



Development of microfluidic cell culture devices towards an in vitro human intestinal barrier model

Tan, Hsih-Yin

Publication date:
2015

Document Version
Publisher's PDF, also known as Version of record

[Link back to DTU Orbit](#)

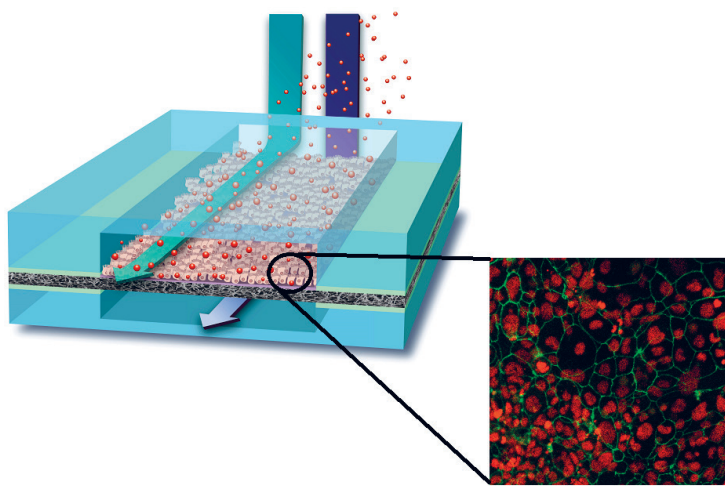
Citation (APA):
Tan, H-Y. (2015). *Development of microfluidic cell culture devices towards an in vitro human intestinal barrier model*. DTU Nanotech.

General rights

Copyright and moral rights for the publications made accessible in the public portal are retained by the authors and/or other copyright owners and it is a condition of accessing publications that users recognise and abide by the legal requirements associated with these rights.

- Users may download and print one copy of any publication from the public portal for the purpose of private study or research.
- You may not further distribute the material or use it for any profit-making activity or commercial gain
- You may freely distribute the URL identifying the publication in the public portal

If you believe that this document breaches copyright please contact us providing details, and we will remove access to the work immediately and investigate your claim.



Development of microfluidic cell culture devices towards an *in vitro* human intestinal barrier model

Hsih-Yin Tan
PhD Thesis October 2015

Development of microfluidic cell culture devices towards an *in vitro* human intestinal barrier model

Hsih-Yin Tan

Department of Micro- and Nanotechnology
Technical University of Denmark

Ph.D. Thesis

October 2015

Main supervisor: Professor Thomas Lars Andresen, Nanotech, DTU

Co-supervisor: Assoc. Professor Martin Dufva, Nanotech, DTU

Co-supervisor: Jörg Peter Kutter, Department of Pharmacy, Copenhagen University

PREFACE

This thesis is presented as a partial fulfilment of the requirements for obtaining a Ph.D. degree from the Technical University of Denmark (DTU). The Ph.D. project was conducted at the department of Micro- and Nanotechnology (DTU Nanotech), from 1st September 2012 until 30th October 2015 and was funded by the DTU Ph.D. Stipend.

The project was supervised by:

Professor Thomas Lars Andresen, DTU Nanotech

Main supervisor

Associate Professor Martin Dufva, DTU Nanotech

Co-supervisor

Professor Jörg P. Kutter, Copenhagen University (KU)

Co-supervisor

Kgs. Lyngby, 30th October 2015

Hsih-Yin Tan

ACKNOWLEDGEMENT

The three years of Ph.D. studies have been an enriching and unforgettable journey. This would not have been possible without the help and support of many people. I would like to take this opportunity to express my sincere gratitude to a number of people.

First and foremost, I would like to thank my main supervisor Thomas Lars Andresen for the opportunity to undertake this Ph.D. project in his research group. His patience, support and the freedom to explore my own ideas made these three years a wonderful experience. I would also like to express my sincere thanks to co-supervisor, Martin Dufva for all the helpful and inspiring discussions. Towards the end of my Ph.D. period, Martin provided his helpful guidance in the writing of this thesis. I would also like to thank my other co-supervisor Jörg P. Kutter for all his helpful suggestions, guidance and discussions.

A special acknowledge goes to my colleagues in Colloids and Biological Interfaces (CBIO), Fluidic Array Systems and Technology (FAST) and ex-ChemLabChip groups in DTU Nanotech for providing a wonderful and harmonious work environment. I am grateful to my colleague, Rikke Søndergaard. I was naïve on biology when I first arrived in DTU. With Rikke's help, I learnt the secrets to cell culturing. The discussions and her guidance have helped me to understand biology better. I am also thankful and indebted to Mette Hemmingsen for her invaluable guidance in the use of the fluidic system for cell culture and microscopy and image processing/analysis. Special thanks goes out to Thomas G. Jensen for his quick and often unconventional ideas for experiments. One of them happened to be a suggestion to use thiol-ene as the material for my microchip fabrication. The suggestion of his became the turning point in my project. I want to also thank him for his Danish translational skills. Pedro Nunes, my office companion for the scientific and non-scientific discussions and his good cheer.

I am very thankful to all my friends especially my closer friends: Solene, Ritika, Silvia and Layla for keeping my head above the water during my three years of Ph.D. studies. They have kept me sane, grounded and well motivated through the difficult times of my research.

Last but not least, I want to express my sincere gratitude and thanks to my family members. Despite the thousands of miles away from home, they have been nothing but supportive of me. I am very grateful for their confidence, patience and love throughout my life.

ABSTRACT

Existing *in vitro* models of the human intestine such as the established epithelial cell line, Caco-2, cultured on porous membranes have been extensively used for assessing and predicting permeability and absorption of oral drugs in the pharmaceutical industries. However, such *in vitro* human intestinal models fail to support any form of luminal flow conditions on the cells in order to more closely mimic *in vivo* conditions. Although these existing systems are easy to use, they require a large amount of cells, culture media, samples and reagents. Microfluidics is a technology that has the potential to revolutionise the way of *in vitro* cell culture. In particular, microfluidics provides avenues for researchers to tailor the cellular microenvironment to better mimic the cell-cell and cell-extracellular matrix interactions, while at the same time reducing the scale of the experimental studies. Moreover, microfluidics also offers the possibility of dynamic cell culture in microperfusion systems to deliver continuous nutrient supplies for long term cell culture. When combined with electronic or optical components such as sensors, actuators, and control logic, microfluidics has the potential to enable real-time detection of cell responses, adjustment of cellular stimulation etc. leading to establishment of conditional experiments.

In this project, microfluidic systems engineering was leveraged to develop an eight chamber multi-layer microchip for intestinal barrier studies. Sandwiched between the layers was a modified Teflon porous membrane for cell culture. The novelty lies in modifying the surface of the porous Teflon support membrane using thiol-ene 'click' chemistry, thus allowing the modified Teflon membrane to be bonded between the chip layers to form an enclosed microchip.

Successful application of the multi-layer microchip was demonstrated by integrating the microchip to an existing cell culture fluidic system to culture the human intestinal epithelial cells, Caco-2, for long term studies. Under the continuous low flow conditions, the cells differentiated into columnar cells displaying folds that closely resembled the intestinal villi and formation of a tight barrier. Furthermore, the microelectrodes embedded in the microchip also allow real-time monitoring of the barrier integrity by means of measuring the trans-epithelial electrical resistance. Demonstrations of transport studies using different compounds on the *in vitro* human intestinal model in the microfluidic device showed comparable results with static cultures.

In addition, a normal commensal intestinal bacteria, *Escherichia coli* (*E. coli*) was successfully co-cultured on the luminal surface of the cultured epithelium without compromising the epithelial cell viability and barrier function. Such a platform paves the way towards an alternative *in vitro* intestinal model for high throughput screening of drugs, chemicals, pathogens, intestinal diseases as well as toxicological studies.

ABSTRAKT

Eksisterende *in vitro*-modeller af den menneskelige tarm, såsom dyrkning af den etablerede epithelial cellelinje, Caco-2, på porøse membraner er ofte blevet anvendt i den farmaceutiske industri til at vurdere og forudsige permeabilitet og absorption af præparater til oral indtagelse. Men sådanne *in vitro* modeller af den menneskelige tarm inddrager ikke strømningsforholdene for cellerne for mere nøje at efterligne *in vivo* betingelserne. Selv om disse eksisterende systemer er nemme at bruge, kræver de en stor mængde celler, kulturmedier, prøver og reagenser. Mikrofluidik er en teknologi, der har potentialet til at revolutionere udviklingen af *in vitro*-cellekulture. Særligt mikrofluidik giver mulighed for forskere til at skræddersy det cellulære mikromiljø for bedre at efterligne celle-celle- og celle-ekstracellulær matrix-interaktioner, mens man på samme tid reducere omfanget af de eksperimentelle undersøgelser. Desuden giver mikrofluidik også mulighed for at systemer, med dynamiske cellekulture i mikroperfusionskamre, kan levere næringsstoffer kontinuerligt til langvarige cellekulture. Når mikrofluidik kombineres med elektroniske eller optiske komponenter, såsom sensorer, aktuatorer og styrelogik, har systemet potentiale til at muliggøre realtids målinger af cellereaktioner, justering af cellulær stimulering, osv.

Til dette projekt blev der udviklet et mikrofluidik-system i flere lag med otte kamre til studier af tarmbarrieren. Celledyrkning foregik på en modificeret porøs membran af Teflon, klemt fast imellem chippens øvrige lag. Det nyskabende i dette forsøg ligger i modificeringen af overfladen af den porøse Teflonmembran ved anvendelse af thiol-ene 'klik' kemi, således at den modificerede Teflonmembran kunne slutte tæt til chippens øvrige lag og derved danne en lukket mikrochip.

Det blev demonstreret at den flerlagede mikrochip succesfuldt kunne integreres i et eksisterende fluidsistem til dyrkning af humane epitelceller i tarmen, Caco-2, for langtidsundersøgelser. Under kontinuerlig gennemstrømning ved lave flowrater differentierede cellerne sig til søjleformede celler, som viste folder, der nøje lignede tarmens villi og dannelse af en tæt barriere. Desuden tillader de indlejrede mikroelektroder i mikrochippen også overvågning af barrierens integritet i realtid ved at måle den trans-epiteliale elektriske modstand. Transport undersøgelser i *in vitro*-modellen af den menneskelige tarm med forskellige kemikalier viste sammenlignelige resultater med statiske kulturer.

Derudover blev normale kommensale tarmbakterier, *Escherichia coli* (*E. coli*) med succes co-dyrket på den lumenale overflade af den dyrkede epitel uden at kompromittere levedygtigheden af cellerne eller barrieres funktion. En sådan platform baner vejen hen imod en alternativ *in vitro* tarm model for high throughput screening af lægemidler, kemikalier, patogener, tarmsygdomme samt toksikologiske undersøgelser.

Everything begins with the resolve to take the first step. From that action, wisdom arises and change begins. Without action, nothing changes.

- Daisaku Ikeda

TABLE OF CONTENTS

Table of contents	vii
List of figures	xiii
List of tables	xvi
List of symbols	xvii
List of abbreviations	xviii
1 Chapter one: Introduction	1
1.1 Background	1
1.2 Aim of project.....	3
1.3 Outline of the thesis	4
References	7
2 Chapter two: Background and premises	8
2.1 Microfluidic phenomena related to cellular studies	8
2.1.1 Laminar flow in microchannels.....	8
2.1.2 Diffusion	10
2.1.3 Fluid shear stress	11
2.2 Caco-2 cells	12
2.2.1 Transport mechanisms across Caco-2 monolayers.....	14
2.3 Microfluidics for cell culture.....	15
2.3.1 Using microfluidic flow conditions to control microenvironments	16
2.3.2 Integrated analysis on microfluidic devices	16
2.3.3 Microfluidic cell culture systems and cell-based assay systems	17
2.4 Device materials and fabrication	19
2.4.1 Material selection	19
2.4.2 Fabrication technologies for microfluidics.....	20
2.4.2.1 Direct writing technique.....	21
2.4.2.2 Replication technique	22
2.4.3 Bonding of polymers	24
2.4.3.1 Indirect bonding	25

2.4.3.2	Direct bonding	25
References	26
3	Chapter three: First generation microchip – PMMA microchip.....	35
3.1	Design considerations	35
3.1.1	Material selection for fabrication of microchip	36
3.1.2	Design of microchip	36
3.1.3	Design of fluidic system	39
3.1.4	Bubble trap designs	39
3.2	Materials and methods	41
3.2.1	Fabrication and assembling of the microfluidic devices	41
3.2.2	Fabrication of bubble traps	43
3.2.2.1	Bubble trap design 1.....	43
3.2.2.2	Bubble trap design 2.....	44
3.2.3	Flow studies with the microfluidic devices and bubble traps.....	44
3.2.4	Cell culturing with PMMA microchip design 2	45
3.3	Results and discussion	46
3.3.1	Flow characterisation in microfluidic chip.....	46
3.3.2	Bubble trap characterisation.....	48
3.3.2.1	Bubble trap design 1.....	48
3.3.2.2	Bubble trap design 2	49
3.3.3	Cell culturing with PMMA microchip and bubble trap design 2	50
3.3.4	Comparison of microfluidic device connected to bubble trap design 2 functioning at room temperature versus at 37 °C	53
3.4	Conclusion	54
3.5	Outlook	54
References	56
4	Chapter four: Second generation microchip – Thiol-ene microchip	59
4.1	Design considerations	59
4.1.1	Material selection	59
4.1.2	Microchip designs	60

4.2	Materials and methods	62
4.2.1	Fabrication of microchips	62
4.2.2	Optimisation of UV-exposure time to cure thiol-ene mixtures	66
4.2.3	Preparation of thiol-ene and PDMS rings for Caco-2 biocompatibility studies	66
4.2.4	Contact angle and wetting properties.....	68
4.2.5	Bond test of microchip.....	68
4.3	Results	69
4.3.1	Thiol-ene biocompatibility test.....	69
4.3.2	Characterisation of polymeric materials for microchip fabrication	71
4.3.2.1	Shrinking of PDMS	71
4.3.2.2	Optimisation of UV-exposure duration for curing thiol-ene mixtures	72
4.3.3	Thiol-ene modified porous Teflon membrane	73
4.3.4	Bond testing of microchip	76
4.4	Discussion	77
4.5	Conclusion	80
	References	81
5	Chapter five: Integrating thiol-ene microchip with fluidic system for cell culture	84
5.1	Fluidic system for microfluidic cell culture	84
5.2	Materials and methods	85
5.2.1	Assembling of the microfluidic perfusion cell culture system	85
5.2.2	Preparation of microfluidic system for cell culture	87
5.2.3	Cell seeding and cell culture in microfluidic system	88
5.2.4	Cell imaging and live/dead cell staining	89
5.2.5	Flow profile in microchamber	89
5.3	Results	90
5.3.1	System evaluation.....	90
5.3.2	Preliminary cell culture with HeLa cells and Caco-2 cells with thiol-ene microchip design 1 and fluidic system	92
5.3.3	Effect of inlet dimensions on flow profile and cell growth in microchamber	94
5.4	Discussion	96
5.4.1	Fluidic system for cell culture.....	97
5.4.2	Thiol-ene microchip for cell culture	97
5.5	Conclusion.....	98

5.6 Outlook.....	99
References	99
6 Chapter six: Embedding electrodes onto thiol-ene microfluidic chip for trans-epithelial electrical resistance (TEER) measurements	102
6.1 Trans-epithelial electrical resistance measurement across Caco-2 monolayer.....	102
6.2 Design considerations	104
6.2.1 Positioning of electrodes	104
6.2.2 Material selection of electrode and fabrication technique.....	105
6.2.3 Electrode design on microfluidic chip	106
6.2.4 System for obtaining TEER measurements.....	107
6.3 Materials and methods	108
6.3.1 Fabrication of electrodes on microchip.....	108
6.3.2 Biocompatibility studies of InBiSn metal	109
6.3.3 Characterization studies of electrodes.....	110
6.3.4 TEER measurements of Caco-2 cells cultured in microchip	110
6.3.5 Introducing membrane enhancer to Caco-2 monolayers in microchip	111
6.3.6 Static Transwell cultures of Caco-2 monolayer.....	112
6.4 Results.....	114
6.4.1 Biocompatibility tests on InBiSn metal	114
6.4.2 Characterization of electrodes on microchip.....	115
6.4.3 TEER measurements of Caco-2 cells cultured in microchip.....	117
6.4.4 Effect of membrane enhancers on TEER measurements	119
6.5 Discussion	120
6.6 Conclusion.....	123
References	124
7 Chapter seven: Thiol-ene based microchip Caco-2 monolayer for passive transport studies	127
7.1 Motivation	127
7.2 Materials and methods	128
7.2.1 Caco-2 cell culture	128
7.2.2 Morphological studies	128
7.2.3 Aminopeptidase studies	129

7.2.4	Permeability studies	130
7.3	Results and discussion	132
7.3.1	Phase contrast imaging of Caco-2 monolayer	132
7.3.2	Fluorescent images of cells	133
7.3.3	Measurement of aminopeptidase activity	135
7.3.4	Permeability studies of FITC–dextran (FD-4), mannitol and insulin in the presence or absence of membrane enhancer	136
7.3.5	TEER measurements across Caco-2 monolayers in the presence or absence of membrane enhancer	138
7.4	Conclusion.....	139
	References	139
8	Chapter eight: Co-culturing of Escherichia Coli (<i>E. coli</i>) with Caco-2 cell	141
8.1	Motivation of this project	142
8.2	Materials and methods	142
8.2.1	Culturing <i>E. coli</i>	142
8.2.2	Co-culturing <i>E. coli</i> in Transwell inserts	142
8.2.2.1	Trans-epithelial electrical resistance (TEER) measurements	143
8.2.2.2	Cell staining.....	143
8.2.2.3	Permeability studies using phenol red.....	144
8.2.3	Co-culturing of <i>E. coli</i> with Caco-2 cells in microfluidic system	144
8.2.3.1	TEER measurements	145
8.2.3.2	Morphological studies	145
8.3	Results	146
8.3.1	Co-culturing of Caco-2 cells with <i>E. coli</i> in Transwell	146
8.3.1.1	Caco-2 cells viability	147
8.3.1.2	Effect of co-culture duration on Caco-2 cells.....	148
8.3.1.3	Morphological studies	152
8.3.2	Co-culturing <i>E. Coli</i> in thiol-ene microfluidic system	152
8.3.2.1	TEER measurements in microfluidic device	153
8.3.2.2	Morphological studies on Caco-2 cell incubated with <i>E. Coli</i> in microfluidic system	154
8.4	Discussion	156
8.4.1	Challenging Caco-2 cells with <i>E. coli</i> in Transwell systems	156

8.4.2	Challenging Caco-2 cells with <i>E. coli</i> in microfluidic system	158
8.5	Conclusion.....	159
8.6	Outlook.....	159
	References	160
9	Chapter nine: Conclusion and Outlook.....	162
9.1	Conclusion	162
9.2	Outlook	163
	Appendix	165
	List of publications.....	165
	A1 Manuscript for peer review journal	166
	B2 Peer reviewed conference proceeding	187

LIST OF FIGURES

Figure 1.1: Schematic illustration of the concept of the microfluidic device for culturing Caco-2 cells	3
Figure 2.1: Schematic illustration of fluid flow in a parallel plate flow chamber	12
Figure 2.2: Schematic view Caco-2 cells cultured in Transwell porous inserts	13
Figure 2.3: Schematic overview of the Caco-2 monolayer forming a tight barrier when grown on the Transwell porous membrane.	14
Figure 2.4: Step-growth photopolymerisation mechanism of thiol-ene.....	20
Figure 2.5: Micromilling	21
Figure 2.6: Soft lithography process	23
Figure 2.7: Chemical structures of thiols and allyl that will be used for creating the different thiol-ene layers in the microfluidic chip in this project	24
Figure 3.1: Exploded views of the different layers in the two different microfluidic chip designs	37
Figure 3.2: Cross-sectional view of the microchambers from the two different microchip designs	38
Figure 3.3: Schematic drawing of the fluidic set-up connected to the microchip	39
Figure 3.4: Cross-sectional view of the bubble trap made from silicon tubes of different inner diameters connected in series	40
Figure 3.5: Schematic cross-sectional view of the Eppendorf tube bubble trap. Blue circles indicating air bubbles	41
Figure 3.6: Images of the assembled microchip devices	42
Figure 3.7: Bubble trap made from connecting different tubing sizes	43
Figure 3.8: Close up view of the Eppendorf bubble trap	44
Figure 3.9: Pictures of microfluidic chips after being infused with colour dyes for 1 hr	47
Figure 3.10: Cell culture medium was continuously perfused into microchip design 2 for 2 hr.....	48
Figure 3.11: Pictures of the cell culture chamber perfused with cell culture medium	49
Figure 3.12: Bubble traps made using 1.5 ml Eppendorf tubes	50
Figure 3.13: Close up view of the cell culture chamber on PMMA microchip containing Hela cells	51
Figure 3.14: Membrane removed from the microchip	52
Figure 3.15: Hela cells cultured in PMMA microchip for 48 hrs	53
Figure 4.1: Exploded views of the 3 layer thiol-ene microchip	61

Figure 4.2: Schematic top view of the two different microchip designs	62
Figure 4.3: PMMA master mold	63
Figure 4.4: Schematic process of fabricating the thiol-ene microchip	65
Figure 4.5: Completed thiol-ene microfluidic chip	66
Figure 4.6: Batch cultures in 12-well microtitre plate	67
Figure 4.7: Burst pressure study for thiol-ene microchip	69
Figure 4.8: Phase contrast pictures of the Caco-2 cells taken over the days of cell culture	70
Figure 4.9: Cured PDMS mold aligned over the PMMA molds	71
Figure 4.10: Scanning electron microscope (SEM) images of Teflon membrane	73
Figure 4.11: Contact angle measurement of materials typically used in microchip fabrication for cell culture	74
Figure 4.12: Contact angle measurement of original Teflon membrane and the protected region of thiol-ene coated Teflon membrane.....	75
Figure 4.13: Porous Teflon membrane modified with a layer of cured thiol-ene mixture (3T+3E)	76
Figure 5.1: Schematic drawing of the assembly of base plate for the cell culture platform	85
Figure 5.2: Assembled thiol-ene microfluidic chip (design 1) with the cell culture platform	86
Figure 5.3: Assembled system with thiol-ene microchip	91
Figure 5.4: Images of Caco-2 cells and Hela cells in the thiol-ene microchip after culturing for 11 days and 6 days respectively	93
Figure 5.5: Phase contrast imaging of Caco-2 cells cultured in thiol-ene microchip (design 1) on day 10	94
Figure 5.6: Simulated flow contours in the microchambers with respect to different inlet and outlet widths	95
Figure 5.7: Effect of channel dimensions on cell growth	96
Figure 6.1: Schematic illustrations of the electrical circuit and flow of current across Caco-2 monolayers .	103
Figure 6.2: Schematic cross-sectional view of the microchamber in a microfluidic chip with electrodes connected to the multimeter	105
Figure 6.3: Schematic drawings of the fluidic layers	107
Figure 6.4: Multi-meter used for recording the TEER measurements from microfluidic chip	108
Figure 6.5: Electrodes on microfluidic chip for TEER measurements	109
Figure 6.6: TEER measurement in Transwell system	113
Figure 6.7: Biocompatibility tests of InBiSn alloy	114
Figure 6.8: Characterisation of electrodes in microfluidic chip	116

Figure 6.9: Baseline resistance of different chambers filled with PBS on the same microchip	117
Figure 6.10: TEER measurements recorded with Caco-2 cells and no Caco-2 cells (Control) in microfluidic device	118
Figure 6.11: TEER measurements of Caco-2 cells cultured in thiol-ene microchip and Transwell inserts ..	119
Figure 6.12: Impact of different concentrations of TDM on TEER measurements	120
Figure 7.1: Phase contrast images of the Caco-2 cells cultured in the microchambers on the thiol-ene microchip over 10 days	133
Figure 7.2: Immunostaining of tight junctions and nucleus of Caco-2 cells cultured in microfluidic device	134
Figure 7.3: Immunofluorescence staining of nucleus and mucus on Caco-2 cells cultured in thiol-ene microchip on day 10 of cell culture	135
Figure 7.4: Differentiation of Caco-2 cells cultured in Transwell set-up and microfluidic device as indicated by the activity of the brush border enzyme aminopeptidase activity	136
Figure 7.5: Permeability of A) mannitol, B) FD4 and C) insulin, alone or with TDM, across caco-2 monolayers grown in the Transwell or microfluidic setup	137
Figure 7.6: Effect of insulin/FD4 alone or with TDM on Caco-2 TEER in the Transwell or microfluidic setup, immediately after the experiment or 24 hr recovery in cell culture medium	138
Figure 8.1: Transwell inserts with <i>E. coli</i> seeded on the apical side of Caco-2 monolayers	147
Figure 8.2: Live/dead cell staining on Caco-2 monolayers cultured in Transwell set-up	148
Figure 8.3: Apparent permeability (P_{app}) of phenol red across Caco-2 monolayers challenged with different concentrations of <i>E. coli</i> for 24 hr incubation period	149
Figure 8.4: Penol red permeability studies carried out on Caco-2 monolayers under different incubation duration with <i>E. coli</i> and 24 hr recovery with normal cell culture medium.....	150
Figure 8.5: Percentage change in TEER measurements on Caco-2 monolayers co-cultured with <i>E. coli</i> for different duration and 24 hr recovery in cell culture medium with antibiotics	151
Figure 8.6: Top view of Caco-2 monolayers stained for nucleus (red) and tight junctions (green)	152
Figure 8.7: Microfluidic chip with <i>E. coli</i> co-cultured on the apical side of the Caco-2 monolayers	153
Figure 8.8: TEER measurements of co-culture studies in microfluidic device	154
Fig 8.10: Live/dead cell staining on Caco-2 monolayers after challenged with <i>E. coli</i> for 24 hr in the microfluidic device	155
Fig 8.11: Immunofluorescent images of Caco-2 cells after 24 hr incubation with <i>E. coli</i>	156

LIST OF TABLES

Table 2.1 Typical diffusion coefficients for various particles in water at room temperature	11
Table 4.1: Increased UV exposure to new PDMS layers resulted in a decreased in on the UV-light transmission through the PDMS layer	72
Table 4.2: Tabulated data of the maximum pressure the different thiol-ene mixtures used for fabricating the microchips could withstand in different temperature conditions	77

LIST OF SYMBOLS

A	Area
HB	Brinell Hardness
l	Characteristic length
\varnothing	Diameter
D	Diffusion coefficient
ρ	Density
T	Temperature
T_g	Glass transition temperature
n	Number of experiments
Pe	Peclet number
τ	Shear stress
Re	Reynolds number
μ	Viscosity
Q	Volumetric flow rate

LIST OF ABBREVIATIONS

2D	Two-dimensional
3D	Three-dimensional
3E	Tri-allyl-tri-azine (tri-allyl moieties)
3T	Trimethylopropane tris-(2-mercaptopropionate) (tri-thiol moieties)
4T	Pentaerythritol tetrakis-3-mercaptopropionate) (tetra-thiol moieties)
[³ H]	Mannitol
Abs	Absorbance
AC	Alternating current
Ag	Silver
AgCl	Silver chloride
Bi	Bismuth
CAD	Computer aided design
CNC	Computer numerical control
CO ₂	Carbon dioxide
DC	Direct current
DMEM	Dulbecco's Modified Eagle's Medium
DMEM ^{-PR}	Dulbecco's Modified Eagle's Medium without phenol red
<i>E. coli</i>	<i>Escherichia coli</i>
FBS	Fetal bovine serum
FD4	Fluorescein isothiocyanate (FITCH)-labeled dextran
HBSS	Hank's Buffer Saline Solution
In	Indium
InBiSn	Indium metal used for microelectrode
L-A4N	L-alanine-4-nitroanilide hydrochloride
LOC	Lab-on-a-chip
MEMS	Microelectromechanical systems
μTAS	Micro total analysis systems
MUC-2	Mucin-2

NaCl	Sodium chloride
NaOH	Sodium hydroxide
NEAA	Non-essential amino acid
OSTE	Off-stoichiometry thiol-ene
OVA	Ovalbumin
P_{app}	Apparent permeability
PBS	Phosphate buffer saline
Pt	Platinum
PC	Polycarbonate
PDMS	Poly-dimethylsiloxane
PMMA	Polymethylmethacrylate
P/S	Penicillin-streptomycin
PS	Polystyrene
PTFE	Polytetrafluoroethylene
RP	Rhodamine phalloidin
SD	Standard deviation
Sn	Tin
TDM	Tetradecyl- β -D-Maltoside
TEER	Trans-epithelial electrical resistance
UV	Ultraviolet
v/v	volume-volume ratio

CHAPTER 1: Introduction

1.1 Background

For almost a century, the science of *in vitro* cell culture is the standard method used around the world for understanding molecular and cell biology. Cell culture is also a model system used extensively in the disciplines of genetics, immunology, cancer, medicine, vaccine production, tissue engineering and many other countless applications [1]. However, the tools and technologies for cell culture did not change significantly over the years. Much of our current understanding of biology derived from *in vitro* studies of cells cultured in Petri dishes, flasks or well plates. Such systems require milliliters of media for culturing cells as suspensions or monolayers. Although these culture systems are relatively robust, predictable and simple, they fail to provide dynamic physiological conditions that are present in *in vivo* conditions. In *in vivo* conditions, cells reside in an environment composed of soluble factors, cell-matrix interactions and cell-cell contacts. They live within an environment with specific physicochemical properties (pH, oxygen tension, temperature, and osmolality) [1]. These parameters function in harmony to regulate the cell structure, function, behaviour, growth and development. As such, the *in vitro* conditions are significantly different from *in vivo* conditions. To better mimic key factors of the human body, much efforts are or have been invested to introduce different parameters to control the microenvironment in cell culture systems [2].

In recent years, researchers explored the possibilities of exploiting microfluidic technology for cell culture. Microfluidics is an area of research that addresses and exploits the fluid dynamics at sub-millimeter scale [1,3]. Microfluidic technology is generally based on devices with networks of microchannels. One of the main advantages of microfluidics is the utilisation of scaling laws to create new effects and better performances in miniaturised devices. Since the emergence of microfluidics in the 1980s, it has been widely used in the development of systems such as microchips for polymerase chain reaction (PCR) of deoxyribonucleic acid (DNA), laser inkjet print-head, sophisticated lab-on-a-chip (LOC) devices, and medical instruments.

Although initially the research in microfluidics was hugely dominated by studies in chemistry and physics, another area that have been gaining rapid development concerning the use of microfluidic systems is cell biology [1,4]. Because microfluidic technology has the ability to manipulate small volumes of fluid in micron-sized channels, it can be leveraged to control parameters of the cellular microenvironments. Additionally, the flexibility in the designing of microfluidic devices, allowed these devices to be tailored to individual cells and cellular co-cultures can also be implemented on the same chip [5]. Therefore making it an attractive technology to bioengineers, biologists and engineers for development of microdevices for biology. This has also led to

new methods of designing and performing biological experiments. Microfluidics has thus paved a way for innovative approaches to understanding fundamental biology and providing new approaches to the solutions of important problems in biomedical analysis [1].

One of the key advantages of microfluidics for biology is the ability to control parameters of the cell microenvironment at relevant length and time scales [1]. In the past decade, researchers tried to leverage microfluidic technologies to create 3-dimensional (3D) microdevices to culture living cells. These 3D microdevices allow the flexibility to artificially engineer key aspects of the *in vivo* microenvironment [6,7]. Toh et. al. [8] reported on developing a 3D microfluidic channel based cell culture system that supported adequate 3D cell-cell and cell-matrix interactions. Through an array of micropillars, maximal cell-cell interaction was achieved. In another study, Hsiao et. al. [9] reported on a microfluidic 3D culture system that recapitulated the *in vivo* growth behaviour of malignant prostrate cancer cells, through construction of an *in vitro* bone metastatic prostate cancer microenvironment. The design allowed gel-free formation of uniformly sized spheroids in a 2-layered microfluidic device to model the 3D metastatic prostate cancer.

In the quest to further mimic *in vivo* conditions, microfluidic cell culture research has also moved towards tissue engineering. Most recently, Choi et. al. reported on developing a microsystem that enabled co-culture of breast tumour spheroids with human mammary ductal epithelial cells and mammary fibroblasts in a compartmentalised 3D microfluidic device to replicate the microarchitecture of breast ductal carcinoma *in situ* [10]. Another recent study demonstrated that the brain microenvironment can be closely mimic by developing a 3D brain model on a microfluidic device [11]. By combining concave microwell arrays with an osmotic micropump system, interstitial level of flow was achieved.

In this sense, applying microfluidic technology to cell culture is a promising approach to more closely mimic *in vivo* cellular microenvironment and simultaneously enabling cell analysis to take place.

1.2 Aim of project

To develop an alternative *in vitro* human intestinal device for transport studies, in this project there are three main objectives to be met. They are listed as follow:

1) To leverage the advances in microfluidic systems engineering to develop an alternative *in vitro* human intestinal model on a multi-layer microchip that provides constant fluid flow and fluidic shear stresses.

The human intestines can be likened to a fluidic tube that is constantly exposed to mechanical stresses due to the presence of fluid flow. One of the major factor missing in conventional *in vitro* intestinal models is the lack of fluid flow that is present in normal human intestines. To simulate the human intestines, this microfluidic chip would consist of upper and lower microchannels separated by a thin porous membrane coated with extra cellular matrix (ECM) that mimics the basement membrane in a human intestine. The upper microchannel of the microchannel will recreate the lumen of the intestine while the bottom layer will recreate the vascular compartment of capillaries *in vivo* (Figure 1.1). Continuous perfusion of culture media in both the upper and lower microchannels would be supplied to ensure the growth and maintenance of the epithelial cells. The convection and diffusion mass transport mechanism found in the body will be reproduced in the microfluidic chip.

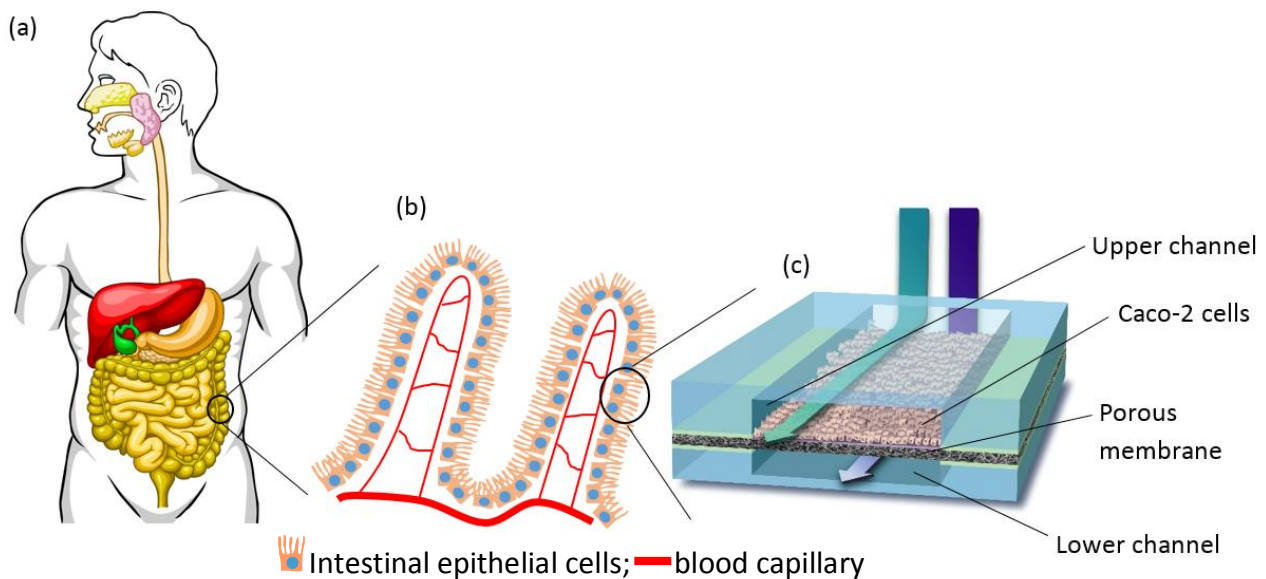


Figure 1.1 Schematic illustration of the concept of the microfluidic device for culturing Caco-2 cells. (a) Human gastrointestinal tract [12]; (b) Schematic view of the human intestinal microvilli comprising of epithelial cells and the vascular network; (c) Artist impression of the architecture of the microfluidic chip. Whereby the microchip comprised of upper microchannel, porous membrane and lower microchannel. Intestinal cells (Caco-2 cells) are cultured on the porous membrane.

Microfluidic system engineering would be leveraged to develop the microfluidic device. In developing the microdevice, the materials chosen must be optically transparent, should be inexpensive and allow rapid prototyping. The work presented in this project will focus on using polymeric materials such as polymethylmethacrylate (PMMA) and thiol-ene to fabricate the microfluidic cell culture device. Microtechnologies like micromilling and soft lithography will be explored as the fabrication techniques.

2) Integration of microelectrodes in the microfluidic device to permit trans-epithelial electrical resistance (TEER) measurements of cells.

One of the simplest and fastest label-free method to monitor the barrier integrity of the cell layer is to acquire the trans-epithelial electrical resistance (TEER). This is possible by using a system consisting of electrodes and electrical measuring equipment such as a volt-ohm meter or multimeter [6,7,13,14]. To realise this aim, design and fabrication of microelectrodes with different electrode materials on the microfluidic chip will be explored.

3) Transport studies conducted with the *in vitro* intestinal model cultured with the microfluidic device for transport studies.

The last objective of the project is to conduct transport studies with the *in vitro* intestinal model in the microfluidic device. Permeability studies with some test compounds will be explored.

1.3 Outline of the thesis

This project is highly inter- disciplinary. The content of this thesis is based on selected work performed throughout the 3-year Ph.D. study. The thesis is divided into nine chapters. In the following list is the brief description of the content in each chapter.

Chapter 1: Introduction

This chapter provides a brief introduction, description of the aims for this project and the organization of the thesis.

Chapter 2: Background/theory

This chapter reviews and discusses on the backgrounds of selected different disciplines and research fields involved. A brief introduction of the physics of microfluidics is discussed, followed by an introduction of Caco-2, the epithelial cell line of interest. This chapter also provides a brief review on the application of microfluidic technology for cell culture, cell handling and membrane studies. Overviews on the different materials used for microfluidic chip fabrication and the different fabrication techniques are also included. Special attention will be paid to thiol-ene, the material of interest that is used for fabricating the microchip for Caco-2 cell cultivation.

Chapter 3: First generation of microchip – PMMA microchips

This chapter introduces the first generation microfluidic chip for cell culture. The microfluidic chip reported is made from polymethylmethacrylate (PMMA). Different microchambers for cell culture were designed, fabricated and tested. The microchip design consists of multiple layers of PMMA layers and a piece of porous cell culture membrane sandwiched between the PMMA layers and clamped together with thick blocks of PMMA acting as the microchip holder. Likewise, some bubble trap designs are discussed in this chapter.

Chapter 4: Second generation microchip – Thiol-ene microchips

Most of the shortcomings highlighted in the previous chapter are addressed in this chapter. The different designs, fabrication and characterisation of the microfluidic chips made from thiol-ene are presented in detail. The chapter also elaborates on the transition from micro-milling machining of the microfluidic chip as reported earlier by the candidate to soft lithography. Bonding of different mixtures of cured thiol-ene pieces to a thiol-ene modified porous membrane for cell culture was subsequently investigated and reported.

Chapter 5: Integrating thiol-ene microchip with fluidic system for cell culture

Integrating of the thiol-ene microfluidic chip with the fluidic platform consisting of some MAINSTREAM components [15–18] are described and discussed. Some preliminary cell culture studies with HeLa cells and Caco-2 cells are experimented with the thiol-ene microchip and presented. The work was presented in conference proceeding 1.

Chapter 6: Embedding electrodes onto thiol-ene microfluidic chip for trans-epithelial electrical resistance (TEER) measurements

The design, fabrication technique of embedding the microelectrodes on the thiol-ene microchip are described. Characterisation of the electrodes were performed. Successful and reliable trans-epithelial electrical resistance (TEER) measurements recorded across Caco-2 cells cultured in the microchip are reported.

Chapter 7: Thiol-ene based microchip Caco-2 monolayer for passive transport studies

Application of the thiol-ene microfluidic chip for long-term Caco-2 cell culture for transport studies is demonstrated. In this chapter, morphological studies of the Caco-2 cells cultured in the microfluidic device are also presented. Permeability studies with different test compounds (with or without membrane enhancers) were conducted on the Caco-2 monolayers cultured in the microfluidic system. Comparison studies were also carried out in the traditional static Transwell system. The bulk of this work is presented in a manuscript prepared for submission.

Chapter 8: Co-culturing of Escherichia coli (*E. coli*) with Caco-2 cells

The work presented here was conducted with a Master intern student, Jorine Brendensen from University of Twente. In this chapter, some preliminary investigations on co-culturing the bacteria, *E. coli* with the Caco-2 monolayers were presented. Co-culturing of the bacteria and Caco-2 cells was carried out in both the Transwell culture systems and microfluidic device. Experimental results were evaluated and presented.

Chapter 9: Conclusion and outlook

This chapter concludes the results presented, followed with suggestions for future work based on the project.

References

- [1] E.W.K. Young, D.J. Beebe, Fundamentals of microfluidic cell culture in controlled microenvironments, *Chem. Soc. Rev.* 39 (2010) 1036–1048.
- [2] A.D. van der Meer, A. van den Berg, Organs-on-chips: breaking the in vitro impasse, *Integr. Biol.* 4 (2012) 461–70.
- [3] N.-T. Nguyen, S.T. Wereley, Fundamentals and applications of microfluidics, 1st ed., Artech House, Boston, 2002.
- [4] G.M. Whitesides, The origins and the future of microfluidics., *Nature.* 442 (2006) 368–73.
- [5] L.Y. Yeo, H.-C. Chang, P.P.Y. Chan, J.R. Friend, Microfluidic devices for bioapplications, *Small.* 7 (2011) 12–48.
- [6] D. Huh, B.D. Matthews, A. Mammoto, M. Montoya-Zavala, H.Y. Hsin, D.E. Ingber, Reconstituting organ-level lung functions on a chip, *Science* (80-.). 328 (2010) 1662–8.
- [7] H.J. Kim, D. Huh, G. Hamilton, D.E. Ingber, Human gut-on-a-chip inhabited by microbial flora that experiences intestinal peristalsis-like motions and flow, *Lab Chip.* 12 (2012) 2165–74.
- [8] Y.-C. Toh, C. Zhang, J. Zhang, Y.M. Khong, S. Chang, V.D. Samper, et al., A novel 3D mammalian cell perfusion-culture system in microfluidic channels, *Lab Chip.* 7 (2007) 302.
- [9] A.Y. Hsiao, Y. Torisawa, Y.-C. Tung, S. Sud, R.S. Taichman, K.J. Pienta, et al., Microfluidic system for formation of PC-3 prostate cancer co-culture spheroids, *Biomaterials.* 30 (2009) 3020–3027.
- [10] Y. Choi, E. Hyun, J. Seo, C. Blundell, H.C. Kim, E. Lee, et al., A microengineered pathophysiological model of early-stage breast cancer, *Lab Chip.* 15 (2015) 3350–3357.
- [11] J. Park, B.K. Lee, G.S. Jeong, J.K. Hyun, C.J. Lee, S.-H. Lee, Three-dimensional brain-on-a-chip with an interstitial level of flow and its application as an in vitro model of Alzheimer’s disease., *Lab Chip.* 15 (2014) 141–50.
- [12] Human gastrointestinal tract, www.cvseventh.com.
- [13] C. Huang, Q. Ramadan, J.B. Wacker, H.C. Tekin, C. Ruffert, G. Vergères, et al., Microfluidic chip for monitoring Ca²⁺ transport through a confluent layer of intestinal cells, *RSC Adv.* 4 (2014) 52887–52891.
- [14] I. Hubatsch, E.G.E. Ragnarsson, P. Artursson, Determination of drug permeability and prediction of drug absorption in Caco-2 monolayers, *Nat. Protoc.* 2 (2007) 2111–9.
- [15] P. Skafte-Pedersen, D. Sabourin, M. Dufva, D. Snakenborg, Multi-channel peristaltic pump for microfluidic applications featuring monolithic PDMS inlay, *Lab Chip.* 9 (2009) 3003–6.
- [16] D. Sabourin, D. Snakenborg, M. Dufva, Interconnection blocks: a method for providing reusable, rapid, multiple, aligned and planar microfluidic interconnections, *J. Micromechanics Microengineering.* 19 (2009) 035021.
- [17] D. Sabourin, D. Snakenborg, M. Dufva, Interconnection blocks with minimal dead volumes permitting planar interconnection to thin microfluidic devices, *Microfluid. Nanofluidics.* 9 (2009) 87–93.
- [18] D. Sabourin, P. Skafte-Pedersen, M.J. Sjøe, M. Hemmingsen, M. Alberti, V. Coman, et al., The MainSTREAM component platform: a holistic approach to microfluidic system design, *J. Lab. Autom.* 18 (2013) 212–28.

CHAPTER 2: Background and premises

Some highlights of the important physics that are dominant in cell culture microfluidic devices will be presented here. Reviews and discussions of some past work on Lab-on-a-chip (LOC) devices for cell culture and Caco-2 cells, are also highlighted. This chapter will also review on some of the popular materials used in fabrication of microchip for cell culture and the material of interest, thiol-ene, used in the fabrication for the culture of Caco-2 cells in this project.

2.1 Microfluidic phenomena related to cellular studies

2.1.1 Laminar flow in microchannels

Microfluidics is an area of research that addresses and exploits the fluid dynamics at sub-millimeter scale [1,2]. To work with microfluidics, it is important to understand the physical phenomena that are dominant at the micrometer scale.

At the microscale, the laws of physics remain the same as in macroscopic systems. However, due to the scaling down of fluids into sub-millimeter scale, some of the forces (e.g. capillary forces) become more dominant over those experienced in everyday life [3]. For example, in the case of fluid flow, the reduction in size will reduce the influence of the inertial forces compared to frictional/viscous forces. This will lead to the formation of laminar flow in microfluidic channels. Therefore, new designs need to be considered to deal with the forces that are dominant when working in the microscale ranges. References [4,5] give comprehensive reviews of the physics associated with both micro- and nanofluidics.

By downscaling the geometry of the channel that is containing the fluid, the effects that become dominant in microfluidics include laminar flow, diffusion, fluidic resistance, surface area to volume ratio, and surface tension [5]. The Reynolds number (Re) of a fluid flow, is a dimensionless quantity used for characterising the fluid behaviours within microfluidic channels. Re is used to quantitatively estimate the tendency of a fluid to develop turbulence. It is defined as the ratio between the inertial and viscous forces on the fluid. The Reynolds number (Re) can be calculated by:

$$\text{Eq. 2.1} \quad Re = \frac{\rho u D_h}{\mu}$$

where ρ ($\text{kg} \cdot \text{m}^{-3}$) is the density of fluid, u ($\text{m} \cdot \text{s}^{-1}$) is the characteristic velocity of fluid and μ ($\text{kg} \cdot \text{s}^{-1} \cdot \text{m}^{-1}$) is the viscosity of fluid. D_h (m) is the hydraulic diameter of the pipe or channel, which is dependent on the cross-section of the channel in which the fluid is flowing across. Flow patterns are often classified into two categories: laminar and turbulent. Laminar flow occurs when $Re < 2100$, and the flow is smooth and predictable. Due to the small size of the microchannels, the flow in a microfluidic channel is almost always laminar [5]. This can be advantageous in some cell biology applications such as the formation of static and dynamic gradients at subcellular resolution in the presence of laminar flow [6].

Pressure driven incompressible flow is described by two equations, the Navier-Stokes equation [7]:

$$\text{Eq. 2.2} \quad \rho \left[\frac{\partial u}{\partial t} + (u \cdot \nabla)u \right] = -\nabla P + \eta \nabla^2 u$$

And the continuity equation is given by:

$$\text{Eq. 2.3:} \quad \nabla \cdot u = 0$$

Where ρ is the density of fluid, u is fluid velocity, t is time, P is the pressure and η is fluid viscosity. When $Re \ll 1$, the flow is described as ‘creeping flow’. The Navier-Stokes equation describes the motion of viscous fluids.

In designing microfluidic channels, the analytical solution for the Navier-Stokes equation can be solved by assuming no-slip boundary conditions. Under pressure-driven flow, the flow profile will always be parabolic. The exact solution is dependent on the cross-sectional geometry of the microfluidic channel. The steady state velocity profile for the rectangular channel can be approximated using parallel plate Poiseuille flow [8]:

$$\text{Eq. 2.4:} \quad v_x = \frac{\Delta P}{2\mu L} (h - y)y$$

Where v_x is the velocity in the x direction. v_x is a function of the position along the channel height y , and h is the channel height, ΔP is the pressure difference between the two ends of the channel, L is the length of channel and μ is the viscosity of fluid.

For fluid flow through shallow microchannels with height, h , and width, w , the average velocity in the microchannel can be calculated as:

Eq. 2.5
$$u = \frac{Q}{w \cdot h}$$

where u is fluid velocity, Q ($\text{m}^3 \cdot \text{s}^{-1}$) is the volumetric flow rate, w (m) is the width of channel and h (m) is the height of channel.

In laminar flow, the liquids are transported in uniform layers of thickness, between fixed boundaries, where the mixing of the streamed liquids occurs by diffusion across the liquid-liquid interfaces.

2.1.2 Diffusion

Diffusion is the process by which a concentrated group of particles (e.g., molecules, particles, cells etc.) will spread out over time. Thus, by means of Brownian motion, the average concentration of particles throughout the volume becomes constant [5]. For a laminar flow in a channel, due to the absence of convective forces acting on the fluid under laminar flow, the contents in the fluid will mix by means of diffusion

Furthermore, the reduction of dimension sizes has a direct influence on the reaction time of the contents. Diffusion of a particle in a channel can be modeled in one-dimensional means by:

Eq. 2.6
$$d = \sqrt{2Dt}$$

Where d is the distance a particle moves at time t , and D is the diffusion coefficient of the particle. From equation 2.6, it is clear the mixing time for diffusion-based mixing increases with the diffusion distance. Therefore, diffusion becomes an important phenomenon in microscale. The degree of mixing particles between adjacent streams is therefore dependent on the channel dimensions, the size of the particle found within the channel and the flow rates within the channel. The velocity of diffusion is related to the diffusion coefficient of the solute of interest. The diffusion coefficient (D) can be estimated with the Stokes-Einstein equation:

Eq 2.7
$$D = \frac{k_B T}{6\pi\eta r}$$

where T (K) is absolute temperature, r (m) is the radius of the particle, k_B is Boltzmann constant and η (Pa·s) is the viscosity of the solute. Generally, the linear size of a molecule varies as the cube root of the molecular weight ($r \approx (\text{MW})^{1/3}$) [9]. Hence, the diffusion coefficient for a large protein is about 50 times smaller than a solute ion. For particles like cells (10 μm in diameter) the diffusion constant could be 2×10^4 times smaller than for a small protein. Table 2.1 shows the diffusion coefficient for various particles.

Particle	Typical size	Diffusion coefficient
Solute ion	0.1 nm	$2 \times 10^3 \text{ m}^2/\text{s}$
Small protein	5 nm	$40 \text{ }\mu\text{m}^2/\text{s}$
Virus	100 nm	$2 \text{ }\mu\text{m}^2/\text{s}$
Bacterium	1 μm	$0.2 \text{ }\mu\text{m}^2/\text{s}$
Mammalian/Human cell	10 μm	$0.02 \text{ }\mu\text{m}^2/\text{s}$

Table 2.1 Typical diffusion coefficients for various particles in water at room temperature [4].

Depending on the fluid dynamic conditions, transport of solutes can be either by convection or diffusion. The dimensionless number Péclet number, Pe , expresses the relative importance of convection to diffusion and is given as [4]:

$$\text{Eq. 2.8} \quad Pe = \frac{ul}{D}$$

where u is the velocity, l is the characteristic length and D is the diffusion coefficient of the particle. In situations where the velocity is high, convective transport will dominate. Conversely, when the length of the microchannel is short, diffusion will dominate. In a microfluidic cell culture system, the Peclet number also provides an estimation of how quickly the nutrients are being replenished by flow compared to the amount diffusing out [1]. For maintaining healthy cells cultures, it is important to maintain favourable mass transport. Consider a situation when the convective transport is too slow, when the rate of replenishing the nutrients is slower than the rate of nutrient consumption by the cells, over time the cells will starve. Conversely, when the convective transport is too fast, signaling factors secreted by the cells will be washed away. Similarly when the diffusional distance is too far, a concentration gradient is generated based on the cell location. While when the diffusion distance is very short, fitting sufficient cells in the limited space becomes a challenge [10].

2.1.3 Fluid shear stress

The mechanical impact of shear stress can be controlled through the geometry and flow conditions. Fluidic shear stresses are generally measured as the ratio of the shearing force over the area which it is acting on. The walls of the microchannel can be likened to two parallel plates and the shear stress that is imposed on the cells is constant over a defined period of time as the flow rate is constant. Typically, the fluid enters from one end and exit from the other end as shown in figure 2.1.

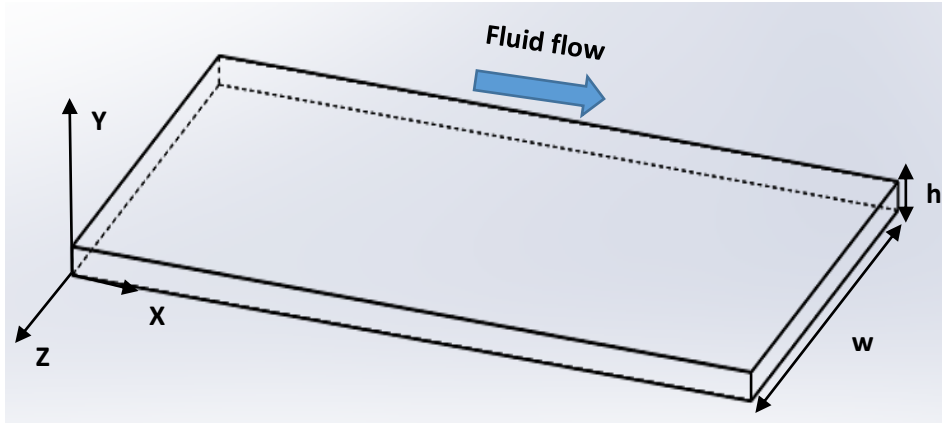


Figure 2.1. Schematic illustration of fluid flow in a parallel plate flow chamber. Flow is entering from one end and exit from the opposite direction. This is also similar to a microfluidic channel for cell culture.

In a chamber or channel where cells are cultured, the bottom layer will be where the cells are cultured. Calculation of the shear stress in a microchannel is expressed as follows [11]:

$$\text{Eq. 2.9} \quad \tau_w = \frac{6\mu Q}{wh^2}$$

where τ_w is the shear stress, μ is the dynamic viscosity of fluid (Pa·s), Q is the volumetric flowrate ($\text{m}^3\cdot\text{s}^{-1}$), h is the channel height (m), and w is the channel width (m). For shear stress calculations using cell culture medium, Dulbecco's Modified Eagle's Medium (DMEM), as the fluid, the viscosity of DMEM at 37 °C is 0.0078 Pa·s [11]. From eq. 2.9, it is expected that by downscaling the height of the microchannels will increase the shear stress for a fixed flow rate or velocity.

2.2 Caco-2 cells

A single layer of epithelial cells is lining the wall of the intestine. The epithelial layers forms the rate limiting barrier towards absorption of dissolved drugs. For decades, numerous experimental models both *in vitro* and *in vivo*, were developed to predict and study the permeability of intestines [12–15]. Animal testing has so far been the preferred method to simulate and predict human response to drugs, chemicals, pathogens and toxins. However, the downside to this is that animal studies are costly, lengthy and they may fail to accurately predict human response to certain compounds or drugs. Beyond that, there are ethical considerations as well [16]. To properly re-constitute an *in vitro* model of the human intestinal for the prediction of drug absorption in humans,

clinicians and researchers had discovered the human carcinoma cell line, Caco-2, is able to serve this purpose well [17,18].

The Caco-2 cell line is an immortalised line of heterogeneous human epithelial colorectal adenocarcinoma cells. This model was developed by the Sloan-Kettering Institute for Cancer Research. When cultured under specific conditions (i.e. porous cell culture inserts – e.g., Transwell inserts) (Figure 2.2), these cells will form a monolayer and spontaneously proliferate and differentiate, exhibiting many features that are similar to the small intestinal villus epithelium [19]. Some of the most prominent features of the differentiated Caco-2 cells are the formation of brush border microvilli on the upper side of the cells, development of intercellular tight junctions and the presence of various metabolic enzymes present in the intestinal epithelium [20,21].

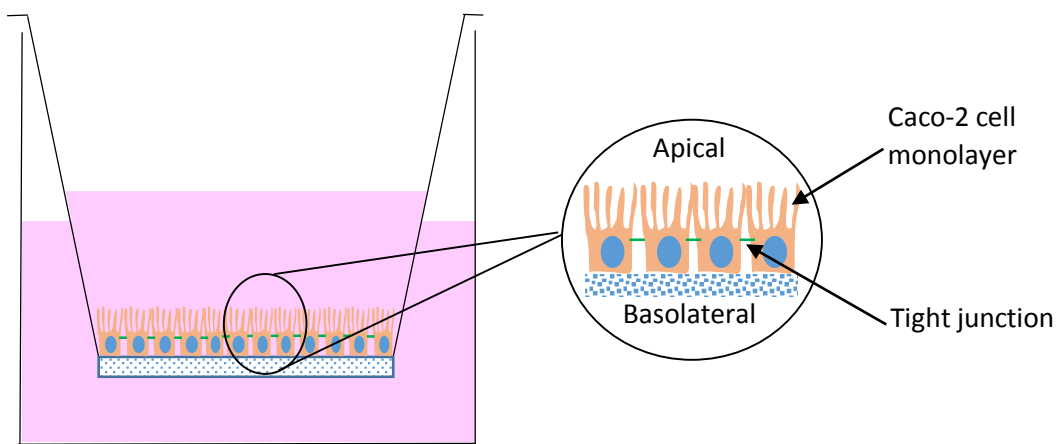


Figure 2.2. Schematic view Caco-2 cells cultured in Transwell porous inserts. Enlarged view of the Caco-2 monolayers with microvilli and tight junctions [19]

About 3 weeks of culture in Transwell porous inserts is required for Caco-2 cells to fully differentiate and form a confluent monolayer [19,22]. During the 3 weeks, the cell culture medium has to be changed every alternate or third day. This can be cumbersome, laborious and costly. There had been reports on the possibilities of developing a more rapid Caco-2 cell culture by modifying the cell culture protocols [23–25]. Acceleration in the growth of the Caco-2 monolayers were achieved by reducing the serum in the cell culture medium but with addition of special supplements [23–25]. Cai et. al. [23] reported that by modifying the composition of the cell culture medium and a higher Caco-2 cell seeding density, a 7-day Caco-2 culture system was achieved. Their results showed that this 7-day Caco-2 culture system displayed better barrier properties. Another study by Lentz et. al. [25] showed that the 4-day Caco-2 culture system they developed, displayed comparable permeability results when compared to 21-day Caco-2 system. However, the Caco-2 monolayers exhibited low brush border enzyme (alkaline phosphatase) activity of 2.46 nmol/min.mg as compared to 87.72 nmol/min.mg for the 21-day culture [25].

2.2.1 Transport mechanisms across Caco-2 monolayers

As mentioned earlier, tight junctions are present between adjacent Caco-2 cells. The formation of the intercellular tight junctions result in a tight cellular barrier separating the apical from the basolateral side (Figure 2.2). Due to this unique characteristic of the polarised Caco-2 monolayer, it provides a physical and biochemical barrier to the passage of ions and small molecules. Therefore, transport across the colonic epithelial barrier is efficiently controlled. There are two modes of transportation across the Caco-2 cell layer: paracellular and transcellular [26].

Paracellular transport is passive diffusion and regulated by the selectively permeable tight junctions between adjacent Caco-2 cells. The transcellular pathway is both transporter-mediated or by simple diffusion. Figure 2.3 shows the schematics of the two different transport pathways across Caco-2 cells.

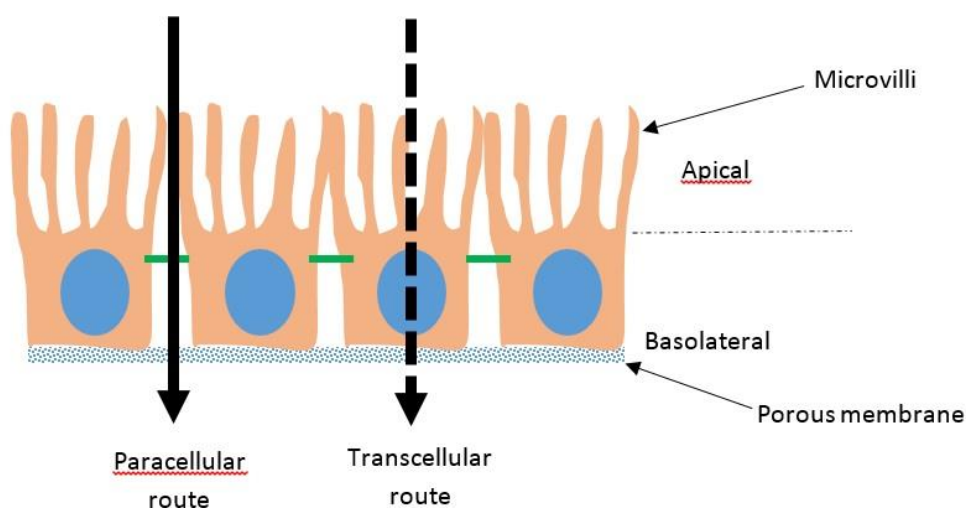


Figure 2.3. Schematic overview of the Caco-2 monolayer forming a tight barrier when grown on the Transwell porous membrane. The two different types of transport in the Caco-2 monolayers are: transcellular pathway and paracellular pathway

Caco-2 monolayers for drug transport studies

Movement of molecules in solutions or molecular transport across the Caco-2 barriers is caused by diffusion. Diffusion is the random movement of molecules in a solution. Therefore, it may only cause a net transport of molecules in the presence of a concentration gradient [27].

The velocity of diffusion is related to the diffusion coefficient of the solute of interest. The diffusion coefficient (D) can be estimated with the Stokes-Einstein equation discussed earlier (eq 2.7). According to eq. 2.7, the diffusion coefficient decreases with increasing molecule size and increasing viscosity of the solvent. The diffusional flux can be determine by applying Fick's first law of diffusion [27]:

Eq. 2.10
$$J = -D \frac{\partial C(x,t)}{\partial(x)}$$

Where J is the flux, ∂C is the concentration in dimensions of (amount of substance per unit volume, $\text{mol}\cdot\text{m}^{-3}$), t (s) is the time and x is the position (m). Fick's first law postulates that under steady-state conditions, the flux goes from regions of high concentration to regions of low concentration.

In a biopharmaceutical context, the use of flux studies are often carried out to investigate the transport of drugs across a barrier tissues by simple diffusion. This is characterised by a permeability of the solute that has been transported across the barrier. In such studies, the compound of interest with initial concentration will be added to the apical side of the cells in a defined volume (donor compartment) and the receiver compartment is on the basolateral side. The flux is measured by taking sample aliquots from the receiver compartment at given time points and new diluent of the same volume as the sample aliquots are added to the basolateral compartment. Therefore, Fick's Law can be simplified as [19,27]:

Eq. 2.11
$$P_{app} = \left(\frac{dQ}{dt}\right) \left(\frac{1}{AC_o}\right)$$

Where P ($\text{cm}\cdot\text{s}^{-1}$) is the permeability coefficient, C_o ($\text{g}\cdot\text{ml}^{-1}$) is the initial concentration of the test compounds in the donor compartment and $\frac{dQ}{dt}$ ($\text{g}\cdot\text{s}^{-1}$) is the steady-state flux and A (cm^2) is the surface area with cells that the test compounds were tested. Eq. 2.11 indicates that the flux is proportional to the concentration gradient and that the permeability is the constant that relates the flux and concentration gradient.

2.3 Microfluidics for cell culture

For almost more than a decade, the microfluidics technology has started to gain much interest in cell biology in applications such as cell sorting and trapping [28–30], cell counting [31,32], cell lysis and extraction [33,34], single cell analysis [35] and cell culture [36–39]. Many believe that the development in microfluidics will steadily expedite advancements in cell biology.

In developing microfluidic devices specifically for cell culture, there are certain aspects that must be considered, both in terms of the perfusion culture system design, cellular microenvironment, material choices and the implementation of fluidic control. Numerous reviews are available that described these different aspects of cell culture and microfluidics [1,5,40–43]. In the next section, some of the implications and considerations are discussed when designing and carrying out studies with the microfluidic cell culture system. Some microfluidic devices applicable for cell biology are also introduced.

2.3.1 Using microfluidic flow conditions to control microenvironments

‘Microenvironment’ can be defined as the immediate small-scale physical, chemical and biological conditions in the vicinity of a living cell where they can be sensed by the cell and have effects on the cell. The *in vivo* microenvironment is a complex environment, comprising of biochemical, biomechanical and bioelectrical signals derived from surrounding cells, extracellular matrix proteins and soluble factors, physical effects by fluid flows and temperature effects [1,40]. These components work in synergistic and antagonistic manner to regulate cellular behaviour. *In vivo* cells continuously sense all these processes and in turn will determine the cell fate.

Microfluidics has the ability to manipulate fluid flows in the submillimetre range, hence offering the possibilities of precise control of dynamic perfusion and extracellular chemicals necessary for individual cells to be cultured [44,45]. In an earlier report, Takayama et. al. exploited microfluidic principles to expose a single cell to asymmetric signals by placing it at the interface of fluid streams. Due to the laminar flow of the fluids, there was minimal mixing when two streams were flowed alongside each other. Because of this effect, part of the cell received soluble factors directly while the other part did not [46].

The development and regulation of functional tissues is dependent on the direct cell-cell communication between adjacent cells. Lee et. al. reported on developing a microfluidic device to selectively trap cell pairs and bring them in contact with each other for cell-cell interaction studies [47]. Song et. al. had reported on creating an artificial microfluidic vasculature to study the intravascular adhesion of metastatic breast cancer cells. By selectively manipulate cancer cells and endothelium over certain intersecting locations with different effector proteins, such as chemokines, serial tumour-endothelial cell interactions can be reproduced with different metastasis-supporting potential in a method similar to the way they occur physiologically [48].

Additionally, the shear stress within the confine microenvironment can also be exploited for investigations on the mechanical impact on cell adhesion [49] or cell responses [50–52].

All these instruments discussed exploit the unique properties of microfluidics to build devices and enable studies that are not possible with traditional cell culture systems.

2.3.2 Integrated analysis on microfluidic devices

In every cell-based study, a reliable method is required to extract information. One of the benefits of the microfluidic system is the possibility of integrating analytical methods to produce information from the cell models. Because real-time microscopic studies are important for cell-based studies, microfluidic devices fabricated for cellular studies are mostly transparent, allowing traditional microscopy techniques like phase contrast imaging, immunocytochemistry, fluorescent and histological stains.

In addition, microfluidic devices capable of analysing cell lysates such as on-chip PCR have also been fabricated and reported by Marcy and colleagues [53]. This integrated microfluidic system contained nine amplification units and allowed selection of individual cells, lysis, sample preparation and amplification.

Furthermore, other analytical tools such as biosensors can be incorporated into the microfluidic device for cell culture. These biosensors can provide rapid and sensitive analysis based on a small number and low reagent volumes. Ges et. al. [54] reported on embedding lactate sensing electrodes within a microfluidic cell to evaluate anaerobic respiration in living fibroblasts. Numerous groups have also demonstrated on embedding electrodes in microfluidic devices to monitor the barrier integrity of epithelial and endothelial cells [52,55–58], cell migration [59] and fluidic pressures [60].

2.3.3 Microfluidic cell culture systems and cell-based assay systems

In recent years, the advancements in microfabrication and microfluidic technologies have enabled the development of various lab-on-a-chip (LOC) devices with cell culturing functionalities. Such micro-scaled systems not only provide new approaches for solutions to address certain challenges in biomedical analysis, they also provide better avenues for studying cellular behaviours and functions, e.g. cells susceptibility to drugs, pathogens, toxins and transport studies in cells. For example, Biffi et. al. [61] reported on developing a microdevice that consisted of a dual channel configuration whereby the cell culture region was partially divided into two sub-compartments. This microchip allowed for cell culture and controlled drug simulation of the neuronal networks. Furthermore, with the ability to reduce experimental variability and the duration of experimentation, allowed for considerable improvements over macroscopic methods. Another report by Antia et al. [62] showed that by replicating the physiological flow conditions in a microfluidic device, allowed for studies of the cyto-adherence and rheological responses of infected red blood cells to host cell ligands.

Performing cell culture and assays with microfluidic devices permit the precise handling of liquid in the micro- and nanoliter ranges, and reduced amount of cells used. This is especially beneficial in studies where rare cells such as stem cells or primary cells are utilised. Additionally, microfluidic cell culture systems offer the possibility of supplying and transferring cell culture medium, buffers, and even air while simultaneously draining the waste products generated from cellular activities. Thus, offering some resemblance to the human circulatory system [63].

Over the past decade, researchers have developed microchips for the study of lungs [64,65], kidney [52,66], liver [67–69], gut [36–39,70–72], blood-brain barrier [55,57], neurons [73–75], cornea [76], bone marrow [77], skin and hair [78], heart [50], muscles [79,80] and many more. Such microfluidic devices used for culturing living cells in a continuously perfused, micro-sized chambers in order to model physiological functions of tissues and organs are also known as organs-on-a-chip [81].

Of particular interest to us is to develop a microchip for the study of human intestines. As mentioned earlier, conventional method of culturing Caco-2 cells to achieve a monolayer for transport or drug studies are often carried out on static porous inserts e.g. Transwell inserts and this entire process require 18-21 days. Although, the Caco-2 cells cultured in Transwell inserts are capable of differentiating to form a polarized epithelial cell monolayer, they fail to reproduce most of the differentiated organ-specific properties of a living intestine [37]. One of the major factor missing in such static culture systems is the presence of continuous fluid flow and stresses that are experienced in the normal human intestines. As such, these static cultures may not be the best *in vitro* models for studying cellular behaviours and functions, e.g., cells susceptibility to drugs, pathogens, toxins and transport studies in cells.

The mammalian intestine can be likened to a type of fluidic tube. Therefore, any form of evaluation of the cells under fluidic conditions is considered more favourable as compared to static experiments conducted with conventional cell culture inserts like the Transwell inserts [36,39,55,70,71]. Furthermore, in *in vivo* conditions, epithelial cells within a monolayer receive their nutrients from the basolateral side. This can be efficiently mimicked in the architecture of a microfluidic device that incorporates a porous membrane (Figure 1.1). The continuous flow of reagents in the top and bottom fluidic layers of the microchip will ensure a constant supply of nutrients and waste removal from the cells.

Kim et. al. [36] reported that with the combination of peristalsis motion and fluid flow in the microfluidic device, the Caco-2 cells displayed intestinal villi and crypt characteristics. The authors reported physiological growth of the Caco-2 monolayers reached up to several hundreds of microns in height, and the cells displayed increased expression of intestine-specific functions, including mucus production. The authors also reported on successfully co-culturing microbes on the Caco-2 monolayers for extended periods without compromising the viability of the cells. Another study by Ramadan et. al. [82] showed that a gastrointestinally motivated microfluidic system was capable of co-culturing Caco-2 cells and U937 cells. This system allowed monitoring of the response of immune cells to pro-inflammatory stimuli. Such a device can be utilise as an *in vitro* model to study the absorption of nutrients and immune-modulatory functions in the human gastrointestinal tract.

Devices that integrate other microfluidic capabilities have also been developed. Recently, Gao et. al. [38] reported on developing a human intestinal model in a microfluidic device with integrated micro solid-phase extraction (SPE) columns for drug permeability assays. The authors claimed that real-time detection of the permeated drugs was achieved by connecting the microfluidic chip to an electrospray ionization quadrupole time-of-flight mass spectrometry (ESI-QTOF-MS).

Most of the above mentioned devices were not designed to screen for multiple compounds at once. Microdevices having the capability to handle more than one input and assess the effects of multiple compounds on cells are valuable for numerous applications.

2.4 Device materials and fabrication

2.4.1 Material selection

One of the most important things that engineers and biologists need to consider is the material to be used for fabricating the microfluidic chip [83]. Since the emergence of microfluidics, microfluidic devices were initially based on non-polymeric materials like silicon or glass. They were fabricated by the well-established integrated circuit production technique – micromechanical systems technology (MEMS) - such as photolithography and e-beam lithography. Such methods of microchip production is costly and time consuming. Furthermore, the microchips produced with silicon are opaque which is incompatible for optical microscopy and the ability to have 3-dimensional (3D) structuring is also limited. Alternative materials such as thermoplastics -polymethylmethacrylate (PMMA), polycarbonate (PC), cyclic olefin copolymer (COC))- and elastomers - polydimethylsiloxane (PDMS)) - had gained much popularity as materials used for fabricating microfluidic device, as they are low-cost, disposable, transparent, biocompatible and easy to fabricate.

Traditionally, polystyrene (PS) is the preferred substrate that cells are cultured on statically [83]. However, microfabrication of PS into microdevices may be challenging. The challenges of fabricating PS microdevices can be attributed to the need to: (1) make molds capable of resisting high temperatures and pressures for hot embossing processes, (2) create inlet and outlet ports for world-to-chip interfacing, and (3) overcome bonding challenges [83]. Though much effort had been made to overcome the challenges for PS microfabrication, the most challenging is the bonding of PS materials or PS with another material.

Numerous teams have sought to use other materials i.e. thermoplastics, PDMS [36,39,55,57,70,73], paper [84], hydrogel [85] for cell culturing in microdevices.

Polymethylmethacrylate (PMMA). Low cost thermoplastic polymers (polymethylmethacrylate (PMMA), polycarbonate (PC), and cyclic olefin copolymer (COC)) have been widely used for fabricating microfluidic devices in high quantities in the industries. Most of these thermoplastics are readily available, have good optical and mechanical characteristics, are low in cost and can be easily handled. Also they had been shown to be biocompatible [86] and applicable for biological applications.

In this project, PMMA was the first material chosen to be used for fabricating the cell culture microchip. The reason being that PMMA is transparent, not costly, has low hydrophobicity, easy to fabricate and good biocompatibility [87,88]. However, due to challenges faced in developing a leak-free microfluidic cell culture device, another alternative material had to be considered and experimented. Fabrication technique of the PMMA microchips, as the first generation microchips are being described in Chapter 3 of the thesis. In Chapter 4, 5 and 6, micromilling of the microchip design onto PMMA pieces are also highlighted.

Thiol-ene. The thiol-ene reaction is an organic reaction between a thiol and an alkene, resulting in the formation of an alkyl sulfide. This reaction is also known as ‘click chemistry’, due to its high stereoselectivity, rapid rate, high yield and thermodynamic driving force. Thus, the thiol-ene ‘click’ chemistries have been widely used in biomaterials applications - drug delivery, tissue engineering and controlled cell culture [89–96].

Thiol-ene polymers are also well known for their uses in UV-curable adhesives (Norland optical adhesives [97]), dental restorations [91,94,95] and recently in microfluidic applications [98–108]. Thiol-ene is ‘cured’ via a step-growth photopolymerisation, hence forming homogenous, photopolymerisable crosslinked polymers [109]. The step-growth process of thiol-ene (Figure 2.4) is based on the radical addition of a thiol to an allyl functional group resulting in a final product that is a combination of the thiol and allyl functional groups. In the step-growth polymerization process, first a thiyl radical is generated as the S-H bond of the thiol group is cleaved during the initiation process. The thiyl radical will then propagate through an addition to the carbon of an allyl functionality. During this process, a hydrogen atom is abstracted from a thiol-group, hence forming a carbon centered radical and a thiyl radical. The propagation and chain transfer mechanisms are continued until termination occurs when a radical is coupled to a radical.

The step-growth photopolymerisation of thiol-ene can be summarised as shown below.

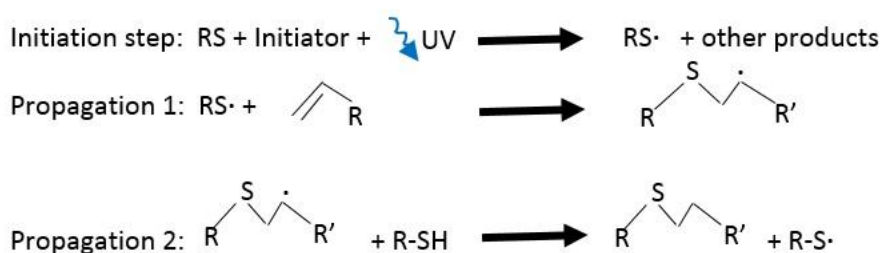


Figure 2.4. Step-growth photopolymerisation mechanism of thiol-ene

Hung et. al. had also reported on the biocompatibility of thiol-ene and its ability to create non-adhesive domains for cell culture experiments [107].

2.4.2 Fabrication technologies for microfluidics

Historically, some of the first microfluidic devices were developed using fabrication technology borrowed from microelectromechanical systems (MEMS) and semiconductor industry. Most of those devices fabricated involved etching of substrates such as silicon or glass and bonding of the different layers. Eventually, other fabrication techniques were developed and they include surface micromachining, deposition and patterning of

various thin film layers. Other fabrication techniques such as soft lithography, laser ablation, injection molding and hot embossing have also been widely employed in microfluidic chip fabrication.

The method for fabricating the microfluidic device is dependent on the material selected. In this project, three major polymeric materials were explored for fabricating of the cell culture microfluidic device. There are two primary methods for creating microfluidic structures in polymers: Direct writing technique and replication technique. The different methods for the device construction are described below.

2.4.2.1 Direct writing technique

Micromilling

Micromilling is a direct writing technique that creates microscale features via cutting tools to remove the bulk material for straight use for microchip devices or a mold for rapid generation of replication process [110–112]. The basic milling system (Figure 2.5a, b), consists of (1) a worktable for positioning the workpiece (secured with double-sided adhesive tape), (2) a cutting tool, and (3) an overhead spindle for securing and rotating the cutting tool. Micromilling is based on computer numerical controlled (CNC) machining as a classical computer aided design and manufacturing (CAD)/(CAM) process. The spindle on the machine has revolution speeds of up to 50.000 min^{-1} . This permits the mounted tool to drill, cut holes and microstructure directly on the substrate (mounted on the worktable) by removing the material in a predefined pattern. The profile and diameter of the cutting tool determine the shape and patterns on the substrate.

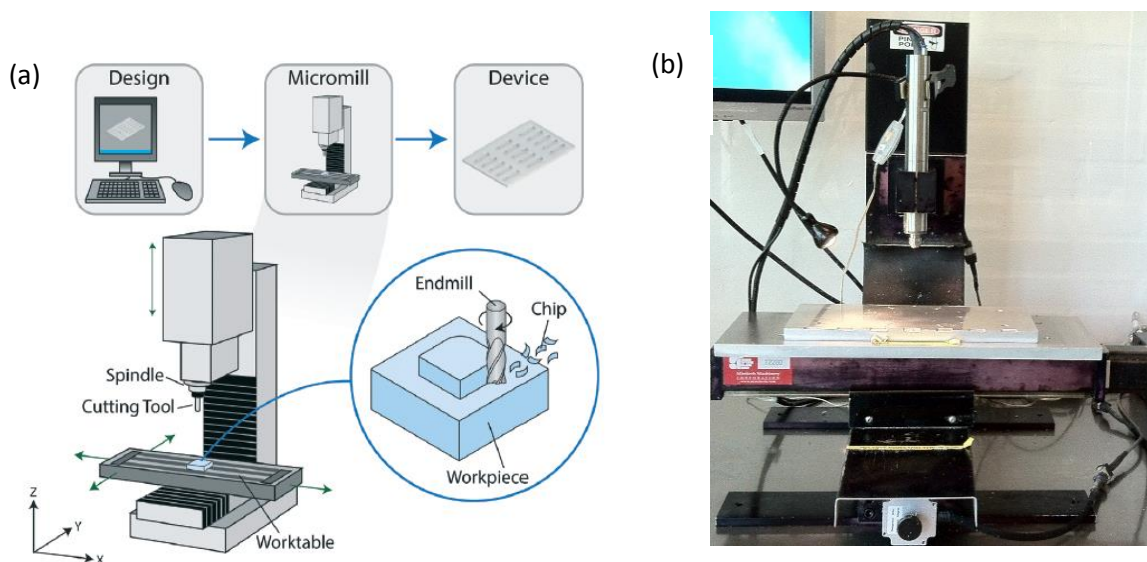


Figure 2.5 Micromilling. a) Schematic process of the micromilling procedure [112]. b) One of the micromilling machines (Mini-Mill/2, Minitech machinery Corp, GA, USA) at DTU Nanotech.

Components and structures produced by micromilling can be precisely aligned ($\approx 50 \mu\text{m}$), hence enabling reproducibility [113]. Surface roughness of micromilled piece is dependent on the cutting tool (e.g., tool features, profile, and wear), and the proper selection of cutting parameters (i.e., feeds and speeds), and adequate use of coolant. Typically, the achieve surface roughness of micromilled features without any post treatment is in the order of 100 - 250 nm [112,114,115]. Since the smallest milling tool available commercially is $5 \mu\text{m}$ [116,117], therefore, micromilling is not suitable for fabricating structures smaller than $5 \mu\text{m}$. However, typical microchannel dimensions for cell culture are in the range of 100 to 1000 μm . The need for larger channel culture regions is to enable enough cells to be cultured in the microchannels to permit population-based analyses [1]. Therefore, micromilling is a suitable technique for fabricating the microchip designs.

2.4.2.2 Replication technique

Casting of PDMS in micromilled PMMA molds. ‘Soft lithography’ technique is a direct pattern transfer technique. The term ‘soft’ refers to an elastomeric stamp with patterned relief structures on its surface. Elastomeric material such as PDMS has been used successfully. PDMS has a low interfacial free energy ($\approx 21.6 \text{ dyn/cm}$), hence preventing most polymeric molecules from adhering onto or reacting with its surface. PDMS is not hydroscopic, that is it does not swell with humidity, has good thermal stability and it is optically transparent ($\approx 300 \text{ nm}$) [118]. Due to the unique properties of PDMS, makes it suitable for the use as ‘stamps’. The “stamps” can be prepared by casting pre-polymers against masters (patterned by conventional lithographic techniques or micromilled), curing and peeling the “stamp” off. The brief procedure for soft lithography is illustrated in Figure 2.6. Soft lithography provides a convenient, effective and low-cost prototyping approach. Furthermore, the technique is easy to learn, straightforward to apply and accessible to a wide range of users.

PDMS also has a number of drawbacks such as swelling [118,119], shrinking [118,120–123] and elastic deformation [118,124]. Therefore, in designing a PDMS part, it is necessary to consider on the shrinking effect upon thermal curing. A number of organic solvents can swell PDMS as well [118,119]. Additionally, the aspect ratio of the designed structure can be limited by elastic deformation. When the aspect ratio is too high, this will lead to two parallel structures attracting to each other. Too low an aspect ratio will lead to sagging of non-contact regions as shown in Figure 2.6. The recommended aspect ratios for PDMS structures are between 0.2 and 2 [118].

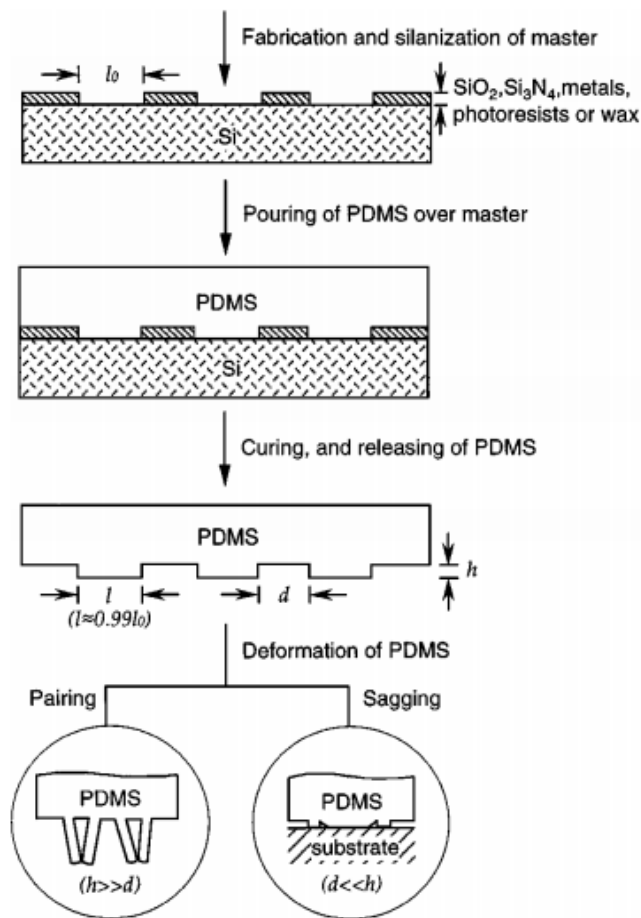


Figure 2.6 Soft lithography process [118]

In this thesis, the master molds for casting the PDMS molds were fabricated by micromilling on PMMA substrates. The fabricated PDMS molds were extensively used for replicating fluidic structures on thiol-ene pieces (the main component for fabricating the cell culture microchip) in chapters 4, 5 and 6.

Casting of thiol-ene using PDMS molds. Replica molding of the thiol-ene is easily carried out by using PDMS molds. Cabral et. al. were the first group to report on using thiol-ene based adhesives for microfluidic chip fabrication. However, the method they proposed required inconvenient photolithography process [108]. Thiol-ene polymers are well suited for microfluidic device applications. This class of polymers have high reaction rates, resistant to different types of solvents including aliphatic and aromatic, low shrinkage stresses and seals to glass, metals and PDMS substrates [107,108]. Therefore, deformation of thin geometries that are commonly found in microfluidic devices is limited.

Carlborg et. al. [99] recently reported on a novel use of off-stoichiometry thiol-ene (OSTE) polymer compositions – with either excess thiol or excess allyl in the thiol-ene mixtures – as another form of material

for rapid prototyping microfluidic devices. The authors reported that the morphology and mechanical properties of the cured OSTE are greatly affected with either excess thiol or excess allyl in the thiol-ene mixtures. The thiol moieties they experimented were pentaerythritol tetrakis-(3-mercaptopropionate) (tetra-thiol moieties) and trimethylpropane tris-(2-mercaptopropionate) (tri-thiol moieties) and the allyl component was tri-allyl-tri-azine (tri-allyl moieties; TTT).

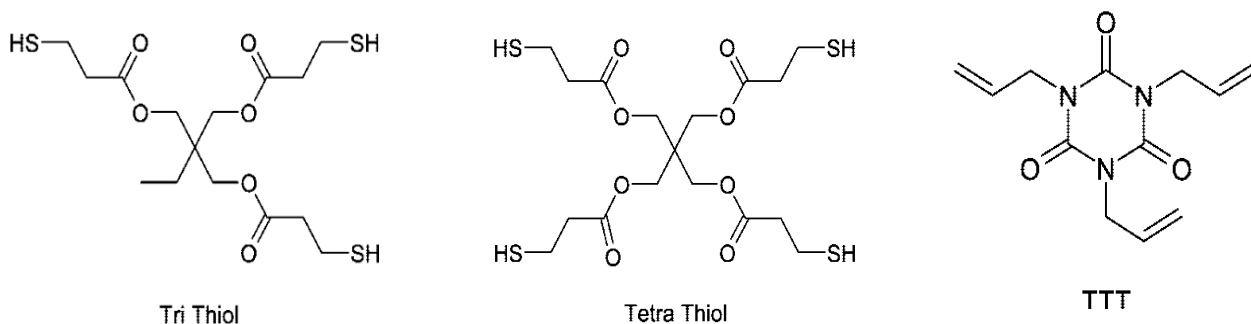


Figure 2.7 Chemical structures of thiols and allyl that will be used for creating the different thiol-ene layers in the microfluidic chip in this project

Master molds are made either of silicon by photolithography or on a thermoplastic like PMMA by micromilling or laser ablation. This PMMA master molds are used to mold the PDMS replica. The prepared thiol-ene mixture (thiol monomer is mixed with the allyl monomer) is poured onto the PDMS mold and cured by UV exposure. Thiol-ene mixtures can be cured between a few seconds to minutes. The duration for curing of thiol-ene mixtures is dependent on the presence of photoinitiator [100,109], strength of UV lamp [109], age and thickness of the PDMS molds. This method of microfluidic device production is rapid and reproducible, hence costs can be reduced and have fast turnaround. More of the microchip fabrication process will be discussed in detail in Chapter 4 of the thesis.

2.4.3 Bonding of polymers

One of the final steps in microchip fabrication is the bonding of the microchip layers. This section will only review and focus on some of the bonding techniques for PMMA and thiol-ene substrates. The bonding technique chosen is dependent on the type of material to be bonded. Tsao et. al. [125] gave a very detailed review on the different bonding methods of thermoplastic polymer in microfluidics. Bonding of microfluidic devices can be classified into either direct or indirect bonding. Indirect bonding involves the use of an adhesive layer to seal two substrates. Direct bonding methods involves mating two substrates of the same material together, without any additional materials added to the interface.

2.4.3.1 Indirect bonding

Adhesive bonding. Adhesive bonding is a very simple and cheap form of bonding two PMMA substrates. Adhesive in the form of glue, epoxy, sticky tapes, UV cured adhesives can be used for this purpose. However, for liquid adhesives, the challenge is to prevent clogging of the microchannels by the adhesives after the adhesives had set. Moreover, many of these adhesives leech chemicals that are not biocompatible. This had been reported by Stangegaard et. al. on observed cytotoxicity induced by epoxy resin and UV-curable glue[126].

Partially cured PDMS has also been investigated as an adhesive layer for bonding of PMMA substrates. Chow et. al. [57] reported that a thin (10 μm to 25 μm) PDMS intermediate layer was spin-coated onto a bare PMMA substrate before placing the other PMMA substrate with channel structure onto it. Toh et. al. [67] also reported a similar procedure, the only difference was that the PDMS mixture was spin coated onto an double-sided adhesive layer. This membrane was than sandwiched between two PMMA layers.

2.4.3.2 Direct bonding

Direct bonding applies to a variety of materials such as silicon, glasses, polymers, ceramics and metals. In direct bonding of thermoplastics, no addition of chemical aids are required. Local or global heating of the structures is required to achieve a thermal fusion between two polymeric surfaces [125]. One of the thermal fusion methods is to heat the entire surface of two substrates to a temperature near or above the glass temperature (T_g) of thermoplastic. Pressure is applied to the substrates to increase the mating contact forces. An advantage of direct thermal bonding of the substrates is the homogenous surface property. The downside of this method is the risk of collapsing microchannel structures [125,127]. Another thermal method is to apply local heating at the interface between two polymer pieces. This can be easily carried out by means of ultrasonics [128,129] or laser welding [125].

Solvent bonding. Generally, chlorocarbon solvents such as chloromethane, dichloromethane and chloroform are highly efficient organic solvents allowing PMMA materials to ‘glue’ together [130]. However, using these organic solvents often result in clogging of the microchannels as they have high PMMA solubility. Lin et. al. [131] reported on the use of low azeotropic solvent to bond PMMA microfluidic devices without causing the microchannels to clog or collapse.

Surface treatment and modification. There have been numerous reports describing the use of surface modification in order to change the thermal properties of the polymers. One of the methods was to expose the surface of the polymer to ultraviolet (UV) rays [132,133]. Doing this will degrade the surface of the polymer, hence lowering the T_g of the first few microns of the surface [133]. Hence, allowing the possibility of softening

the bonding interface and thermal fusion between the bonding surface can be achieved at temperatures below the T_g of the bulk material.

References

- [1] E.W.K. Young, D.J. Beebe, Fundamentals of microfluidic cell culture in controlled microenvironments, *Chem. Soc. Rev.* 39 (2010) 1036–1048.
- [2] N.-T. Nguyen, S.T. Wereley, Fundamentals and applications of microfluidics, 1st ed., Artech House, Boston, 2002.
- [3] J.P. Brody, P. Yager, R.E. Goldstein, R.H. Austin, Biotechnology at low Reynolds numbers, *Biophys. J.* 71 (1996) 3430–41.
- [4] T.M. Squires, S.R. Quake, Microfluidics: Fluid physics at the nanoliter scale, *Rev. Mod. Phys.* 77 (2005) 997–1026.
- [5] D.J. Beebe, G.A. Mensing, G.M. Walker, Physics and applications of microfluidics in biology, *Annu. Rev. Biomed. Eng.* 4 (2002) 261–86.
- [6] G. Velve-Casquillas, M. Le Berre, M. Piel, P.T. Tran, Microfluidic tools for cell biological research, *Nano Today*. 5 (2010) 28–47.
- [7] R.W. Fox, A.T. McDonald, P.J. Pritchard, Fundamentals of Fluid Mechanics, 6th Edition, John Wiley and Sons, 2003.
- [8] H. Bruus, Theoretical microfluidics vol. 1, Oxford University Press, New York, 2008.
- [9] M.E. Young, P.A. Carroad, R.L. Bell, Estimation of diffusion coefficients of proteins, *Biotechnol. Bioeng.* 22 (1980) 947–955.
- [10] P. Lee, T. Gaige, P. Hung, Microfluidic systems for live cell imaging, *Recent Adv. Cytom. Part A*, 5th ed., Elsevier Academic Press Inc., 2011.
- [11] R.G. Bacabac, T.H. Smit, S.C. Cowin, J.J.W.A. Van Loon, F.T.M. Nieuwstadt, R. Heethaar, et al., Dynamic shear stress in parallel-plate flow chambers, *J. Biomech.* 38 (2005) 159–67.
- [12] U.S.H. Svensson, R. Sandström, Ö. Carlborg, H. Lennernäs, M. Ashton, High in situ rat intestinal permeability is unaffected by multiple dosing and with no evidence of P-glycoprotein involvement, *Drug Metab. Dispos.* 27 (1999) 227–232.
- [13] B. Stewart, O.H. Chan, R.H. Lu, E.L. Reyner, H.L. Schmid, H.W. Hamilton, et al., Comparison of intestinal permeabilities determined in multiple in vitro and in situ models: Relationship to absorption in humans, *Pharm. Res.* 12 (1995) 693–699.

- [14] P. Zakeri-Milania, H. Valizadeha, H. Tajerzadehc, Y. Azarmia, Z. Islambolchilara, S. Barzegara, et al., Human intestinal permeability using intestinal perfusion in rat, *J. Pharm. Pharm. Sci.* 10 (2007) 368–379.
- [15] I. Lozoya-Agullo, I. González-Álvarez, M. González-Álvarez, M. Merino-Sanjuán, M. Bermejo, In Situ perfusion model in rat colon for drug absorption studies: comparison with small intestine and Caco-2 cell model, *J. Pharm. Sci.* 104 (2015) 3136–45.
- [16] A.M. Holmes, S. Creton, K. Chapman, Working in partnership to advance the 3Rs in toxicity testing, *Toxicology*. 267 (2010) 14–9.
- [17] A.R. Hilgers, R.A. Conradi, P.S. Burton, Caco-2 cell monolayers as a model for drug transport across the intestinal mucosa, *Pharm. Res.* 7 (1990) 902–910.
- [18] P. Stenberg, U. Norinder, K. Luthman, P. Artursson, Experimental and computational screening models for the prediction of intestinal drug absorption, *J. Med. Chem.* 44 (2001) 1927–1937.
- [19] I. Hubatsch, E.G.E. Ragnarsson, P. Artursson, Determination of drug permeability and prediction of drug absorption in Caco-2 monolayers, *Nat. Protoc.* 2 (2007) 2111–9.
- [20] S. Howell, A.J. Kenny, A.J. Turner, A survey of membrane peptidases in two human colonic cell lines Caco-2 and HT-29, *Biochem. J.* 284 (1992) 595–601.
- [21] M. Pinto, S. Robine-Leon, M.-D. Appay, M. Kedinger, N. Triadou, E. Dussaulx, et al., Enterocyte-like differentiation and polarization, *Biol. Cell.* 47 (1983) 323–330.
- [22] M.J. Briske-Anderson, J.W. Finley, S.M. Newman, The influence of culture time and passage number on the morphological and physiological development of Caco-2 cells, *Proc. Soc. Exp. Biol. Med.* 21 (1997) 248–257.
- [23] Y. Cai, C. Xu, P. Chen, J. Hu, R. Hu, M. Huang, et al., Development, validation, and application of a novel 7-day Caco-2 cell culture system, *J. Pharmacol. Toxicol. Methods.* 70 (2014) 175–81.
- [24] V. Gupta, N. Doshi, S. Mitragotri, Permeation of insulin, calcitonin and exenatide across Caco-2 monolayers: measurement using a rapid, 3-day system, *PLoS One.* 8 (2013) e57136.
- [25] K.A. Lentz, J. Hayashi, L.J. Lucisano, J.E. Polli, Development of a more rapid, reduced serum culture system for Caco-2 monolayers and application to the biopharmaceutics classification system, *Int. J. Pharm.* 200 (2000) 41–51.
- [26] B. Alberts, A. Johnson, J. Lewis, M. Raff, K. Roberts, P. Walter, *Molecular biology of the cell*, 4th ed., Garland Science, New York, 2002.
- [27] B. Brodin, B. Steffansen, C.U. Nielsen, *Passive diffusion of drug substances: The concepts of flux and permeability*, Mol. Biopharm., First edit, Royal Pharmaceutical Press, 2009: pp. 135–152.
- [28] C. Wyatt Shields IV, C.D. Reyes, G.P. López, Microfluidic cell sorting: a review of the advances in the separation of cells from debulking to rare cell isolation, *Lab Chip.* 15 (2015) 1230–1249.
- [29] C. Liberale, G. Cojoc, F. Bragheri, P. Minzioni, G. Perozziello, R. La Rocca, et al., Integrated microfluidic device for single-cell trapping and spectroscopy, *Sci. Rep.* 3 (2013) 1–6.

- [30] M.M. Wang, E. Tu, D.E. Raymond, J.M. Yang, H. Zhang, N. Hagen, et al., Microfluidic sorting of mammalian cells by optical force switching, *Nat. Biotechnol.* 23 (2005) 83–87.
- [31] S.M. Imaad, N. Lord, G. Kulsharova, G.L. Liu, Microparticle and cell counting with digital microfluidic compact disc using standard CD drive, *Lab Chip.* 11 (2011) 1448–1456.
- [32] U. Hassan, N.N. Watkins, C. Edwards, R. Bashir, Flow metering characterization within an electrical cell counting microfluidic device, *Lab Chip.* 14 (2014) 1469.
- [33] E.A. Schilling, A.E. Kamholz, P. Yager, Cell lysis and protein extraction in a microfluidic device with detection by a fluorogenic enzyme assay, *Anal. Chem.* 74 (2002) 1798–1804.
- [34] X. Chen, D.F. Cui, C.C. Liu, On-line cell lysis and DNA extraction on a microfluidic biochip fabricated by microelectromechanical system technology, *Electrophoresis.* 29 (2008) 1844–1851.
- [35] H. Yin, D. Marshall, Microfluidics for single cell analysis, *Curr. Opin. Biotechnol.* 23 (2012) 110–119.
- [36] H.J. Kim, D. Huh, G. Hamilton, D.E. Ingber, Human gut-on-a-chip inhabited by microbial flora that experiences intestinal peristalsis-like motions and flow, *Lab Chip.* 12 (2012) 2165–74.
- [37] H.J. Kim, D.E. Ingber, Gut-on-a-chip microenvironment induces human intestinal cells to undergo villus differentiation, *Integr. Biol.* 5 (2013) 1130–40.
- [38] D. Gao, H. Liu, J.-M. Lin, Y. Wang, Y. Jiang, Characterization of drug permeability in Caco-2 monolayers by mass spectrometry on a membrane-based microfluidic device, *Lab Chip.* 13 (2013) 978–85.
- [39] Y. Imura, Y. Asano, K. Sato, E. Yoshimura, A microfluidic system to evaluate intestinal absorption, *Anal. Sci. Int. J. Japan Soc. Anal. Chem.* 25 (2009) 1403–1407.
- [40] I. Meyvantsson, D.J. Beebe, Cell culture models in microfluidic systems, *Annu. Rev. Anal. Chem.* 1 (2008) 423–49.
- [41] L. Kim, Y.-C. Toh, J. Voldman, H. Yu, A practical guide to microfluidic perfusion culture of adherent mammalian cells, *Lab Chip.* 7 (2007) 681–94.
- [42] E.W.K. Young, C.A. Simmons, Macro- and microscale fluid flow systems for endothelial cell biology, *Lab Chip.* 10 (2010) 143–160.
- [43] G.M. Walker, H.C. Zeringue, D.J. Beebe, Microenvironment design considerations for cellular scale studies, *Lab Chip.* 4 (2004) 91–97.
- [44] J.Y. Park, S. Takayama, S.-H. Lee, Regulating microenvironmental stimuli for stem cells and cancer cells using microsystems, *Integr. Biol.* 2 (2010) 229–240.
- [45] L. Przybyla, J. Voldman, Probing embryonic stem cell autocrine and paracrine signaling using microfluidics, *Annu. Rev. Anal. Chem.* 5 (2012) 293–315.
- [46] S. Takayama, E. Ostuni, P. LeDuc, K. Naruse, D.E. Ingber, G.M. Whitesides, Two neuronal, nuclear-localized RNA binding proteins involved in synaptic transmission, *Chem. Biol.* 10 (2003) 123–130.

- [47] P.J. Lee, P.J. Hung, R. Shaw, L. Jan, L.P. Lee, Microfluidic application-specific integrated device for monitoring direct cell-cell communication via gap junctions between individual cell pairs, *Appl. Phys. Lett.* 86 (2005) 1–3.
- [48] J.W. Song, S.P. Cavnar, A.C. Walker, K.E. Luker, M. Gupta, Y.-C. Tung, et al., Microfluidic endothelium for studying the intravascular adhesion of metastatic breast cancer cells, *PLoS One.* 4 (2009) e5756.
- [49] D.P. Gaver, S.M. Kute, A theoretical model study of the influence of fluid stresses on a cell adhering to a microchannel wall, *Biophys. J.* 75 (1998) 721–33.
- [50] A. Agarwal, J.A. Goss, A. Cho, M.L. McCain, K.K. Parker, Microfluidic heart on a chip for higher throughput pharmacological studies., *Lab Chip.* 13 (2013) 3599–608.
- [51] K.M. Ainslie, J.S. Garanich, R.O. Dull, J.M. Tarbell, Vascular smooth muscle cell glycocalyx influences shear stress-mediated contractile response., *J. Appl. Physiol.* 98 (2005) 242–9.
- [52] N. Ferrell, R.R. Desai, A.J. Fleischman, S. Roy, H.D. Humes, W.H. Fissell, A microfluidic bioreactor with integrated transepithelial electrical resistance (TEER) measurement electrodes for evaluation of renal epithelial cells, *Biotechnol. Bioeng.* 107 (2010) 707–16.
- [53] Y. Marcy, C. Ouverney, E.M. Bik, T. Lösekann, N. Ivanova, H.G. Martin, et al., Dissecting biological “dark matter” with single-cell genetic analysis of rare and uncultivated TM7 microbes from the human mouth, *Proc. Natl. Acad. Sci. U. S. A.* 104 (2007) 11889–11894.
- [54] I.A. Ges, F. Baudenbacher, Enzyme-coated microelectrodes to monitor lactate production in a nanoliter microfluidic cell culture device, *Biosens. Bioelectron.* 26 (2010) 828–833.
- [55] R. Booth, H. Kim, Characterization of a microfluidic in vitro model of the blood-brain barrier (μ BBB), *Lab Chip.* 12 (2012) 1784–92.
- [56] N.J. Douville, Y.-C. Tung, R. Li, J.D. Wang, M.E.H. El-Sayed, S. Takayama, Fabrication of two-layered channel system with embedded electrodes to measure resistance across epithelial and endothelial barriers, *Anal. Chem.* 82 (2010) 2505–11.
- [57] L.M. Griep, F. Wolbers, B. de Wagenaar, P.M. ter Braak, B.B. Weksler, I.A. Romero, et al., BBB on chip: microfluidic platform to mechanically and biochemically modulate blood-brain barrier function, *Biomed. Microdevices.* 15 (2013) 145–50.
- [58] C. Huang, Q. Ramadan, J.B. Wacker, H.C. Tekin, C. Ruffert, G. Vergères, et al., Microfluidic chip for monitoring Ca²⁺ transport through a confluent layer of intestinal cells, *RSC Adv.* 4 (2014) 52887–52891.
- [59] T.A. Nguyen, T.-I. Yin, D. Reyes, G.A. Urban, Microfluidic Chip with integrated electrical cell-impedance sensing for monitoring single cancer cell migration in three-dimensional matrixes, *Anal. Chem.* 85 (2013) 11068–11076.
- [60] M.-C. Liu, H.-C. Shih, J.-G. Wu, T.-W. Weng, C.-Y. Wu, J.-C. Lu, et al., Electrofluidic pressure sensor embedded microfluidic device: a study of endothelial cells under hydrostatic pressure and shear stress combinations, *Lab Chip.* 13 (2013) 1743–53.

- [61] E. Biffi, F. Piraino, A. Pedrocchi, G.B. Fiore, G. Ferrigno, A. Redaelli, et al., A microfluidic platform for controlled biochemical stimulation of twin neuronal networks, *Biomicrofluidics*. 6 (2012) 1–10.
- [62] M. Antia, T. Herricks, P.K. Rathod, Microfluidic Modeling of Cell–Cell Interactions in Malaria Pathogenesis, *PLoS Pathog*. 3 (2007) e99.
- [63] J.H. Yeon, J. Park, Microfluidic cell culture systems for cellular analysis, *Biochip J*. 1 (2007) 17–27.
- [64] M. Ghaedi, J.J. Mendez, P.F. Bove, A. Sivarapatna, M.S.B. Raredon, L.E. Niklason, Alveolar epithelial differentiation of human induced pluripotent stem cells in a rotating bioreactor, *Biomaterials*. 35 (2014) 699–710.
- [65] D. Huh, D.C. Leslie, B.D. Matthews, J.P. Fraser, S. Jurek, G.A. Hamilton, et al., A human disease model of drug toxicity-induced pulmonary edema in a lung-on-a-chip microdevice, *Sci. Transl. Med*. 4 (2012) 159ra147.
- [66] K.-J. Jang, K.-Y. Suh, A multi-layer microfluidic device for efficient culture and analysis of renal tubular cells, *Lab Chip*. 10 (2010) 36–42.
- [67] P. Chao, T. Maguire, E. Novik, K.-C. Cheng, M.L. Yarmush, Evaluation of a microfluidic based cell culture platform with primary human hepatocytes for the prediction of hepatic clearance in human, *Biochem. Pharmacol*. 78 (2009) 625–632.
- [68] P.J. Lee, P.J. Hung, L.P. Lee, An artificial liver sinusoid with a microfluidic endothelial-like barrier for primary hepatocyte culture, *Biotechnol. Bioeng*. 97 (2007) 1340–1346.
- [69] B.J. Kane, M.J. Zinner, M.L. Yarmush, M. Toner, Liver-specific functional studies in a microfluidic array of primary mammalian hepatocytes, *Anal. Chem*. 78 (2006) 4291–8.
- [70] H. Kimura, T. Yamamoto, H. Sakai, Y. Sakai, T. Fujii, An integrated microfluidic system for long-term perfusion culture and on-line monitoring of intestinal tissue models, *Lab Chip*. 8 (2008) 741–6.
- [71] Y. Imura, K. Sato, E. Yoshimura, Micro total bioassay system for ingested substances: assessment of intestinal absorption, hepatic metabolism, and bioactivity, *Anal. Chem*. 82 (2010) 9983–9988.
- [72] G.J. Mahler, M.B. Esch, R.P. Glahn, M.L. Shuler, Characterization of a gastrointestinal tract microscale cell culture analog used to predict drug toxicity, *Biotechnol. Bioeng*. 104 (2009) 193–205.
- [73] K.A. Southam, A.E. King, C.A. Blizzard, G.H. McCormack, T.C. Dickson, Microfluidic primary culture model of the lower motor neuron-neuromuscular junction circuit, *J. Neurosci. Methods*. 218 (2013) 164–9.
- [74] J. Park, S. Kim, S.I. Park, Y. Choe, J. Li, A. Han, A microchip for quantitative analysis of CNS axon growth under localized biomolecular treatments, *J. Neurosci. Methods*. 221 (2014) 166–74.
- [75] T.F. Didar, K. Li, T. Veres, M. Tabrizian, Separation of rare oligodendrocyte progenitor cells from brain using a high-throughput multilayer thermoplastic-based microfluidic device, *Biomaterials*. 34 (2013) 5588–93.

- [76] C.M. Puleo, W.M. Ambrose, T. Takezawa, J. Elisseeff, T.-H. Wang, Integration and application of vitrified collagen in multilayered microfluidic devices for corneal microtissue culture, *Lab Chip*. 9 (2009) 3221–7.
- [77] Y. Torisawa, C.S. Spina, T. Mammoto, A. Mammoto, J.C. Weaver, T. Tat, et al., Bone marrow-on-a-chip replicates hematopoietic niche physiology in vitro, *Nat. Methods*. 11 (2014) 663–9.
- [78] B. Ataç, I. Wagner, R. Horland, R. Lauster, U. Marx, A.G. Tonevitsky, et al., Skin and hair on-a-chip: in vitro skin models versus ex vivo tissue maintenance with dynamic perfusion., *Lab Chip*. 13 (2013) 3555–61.
- [79] E.E. Zahavi, A. Ionescu, S. Gluska, T. Gradus, K. Ben-Yaakov, E. Perlson, A compartmentalized microfluidic neuromuscular co-culture system reveals spatial aspects of GDNF functions, *J. Cell Sci*. 128 (2015) 1241–52.
- [80] K. Shimizu, H. Araki, K. Sakata, W. Tonomura, M. Hashida, S. Konishi, Microfluidic devices for construction of contractile skeletal muscle microtissues, *J. Biosci. Bioeng*. 119 (2015) 212–6.
- [81] S.N. Bhatia, D.E. Ingber, Microfluidic organs-on-chips, *Nat. Biotechnol*. 32 (2014) 760–772.
- [82] Q. Ramadan, H. Jafarpoorchehab, C. Huang, P. Silacci, S. Carrara, G. Koklü, et al., NutriChip: nutrition analysis meets microfluidics, *Lab Chip*. 13 (2013) 196–203.
- [83] E. Berthier, E.W.K. Young, D. Beebe, Engineers are from PDMS-land, Biologists are from Polystyrenia., *Lab Chip*. 12 (2012) 1224–37.
- [84] R. Derda, S.K.Y. Tang, A. Laromaine, B. Mosadegh, E. Hong, M. Mwangi, et al., Multizone paper platform for 3D cell cultures, *PLoS One*. 6 (2011) e18940.
- [85] J.H. Sung, J. Yu, D. Luo, M.L. Shuler, J.C. March, Microscale 3-D hydrogel scaffold for biomimetic gastrointestinal (GI) tract model, *Lab Chip*. 11 (2011) 389–92.
- [86] P.M. van Midwoud, A. Janse, M.T. Merema, G.M.M. Groothuis, E. Verpoorte, Comparison of biocompatibility and adsorption properties of different plastics for advanced microfluidic cell and tissue culture models, *Anal. Chem*. 84 (2012) 3938–44.
- [87] P. Skafte-Pedersen, M. Hemmingsen, D. Sabourin, F.S. Blaga, H. Bruus, M. Dufva, A self-contained, programmable microfluidic cell culture system with real-time microscopy access, *Biomed. Microdevices*. 14 (2012) 385–99.
- [88] S. Petronis, M. Stangegaard, C.B.V. Christensen, M. Dufva, Transparent polymeric cell culture chip with integrated temperature control and uniform media perfusion, *Biotechniques*. 40 (2006) 368–376.
- [89] A.A. Aimetti, A.J. Machen, K.S. Anseth, Poly(ethylene glycol) hydrogels formed by thiol-ene photopolymerization for enzyme-responsive protein delivery, *Biomaterials*. 30 (2009) 6048–54.
- [90] S. Caldwell, D.W. Johnson, M.P. Didsbury, B.A. Murray, J.J. Wu, S.A. Przyborski, et al., Degradable emulsion-templated scaffolds for tissue engineering from thiol–ene photopolymerisation, *Soft Matter*. 8 (2012) 10344.

- [91] J.A. Carioscia, H. Lu, J.W. Stanbury, C.N. Bowman, Thiol-ene oligomers as dental restorative materials., *Dent. Mater.* 21 (2005) 1137–43.
- [92] H. Du, G. Zha, L. Gao, H. Wang, X. Li, Z. Shen, et al., Fully biodegradable antibacterial hydrogels via thiol–ene “click” chemistry, *Polym. Chem.* 5 (2014) 4002.
- [93] T.M. O’Shea, A.A. Aimetti, E. Kim, V. Yesilyurt, R. Langer, Synthesis and characterization of a library of in-situ curing, nonswelling ethoxylated polyol thiol-ene hydrogels for tailorable macromolecule delivery, *Adv. Mater.* 27 (2015) 65–72.
- [94] S. Reinelt, M. Tabatabai, N. Moszner, U.K. Fischer, A. Utterodt, H. Ritter, Synthesis and photopolymerization of thiol-modified triazine-based monomers and oligomers for the use in thiol-ene-based dental composites, *Macromol. Chem. Phys.* 215 (2014) 1415–1425.
- [95] H. Lu, J.A. Carioscia, J.W. Stansbury, C.N. Bowman, Investigations of step-growth thiol-ene polymerizations for novel dental restoratives, *Dent. Mater.* 21 (2005) 1129–36.
- [96] L.A. Sawicki, A.M. Kloxin, Design of thiol-ene photoclick hydrogels using facile techniques for cell culture applications, *Biomater. Sci.* 2 (2014) 1612–1626.
- [97] www.norlandprod.com, www.norlandprod.com.
- [98] C.O. Bounds, J. Upadhyay, N. Totaro, S. Thakuri, L. Garber, M. Vincent, et al., Fabrication and characterization of stable hydrophilic microfluidic devices prepared via the in situ tertiary-amine catalyzed Michael addition of multifunctional thiols to multifunctional acrylates, *Appl. Mater. Interfaces.* 5 (2013) 1643–1655.
- [99] C.F. Carlborg, T. Haraldsson, K. Öberg, M. Malkoch, W. van der Wijngaart, Beyond PDMS: off-stoichiometry thiol-ene (OSTE) based soft lithography for rapid prototyping of microfluidic devices., *Lab Chip.* 11 (2011) 3136–47.
- [100] C.F. Carlborg, A. Vastesson, Y. Liu, W. van der Wijngaart, M. Johansson, T. Haraldsson, Functional off-stoichiometry thiol-ene-epoxy thermosets featuring temporally controlled curing stages via an UV/UV dual cure process, *J. Polym. Sci. Part A Polym. Chem.* 52 (2014) 2604–2615.
- [101] N.A. Feidenhans’l, J.P. Lafleur, T.G. Jensen, J.P. Kutter, Surface functionalized thiol-ene waveguides for fluorescence biosensing in microfluidic devices, *Electrophoresis.* 35 (2013) 282–288.
- [102] J.P. Lafleur, R. Kwapiszewski, T.G. Jensen, J.P. Kutter, Rapid photochemical surface patterning of proteins in thiol-ene based microfluidic devices, *Analyst.* 138 (2013) 845–9.
- [103] M. Natali, S. Begolo, T. Carofiglio, G. Mistura, Rapid prototyping of multilayer thiolene microfluidic chips by photopolymerization and transfer lamination, *Lab Chip.* 8 (2008) 492–4.
- [104] F. Saharil, C.F. Carlborg, T. Haraldsson, W. van der Wijngaart, Biocompatible “click” wafer bonding for microfluidic devices, *Lab Chip.* 12 (2012) 3032–5.
- [105] T.M. Sikanen, J.P. Lafleur, M.-E. Moilanen, G. Zhuang, T.G. Jensen, J.P. Kutter, Fabrication and bonding of thiol-ene-based microfluidic devices, *J. Micromechanics Microengineering.* 23 (2013) 037002.

- [106] S. Silvestrini, D. Ferraro, T. Tóth, M. Pierno, T. Carofiglio, G. Mistura, et al., Tailoring the wetting properties of thiolene microfluidic materials, *Lab Chip*. 12 (2012) 4041–3.
- [107] L.-H. Hung, R. Lin, A.P. Lee, Rapid microfabrication of solvent-resistant biocompatible microfluidic devices, *Lab Chip*. 8 (2008) 983–7.
- [108] T. Cabral, K.L. Beers, E.J. Amis, Microfluidic platform for the generation of organic-phase, *Langmuir*. 21 (2005) 3629–3634.
- [109] C.E. Hoyle, T.Y. Lee, T. Roper, Thiol-enes: Chemistry of the past with promise for the future, *J. Polym. Sci. Part A Polym. Chem.* 42 (2004) 5301–5338.
- [110] A. Alrifaiy, O.A. Lindahl, K. Ramser, Polymer-based microfluidic devices for pharmacy, biology and tissue engineering, *Polymers (Basel)*. 4 (2012) 1349–1398.
- [111] H. Becker, C. Gärtner, Polymer microfabrication technologies for microfluidic systems, *Anal. Bioanal. Chem.* 390 (2008) 89–111.
- [112] D.J. Guckenberger, T.E. de Groot, A.M.-D. Wan, D.J. Beebe, E.W.K. Young, Micromilling: A method for ultra-rapid prototyping of plastic microfluidic devices, *Lab Chip*. 15 (2015) 2364–2378.
- [113] G. Perozziello, F. Bundgaard, O. Geschke, Fluidic interconnections for microfluidic systems: A new integrated fluidic interconnection allowing plug “n” play functionality, *Sensors Actuators B Chem.* 130 (2008) 947–953.
- [114] A.L. Jáuregui, H.R. Siller, C.A. Rodríguez, A. Elías-Zúñiga, Evaluation of micromechanical manufacturing processes for microfluidic devices, *Int. J. Adv. Manuf. Technol.* 48 (2009) 963–972.
- [115] G. Perozziello, G. Simone, P. Candeloro, F. Gentile, N. Malara, R. Larocca, et al., A fluidic motherboard for multiplexed simultaneous and modular detection in microfluidic systems for biological application, *Micro Nanosyst.* 2 (2010) 227–238.
- [116] Kyocera, Micro Industrial Cutting Tools, <http://www.kyoceramicrotools.com/>.
- [117] Performance Micro Tools, <http://www.pmtnow.com/>.
- [118] Y. Xia, G.M. Whitesides, Soft lithography, *Annu. Rev. Mater. Sci.* 28 (1998) 153–184.
- [119] J.N. Lee, C. Park, G.M. Whitesides, Solvent compatibility of poly(dimethylsiloxane)-based microfluidic devices, *Anal. Chem.* 75 (2003) 6544–54.
- [120] O.C. Jeong, S. Konishi, Controlling the size of replicable polydimethylsiloxane (PDMS) molds/stamps using a stepwise thermal shrinkage process, *Microelectron. Eng.* 88 (2011) 2286–2289.
- [121] J.S. Marcus, W.F. Anderson, S.R. Quake, Microfluidic single-cell mRNA isolation and analysis, *Anal. Chem.* 78 (2006) 3084–9.
- [122] C. Moraes, Y. Sun, C.A. Simmons, Solving the shrinkage-induced PDMS alignment registration issue in multilayer soft lithography, *J. Micromechanics Microengineering*. 19 (2009) 065015.

- [123] S.W. Lee, S.S. Lee, Shrinkage ratio of PDMS and its alignment method for the wafer level process, *Microsyst. Technol.* 14 (2007) 205–208.
- [124] H. Madadi, M. Mohammadi, J. Casals-Terré, R.C. López, A novel fabrication technique to minimize poly(dimethylsiloxane)-microchannels deformation under high-pressure operation, *Electrophoresis*. 34 (2013) 3126–32.
- [125] C.-W. Tsao, D.L. DeVoe, Bonding of thermoplastic polymer microfluidics, *Microfluid. Nanofluidics*. 6 (2008) 1–16.
- [126] M. Stangegaard, A biocompatible micro cell culture chamber (μ CCC) for culturing and on-line monitoring of Eukaryotic cells, Technical University of Denmark, 2005.
- [127] H. Becker, C. Gärtner, Polymer microfabrication methods for microfluidic analytical applications, *Electrophoresis*. 21 (2000) 12–26.
- [128] Y. Sun, Y. Luo, X. Wang, Micro energy director array in ultrasonic precise bonding for thermoplastic micro assembly, *J. Mater. Process. Technol.* 212 (2012) 1331–1337.
- [129] H.Y. Tan, W.K. Loke, N.-T. Nguyen, S.N. Tan, N.B. Tay, W. Wang, et al., Lab-on-a-chip for rapid electrochemical detection of nerve agent Sarin, *Biomed. Microdevices*. 16 (2014) 269–75.
- [130] H. Zhang, X. Liu, T. Li, X. Han, Miscible organic solvents soak bonding method use in a PMMA multilayer microfluidic device, *Micromachines*. 5 (2014) 1416–1428.
- [131] C.-H. Lin, C.-H. Chao, C.-W. Lan, Low azeotropic solvent for bonding of PMMA microfluidic devices, *Sensors Actuators B Chem.* 121 (2007) 698–705.
- [132] C.W. Tsao, L. Hromada, J. Liu, P. Kumar, D.L. DeVoe, Low temperature bonding of PMMA and COC microfluidic substrates using UV/ozone surface treatment, *Lab Chip*. 7 (2007) 499–505.
- [133] R. Truckenmiiller, P. Henzi, D. Herrmann, V. Saile, W.K. Schomburg, Bonding of polymer microstructures by UV irradiation and subsequent welding at low temperatures, *Microsyst. Technol.* 10 (2004) 372–374.

CHAPTER 3: First generation microchip – PMMA microchip

Certain criteria must be met in designing and fabricating a cell culture microchip for transport studies. The microchip should be easy to fabricate, thickness of chip should allow for confocal microscopy images to be taken, and the material chosen for the microchip should be biocompatible and negligible absorption of molecules. In this chapter, the first generation microchip designs and fabrication techniques are presented. The bulk of the substrate used for microchip fabrication was polymethylmethacrylate (PMMA).

In this chapter, designs and fabrication of bubble traps are also presented. Some preliminary cell culture studies were conducted with the PMMA microfluidic device. Finally, the major shortcomings of the PMMA microfluidic cell culture system are addressed.

3.1 Design considerations

As mentioned earlier in chapter 1, the aim of the project was to design and fabricate a microchip that support long term cell culture. In order to simulate the intestinal barrier functions, the microchamber where the cells are cultured will have an upper and lower fluidic layers separated by a porous membrane (as shown in figure 1.1c). The upper fluidic layer would represent the apical side of the cells and the bottom fluidic layer representing the basolateral side of the cells. For proper transport studies to be conducted across Caco-2 cells, the Caco-2 cells must form confluent monolayers in the cell culture system. Reported literature mentioned that Caco-2 cells cultured in traditional systems like the Transwell inserts required at least two weeks of culture before they were used for permeation studies [1–3]. Furthermore, as mentioned earlier in chapter 1, these Transwell inserts fail to provide dynamic physiological conditions e.g., fluidic flow, fluidic shear stresses.

Recently, there were reports on attempts in culturing Caco-2 cells in microfluidic devices [4,5]. At least 10 days of cell culture were required for the Caco-2 cells to form monolayers in microfluidic devices. Therefore, it was vital that the microfluidic device of interest be capable of supporting long term cell culture (> 10 days) under continuous perfusion. The microchip should also allow for real-time microscopic monitoring of the cells.

3.1.1 Material selection for fabrication of microchip

Many decisions are required in designing and fabricating a cell culture microfluidic device. One of the first most important decision required was the selection of materials used in fabricating the device. In this project, we were interested in fabricating a polymeric microfluidic device for cell culture.

When choosing the polymeric material for the microchip, it is important to note some of the important requirements of the chosen material:

- 1) Easy integration of the microchip with the chosen fluidic system
- 2) Uncomplicated assembly of the different fluidic layers
- 3) Keeping the porous membrane in place on the microfluidic chip
- 4) Low affinity in absorbing molecules
- 5) Compatible with online and real-time microscopy imaging

Keeping all these in mind, the material that was chosen for fabricating the microfluidic designs was polymethylmethacrylate (PMMA).

Moreover, PMMA is readily available, have good optical and mechanical characteristics, low cost [6,7], biocompatible for long term cell culture [8,9] and have low affinity to absorption of small molecules [10]. PMMA was chosen as it has low absorption of water and excellent optical transmissivity [7]. Additionally, PMMA can be easily fabricated by either laser ablation [11] or micromilling [8,12].

Due to the listed favourable properties of PMMA, PMMA was chosen as the material for fabricating the microfluidic devices in this chapter.

3.1.2 Microchip design

Conventional static culture systems like the Transwell systems are widely used for culturing epithelial cell-lines for studies on cell functions [13,14], drugs [1–3,15], cytotoxicity [16] etc. The Transwell system comprises of two chambers (Figure 2.2), whereby the insert contains a porous membrane on which the cells are cultured. This forms the apical side of the cells. The hanging porous insert is placed into a microwell, where the microwell is the lower compartment. The lower compartment is also known as the basolateral side of the cells.

To simulate the two-compartment design of the Transwell system, the microfluidic device was designed to contain two compartments separated by a porous membrane (Figure 3.1). Whereby the top fluidic layer contained fluidic channels that would allow the supply of nutrients to the cells cultured on a porous membrane. Subsequently, the bottom fluidic layer would also contain microchannels allowing the perfusion of cell culture. As mentioned earlier, the material chosen for fabricating the multi-layer microfluidic chip was PMMA. Clamped between the top and bottom fluidic layers, was a thin porous polyethylene terephthalate (PET) membrane for cell culture.

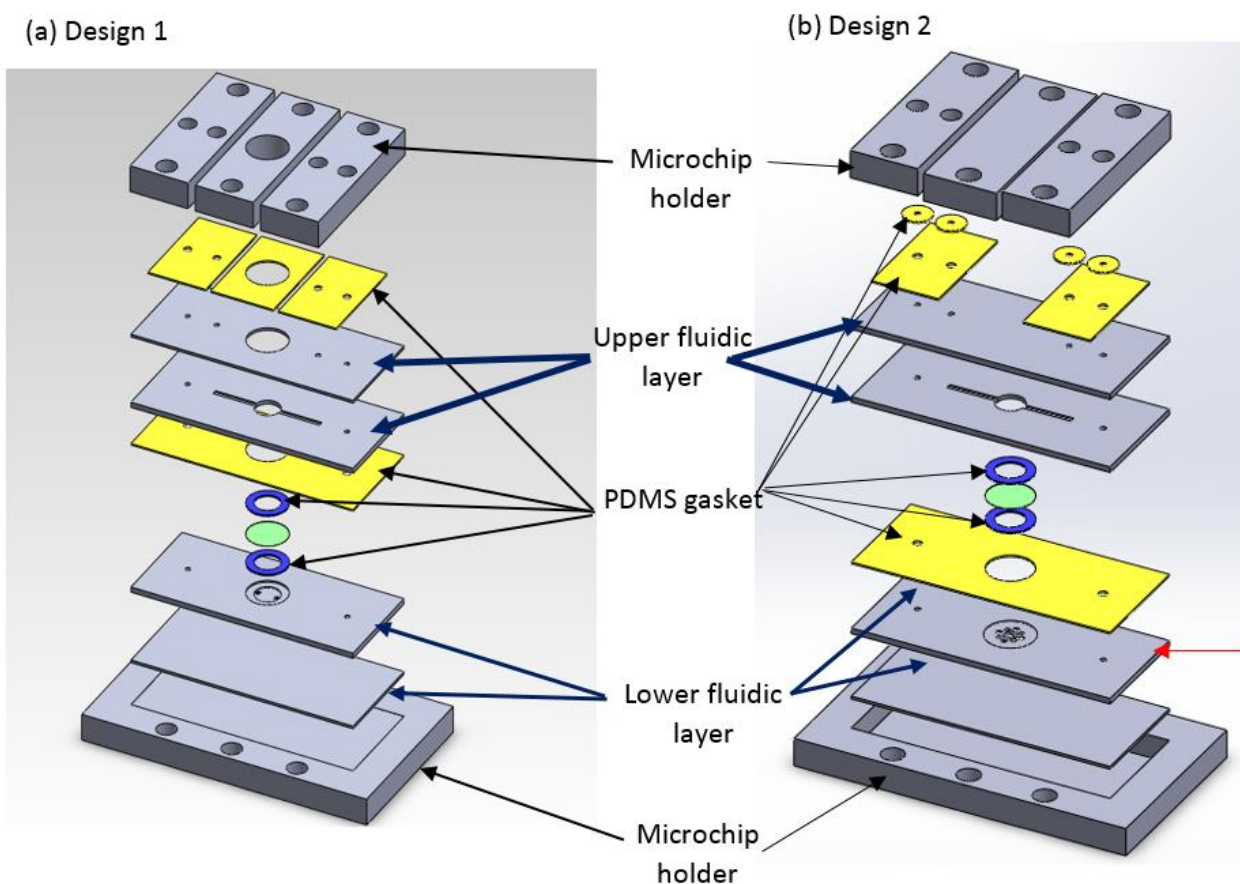


Figure 3.1 (a) Exploded view of all the different layers in the set-up. Two pieces of 0.5 mm thick PDMS pieces, acting as gaskets, were placed on and below the membrane. The fluidic channels in the top and bottom layers pass above and below the cell culture chamber. Each channel would be connected to its own inlet and outlet. A through hole was milled into the chip holder, to allow pipetting of the re-suspended cell mixture directly onto the membrane. (b) Exploded view of microchip design 2. The entire microchip for cell culture was sealed. Through holes would be drilled into the layer (red arrow) to allow even distribution of the fluid to the membrane.

The microchip design 1 consisted of straight microchannels (1 mm (width) x 0.5 mm (height)) and a circular microchamber (4 mm (diameter) x 0.5 mm (height)) (Figure 3.1a). This circular microchamber was the region where cells were cultured in the microfluidic chip.

The architecture of the microdevice was designed to: 1) Ensure fluid from the bottom layer could flow through the inlet hole, wet the porous membrane and exit from the outlet hole (Figure 3.2a). 2) Support the thin porous PET membrane (10 μm thickness), the microchamber must have a bottom plate (Figure 3.1). Figure 3.1a shows that two holes with diameter of 1 mm were present in the microchamber. One of the holes were positioned at the entrance of the inlet and the other hole was positioned at the outlet of the microchamber. Figure 3.2a shows the cross-sectional view of the microchamber for microchip design 1.

The microchamber in the top fluidic layer bore an open microchamber concept. Cell suspension could be loaded directly into the microchamber with a pipette or syringe. The open cavity of the microchamber could be sealed easily by force fitting a block of PDMS. This would ensure the entire system was enclosed during continuous perfusion of cell culture medium.

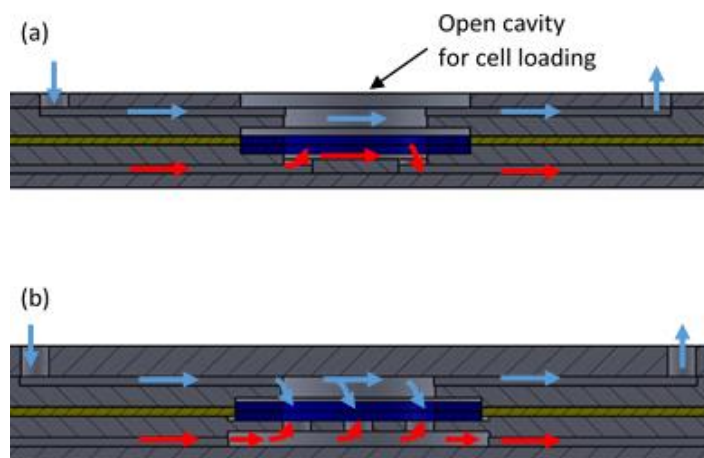


Figure 3.2 Cross-sectional view of the microchamber. (a) Design 1 bore an open cavity in the cell culture chamber; (b) Design 2. Microchamber is entirely enclosed. Blue arrows indicating fluid flow in the upper fluidic layer and red arrows indicating fluid flow in the lower fluidic layer.

Another design of the microfluidic device is shown in Figure 3.1b. The dimensions of the microchannels were similar to that of design 1. The circular microchamber in design 2 also bore the same dimensions as design 1. However, there were three major differences between design 2 and design 1. The first difference was that the microchamber in design 2 was entirely enclosed (Figure 3.1b). The second difference was the presence of additional circular PDMS gaskets between the microchip holder and the flat PDMS sheet for the inlet and outlet ports. The third difference was the presence of holes of two different diameters (diameter = 0.5 mm and diameter = 1 mm) on the bottom layer of the cell culture chamber (indicated by red arrow in Figure 3.1b). These holes were designed to allow a better distribution of fluid within the cell culture chamber. Figure 3.2b shows the schematic cross-sectional view of the microchamber from design 2.

3.1.3 Design of fluidic system

In designing microfluidic cell culture systems, there are several decisions to consider and one of them is the fluidic system for transporting the reagents from region to region. This is possible with the aid of pumps and valves. In this project, the pumps are required to continuously perfuse the reagents to the microchip for long duration. To serve this purpose, a syringe pump was chosen to perfuse the reagents into the microchip. The syringe pump was chosen as it allowed flow conditions to be changed readily and it also allowed the easy connection to the microfluidic chip via tubings and connectors (syringe needles). Furthermore, many available literature reported on carrying out successful cell culturing in microfluidic devices by using the syringe pump to perfuse reagents to the cells for at least 10 days [4,5,17,18]. Figure 3.3 illustrated the schematic fluidic system connected to the microfluidic chip.

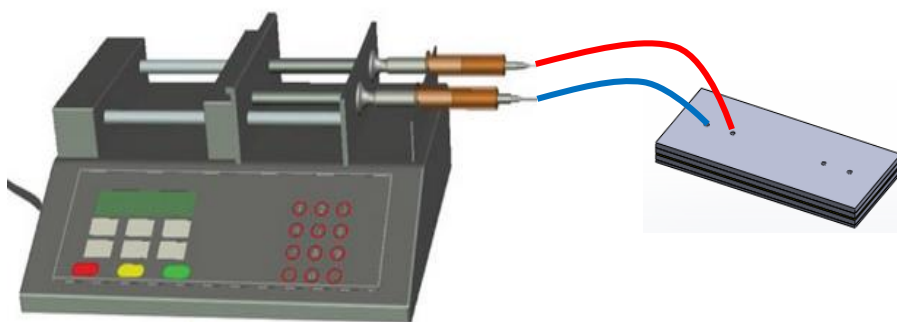


Figure 3.3 Schematic drawing of the fluidic set-up connected to the microchip.

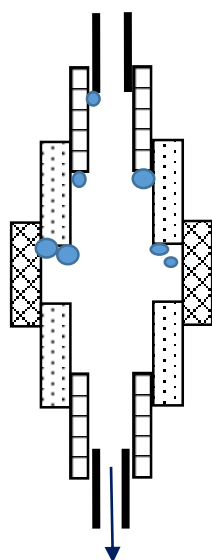
3.1.4 Bubble trap design considerations

Another important thing to consider while designing the microfluidic set-up is the occurrence of air bubbles. Air bubbles are well known to be detrimental to cell cultures. They can rupture cell membranes when they burst [19]. The presence of bubbles can block the entire microchannel or impede fluid flow and this may disturb the cell culture microenvironments [19]. The appearance of bubbles in the microchannels could be due to the temperature changes, channel geometry, flow focusing or configuration of connectors, adaptors and valves that are connected to the microfluidic chip. Numerous available literature discussed on the different bubble traps designs or materials to eliminate bubbles [5,20–24]. These bubble traps could be implemented on the microchip or off microchip.

As mentioned earlier, the material chosen to fabricate the microfluidic chip was PMMA. PMMA is known to have poor gas permeability [25]. Therefore, to remove any bubbles that might form in the tubings before

entering the microfluidic device, bubble traps must be positioned between the pumps and the microfluidic chip. In this chapter, two different bubble trap designs were considered, fabricated and experimented.

Bubble trap design 1. Imura et. al. [5] reported on using silicon tubings with different inner diameters, forced fit in series. The bubble trap made from a series of tubings was to create a gradual decrease in the volume of the tubings while increasing the resistance of the tubings. In order for the bubble trap to work effectively, this bubble trap must be held up vertically above the inlet of the microfluidic chip. Air bubbles have a lower density as compared to liquid, therefore the air bubbles would rise and be trapped at the protruding edges formed by the tubes. This phenomenon coupled with the increased resistance in the tubings would prevent air bubbles from being pumped into the microchip.



Flow to microchip

Figure 3.4 Cross-sectional view of the bubble trap made from silicon tubes of different inner diameters connected in series. Circles represent the bubbles that would be trapped in the regions of the tubings.

Bubble trap design 2. In situations where a huge bubble enters the bubble trap, bubble trap design 1 will not be capable of trapping the bubble effectively. This happens because bubble trap 1 has limited volume for trapping bubbles. To resolve this issue, a second bubble trap with a larger capacity to trap bubbles was designed. This bubble trap design 2 was designed using 1.5 ml Eppendorf tubes as the footprint. The bubble trap comprised of two fluidic tubes (Figure 3.5). Whereby, one of the tubing would be connected to the syringe pump and the other tubing would be connected to the microchip. The tubing connected to the syringe would be inserted to the bottom of the tube while the tube connecting to the microchip was to be inserted to mid-way

of the Eppendorf tube (Figure 3.5). Should any air enter the Eppendorf tube, it would rise to the surface of the reagent in the Eppendorf tube. Since the tube connected to the microchip was inserted to half-way in the reagent, the fluid entering this tube would therefore be bubble free. Figure 3.5 shows the schematics of bubble trap fashioned out of the Eppendorf tube. The tubing from the bubble trap to the microchip should be as short as possible. This was to prevent any further formation of bubbles in the media.

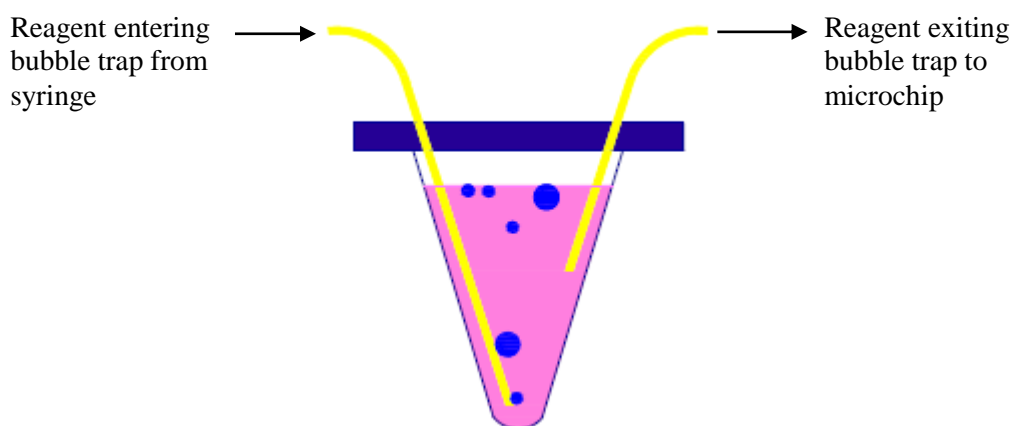


Figure 3.5 Schematic cross-sectional view of the Eppendorf tube bubble trap. Blue circles indicating air bubbles.

3.2 Materials and methods

3.2.1 Fabrication and assembling of the microfluidic devices

Fabrication of PMMA microchip layers. The two different designs of the microchips shown in the earlier section, were drawn using a CAD software, Autocad 2012. The microchip designs were all fabricated using CNC micromilling (Mini-Mil/3, Minitech Machinery Corporation, GA, USA) on 1 mm thick PMMA sheets. The microchip holders (Figure 3.1) were micromilled on 5 mm thick PMMA blocks.

The fabrication process for both microfluidic chip designs were similar. The micromilled 1mm thick PMMA layers were cleaned with MilliQ water and dried. The cleaned surfaces of the PMMA pieces were exposed to UV light (Dymax 5000-EC Series UV curing flood lamp, Dymax Corp., Torrington, CT, USA, $\sim 40 \text{ mW cm}^{-2}$ at 365 nm) for 60 s. Following UV-exposure, the prepared PMMA pieces were sandwiched between two clean glass slides. The ensemble was placed in a laboratory press (PW 10 H, P/O/Weber, Germany) and thermally bonded at 85 °C for 90 min under a compression pressure of 8 kN. A circular porous polyethylene terephthalate (PET; Millipore, Denmark) membrane of 4.5 mm in diameter was cut out from Transwell inserts. The 10 μm thick porous membrane bore pore sizes of 0.4 μm . The cut-out porous membrane was sandwiched between the

upper and lower fluidic layers of the microfluidic chip (Figure 3.1). Circular PDMS, acting as gaskets (thickness 0.2 mm, Figure 3.1), sandwiched the porous membrane in the microchamber.

Fabrication of PDMS gaskets. PDMS (DowCorning, Germany) was prepared by mixing in the ratio of 1:10 (pre-polymer:curing agent), degassed under vacuum and poured onto a glass petri dish (90 mm (diameter) x 12 mm (height)). The PDMS mixture was cured at 75 °C overnight in an oven. The circular PDMS gaskets (external diameter 4 mm and internal diameter of 3 mm) for clamping the porous membrane (blue circles in Figure 3.1) were cut out using biopsy punchers (Ted Pella, USA). The PDMS sheets that were placed between the microchip holder and microchip and between the top and lower fluidic layers (yellow PDMS sheet in Figure 3.1) were cut out using a scalpel. The holes on the PDMS sheet were punched out using biopsy punchers.

For microchip design 1 (Figure 3.1), a thick PDMS block (thickness of 10 mm) was required to force-fit into the microchamber cavity on the microchip holder (Figure 3.6a). This thick PDMS block was prepared as the procedure mentioned above. The circular PDMS block was punched out using a biopsy punch with a diameter of 4.5 mm.

Assembling of microchip layers with the microchip holder. Once the different layers of the microchip and PDMS gaskets were aligned and assembled, they were clamped between the microchip holder (Figure 3.1). 6 screws and bolts were used to hold the layers together in place (Figure 3.6).

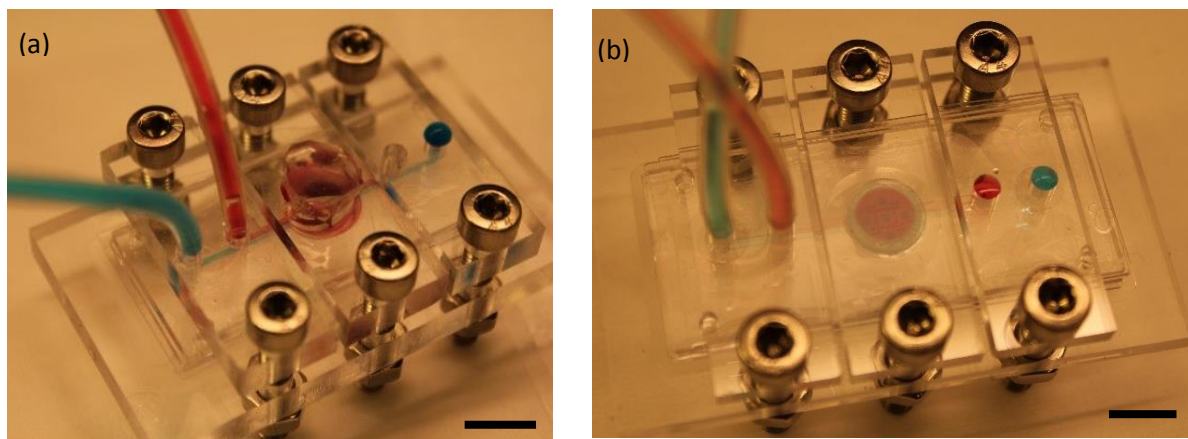


Figure 3.6 Images of the assembled microchip devices. (a) Assembled microchip_design 1 and microchip holder. A thick block of PDMS was force fit into the microchamber cavity on the microchip holder. (b) Assembled set-up of microchip_design 2. In both set-ups, red and blue dyes were flowed into the fabricated microchip. (Scale = 5 mm)

For the microchip design 1, after assembling the microchip with the microchip holder, a thick block of PDMS was force-fit into the cavity of the microchamber. This thick block of PDMS would ensure the microfluidic system was enclosed to prevent leaking during perfusion of fluids through the microchannels.

Silicon tubings (inner diameter = 1.5 mm; external diameter = 3.5 mm) (Oledich, Denmark) were forced fit to the inlet and outlet ports on the microchip holder to allow the perfusion of fluids to and from the microchip (Figure 3.6a, b).

3.2.2 Fabrication of bubble traps

3.2.2.1 Bubble trap design 1

The first bubble trap design was fabricated by connecting four pieces of silicon tubings (Oledich, Denmark) with different inner diameters. The different tubing sizes used to make the bubble trap are 1) inner diameter = 0.8 mm, 2) inner diameter = 1 mm, 3) inner diameter = 2 mm, 4) inner diameter = 3 mm as shown in Figure 3.7a. The length of each silicon tubing was 2 cm except for the tubings that were connected to the pump and microfluidic chip. The tubings were connected by force fitting into each other. To ensure the tubings were immobilized in place, epoxy (Loctite, USA) was applied at the fitting of two tubings.

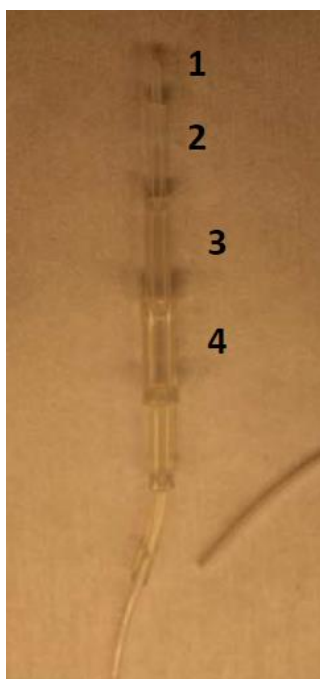


Figure 3.7 Bubble trap made from connecting different tubing sizes. (A) The different tubing sizes used are 1) inner diameter = 0.8 mm, 2) inner diameter = 1 mm, 3) inner diameter = 2 mm, 4) inner diameter = 3mm.

3.2.2.2 Bubble trap design 2

The second bubble trap was made from 1.5 Eppendorf tube (Eppendorf, Denmark). Holes of diameter 2.7 mm were drilled into the caps of the Eppendorf tubes. Two silicon tubings (external $\text{\O} = 3$ mm, inner $\text{\O} = 1$ mm) (Bola, Denmark) were force-fit into the holes. The silicon tubings were immobilized in position by applying epoxy (Loctite, USA) at the point where the tubing was forced fitted to the Eppendorf cap. Two Teflon tubing (inner $\text{\O} = 0.8$ mm, external $\text{\O} = 1.6$ mm) were forced fit into the silicon tubings. The two Teflon tubings were inserted to different depths in the Eppendorf tube. The Teflon tubing that would be connected to the syringe pump, was inserted to the bottom of the Eppendorf tube (indicated by black arrow in Figure 3.8). Another Teflon tubing (inner $\text{\O} = 0.2$ mm, external $\text{\O} = 1.6$ mm) was fitted to the other Silicone tubing. One end of this tubing was connected to the inlet of the microchip and the other was inserted to half-way in the Eppendorf tube (indicated by blue arrow in Figure 3.8). Figure 3.8 shows the assembled bubble trap design 2.

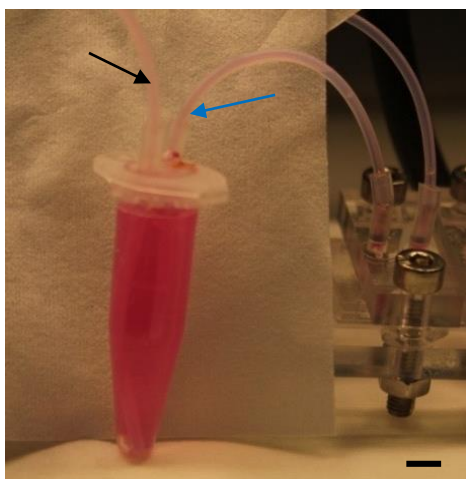


Figure 3.8 Close up view of the Eppendorf bubble trap. The tubing indicated by the black arrow was inserted to the bottom of the Eppendorf tube. This tube was connected to the syringe pump. The tubing indicated by the blue arrow was connected to the microchip. This tubing was inserted to midway of the Eppendorf tube. (Scale bar = 5 mm)

3.2.3 Flow studies with the microfluidic devices and bubble traps

Two different colour dyes were prepared to investigate whether the two microfluidic designs were leak-free. The two different colour dyes, red and blue dyes (Dr. Oetker, Denmark) were prepared by diluting 100 μl of the food dye in 20 ml of de-ionised (DI) water. Before conducting the flow studies, the prepared dye solutions were filtered using syringe filters (pore size 0.2 μm , VWR, Denmark). Subsequently, the filtered dye solutions were pumped into the respective fluidic layers at a flow rate of 5 $\mu\text{l}/\text{min}$ by a syringe pump (Harvard syringe pump, USA). The flow characterization studies were conducted in room temperature.

3.2.4 Cell culturing with PMMA microchip design 2

Sterilisation of microfluidic system for cell culture. Sterility is non-negotiable criteria in cell culture systems. Before cell culture, the microchip and tubings were sterilized by flowing 0.5 M sodium hydroxide (NaOH) at a flow rate of 5 $\mu\text{l}/\text{ml}$ for 1 hr. Subsequently, the entire system was rinsed with sterile water for at least 1 hr at a flow rate of 5 $\mu\text{l}/\text{ml}$. Following that, cell culture medium, Dulbecco's Modified Eagle's medium (DMEM, Sigma, Denmark) was pumped into the microfluidic device for at least 1 hr at a flow rate of 5 $\mu\text{l}/\text{min}$.

Preparation of HeLa cell suspension for microfluidic device. HeLa cells were chosen for the preliminary testing as HeLa cells are known for its rapid proliferation and robustness. HeLa cells (Passage 40) cultured in normal cell culture flask were harvested with trypsin/ETDA solution (Gibco, Denmark). The cell suspension was then centrifuged at 125 $\times g$ for 5 min. Extra care was taken to remove the supernatant, before adding fresh cell culture medium (Dulbecco's Modified Eagle's medium (DMEM); Sigma, Denmark) supplemented with 10% (v/v) heat-inactivated fetal bovine serum (FBS; Sigma, Denmark) and 1% (v/v) penicillin-streptomycin (P/S; Gibco, Denmark) to the cell pellet. The HeLa cells were suspended, counted with a cell counter (Moxi-Z; Orflo, Denmark) and prepared to a concentration of 1.5×10^5 cells/ml.

Seeding of HeLa cells in microfluidic device. HeLa cells were seeded onto the porous membrane in the microfluidic device by gently pushing the prepared HeLa cell suspension into the upper fluidic channel with a sterile syringe (1 ml Luer Lock syringe; BD, Denmark) coupled to a sterile needle (21 g, 0.8 mm; BD, Denmark). Once the cells were loaded in the microfluidic device, the inlet tubing was carefully disconnected from the syringe and re-connected to the syringe containing cell culture medium. The syringe containing cell culture medium was mounted onto the syringe pump.

Only the microfluidic system was placed in an incubator at 37 $^{\circ}\text{C}$, 5 % CO_2 . The syringes containing cell culture medium and the syringe pump were placed outside of the incubator. Subsequently, cell culture medium was perfused into the upper and lower layers of the microfluidic chip for 48 hr at a flow rate of 0.5 $\mu\text{l}/\text{min}$.

Fluorescent cell imaging. As described in the fabrication process of the microchip, the membrane was clamped between the top and bottom fluidic layers (Figure 3.1). The porous membrane could be easily removed from the microfluidic chip by removing the screws and bolts that held the layers together. Once the membrane was removed from the microfluidic layers, it was placed into a microwell in a 6 well microtiter plate. First, the membrane was rinsed with phosphate buffered saline (PBS; Sigma, Denmark) for three times. Next, the cells were fixed with 4 % formaldehyde (Sigma, Denmark) for 10 min. The fixed cells were rinsed with PBS followed by permeabilising them with 0.1 % Triton-X (Sigma, Denmark) for another 10 min. Subsequently, the cells were rinsed with PBS. Nuclear stain, To-Pro (Invitrogen, Denmark) prepared by diluting with PBS in the ratio of 1:300, was added to the cells to stain the nucleus of the HeLa cells. The cells were incubated with TO-PRO for 15 min in room temperature. Next, the cells were rinsed three times with PBS before being

mounted onto a glass slide. Mounting media (Vectashield; VWR, Denmark) was added onto the stained cells. Lastly, a glass cover slip was placed over the stained cells and incubated overnight at 4°C in a fridge. The fluorescently stained cells were imaged with a confocal microscope (Leica, Germany) at an excitation wavelength of 642 and emission wavelength of 661 nm.

3.3 Results and discussion

3.3.1 Flow characterization in microfluidic chip

Colour dyes used for flow characterization studies. The layers that made up the microchip were of different materials. Therefore, it was important to investigate on the leakage-proof packaging of the microchip layers. Two different colour dyes, red and blue dyes were perfused into the top and bottom layer respectively. The use of different colour dyes for the different layers of the microchip allowed for better observation of the flow through the microchannels and microchamber.

Once the dyes were infused to both the top and bottom layers of the microfluidic chips, for design 1 the fluids were observed to leak between the layers (black arrows in Figure 3.9). Leaking was observed at:

1. The interface between the chip holder and the top layer microfluidic chip.
2. At the interface between the microchamber and the top fluidic layer.

The presence of leaking clearly signified that the flat pieces of PDMS gaskets were not able to seal the layers tightly. Therefore, this particular design was not ideal for the final application of cell culture.

Due to the presence of holes in the bottom layer of the cell culture chamber and porous membrane, one would expect the dyes to mix in the microchamber. However, there was almost no mixing of the dyes in the microchamber as the distinct red colour of the dye was observed exiting from the upper layer and blue dye was exiting from the bottom.

Unlike the microfluidic chip design 1, there were no observable leaking between the layers at the inlet and outlet ports in microfluidic chip design 2 (Figure 3.9b). It was believed that the additional circular PDMS gaskets placed between the chip holder and the flat PDMS sheets at the inlet and outlet ports (Red arrows in Figure 3.9b), provided the required seal to prevent leaking. There were also no other observable leaking between the layers in microchip design 2.

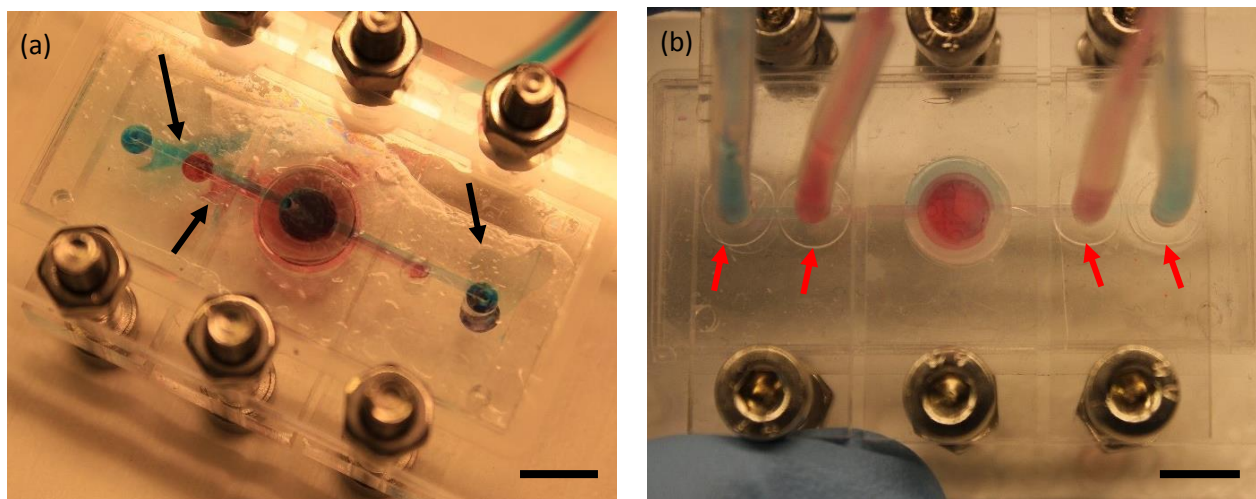


Figure 3.9 Pictures of microfluidic chips after being infused with colour dyes for 1 hour. (a) Underside of microfluidic chip design 1. Black arrows indicating leaking between the layers; (b) Top view of microfluidic chip design 2. Red arrows indicating the additional circular PDMS gaskets. (Scale = 5mm)

The reagents were also evenly distributed throughout the microchamber in design 2 (Figure 3.9b). Similar to design 1, the dyes in design 2 also did not mix in the microchamber. Red dye was exiting from the outlet of the top layer and blue dye was exiting from the bottom of the fluidic layer. We believe the absence of mixing of the food dyes in the microchamber could be due to two reasons. The first reason is the presence of high flow velocities within the micorchamber. Referring to eq. 2.8: $Pe = ul/D$, where u is velocity, l is the length of microchannel and D is the diffusivity of the particle, the mass transport along the length of the microchannel in the microfluidic device was dependent on convective transport. While across the cross-section of the microchamber, molecules were transported by diffusion. This form of transportation and mixing (by means of diffusion) of molecules, is slow. When the flow rate of the reagents was sufficiently high, this would result in higher fluid velocities within the microchannels. Therefore, the red and blue dye molecules might not have sufficient time to mix before flushing them away from the microchamber.

The second reason was the high dilution rate of the mixed dye molecules. Perhaps there were some form of mixing between the two different dyes. However, the continuous perfusion of reagents might have diluted the reacted dye solutions. Moreover, the flow study results in figure 3.9 were observed visually. There was no proper quantification of the reagents at the outlets. Hence, visual observation was not able to accurately quantify the outcome of the reacted dyes.

For future optimization and cell culture studies in this chapter, microchip design 2 was chosen over design 1.

Using cell culture medium for flow characterization studies. Eventually cell culture medium is the fluid that is perfused through the microfluidic device during cell culture. Therefore, it was important to investigate the flow characteristics and any formation of bubbles using cell culture medium. A similar flow characterization study to the above-mentioned colour dye flow study was conducted. During the 2 hr of continuous perfusion of cell culture medium, there were no observable leakage from the microfluidic device.

During the first hour of continuous perfusion of the cell culture medium, there were no observable air bubbles. However, after 2 hr of continuous perfusion of cell culture medium, a couple of small air bubbles appeared in the microchamber (Figure 3.10).

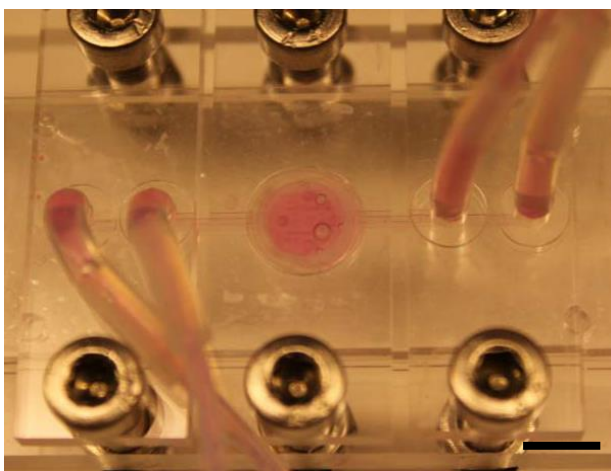


Figure 3.10 Cell culture medium was continuously perfused into microchip design 2 for 2 hr. Air bubbles were trapped inside the microchamber. (Scale bar = 5 mm)

3.3.2 Bubble trap characterization

The two different designs of bubble traps were tested to determine which was the better design to trap bubbles. To investigate the feasibility of the different bubble trap designs, the bubble traps were connected to the microfluidic chip design 2.

3.3.2.1 Bubble trap design 1

The bubble trap made from a series of tubings was to create a gradual decrease in the volume of the tubings while increasing the resistance of the tubings. This will allow the bubbles to be retained in the larger tubings before entering the microchip. To investigate the feasibility of the bubble trap, one end of the bubble trap was connected to the syringe pump while the other end was connected to the microchip.

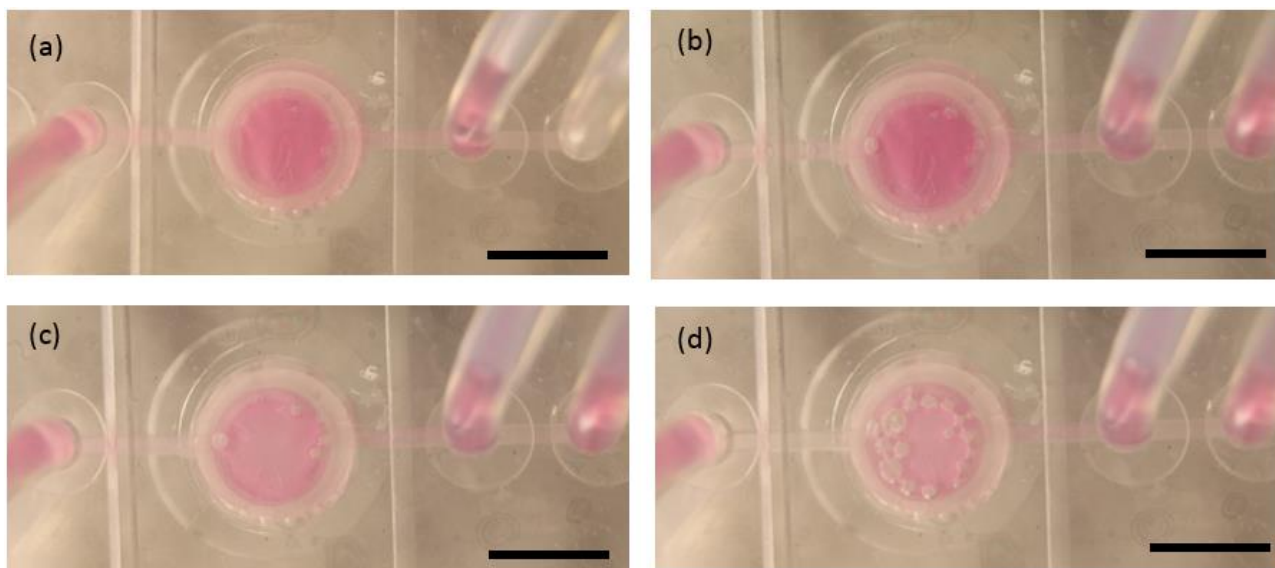


Figure 3.11 Pictures of the cell culture chamber perfused with cell culture medium. (a) 0 hr after activating the pump; (b) 1 hr after activating the pump; (c) 2 hr after activating the pump; (d) 3 hr after activating the pump. (Scale bar = 5mm)

The bubble trap was effective in trapping the bubbles during the first 2 hrs of continuous perfusion of the cell culture medium (Figure 3.11 a-c). However, between 2-3 hr of continuous perfusion of cell culture medium, bubbles started to appear in the microchamber (Figure 3.11d). Numerous air bubbles were observed in the microchamber that were previously not present at the 2 hr mark (Figure 3.11d). This bubble trap design although was effective in trapping bubbles during the first 2 hrs of continuous perfusion, it was not effective in trapping bubbles beyond 2 hrs of continuous perfusion at a flow rate of 5 $\mu\text{l}/\text{min}$.

Moreover, in situations when the air bubble was huge or when the trapped bubbles in the bubble trap coalesced to form a huge bubble in the bubble trap, under continuous perfusion condition this air bubble was pushed into the microchip. Once the air bubble flowed into the microchip, it was trapped in the microchamber. We believed that due to the limited volume of the bubble trap design 1, effective trapping of air bubble could not be achieved. Hence, this bubble trap design was not applicable to be integrated to the microfluidic device for long term cell culture.

3.3.2.2 Bubble trap design 2

We next sought to investigate the effectiveness of trapping bubbles with bubble trap design 2. The Eppendorf bubble traps were connected to the syringe pump and microfluidic chip as shown in Figure 3.12a. Cell culture medium was perfused into the set-up at a flow rate of 5 $\mu\text{l}/\text{min}$. After the syringe pump was activated to pump

at a flow rate of 5 $\mu\text{l}/\text{min}$, there was no observable leaking in the entire system. It was observed that when the air bubble enter the Eppendorf tube from the tube connecting to the syringe pump, the air bubble rose to the surface of the cell culture medium in the Eppendorf tube. The black arrow in Figure 3.12a indicated the air bubble that entered the Eppendorf tube from the inlet tube. As mentioned earlier, the cell culture medium inside the Eppendorf tube was bubble-free. With the tube connecting the Eppendorf tube to the microchip inserted to mid-way of the Eppendorf tube, the cell culture medium entering the microchip was bubble-free.

However, after continuous perfusion of cell culture medium for 165 hr, a bubble appeared in the microchamber (Figure 3.12b).

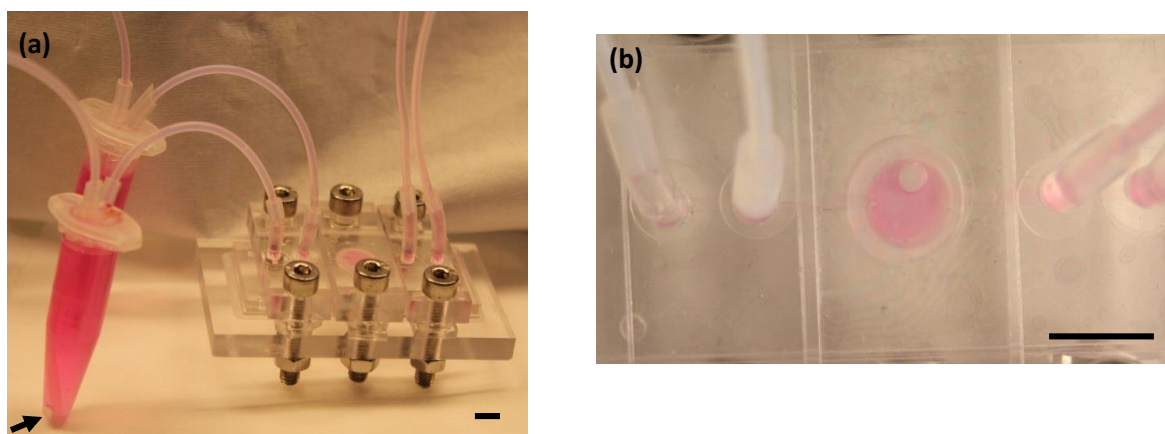


Figure 3.12 Bubble traps made using 1.5 ml Eppendorf tubes. (a) Overall view of the Eppendorf bubble traps connected to the microchip via silicon tubings. Black arrow indicating a bubble in the bubble trap. (b) Close up view of the cell culture chamber after continuous flow of cell culture media in the system using the Eppendorf bubble traps for 165 hrs. A bubble appeared in the cell culture chamber. (Scale bar = 5 mm)

This study showed that the bubble trap design 2 was more effective in trapping the air bubbles as compared to bubble trap design 1. We believe bubble trap design 2 was able to trap more bubbles effectively due to the larger volume of the Eppendorf tubes as compared to the volume of the silicon tubes.

3.3.3 Cell culturing with PMMA microchip and bubble trap design 2

Previously we showed that the entire system was leak-free and bubble-free for at least 165 hr when the microchip design 2 was integrated with bubble trap design 2. To investigate the feasibility of the system for cell culture, some preliminary cell culture studies were conducted. In this study, HeLa cells were seeded and cultured in the microfluidic device. After 48 hr of continuous perfusion of cell culture medium in the incubator, bubbles were observed in the cell culture chamber (Figure. 3.12). The bubbles were pushed into the

microchamber between 36 - 48 hr (results not shown). Moreover, the flow of the cell culture medium stopped between 36 hrs - 48 hrs. Upon opening and closing the caps of the Eppendorf tubes (bubble traps), the flow was re-established. It was suspected that the release of air bubbles from the culture medium into the bubble trap could have built-up the pressure in the bubble traps. The flow of cell culture medium might have been stalled by the built up of pressure within the bubble traps. By opening the caps of the Eppendorf tubes allowed the release of the built-up pressure. However, the opening and closing of the caps of the Eppendorf tubes was not an ideal solution for cell culture, as this was tedious and time dependent. Additionally, the constant opening and closing of the Eppendorf tubes increased the risk of contaminating the entire system.

Furthermore, the volume of the Eppendorf tube is 1.5 ml. For every cell culture study conducted with this bubble trap design, we must always consider the extra 1.5 ml as dead volume. In studies where expensive drugs are to be used, such bubble traps will incur more costs and this is undesirable.

Due to the appearance of the air bubbles in the microchamber, the cell culture study was terminated after 48 hr of continuous perfusion.

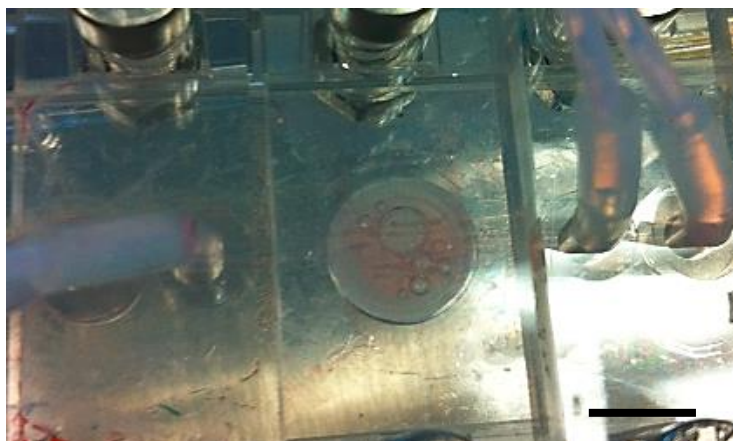


Figure 3.13 Close up view of the cell culture chamber on PMMA microchip containing HeLa cells. Air bubbles had appeared in the cell culture chamber after 48 hrs of continuous perfusion of DMEM. (Scale bar = 5 mm)

Porous PET membrane for HeLa cell culture. Previously in section 3.2.1, it was mentioned that the microfluidic chip layers were assembled by using six screws and bolts. Therefore, the porous membrane clamped between the fluidic could be manually removed. By removing, the porous membrane from the microchip layers allowed the staining of cells to be carried out off chip.

Furrows and folds were observed on the membrane (Figure 3.13). It was believed that these furrows and folds on the membrane were resulted from the tightening of the screws on the entire system. When the screws were tightened this might have caused some stresses on the membrane. As the membrane was very thin, the unequal

stresses acting on the membrane caused the folding and crinkling of the membrane. The presence of these furrows and folds, may pose some challenges in observing the cells microscopically. Consequently, these furrows and folds on the membrane might also prevent the cultured cells from forming confluent layers. Such outcome would be undesirable for transport studies as tight, confluent monolayers are required.

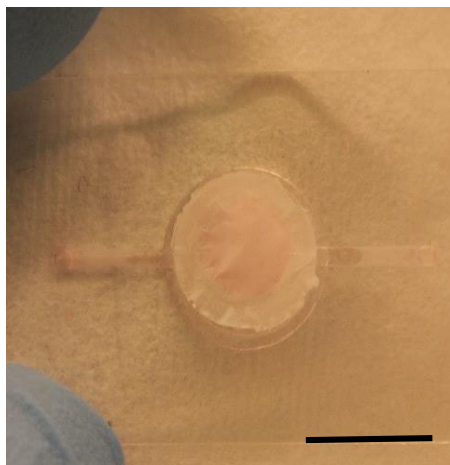


Figure 3.14 Membrane removed from the microchip. (Scale bar = 5 mm)

Fluorescent imaging of HeLa cells cultured in microchip. Microscopic phase contrast or bright field imaging could not be carried out on the cells cultured on the membrane. The reason being the porous PET membrane is not transparent when wetted. To investigate the viability of the HeLa cells cultured in the microchip, the nucleus of the HeLa cells were stained with fluorescent dye, To-PRO. Microscopic fluorescent images of the HeLa cells cultured in the microfluidic device showed that the HeLa cells survived in the PMMA microchip (Figure 3.15). The HeLa cells were sparsely spaced on the PET membrane (Figure 3.15). This observed phenomenon could be due to several reasons:

1) The presence of the air bubbles in the cell culture chamber. As mentioned earlier the presence of air bubbles may cause abrupt changes to the microenvironment in the cell culture chamber. This will result in cell damage and even cause cell death when the surface tension of the air-liquid interface is sufficient to rupture the cell membrane [23,26].

2) The cells failing to multiply. Perhaps the microenvironment in the microfluidic device was not conducive for cell culture. Numerous available literature reported that the microchambers for cell culture were often coated with a layer of extra cellular matrix (ECM) [4,5,17,18,26,27]. The ECM has the possibility of affecting the growth and differentiation of cells [28]. However, the cell culture studies conducted with the microfluidic device in this chapter were not cultured in ECM-coated microchambers.

3) Non-uniform seeding of cells on the porous membrane. As mentioned earlier, the cells were seeded by manually pushing the cell suspension into the cell culture chamber with a disposable syringe. This method of seeding cells might not have ensure proper uniform coverage of cells on the porous membrane. Poor coverage of cells on the cell membrane would affect the rate of cell proliferation.

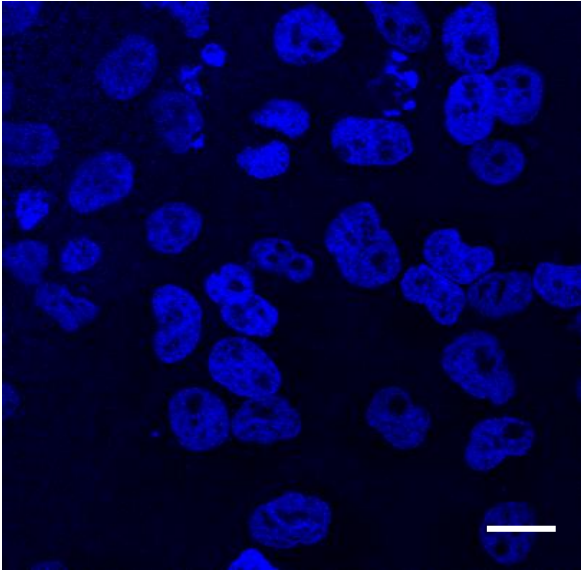


Figure 3.15 HeLa cells cultured in PMMA microchip for 48 hrs. The nucleus of the HeLa cells were stained with TO-PRO and imaged with a confocal microscope at Ex/Em 642/661 nm. Magnification of 15x. (Scale bar = 20 μm)

3.3.4 Comparison of microfluidic device connected to bubble trap design 2 functioning at room temperature versus at 37 °C

We showed earlier that the bubble trap design 2 was effective in trapping bubbles for at least 165 hr (Figure 3.12). However, when the entire system was placed inside an incubator (37 °C), our images showed that air bubbles appeared in the microchamber after 48 hr of continuous perfusion (Figure 3.13). Our results showed that the air bubbles appeared quicker in the microchamber at elevated temperatures (37 °C) as compared to room temperature. This phenomenon could be due to the dissolution of gases. In situations where the supersaturated liquids are introduced into a device at a lower temperature (e.g., at room temperature) and are subsequently heated to physiological temperature (i.e. 37 °C), will result in de-gassing of the liquids in the form of bubbles [21].

3.4 Conclusion

In this chapter, two preliminary designs of the microfluidic chip were fabricated by means of CNC micromilling on PMMA. In this chapter, it was demonstrated PMMA could be easily fabricated and was biocompatible. However, for cell culture, it was necessary to ensure that the microchip is leak-free and bubble-free. The two microchip designs discussed in this chapter were not 100 % leak-free nor were they bubble-free. Although the bubble trap design 2 was effective in removing bubbles for 165 hr in room temperature, when the system was placed inside an incubator, the bubble trap could not function for more than 48 hr. The results showed that none of the tested bubble traps were usable for long term cell culture.

Additionally, the method of sandwiching the porous membrane between the PMMA layers and tightening the layer with screws and bolts was not the ideal method of sealing the microchip layers. When the membrane was removed from the microchip layers, folds and furrows were observed on the porous membrane. These furrows and folds on the membrane will prevent the formation of monolayer of cells. Without the formation of a monolayer of cells on the porous membrane, transport studies cannot be conducted across the cell layer. Besides, the presence of these furrows and folds on the membrane will also pose some challenges in microscopic observations of the cells.

3.5 Outlook

The designs of the microchip described and presented in this chapter are undesirable and not suitable for cell culture. The microchip designs and the fluidic system showed too many shortcomings. In order to achieve the desired performance on and from the microchip, the entire project and the shortcoming of the experiments presented in this chapter must be addressed from the start:

1. **New material for microchip fabrication.** Although PMMA is biocompatible, with the discussed fabrication technique and assembly, the microchip made from PMMA did not achieved any of the project aims. A new design consideration, decision and selection of a new material were required to fabricate the microchip. This new material must be biocompatible and allows the embedding of the porous membrane for culturing of cells. The new material chosen must be transparent to permit real-time microscopy of the cells.

2. **Leak-free microchip.** PDMS gaskets used in the microchip designs were supposed to provide proper sealing between the microfluidic layers. However, as demonstrated in this chapter, the PDMS gaskets in the microfluidic device assemble, failed to provide the required leak-free seal.

In order to support continuous perfusion of cell culture medium in the microfluidic device, it was vital that the microchip be leak-free. This would ensure a sterile and conducive microenvironment be maintained for the cells. Hence, investigation of a new method of bonding the microfluidic layers was required. The bonding technique was dependent on the material chosen for the microchip.

3. **Porous membrane for cell culture.** The porous PET membrane discussed in this chapter was not transparent. Although it was biocompatible, it prevented online and real-time microscopy cell imaging of the cultured cells. Investigations of a new porous biocompatible membrane was required. This porous membrane must also allow it to be bonded to the microchip layers to form a leak-free microchip. Additionally, this porous membrane must not crinkle or form furrows after embedding it between the fluidic layers of the microchip.
4. **New fluidic system to support cell culture.** In all the preliminary studies discussed and presented in this chapter, a syringe pump was utilized to pump the reagents into the microfluidic chip. The syringe pump was bulky and much maneuvering of the entire set-up needed to be considered if microscopic real time- monitoring of the cells were to be performed on the chip. Besides, with the fluidic system (presented above) connected to the microchip, air bubbles were consistently appearing and forming in the cell culture chamber. As mentioned earlier, the formation of bubbles was mainly due to the temperature changes, channel geometry, flow focusing or configuration of connectors, adaptor and valves that were connected to the microfluidic chip. Introduction of bubble traps [5,24,29] or putting the entire cell culture system under pressure [8,12] could prevent air bubbles from entering the microchips. Air bubble traps were experimented and discussed in this chapter. However, they were not successful in eliminating the air bubbles. To eliminate the formation of air bubbles, the latter method of subjecting the entire system to pressure should be explored. Permeable parts of the system such as the interconnections can function as degassing components due to the pressure difference. A new fluidic system was necessary to support the microchip for cell culture. This fluidic system must be leak-free and permit the continuous perfusion of cell culture medium to the cells for long periods.
5. **Parallelizing cell culture on a single microchip.** In biology, performing parallel cell cultures and combinatorial assays is important from the single-cell level to the system level [30]. The microchip designs discussed in this chapter only has one chamber for cell culture. Therefore, a new design of the microchip was necessary to increase the throughput of the microchip.

References

- [1] I. Hubatsch, E.G.E. Ragnarsson, P. Artursson, Determination of drug permeability and prediction of drug absorption in Caco-2 monolayers, *Nat. Protoc.* 2 (2007) 2111–9.
- [2] S.B. Petersen, L.G. Nielsen, U.L. Rahbek, M. Guldbrandt, D.J. Brayden, Colonic absorption of salmon calcitonin using tetradecyl maltoside (TDM) as a permeation enhancer, *Eur. J. Pharm. Sci.* 48 (2013) 726–34.
- [3] S.B. Petersen, G. Nolan, S. Maher, U.L. Rahbek, M. Guldbrandt, D.J. Brayden, Evaluation of alkylmaltosides as intestinal permeation enhancers: comparison between rat intestinal mucosal sheets and Caco-2 monolayers, *Eur. J. Pharm. Sci.* 47 (2012) 701–12.
- [4] H.J. Kim, D. Huh, G. Hamilton, D.E. Ingber, Human gut-on-a-chip inhabited by microbial flora that experiences intestinal peristalsis-like motions and flow, *Lab Chip.* 12 (2012) 2165–74.
- [5] Y. Imura, Y. Asano, K. Sato, E. Yoshimura, A microfluidic system to evaluate intestinal absorption, *Anal. Sci. Int. J. Japan Soc. Anal. Chem.* 25 (2009) 1403–1407.
- [6] H. Becker, C. Gärtner, Polymer microfabrication technologies for microfluidic systems, *Anal. Bioanal. Chem.* 390 (2008) 89–111.
- [7] C.-W. Tsao, D.L. DeVoe, Bonding of thermoplastic polymer microfluidics, *Microfluid. Nanofluidics.* 6 (2008) 1–16.
- [8] P. Skaftø-Pedersen, M. Hemmingsen, D. Sabourin, F.S. Blaga, H. Bruus, M. Dufva, A self-contained, programmable microfluidic cell culture system with real-time microscopy access, *Biomed. Microdevices.* 14 (2012) 385–99.
- [9] M. Stangegaard, A biocompatible micro cell culture chamber (μ CCC) for culturing and on-line monitoring of Eukaryotic cells, Technical University of Denmark, 2005.
- [10] P.M. van Midwoud, A. Janse, M.T. Merema, G.M.M. Groothuis, E. Verpoorte, Comparison of biocompatibility and adsorption properties of different plastics for advanced microfluidic cell and tissue culture models, *Anal. Chem.* 84 (2012) 3938–44.
- [11] H.Y. Tan, W.K. Loke, Y.T. Tan, N.-T. Nguyen, A lab-on-a-chip for detection of nerve agent sarin in blood, *Lab Chip.* 8 (2008) 885–91.
- [12] D. Sabourin, P. Skaftø-Pedersen, M.J. Sjøe, M. Hemmingsen, M. Alberti, V. Coman, et al., The MainSTREAM component platform: a holistic approach to microfluidic system design, *J. Lab. Autom.* 18 (2013) 212–28.
- [13] F. Sallustio, V. Costantino, S.N. Cox, A. Loverre, C. Divella, M. Rizzi, et al., Human renal stem/progenitor cells repair tubular epithelial cell injury through TLR2-driven inhibin-A and microvesicle-shuttled decorin, *Kidney Int.* 83 (2013) 392–403.
- [14] W. Xu, A.J. Janocha, R.A. Leahy, R. Klatte, D. Dudzinski, L. A. Mavrikakis, et al., A novel method for pulmonary research: Assessment of bioenergetic function at the air–liquid interface, *Redox Biol.* 2 (2014) 513–519.
- [15] P. Artursson, R.T. Borchardt, Intestinal drug absorption and metabolism in cell cultures: Caco-2 and beyond, *Pharm. Res.* 4 (1998) 1655–1658.
- [16] T. Toimela, H. Mäenpää, M. Mannerström, H. Tähti, Development of an in vitro blood–brain barrier model—cytotoxicity of mercury and aluminum, *Toxicol. Appl. Pharmacol.* 195 (2004) 73–82.

- [17] L.M. Griep, F. Wolbers, B. de Wagenaar, P.M. ter Braak, B.B. Weksler, I.A. Romero, et al., BBB on chip: microfluidic platform to mechanically and biochemically modulate blood-brain barrier function, *Biomed. Microdevices*. 15 (2013) 145–50.
- [18] D. Huh, B.D. Matthews, A. Mammoto, M. Montoya-Zavala, H.Y. Hsin, D.E. Ingber, Reconstituting organ-level lung functions on a chip, *Science* (80-.). 328 (2010) 1662–8.
- [19] E.W.K. Young, D.J. Beebe, Fundamentals of microfluidic cell culture in controlled microenvironments, *Chem. Soc. Rev.* 39 (2010) 1036–1048.
- [20] C. Liu, J.A. Thompson, H.H. Bau, A membrane-based, high-efficiency, microfluidic debubbler, *Lab Chip*. 11 (2011) 1688–93.
- [21] C. Lochovsky, S. Yasotharan, A. Günther, Bubbles no more: in-plane trapping and removal of bubbles in microfluidic devices, *Lab Chip*. 12 (2012) 595–601.
- [22] H. van Lintel, G. Mernier, P. Renaud, High-throughput micro-debubblers for bubble removal with sub-microliter dead volume, *Micromachines*. 3 (2012) 218–224.
- [23] Y. Wang, D. Lee, L. Zhang, H. Jeon, J.E. Mendoza-Elias, T.A. Harvat, et al., Systematic prevention of bubble formation and accumulation for long-term culture of pancreatic islet cells in microfluidic device, *Biomed. Microdevices*. 14 (2012) 419–26.
- [24] W. Zheng, Z. Wang, W. Zhang, X. Jiang, A simple PDMS-based microfluidic channel design that removes bubbles for long-term on-chip culture of mammalian cells, *Lab Chip*. 10 (2010) 2906–10.
- [25] J.C. Salamone, *Polymeric Materials Encyclopedia*, CRC Press Taylor & Francis Group, 1996.
- [26] R. Booth, H. Kim, Characterization of a microfluidic in vitro model of the blood-brain barrier (μ BBB)., *Lab Chip*. 12 (2012) 1784–92.
- [27] N. Ferrell, R.R. Desai, A.J. Fleischman, S. Roy, H.D. Humes, W.H. Fissell, A microfluidic bioreactor with integrated transepithelial electrical resistance (TEER) measurement electrodes for evaluation of renal epithelial cells, *Biotechnol. Bioeng.* 107 (2010) 707–16.
- [28] C.J. Flaim, S. Chien, S.N. Bhatia, An extracellular matrix microarray for probing cellular differentiation, *Nat. Methods*. 2 (2005) 119–125.
- [29] L. Kim, M.D. Vahey, H.-Y. Lee, J. Voldman, Microfluidic arrays for logarithmically perfused embryonic stem cell culture, *Lab Chip*. 6 (2006) 394.
- [30] Z.T.F. Yu, K. Kamei, H. Takahashi, C.J. Shu, X. Wang, G.W. He, et al., Integrated microfluidic devices for combinatorial cell-based assays, *Biomed. Microdevices*. 11 (2009) 547–55.

CHAPTER 4: Second generation microchip – Thiol-ene microchip

Previously in Chapter 3, the PMMA microchip and fluidic platform described and discussed was unsuitable for long-term cell culture. To address all the shortcomings listed in section 3.5, a new material and design of microchip was considered. The microfluidic chip was fabricated using the polymer thiol-ene. The porous membrane to be embedded between the fluidic layers was changed to a porous Teflon membrane. Attempts in modifying the porous Teflon membrane were investigated to enable bonding of the different layers in the microchip. This chapter describes all the designs, optimization and fabrication of the thiol-ene microchip.

4.1 Design considerations

As mentioned earlier, the aim of the project is to design and fabricate a microchip for long-term cell culture for transport studies. Previously in chapter 3, it was clearly demonstrated that the material (PMMA) and fabrication technique were unsuitable for producing a microchip to meet the aim of the project. To resolve the challenges faced in the previous chapter there were three major design considerations that were revised.

- 1) The fluidic system required to control and automate the fluid to and from the microchip.
- 2) The choice of material used for fabricating the microchip. This material must allow easy integration to the chosen fluidic system.
- 3) The membrane which needs to be transparent when wetted.

The fluidic system (comprising of MAINSTREAM components [1–4]) chosen to drive the microfluidic chip for cell culture will be discussed further in detail in Chapter 5.

4.1.1 Material selection

Material for microchip fabrication. The requirements for choosing the new material to fabricate the new microfluidic chip design were similar to those listed in section 3.1.1 in chapter 3 of the thesis. In recent years, several groups reported on exploiting the advantages of thiol-ene's 'click' chemistry to fabricate microfluidic

devices [5–13]. The mechanism of thiol-ene ‘click’ chemistry was already discussed in Chapter 2. The method employed for fabricating microfluidic devices with thiol-ene polymers is fast (device layers are fabricated in the order of seconds) and the entire fabrication process can be carried out in ambient temperatures [5–8,11,13]. This form of rapid prototyping of microfluidic devices is suitable for small scale commercial series production [8]. Furthermore, the mechanical and chemical properties of cured thiol-ene polymers can be controlled [7]. This may be advantageous for fabricating the microchip, especially in keeping the porous membrane in place on the microchip. Moreover, cured thiol-ene polymers are reported to have low affinity in absorbing molecules and low volume shrinkage [8,9]. These properties make thiol-ene a suitable material for fabricating the new microchip.

Finally, thiol-ene maybe biocompatible for cell culture. There was a brief study conducted to investigate the biocompatibility of thio-ene [12]. Errando-Vastesson et. al reported on observing similar cell viability of HEK293A cells cultured on thiol-ene mixtures (without photoinitiator) when compared to polystyrene (PS). PS is the most commonly used material for laboratory cultureware [14]. Due to some of the listed promising qualities of thiol-ene polymers, thiol-ene was chosen as the material for fabricating the microfluidic chip in this project.

Material of porous membrane for cell culture. Previously, in chapter 3, the porous membrane used in fabricating the first generation microchips was polyethylene terephthalate (PET). Although PET is suitable for cell culture, it is not transparent to visible light when wetted. Therefore, real-time microscopic studies on the Caco-2 cells in the intended microfluidic chip could not be performed. We decided to use a porous Teflon membrane (Millipore, Denmark) known to be suitable for cell culture in the chip. First of all, this Teflon membrane becomes transparent to visible light when wetted. This property is advantageous as it enables real-time microscopic imaging of the cells cultured on it. Second, the porous membrane can be purchased in big sheets instead of cutting them from Transwell inserts. This allowed for easy of tailoring the membrane to the size required in the fabrication procedure.

4.1.2 Microchip designs

To perform transport studies with the Caco-2 cells cultured in the microfluidic chip later in the project, it is important that the microchip is multi-layered. Additionally, the microfluidic chip must allow for perfusion of reagents to both the apical and basolateral side of the cells. To increase the throughput of the microchip, the microchip was designed to contain eight microchambers. Each of the microchambers was connected to its individual inlet and outlet channels. Altogether, there were 32 inlet and outlet ports on the microchip. Integration of the microfluidic chip with the fluidic system will be further discussed in chapter 5. Two designs of the microchip were drawn using the CAD software, Autocad 2012.

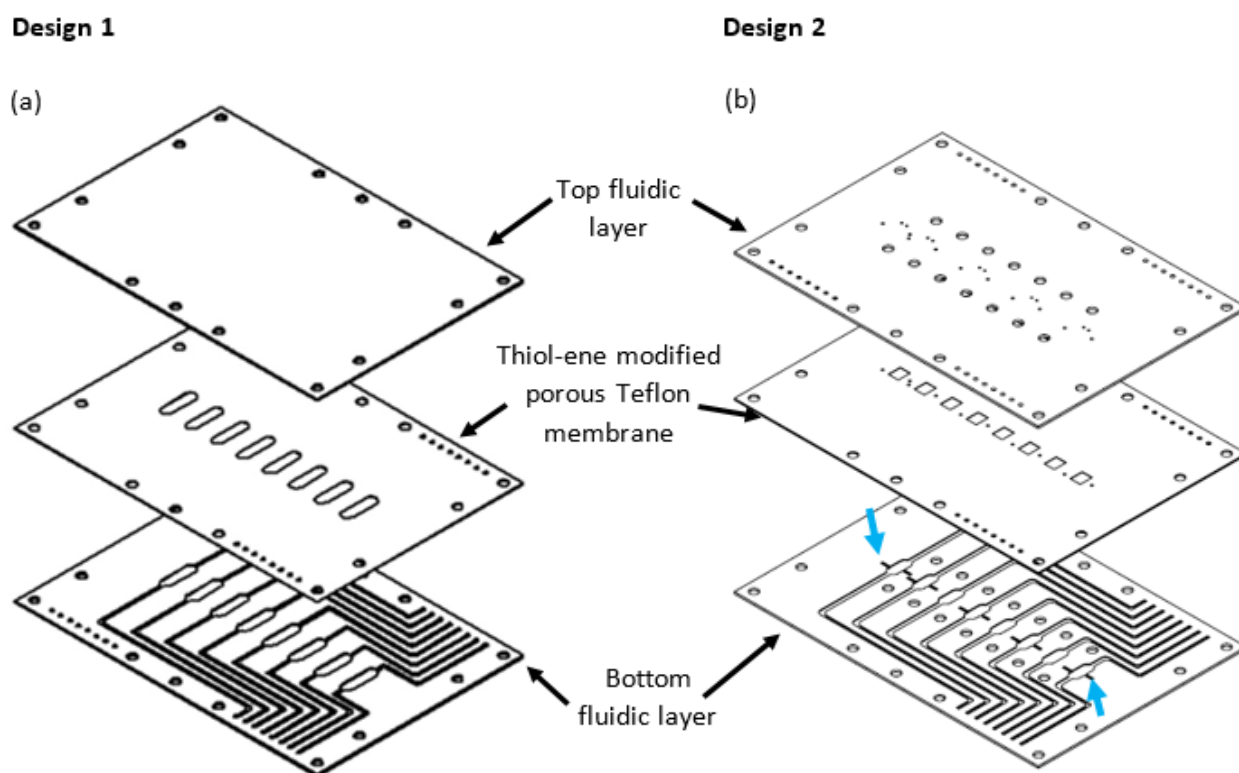


Figure 4.1. Exploded views of the 3 layer thiol-ene microchip. Dimension of microchip: 76 mm x 52 mm x 2.7 mm. Thickness of membrane is 0.3 mm. Fluids are perfused through the upper and lower layers. (a) Microchamber has an elliptical shape of width = 2.5 mm and length = 11 mm; (b) Microchamber has a size of a rectangular shape with a dimension of 3 mm (length) x 2.5 mm (width). Microgrooves (blue arrows) with dimensions of 2 mm (length) x 0.5 (width) x 0.2 mm (height) for the placement of the microelectrodes for trans-epithelial electrical resistance (TEER) measurements, were micromilled only to the bottom fluidic layer.

The microchip has an external dimension of 76 mm (length) x 52 mm (width) x 2.7 mm (height). Sandwiched between the top and bottom fluidic layers was the porous membrane (Figure 4.1). Cells will be cultured on the porous membrane. The difference between the two designs was the size of the microchamber. In Design 1, the microchambers were elliptical shape with the dimensions of 2.5 mm (width) x 11 mm (length) per chamber (Figure 4.2 a-b). The microchambers in design 2 were rectangular in shape with dimensions of 2.5 mm (width) x 3 mm (length) per chamber (Figure 4.4c-d). The shaded regions shown in Figure 4.2b and Figure 4.4d are the open porous Teflon membrane for cell culture. The cell culture chambers in design 2 were positioned at a distance from the inlet channel (Figure 4.2 c-d). This was to allow a better distribution of the reagents within the microchamber. Fluid distribution in the microchamber and the effects of fluid on cell growth will be discussed in chapter 5.

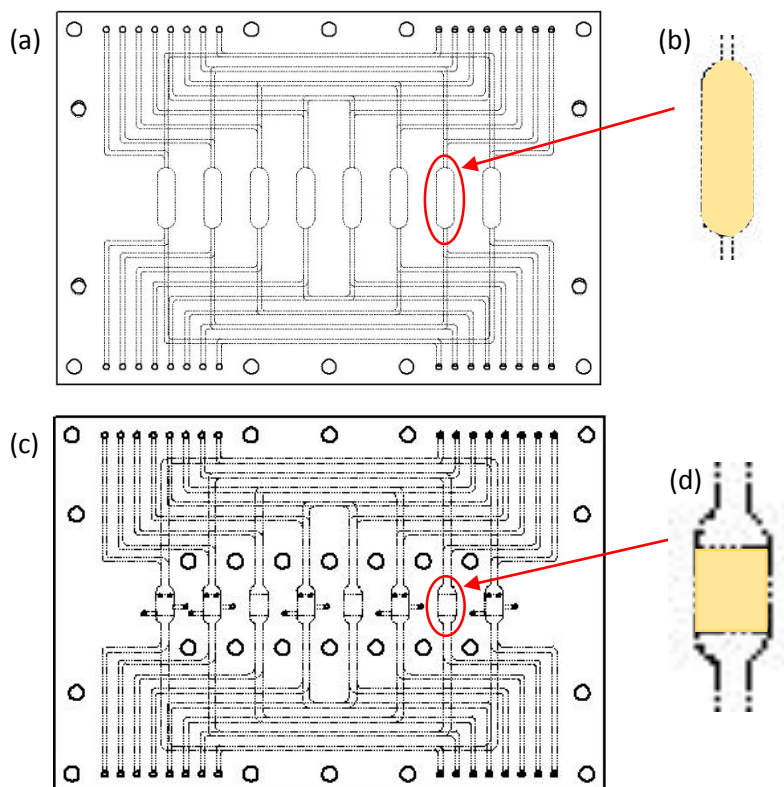


Figure 4.2 Schematic top view of the two different microchip designs. a) Top view of the assembled microfluidic chip design 1; (b) Expanded view of the cell culture chamber (top view). Shaded region is the open porous Teflon membrane; (c) Top view of the assembled layers of microchip design 2; (d) Expanded view of the cell culture chamber. Shaded region is the open porous Teflon membrane (top view)

The new designs of the microchip do not require additional gaskets to seal the different layers of the microchip as the chip is essentially glued together using thiol-ene. The presented schematics of the assembly of the new microfluidic chip designs is greatly simplified as compared to the complicated assembly of the PMMA chips that were previously described in Chapter 3.

4.2 Materials and methods

4.2.1 Fabrication of microchip

Two sets of molds were required to fabricate the fluidic layers of the thiol-ene microchip. The first mold was fabricated on polymethylmethacrylate (PMMA). The design of this mold was the exact replica of the thiol-ene microchip design. A second mold made from PDMS was the inverse design of the PMMA mold.

Fabrication of first mold. The first master mold was fabricated by CNC micromilling (Mini-Mill/3, Minitech Machinery Corporation, GA, USA) on 5 mm PMMA blocks. The microchambers on the PMMA molds were milled through (red circle in Figure 4.3 a). The microchamber inserts (Figure 4.3b) were milled separately and inserted into the milled-through cavities (black arrows in Figure 4.3a). By carrying out this procedure, flat and clear surfaces of the microchambers were yielded. This would enable better microscopic imaging of the cells in the studies later on.

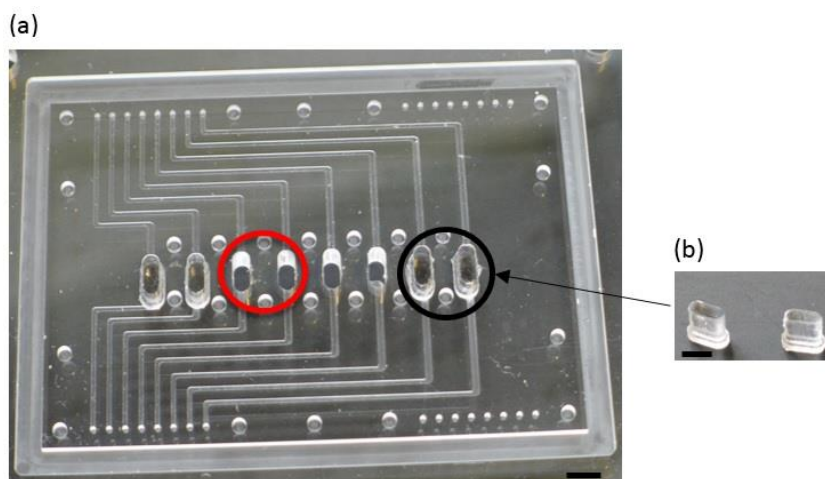


Figure 4.3 PMMA master mold. a) Red circle indicate the milled out microchambers. Black circle indicate the microchambers with the inserts. b) Expanded view of the inserts. (Scale bar = 5 mm)

Fabrication of second mold. The second mold was fabricated by mixing polydimethylsiloxane (PDMS; DowCorning, Germany) in the ratio of 1:10 (curing agent: pre-polymer), degassed under vacuum and poured onto the PMMA master mold. The liquid PDMS was cured at 70 °C for more than 20 hrs. Once the PDMS mold was cured, it was de-molded from PMMA mold, bearing the replicated design of the microchip layer. The PDMS master mold would be highly used for the thiol-ene curing process. Figure 4.4 shows the schematic flow for fabricating the thiol-ene microchip.

Fabrication of thiol-ene microchip. The top and bottom layers of the thiol-ene microchip were fabricated via the method reported by Lafleur et. al. [11]. Two different mixtures of thiol-ene were prepared for the microchip fabrication. The top and bottom layers were fabricated with a mixture of pentaerythritol tetrakis-(3-mercaptopropionate) (tetra-thiol moieties, 4T; Sigma, Denmark) and 1,3,5-triallyl-1,3,5-triazine-2,4,6(1H,3H,5H)-trione (tri-allyl moieties, 3E; Sigma, Denmark) in stoichiometric ratios (1:1) by weight in a plastic beaker. After mixing the two different monomers, the mixture was poured onto the PDMS mold bearing the microchip designs (Step 1 in Figure 4.4A). A PDMS block (3mm thick) was carefully placed over the mold to prevent any trapping of air bubbles. The closed mold was exposed to UV light (Dymax 5000-EC Series UV

curing flood lamp, Dymax Corp., Torrington, CT, USA, $\sim 40 \text{ mWcm}^{-2}$ at 365 nm) for 40 s on both sides (Step 2 and 3 in Figure 4.4A). Immediately after curing, the thiol-ene layers were demolded from the PDMS molds (Step 4 in Figure 4.4A). Next, holes for the inlet, outlet ports and electrode ports (in design 2 Figure 4.1) were drilled through the cured thiol-ene layers.

The porous Teflon membrane (0.4 μm in pore size; 40 μm in thickness) (Millipore, Denmark) was modified to enable bonding of the membrane to the thiol-ene parts containing the fluidic manifolds. A thiol-ene mixture consisting of trimethylpropane tris-(2-mercaptopropionate) (tri-thiol moieties, 3T); Sigma, Denmark) and the same allyl moiety, 3E, was prepared in stoichiometric ratios (1:1) by weight in a plastic beaker. This mixture was used to coat the membrane (Step 1 in Figure 4.4B). The coated membrane was exposed to UV radiation for 25 s through a plastic mask (Infinite Graphics, Singapore) that protected the cell culture regions (Step 2 Figure 4.4B). Hereafter, the entire membrane was rinsed with methanol (Sigma, Denmark) to remove any uncured thiol-ene (Step 3 in Figure 4.4B). The same process was carried out on the underside of the Teflon membrane (Step 4 and 5 in Figure 4.4B). Before bonding the layers, holes for the inlets, outlets connecting to the bottom fluidic layer and electrode ports were drilled through the thiol-ene modified membrane. Subsequently, the different layers were placed into the oven (temperature = 75 °C) for about 10 min. This was necessary to allow the thiol-ene layers to soften. Softening the layers will allow the layers to adhere and conform to each other better. Following that, the layers were aligned onto each other and slight pressure was applied with a roller over the layers to ensure good contact between the surfaces. As the surfaces of the different layers were a little 'sticky', they would adhere to each other easily. To finalise the bonding, the combined layers were exposed to UV radiation for another minute on each side (Final fabrication step in Figure 4.4). This will also yield complete conversion of the thiol- and allyl groups in the thiol-ene layers.

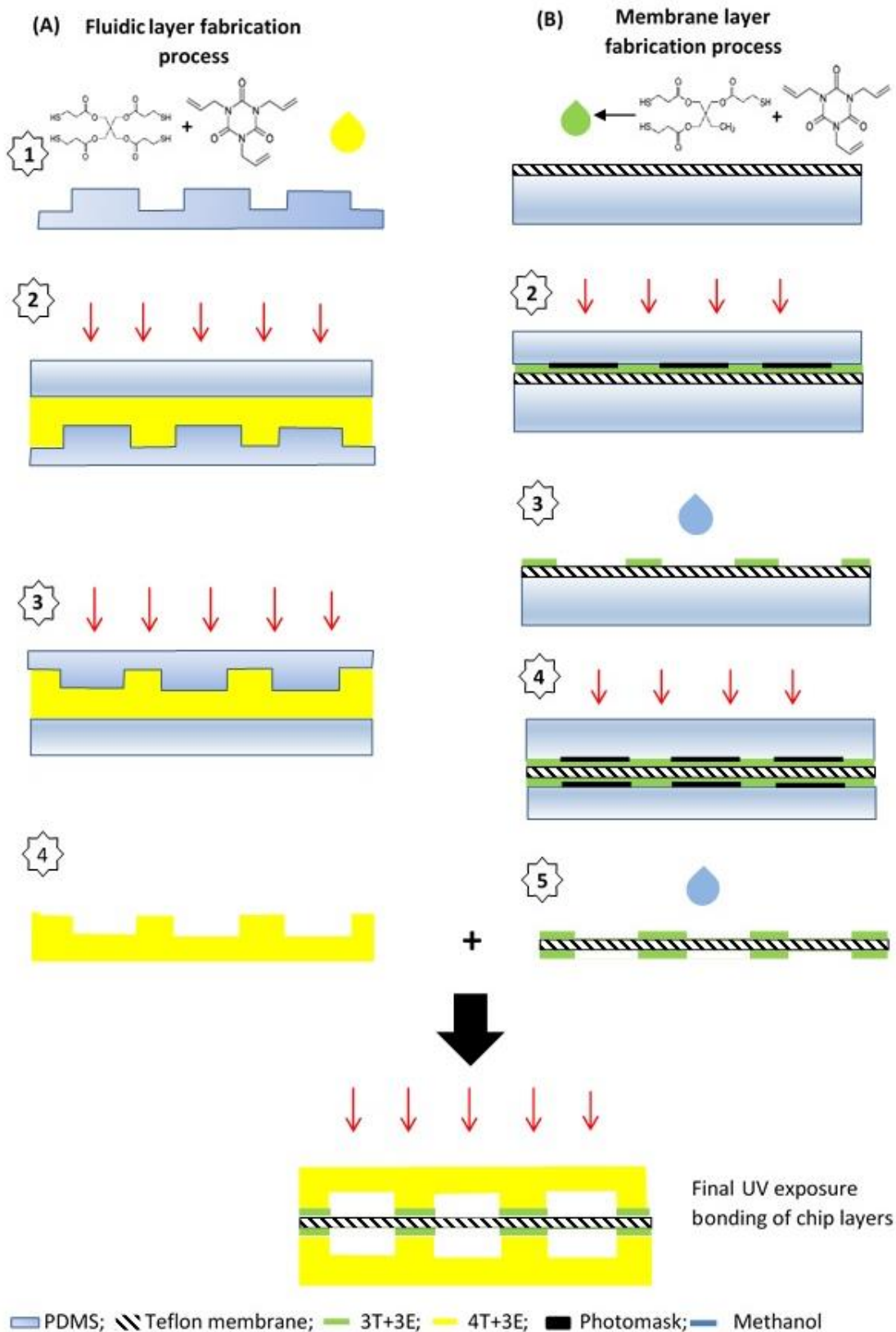


Figure 4.4 Schematic process of fabricating the thiol-ene microchip. A) The upper and lower fluidic layer; B) The thiol-ene coated Teflon membrane.

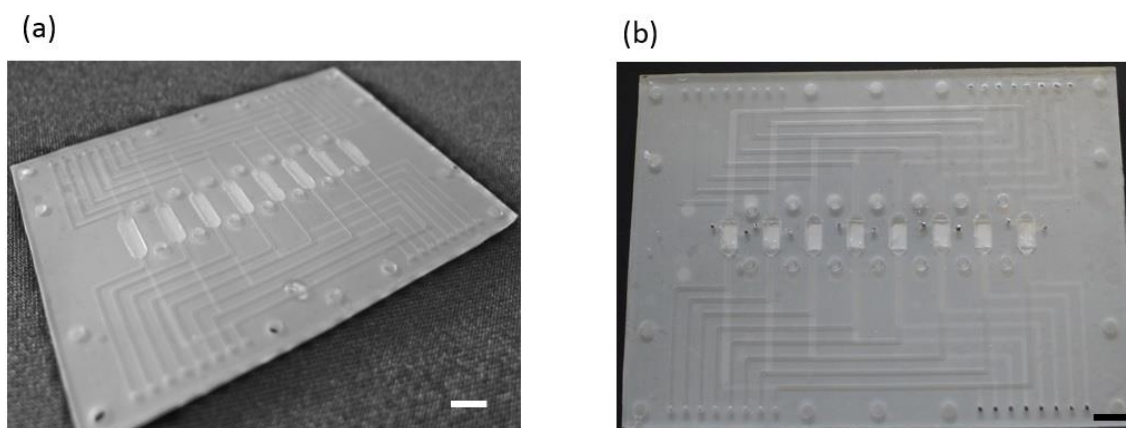


Figure 4.5 Completed thiol-ene microfluidic chip. (a) Design 1; (b) Design 2 (Scale bar = 5 mm)

4.2.2 Optimisation of UV-exposure time to cure thiol-ene mixtures

Clean and new PDMS molds of 5 mm in thickness were subjected to different durations of UV exposure: 0 to 30 min. A spectrometer (U-Vis spectrophotometer; Shimadzu, Japan) was used to analyse the UV light transmittance through the PDMS molds.

4.2.3 Preparation of thiol-ene and PDMS rings for Caco-2 biocompatibility studies

Fabrication of thiol-ene rings. To investigate the biocompatibility of the cured thiol-ene, rings fitting into 12-well microtiter plates of different thiol-ene mixtures were fabricated. The two different thiol-ene mixtures were prepared using the thiol and allyl moieties discussed in Chapter 2. One of the mixture was prepared with 3T and 3E, while the other mixture was prepared with 4T and 3E. The thiol and allyl monomers were prepared in stoichiometric ratios (1:1) by weight in a plastic beaker. Next, the monomers were carefully mixed and poured onto the PDMS molds bearing the ring structures. Another layer of PDMS (3 mm thick) was carefully placed over the molds to prevent any trapping of air bubbles. The closed mold of thiol-ene mixtures were exposed to UV light for 1 min. Next the mold was flipped and exposed through the bottom for another 1 min. Immediately after the second UV-exposure, the cured thiol-ene rings (Figure 4.6b) were de-molded from the PDMS molds. These rings have an external diameter of 8 mm, inner diameter of 5 mm and 10 mm in thickness (Figure 4.6b).

Fabrication of PDMS rings. PDMS was prepared by mixing the pre-polymer : curing agent in the ratio of 1:10. PDMS mixture was degassed under vacuum and poured onto the PMMA molds and cured at 75 °C for

at least 20 hrs. The wells containing the PDMS rings will serve as controls for the biocompatibility study. Dimension of the rings are similar to the thiol-ene rings.

Preparation of rings for Caco-2 biocompatibility studies. The respective materials (PDMS, 3T+3E, 4T+3E) were first sterilized by washing thoroughly with 70 % ethanol. Next the different materials were treated in three different conditions: i) 24 hr soaking in ethanol followed with wiping with cell culture medium, ii) soaking for 24 hr in cell culture medium or iii) briefly wiped with cell culture medium. Subsequently, the different treated materials were placed into respective wells of a 12 well microtitre plate (Nunc, Denmark).

Preparation of Caco-2 cells for biocompatibility studies. Human Caco-2 intestinal epithelial cells were obtained from American Type Culture Collection ((ATCC), HTB-37, Germany). The Caco-2 cells were cultured routinely in Dubelco's Modified Eagle Medium (DMEM; Sigma, Denmark). The culture medium was supplemented with 10 % (v/v) heat-inactivated fetal bovine serum (FBS; Sigma, Denmark), 1% (v/v) nonessential amino acids (NEAA; Gibco, Denmark) and 1% (v/v) penicillin-streptomycin (P/S; Gibco, Denmark). Caco-2 cells of Passage 48 (P48) were harvested using a trypsin/EDTA solution (Sigma; Denmark). Following that, they were centrifuged at 125g for 5 min, before re-suspending the cell pellets with fresh cell culture medium. A cell counter (Moxi-Z; Orflo, Denmark) was used to count the re-suspended Caco-2 cells. A concentration of 1.5×10^5 cells/ml was prepared. 2ml of the prepared Caco-2 cells were transferred into the respective wells. Following that, the microtitre plate was placed in the incubator (37 °C; 5 % CO₂) and cultured for 14 days. Cell culture medium was changed on alternate days of cell culture. Microscopic phase contrast images of the cells were taken on alternate days to monitor the growth of the Caco-2 cells.

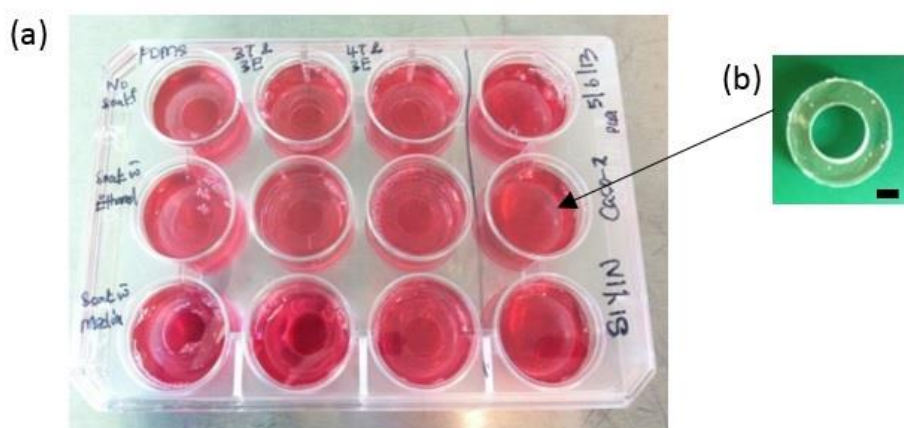


Figure 4.6 Batch cultures in 12-well microtitre plate. (a) Top view of the wells containing the different materials subjected to different treatments prior to cell seeding. Last column on the right is the control (without any material). (b) Enlarged view of the thiol-ene ring. Dimension of ring: external diameter = 8 mm, inner diameter = 5 mm; thickness = 10 mm. (scale bar = 2 mm)

4.2.4 Contact angle and wetting properties

Contact angle measurements were carried out on five different materials: Cured thiol-ene layer, thiol-ene modified Teflon membrane, un-modified Teflon membrane, PDMS, PMMA and polycarbonate (PC). In the wettability studies, the material of interest was mounted onto the stage of the equipment (Contact angle system OCA20; Dataphysics, Germany). A drop of de-ionised (DI) water (volume = 4 μ l or 2 μ l) was dropped onto the surface of the material. The angle at which the liquid and surface interact, was recorded as the contact angle.

4.2.5 Bond test of microchip

The burst pressure test of the different thiol-ene microfluidic chips were carried out at two different temperatures, namely room temperature (25°C) and incubator temperature (37 °C). The bond strength between the layers were investigated at 37 °C, which was the required temperature for cell culture of Caco2 cells. Therefore, this will also be the temperature that the microfluidic chip would be subjected to for long periods. For the studies carried out at 37 °C, the microchip was first placed into an oven set at 37 °C, then transferred to a hotplate set at 37°C during the burst pressure tests.

The system and method reported by Silkane et. al. [6] was used to carry out the burst pressure studies. The microchannels were first filled with diluted red food colour dye. Red dye was used to allow better visual observations during the pressure experiments. When testing the top layer, the inlets and outlets of the bottom layer and the outlet of the top layer were sealed with a layer of cured thiol-ene. These ports were sealed to prevent any leakage of pressure during the studies. The same procedure was carried out when testing the bottom fluidic layer. The instrument for the pressure test, as well as the chip filled with dye are shown in figure 4.7.

Next, the microchip was connected to a mechanical clamp, where a pressure sensor was mounted onto a polycarbonate block. Via a tube, the system was connected to two 10 ml syringes. Pressure in the microchip was increased, by using the clamp to compress the air in the syringes. The entire system for the burst pressure test is shown schematically in Figure 4.7a. The output of the pressure sensor was measured with an in-house written Labview program (National Instruments, Austin, TX, USA).

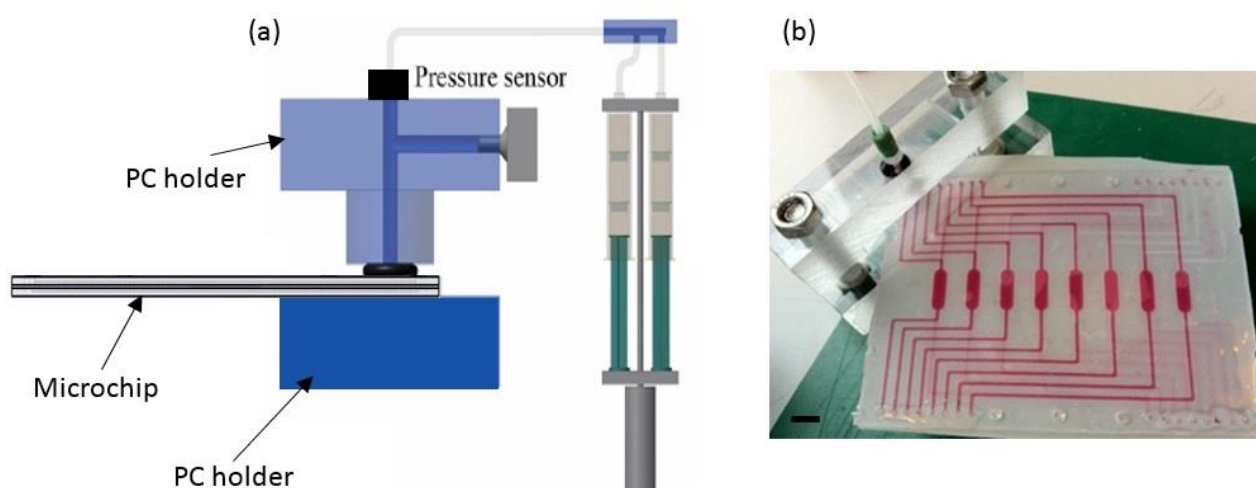


Figure 4.7 Burst pressure study for thiol-ene microchip. (a) Schematic view of the pressure system [6]. The thiol-ene microchip was clamped between the PC holders. The pressure sensor on the top of the PC holder will measure the pressure of the set-up. The syringes are compressed to provide the pressure into the microchip. (b) Microfluidic chip filled with red dye. The inlet and outlet ports for the bottom fluidic layer and outlet for the top layer were sealed with cured thiol-ene. The inlet port of the top fluidic layer is clamped between the mechanical device.

4.3 Results

4.3.1 Thiol-ene biocompatibility tests

As mentioned earlier, it is very important to choose a material that must be biocompatible for cell culture. One of the first studies conducted prior to fabricating the microfluidic device was to investigate the biocompatibility of thiol-ene with Caco-2 cells. In our biocompatibility studies, Caco-2 cells were cultured in different wells on a 12-well microtiter plate. The growth of the Caco-2 cells were microscopically monitored on alternate cell culture days. The phase contrast pictures (Figure 4.8) clearly displayed that the different cured thiol-ene mixtures did not have any adverse effects on the growth and morphology of the Caco-2 cells. On the day after seeding, the cultures were composed of both round and flattened cells. Clumps of cells showing varying degrees of attachment to each other were also observed. By day 3 of cell culture, the cultures consisted almost entirely of flattened cells. Most of the cells observed on this day were elongated. It has been reported that this form of elongated Caco-2 cells are observed just before cell division [15]. Seeing these form of elongated Caco-2 cells in all the wells, was also a clear indication that the materials were not leaching any form of cytotoxic monomers into the cell culture medium.

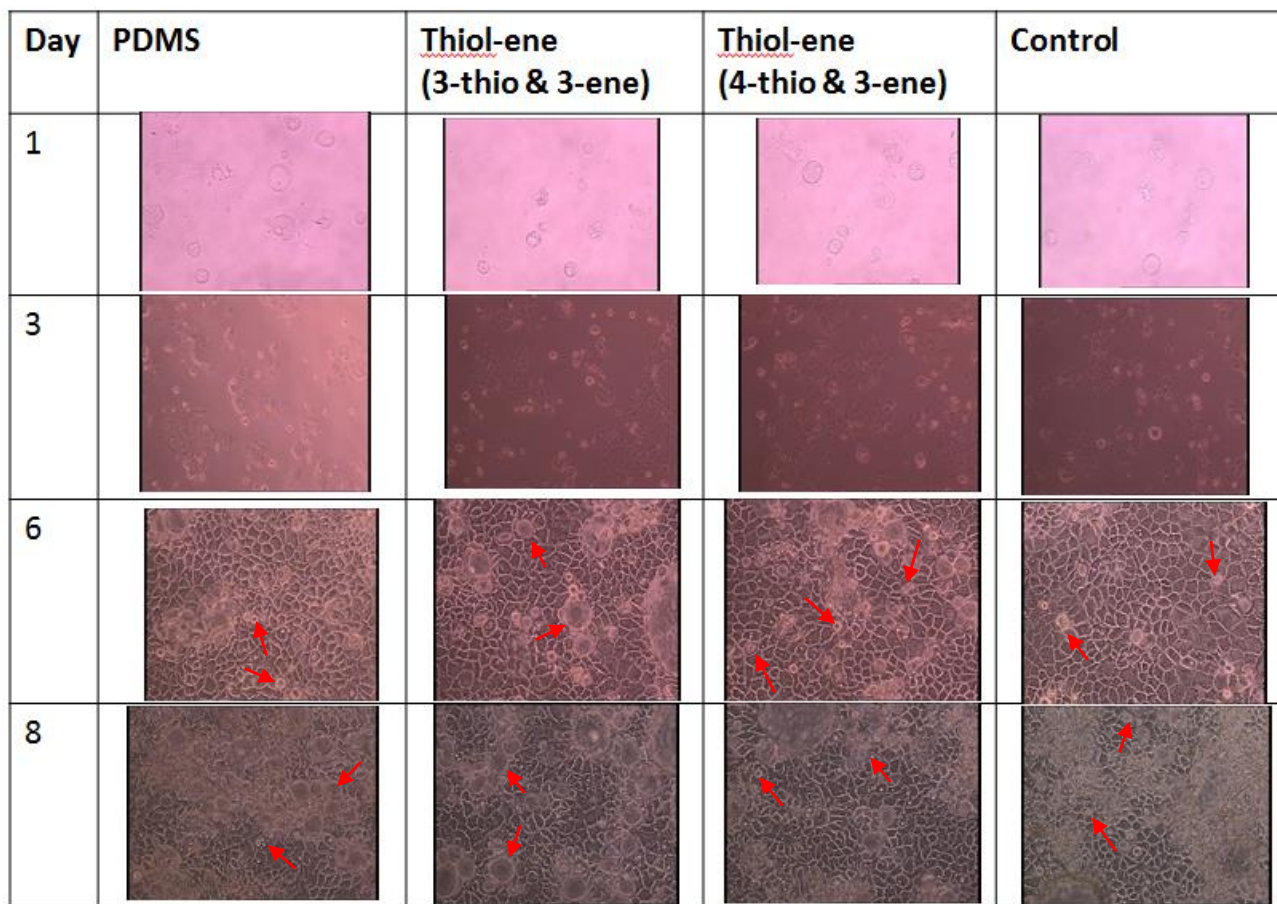


Figure 4.8 Phase contrast pictures of the Caco-2 cells taken over the days of cell culture. Control = cells cultured in the wells where there are no foreign materials. The pictures taken for the three different materials were from the worst condition, i.e. the rings were not treated with ethanol or media. (Magnification 10x)

By day 6, the Caco-2 cells multiplied and there was about 90 % confluence of the respective wells. Polygonal shaped cells with clear, sharp boundaries between the cells were observed in all the wells. By day 8, the Caco-2 cells multiplied even more and 100 % confluency was reached for all microwells. There was also an increase of circular vacuoles in the cytoplasm of the cells (indicated by red arrows). The appearance of these vacuoles is an indication of the Caco-2 cell density increasing to confluence. The phase contrast pictures clearly confirmed that the different cured thiol-ene mixtures did not have any adverse effects on the growth of the Caco-2 monolayers. Therefore, the chosen thiol-ene mixtures for the microchip fabrication were biocompatible for Caco-2 cell culture.

4.3.2 Characterisation of polymeric materials for microchip fabrication

4.3.2.1 Shrinkage of PDMS

PMMA, PDMS and thiol-ene were the three main polymers required for fabricating the molds of the microchip and the microchip respectively. During the curing procedures of PDMS mixture and thiol-ene mixture, both polymers undergo phase changes. It is known that when polymers undergo phase changes, this will directly influence the specific volume of the polymer [16]. This in turn will have significant influence on the dimensional accuracy and dimensional stability of the final product [17]. Investigations on possible polymer shrinkage after undergoing the different curing procedures were performed.

When the cured thiol-ene layers were aligned against the PDMS mold, it was observed that the pieces lined up perfectly. This was a clear indication that the cured thiol-ene layer did not shrink significantly. This is consistent to previous reports [8,10]. However, when the cured thiol-ene was aligned against the original PMMA molds, misalignment of the structures on the thiol-ene and PMMA were observed.

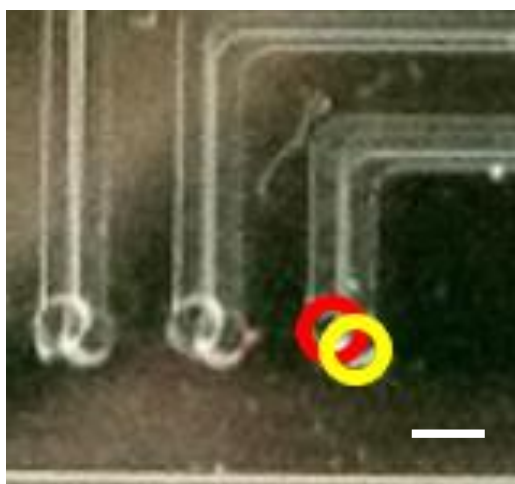


Figure 4.9 Cured PDMS mold aligned over the PMMA molds. Red circle indicate the outlet on the PDMS mold and yellow circle indicate the outlet on the PMMA mold. (Scale bar = 1 mm)

The PDMS molds were also aligned against the PMMA master mold. It was observed that the PDMS molds could not be aligned with the patterns on the PMMA mold (Figure 4.9). Based on the measurements of the misalignment of the PDMS patterns against the PMMA mold, it was calculated that the PDMS shrunk by about 0.7%. To compensate the shrinking of features during the PDMS curing step, the Autocad designs for the PMMA master molds were scaled up by 0.7%. The resulting cured PDMS molds could be aligned with the patterns of the original PMMA molds.

4.3.2.2 Optimisation of UV-exposure duration for curing thiol-ene mixtures

PDMS materials can suffer from ageing effects when exposed to UV irradiation [18]. Constant exposure of PDMS to UV irradiation will result in changed Young's modulus, chemical properties and changed colouration that will affect its light transmission [19–21]. Of particular interest for the fabrication process described here is the amount of light transmitted through the PDMS block when it was subjected to UV irradiation over time. The changed properties will affect how well the thiol-ene mixtures could be cured in the PDMS molds during UV irradiation. To investigate the changed property and better control the duration of UV irradiation for curing thiol-ene mixtures, a characterization experiment was performed. Table 4.1 clearly shows that exposing PDMS to increasing duration of UV irradiation will decrease the transmittance of UV light through the PDMS. With lesser amount of light transmitted across the PDMS mold would directly affect the duration required for curing thiol-ene mixtures in the PDMS molds (Table 4.1).

Duration of UV exposure (min)	Average UV light transmission	4T+3E Thiol-ene curing duration (s) on each side
0	77.43	35
1	72.43	35
3	71.61	35
8	63.07	40
12	63.42	45
30	47.00	60

Table 4.1. Increased UV exposure to new PDMS layers resulted in a decreased in on the UV-light transmission through the PDMS layer. The amount of UV-light being transmitted through the PDMS will affect the duration required to cure the 4T3E thiol-ene layers. (n = 6)

It was observed that using an older PDMS mold required a longer duration of UV-exposure to cure the thiol-ene mixture in the PDMS molds. This characterization study allow for better control on the duration of UV-exposure to cure or partial-cure thiol-ene layers. This would also ensure the microchips fabricated were similar from batch to batch. Therefore, it was necessary to change the PDMS molds when the duration for curing the thiol-ene mixture required more than 60 min.

4.3.3 Thiol-ene modified porous Teflon membrane

Investigation of Teflon membrane surface using scanning electron microscopic imaging. We next sought to investigate the surface structure of the Teflon membrane after applying and curing the layer of thiol-ene. This was carried out using scanning electron microscopy imaging. Figure 4.10b shows scanning electron microscope (SEM) images detailing the surface morphology of the Teflon membrane after curing a layer of thiol-ene. From the SEM images, the region of the porous Teflon membrane that was cured with a layer of thiol-ene, showed a smooth surface (indicated by blue arrow). However, for the regions that were masked-off and rinsed with methanol, the porous structure of the Teflon membrane [22] was still present (Figure 4.10a). This procedure clearly displayed that the thiol-ene ‘click’ chemistry could be exploited for functionalizing and patterning a membrane as well as surfaces as previously described [8,13].

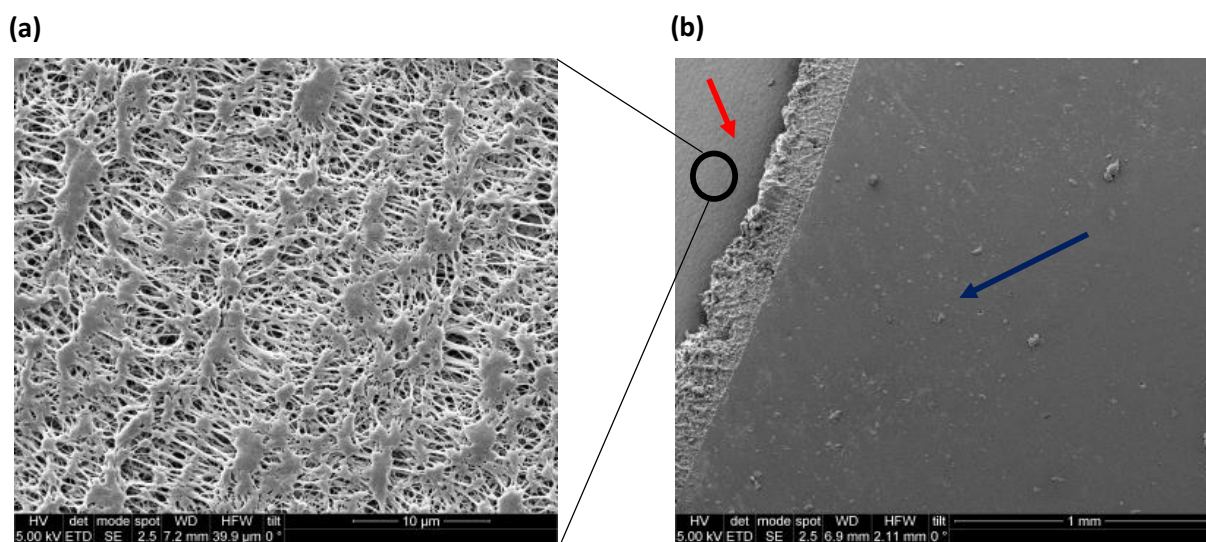


Figure 4.10 Scanning electron microscope (SEM) images of Teflon membrane. Surface morphology was changed significantly after coating a layer of thiol-ene. (A) Expanded view of the un-modified region on Teflon membrane. Observable pores in the membrane; (B) Teflon membrane after coating and curing a layer of thiol-ene. The red arrow indicates the region of membrane that was not coated with thiol-ene. The blue arrow indicate the region that was cured with a coat of thiol-ene. Thickness of thiol-ene coated on membrane is 100 μm .

Wettability of thiol-ene modified Teflon membrane. Wetting behaviours of the membrane were analysed by measuring the contact angle of a drop of DI water on the membrane surface. High wettability correspond to small contact angles ($\leq 90^\circ$), while low wettability correspond to large contact angles ($\geq 90^\circ$). PDMS, PMMA and PC were included in the studies as they are more commonly used as materials in microchip fabrication for cell culture [3,23–28].

The contact angle measurements showed that both PMMA and PC were slightly hydrophilic (Figure 4.11) and PDMS was hydrophobic. The results for these three materials were consistent with reported studies [29–31]. From the contact angle measurements, it was obvious that the thiol-ene layers exhibit a slightly hydrophobic surface (Figure 4.11). Similarly, the thiol-ene coated membrane also exhibited a slight hydrophobic surface (Figure 4.11). A similar test was carried out on the un-coated Teflon membrane. When the drop of liquid was dropped onto the porous Teflon membrane, all the liquid was absorbed (results not shown). The results showed that the layer of cured thiol-ene on the porous membrane changed the wettability of the membrane.

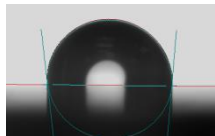
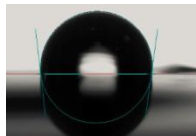
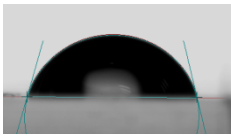
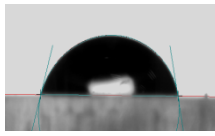
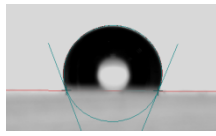
Thiol-ene	Thiol-ene coated membrane	PMMA	PC	PDMS
				
$\alpha = 95.87^\circ$ $\beta = 95.03^\circ$	$\alpha = 96.4^\circ$ $\beta = 96.57^\circ$	$\alpha = 76.73^\circ$ $\beta = 77.13^\circ$	$\alpha = 74.2^\circ$ B = 76.37°	$\alpha = 113.13^\circ$ $\beta = 113.93^\circ$

Figure 4.11 Contact angle measurement of materials typically used in microchip fabrication for cell culture. The contact angle measured on thiol-ene was compared to the other materials. Volume of droplet used for contact angle measurement was 4 μl . Where α = left angle and β = right angle of the droplet. The thiol-ene coated membrane was found to be slightly hydrophobic.

Wettability studies were also carried out on un-modified Teflon membrane and the membrane that was protected during UV exposure. The results showed that both membrane exhibited slight hydrophobicity immediately after the droplet was dispensed. Because the membrane was porous, the membrane absorbed the droplet thus causing the size of the droplet to change gradually over time. Therefore, to determine the contact angle of the droplets on both surfaces, contact angle measurements were recorded at 0 min when the droplet was dispensed onto the surfaces and ≈ 4 min when the droplet was absorbed by the membrane (Figure 4.12). In both membranes, there was no observable droplet on the membrane. The contact angles measured were 0° - 5.1° (Figure 4.11). The results showed the protected regions of thiol-ene coated Teflon membrane that were rinsed with methanol did not affect the wettability property of the membrane.

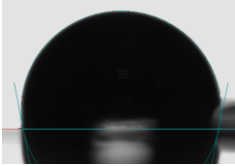

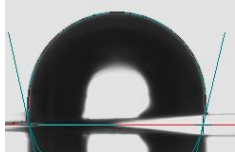

	0 min after dispensing droplet	≈ 4 min after dispensing droplet
Original Teflon membrane	 $\alpha = 101.2^\circ$ $\beta = 101.4^\circ$	 $\alpha = 5.1^\circ$ $\beta = 5.1^\circ$
Protected region of thiol-ene coated membrane	 $\alpha = 102.4^\circ$ $\beta = 103.2^\circ$	 $\alpha = 0^\circ$ $\beta = 0^\circ$

Figure 4.12 Contact angle measurement of original Teflon membrane and the protected region of thiol-ene coated Teflon membrane. Volume of droplet used for contact angle measurement was 2 μl . Where α = left angle and β = right angle of the droplet. The thiol-ene coated membrane was found to be slightly hydrophobic.

Optical transparency of the membrane. By visual observation, the regions where thiol-ene was coated and cured appeared shiny and smooth. Visible light was not able to penetrate through the cured thiol-ene regions on the membrane. In the regions, where the Teflon membrane was protected by the plastic mask during UV-exposure, the membrane looks like the original membrane before thiol-ene modification (black arrow Figure 4.13a).

When the membrane was dry, it appeared white and opaque (black arrow Figure 4.13a). To investigate the wettability and visibility of the regions on the membrane that were protected by the plastic mask during UV-exposure, DI water was dropped onto these surfaces. Once the membrane was wetted, the Teflon membrane became transparent to visible light (red arrows Figure 4.13b).

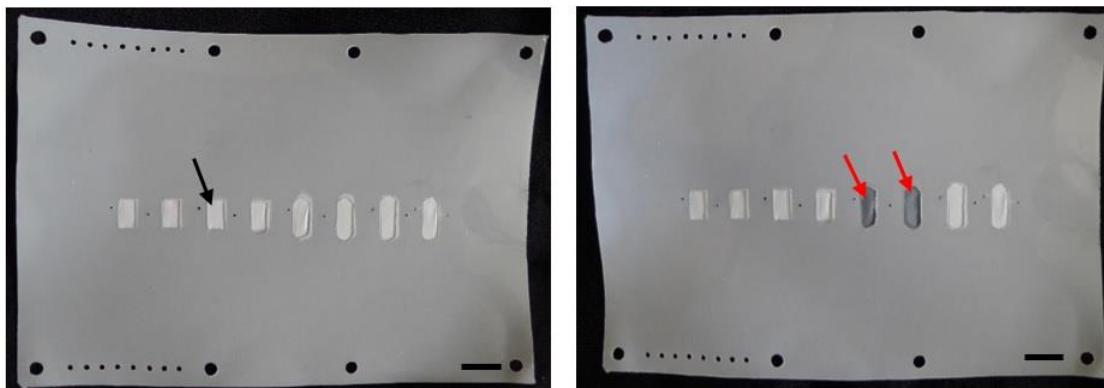


Figure 4.13 Porous Teflon membrane modified with a layer of cured thiol-ene mixture (3T+3E). Black arrow indicating the region on porous membrane that was protected by a plastic mask during UV-exposure. When dry, the region appeared white and opaque. (b) Two chambers were wetted with DI water, as indicated by red arrows. Teflon membrane becomes transparent in visible light. (Scale bar = 5 mm)

4.3.4 Bond testing of microchip

Previously, Silkane et. al. [6] reported their investigations on the bond strength of thiol-ene layers. The thiol-ene layers were fabricated using extra thiol- groups or extra allyl groups in the thiol-ene mixtures. There have been no reports thus far on fabricating thiol-ene microchips comprising of different thiol- and allyl mixtures in stoichiometric ratios. To understand if the bonding of the thiol-ene layers was feasible for the pressure driven flow (generated by the fluidic system), a burst pressure test was carried out. It was also necessary to investigate the bond strength of the different thiol-ene layers at 37 °C, the temperature for cell culture. Three different types of microchips comprising of different thiol-ene layers were subjected to the burst pressure test at two different temperatures.

At 25 °C, 3T3E + 3T3E microchip was stiff and it could withstand burst pressures of 2.0 ± 0.66 Bar. However, when it was heated to 37 °C, the microchip softened tremendously and was readily bendable. The pressures that the microchip could withstand was reduced to < 0.3 bar and it was a challenge to record as the layers delaminated immediately upon supplying little pressure to the microchip.

The pressure test for the microchip that was fabricated using the 4T3T + 4T3E combination could not be carried out at both temperatures. The cured thiol-ene layers could not adhere to each other during the final curing process (Final fabrication step in Figure 4.3)

For the last microchip combination 4T3E + 3T4E (Table 4.2), at both temperatures, there were no observable changes to the pressures that the microchip was able to withstand. This microchip was able to withstand pressures of more than 6 Bars. This value was more than the 0.3 bar [32,33] that the entire system will be

subjected to during the entire cell culture period. Brute force was used to pry the 4T3E, 3T3E layers apart. By doing so, the thiol-ene layers were totally destroyed.

Sample	Maximum pressure (Bars)	Temperature
3T3E + 3T3E	2.0 ± 0.66	25 °C
4T3E + 4T3E	Layers could not be bonded	
4T3E + 3T3E	> 6.0	
3T3E + 3T3E	< 0.3	37 °C
4T3E + 4T3E	Layers could not be bonded	
4T3E + 3T3E	> 6.0	

Table 4.2 Tabulated data of the maximum pressure the different thiol-ene mixtures used for fabricating the microchips could withstand in different temperature conditions. All thiol-ene mixtures were prepared in stoichiometric ratios. Where 4T = tetra-thiol, 3T = tri-thiol and 3E = tri-allyl. (n = 6)

4.4 Discussion

Shrinkage of PDMS molds

In designing and fabricating a microfluidic chip, there are many issues requiring much attention and consideration. One of the first issues to resolve in fabricating the thiol-ene microchip was the shrinkage of PDMS molds during thermal curing. Previous literature reported on PDMS undergoing a small degree of shrinkage during thermal curing [34–37]. As shown from the reported results in this chapter, the PDMS molds shrank by 0.7 % after thermal curing (Figure 4.9). This reduction in the PDMS mold was later transferred to the cured thiol-ene layer. Shrinkage of the PDMS may eventually pose some challenges in systems where alignment of components are crucial. For example the cell culture platform chosen to integrate the thiol-ene microchip for cell culture, the necessary MainSTREAM components on the platform for cell culture are fixed in positions with screws [2,3]. The distance between each inlet holes (diameter 0.24 mm) of the fluidic interconnections on the fluidic platform is 2.25 mm (this will be further discuss in chapter 5). For the fluidic system to effectively pump reagents to and from the microchip, the inlet and outlet ports on the microchip must be well aligned with the MainSTREAM components to avoid leakage. Several approaches reported in literature to resolve the shrinkage of PDMS included modifying PDMS material [38], curing PDMS in room temperature [39] and to characterise the degree of shrinkage of PDMS and scale the master size accordingly

[35]. In this project, to resolve the issue of the PDMS shrinkage, the Autocad designs of the PMMA master molds were enlarged by 0.7 %.

Effect of aged PDMS molds on microchip fabrication

How well the thiol-ene mixtures cured in the PDMS molds is dependent on the duration of UV-exposure and strength of UV light [13] on the thiol-ene mixtures. This would also indirectly affect the bond strength between cured thiol-ene layers. Additionally, any monomers that are not cross-linked, can leach into the fluidic streams and this may cause undesirable effects to the cell cultures. The characterization studies on the duration of UV irradiation on PDMS and the implications on the duration for curing thiol-ene mixtures were displayed in Table 4.1. Having this knowledge of UV irradiation on the PDMS is powerful as this enable the user to control how well the thiol-ene mixture could be cured. Furthermore, PDMS molds have a limited number of use. Therefore, this knowledge would also ensure the fabrication of reproducible microchips.

Enhancing bond strength between thiol-ene layers by controlling the duration of UV-irradiation

Recently, Calborg et. al. [7] reported on carrying out two step UV exposure (using 2 different UV wavelengths) on the off-stoichiometric thiol-ene epoxy (OSTE+). The authors reported, in the first curing process, the thiol-ene layers were partially cured due to partial conversion of the thiol groups. However, with the second UV-exposure, full conversion of thiol and allyl groups would enhance the mechanical properties of the OSTE+. Natali et. al. [13] also reported on carrying out 2-step UV curing of thiol-ene mixtures to improve the bond strength between the thiol-ene layers. The authors reported that a partially cured thiol-ene was produced in the first step of UV curing. Following that, the second UV-exposure (hard cure) would yield a hard assembly of thiol-ene layers.

In the fabrication process of the thiol-ene microchip described here, a two-step curing process of the different thiol-ene mixtures was also carried out. Instead of exposing the thiol-ene mixtures to different UV wavelengths, in the first curing step (curing of the thiol-ene fluidic layers), the duration was shortened (40 s instead of 45 s) to yield partial cured thiol-ene layers. The partial cured thiol-ene layers exhibited sticky surfaces and were pliable. The sticky surface of the partial cured thiol-ene layer allowed better adherence to another surface. The sticky surface of the partially cured thiol-ene layer was due to the presence of partial conversion of thiol and allyl groups [9]. Since the functional group conversion with UV exposure follows an asymptotic curve [9], the second UV exposure would result in complete conversion of the thiol and allyl groups. This will yield a hard and well bonded multi-layer microchip. This was demonstrated from the pressure burst studies (Table 4.2). The studies revealed that using the 2-step curing of the thiol-ene mixtures (microchips

fabricated with 4T3E + 3T3E) enabled the chips to withstand burst pressures of more than 6 bars. This would also ensure that the microchip could withstand the pressure (0.3 Bars) that the entire device would be subjected to during cell culture. This would be further discussed in chapter 5.

Modifying porous Teflon membrane with Thiol-ene.

One of the most critical steps in microchip fabrication is sealing of open microchannels to produce the final enclosed microfluidic chip. A number of considerations must be taken into account when selecting and implementing the appropriate bonding method. Bonding of dissimilar materials is always a big challenge because the materials have different surface chemistry and may not be compatible. This was also mentioned previously in Chapter 3 on the bonding of the porous membrane between the fluidic layers. Ferrell et. al. [40] recommended using medical grade epoxy for bonding of porous membrane to the fluidic layers. Few groups reported on using a PDMS mortar to ensure a tight sealing [25,41–43]. This method required a thin layer of PDMS prepolymer, spin-coated on a glass slide, was transferred to PDMS substrates with channel features as well as to the edges of the porous membrane by stamping. Following that, the entire device was thermally cured. However, this method is not applicable for the thiol-ene microfluidic chip as the fluidic layers are not fabricated with PDMS. One of the simplest method for bonding of dissimilar materials (especially a thermoset to thermoplastic) is by means of adhesive materials. However it was shown previously [27] epoxy resin was capable of inducing cytotoxicity.

Although there are numerous methods for bonding dissimilar materials, however, none of them were suitable for bonding the porous membrane to the thiol-ene fluidic layers. Nevertheless, by modifying the surface of the Teflon membrane with thiol-ene enabled the porous membrane to be bonded to the thiol-ene fluidic layers. To date there are no reports on the ability to modify the surface of the porous Teflon membrane with thiol-ene to enable it to be bonded with another thiol-ene surface. This form of microchip fabrication paves a new way of bonding a thermoplastic with a thermoset. Furthermore, the possibility of using a plastic mask to prevent localised regions on the porous membrane from being modified during UV irradiation is advantageous. We have demonstrated that these unmodified regions were transparent to white light when wetted. This is beneficial for real-time microscopic studies to be performed when the cells are cultured in these regions. Furthermore, the ability of wetting only the regions where the membrane's porosity and structure were not modified was advantageous. This changed property of the membrane, would eliminate the chances of cross-contamination between microchannels and microchambers during perfusion of reagents into the microfluidic chip. This would be further proven in the cell culture experiments (Chapter 5, 6, 7) and in chapter 8 where Caco-2 cells were co-cultured with *E. coli*.

However, when performing the modification of the Teflon membrane, the plastic mask for protecting the microchambers from being exposed to UV irradiation in step 4 of Figure 4.4B must be well aligned. Otherwise, some other complications may arise when performing transport studies across the cells.

Biocompatibility studies of thiol-ene with Caco-2 cells

In designing a microfluidic chip for cell culture, the material chosen for fabricating the microchip must be non-cytotoxic. Otherwise, complications will arise during cell culture. To our knowledge, there are no literature available reporting on the biocompatibility of thiol-ene with Caco-2 cell culture. The results of the biocompatibility studies presented in section 4.4.1 showed that the Caco-2 cells cultured in the presence of the thiol-ene materials were comparable to the Caco-2 cells in the control wells (Figure 4.8). Although the cells were observed to multiply, there is a need to further investigate the viability of the cells. Live/dead cell staining of the cell cultured in the thiol-ene microfluidic chip will be further discussed in chapter 5 of the thesis. Importantly, the results presented in this chapter, showed that thiol-ene is a promising material for long term Caco-2 cell culturing.

4.5 Conclusion

In this chapter, two totally new designs of the microfluidic chip architecture were discussed. The newly designed microfluidic chips comprised of three layers and contained a total of eight microchambers each having its own inlet and outlet. The presence of eight microchambers, will increase the throughput for biological experiments. In the new microfluidic chip designs, the assembly of the microchip simplified tremendously compared to the complicated assembly of the PMMA chip discussed in chapter 3.

With the thiol-ene microfluidic chip presented in this chapter, much optimisation and characterisation studies on the material were performed. One of the first studies carried out was to investigate on the biocompatibility of thiol-ene. The biocompatibility studies clearly showed thiol-ene is biocompatible for Caco-2 cell culture. In this chapter, it was also clearly demonstrated that wettability and functionality of a porous Teflon membrane could be potentially changed by coating and curing a layer of thiol-ene mixture on it. Besides, the thiol-ene ‘click’ chemistry could be leverage for patterning the thiol-ene coated Teflon membrane.

To yield the best bonding between the different layers, a partial curing of the thiol-ene mixtures in the first UV-exposure was implemented. Once the layer were aligned, a second curing step completed the reaction

between the available thiol- and allyl groups from the first partial cure. Hence yielding a very hard microfluidic chip that could withstand more than 6 Bars. From all the characterisation and optimisation studies carried out with the different cured thiol-ene layers, it was clearly demonstrated that the thiol-ene microfluidic chip comprising of 4T+3E for the fluidic layers and 3T + 3E for the membrane layer yielded the best bond strength. The results presented in this chapter showed that the thiol-ene microchip is a very promising device for long time cell culture.

References

- [1] D. Sabourin, D. Snakenborg, M. Dufva, Interconnection blocks with minimal dead volumes permitting planar interconnection to thin microfluidic devices, *Microfluid. Nanofluidics*. 9 (2009) 87–93..
- [2] D. Sabourin, P. Skaft-Pedersen, M.J. Sjøe, M. Hemmingsen, M. Alberti, V. Coman, et al., The MainSTREAM component platform: a holistic approach to microfluidic system design, *J. Lab. Autom.* 18 (2013) 212–28.
- [3] P. Skaft-Pedersen, M. Hemmingsen, D. Sabourin, F.S. Blaga, H. Bruus, M. Dufva, A self-contained, programmable microfluidic cell culture system with real-time microscopy access, *Biomed. Microdevices*. 14 (2012) 385–99.
- [4] P. Skaft-Pedersen, D. Sabourin, M. Dufva, D. Snakenborg, Multi-channel peristaltic pump for microfluidic applications featuring monolithic PDMS inlay, *Lab Chip*. 9 (2009) 3003–6.
- [5] N.A. Feidenhans'l, J.P. Lafleur, T.G. Jensen, J.P. Kutter, Surface functionalized thiol-ene waveguides for fluorescence biosensing in microfluidic devices, *Electrophoresis*. 35 (2013) 282–288.
- [6] T.M. Sikanen, J.P. Lafleur, M.-E. Moilanen, G. Zhuang, T.G. Jensen, J.P. Kutter, Fabrication and bonding of thiol-ene-based microfluidic devices, *J. Micromechanics Microengineering*. 23 (2013) 037002.
- [7] C.F. Carlborg, A. Vastesson, Y. Liu, W. van der Wijngaart, M. Johansson, T. Haraldsson, Functional off-stoichiometry thiol-ene-epoxy thermosets featuring temporally controlled curing stages via an UV/UV dual cure process, *J. Polym. Sci. Part A Polym. Chem.* 52 (2014) 2604–2615.
- [8] C.F. Carlborg, T. Haraldsson, K. Öberg, M. Malkoch, W. van der Wijngaart, Beyond PDMS: off-stoichiometry thiol-ene (OSTE) based soft lithography for rapid prototyping of microfluidic devices., *Lab Chip*. 11 (2011) 3136–47.
- [9] C.E. Hoyle, T.Y. Lee, T. Roper, Thiol-enes: Chemistry of the past with promise for the future, *J. Polym. Sci. Part A Polym. Chem.* 42 (2004) 5301–5338.
- [10] C.E. Hoyle, C.N. Bowman, Thiol-ene click chemistry, *Angew. Chemie*. 49 (2010) 1540–73.
- [11] J.P. Lafleur, R. Kwapiszewski, T.G. Jensen, J.P. Kutter, Rapid photochemical surface patterning of proteins in thiol-ene based microfluidic devices, *Analyst*. 138 (2013) 845–9.

- [12] C. Errando-Vastesson, H. Alexander, M. Zelenina, G. Pardon, B. Gunnar, W. van der Wijngaart, et al., Biocompatibility of OSTE polymers studies by cell growth experiments, in: 17th Int. Conf. Miniaturized Syst. Chem. Life Sci., Freiburg, 2013: pp. 143–145.
- [13] M. Natali, S. Begolo, T. Carofiglio, G. Mistura, Rapid prototyping of multilayer thiolene microfluidic chips by photopolymerization and transfer lamination, *Lab Chip*. 8 (2008) 492–4.
- [14] E. Berthier, E.W.K. Young, D. Beebe, Engineers are from PDMS-land, Biologists are from Polystyrenia., *Lab Chip*. 12 (2012) 1224–37.
- [15] S.Z. Jokhadar, V. Suštar, S. Svetina, U. Batista, Time lapse monitoring of Caco-2 cell shapes and shape dependence of the distribution of integrin $\beta 1$ and F-actin on their basal membrane, *Cell Commun. Adhes.* 16 (2009) 1–13.
- [16] J.C. Salamone, *Polymeric Materials Encyclopedia*, CRC Press Taylor & Francis Group, 1996.
- [17] J.M. Fisher, *Handbook of molded part shrinkage and warpage*, 1st ed., Cambridge University Press, 2003.
- [18] W.T.S. Huck, N. Bowden, P. Onck, T. Pardoën, J.W. Hutchinson, G.M. Whitesides, Ordering of spontaneously formed buckles on planar surfaces, *Langmuir*. 16 (2000) 3497–3501.
- [19] C.G. Zimmermann, On the kinetics of photodegradation in transparent silicones, *J. Appl. Phys.* 103 (2008) 083547.
- [20] B. Schnyder, T. Lippert, R. Kötz, A. Wokaun, V.-M. Graubner, O. Nuyken, UV-irradiation induced modification of PDMS films investigated by XPS and spectroscopic ellipsometry, *Surf. Sci.* 523 (2003) 1067–1071.
- [21] H.R. Fischer, C. Semprimoschnig, C. Mooney, T. Rohr, E.R.H. van Eck, M.H.W. Verkuijen, Degradation mechanism of silicone glues under UV irradiation and options for designing materials with increased stability, *Polym. Degrad. Stab.* 98 (2013) 720–726.
- [22] Transwell inserts, www.corning.com.
- [23] H.J. Kim, D. Huh, G. Hamilton, D.E. Ingber, Human gut-on-a-chip inhabited by microbial flora that experiences intestinal peristalsis-like motions and flow, *Lab Chip*. 12 (2012) 2165–74.
- [24] H.J. Kim, D.E. Ingber, Gut-on-a-chip microenvironment induces human intestinal cells to undergo villus differentiation, *Integr. Biol.* 5 (2013) 1130–40.
- [25] D. Gao, H. Liu, J.-M. Lin, Y. Wang, Y. Jiang, Characterization of drug permeability in Caco-2 monolayers by mass spectrometry on a membrane-based microfluidic device, *Lab Chip*. 13 (2013) 978–85.
- [26] Y. Imura, Y. Asano, K. Sato, E. Yoshimura, A microfluidic system to evaluate intestinal absorption, *Anal. Sci. Int. J. Japan Soc. Anal. Chem.* 25 (2009) 1403–1407.
- [27] M. Stangegaard, A biocompatible micro cell culture chamber (μ CCC) for culturing and on-line monitoring of Eukaryotic cells, Technical University of Denmark, 2005.
- [28] M. Tehranirokh, A.Z. Kouzani, P.S. Francis, J.R. Kanwar, Microfluidic devices for cell cultivation and proliferation, *Biomicrofluidics*. 7 (2013) 1–32.
- [29] J. Wu, N.Y. Lee, One-step surface modification for irreversible bonding of various plastics with a poly(dimethylsiloxane) elastomer at room temperature, *Lab Chip*. 14 (2014) 1564–71.

- [30] K. Tokuda, T. Ogino, M. Kotera, T. Nishino, Simple method for lowering poly(methyl methacrylate) surface energy with fluorination, *Polym. J.* 47 (2014) 66–70.
- [31] D. Briggs, H. Chan, M.J. Hearn, D.I. McBriar, H.S. Munro, The contact angle of poly(methyl methacrylate) cast against glass, *Langmuir.* 1 (1990) 420–424.
- [32] M. Hemmingsen, Usability and Applicability of Microfluidic Cell Culture Systems, Technical University of Denmark, 2012.
- [33] P. Skafte-Pedersen, Microfluidic cell culture systems for real-time studies of cells, Technical University of Denmark, 2011.
- [34] O.C. Jeong, S. Konishi, Controlling the size of replicable polydimethylsiloxane (PDMS) molds/stamps using a stepwise thermal shrinkage process, *Microelectron. Eng.* 88 (2011) 2286–2289.
- [35] J.S. Marcus, W.F. Anderson, S.R. Quake, Microfluidic single-cell mRNA isolation and analysis, *Anal. Chem.* 78 (2006) 3084–9.
- [36] C. Moraes, Y. Sun, C.A. Simmons, Solving the shrinkage-induced PDMS alignment registration issue in multilayer soft lithography, *J. Micromechanics Microengineering.* 19 (2009) 065015.
- [37] S.W. Lee, S.S. Lee, Shrinkage ratio of PDMS and its alignment method for the wafer level process, *Microsyst. Technol.* 14 (2007) 205–208.
- [38] K.M. Choi, J.A. Rogers, A photocurable poly(dimethylsiloxane) chemistry designed for soft lithographic molding and printing in the nanometer regime, *J. Am. Chem. Soc.* 125 (2003) 4060–1.
- [39] H. Wu, T.W. Odom, D.T. Chiu, G.M. Whitesides, Fabrication of complex three-dimensional microchannel systems in PDMS, *J. Am. Chem. Soc.* 125 (2003) 554–9.
- [40] N. Ferrell, R.R. Desai, A.J. Fleischman, S. Roy, H.D. Humes, W.H. Fissell, A microfluidic bioreactor with integrated transepithelial electrical resistance (TEER) measurement electrodes for evaluation of renal epithelial cells, *Biotechnol. Bioeng.* 107 (2010) 707–16.
- [41] R. Booth, H. Kim, Characterization of a microfluidic in vitro model of the blood-brain barrier (μ BBB)., *Lab Chip.* 12 (2012) 1784–92.
- [42] N.J. Douville, Y.-C. Tung, R. Li, J.D. Wang, M.E.H. El-Sayed, S. Takayama, Fabrication of two-layered channel system with embedded electrodes to measure resistance across epithelial and endothelial barriers, *Anal. Chem.* 82 (2010) 2505–11.
- [43] B.H. Chueh, D. Huh, C.R. Kyrtsos, T. Houssin, N. Futai, S. Takayama, Leakage-free bonding of porous membranes into layered microfluidic array systems, *Anal. Chem.* 79 (2007) 3504–3508.

CHAPTER 5: Integrating thiol-ene microchip with fluidic system for cell culture

In designing and fabricating a microfluidic perfusion cell culture system, a very large part of the reported literature have been focused on the microchip level [1–5]. However, for the microfluidic chip device to function fully, fluid volumes must be transported and displaced from region to region in the chip. This is possible by using valves and pumps that can be externally connected to the microfluidic device or directly built into the system [6].

Earlier in Chapter 4, the two different thiol-ene microchip designs presented each had 16 inlets (eight inlets for each fluidic layer) and 16 outlet ports (eight outlets or each fluidic layer). To realise the possibility of parallel perfusion of reagents in and out from all 32 ports on the microchip, the MainSTREAM components [7,8] were adopted to the thiol-ene chip. In the following chapter, integration of the two different designs of the thiol-ene microfluidic chips (Chapter 4) to the fluidic system is described. Some preliminary cell cultures were attempted to investigate the better microchip design for long term-cell culture.

5.1 Fluidic system for microfluidic cell culture

For a microfluidic perfusion culture system to perform successfully, robust packaging is a crucial factor. Some of the major packaging challenges are in the sealing of the microfluidic chip, the chip-to-world interface, portability of the system and bubble-free operation [9]. The chip-to-world interface refers to the connections between the microfluidic network and macroscale components such as valves and pumps. To overcome the above mentioned challenges, we adopted the MainSTREAM components [8,10,11] onto a platform.

As described previously in chapter 4, each of the thiol-ene microchip designs (Figure 4.1) contained eight microchambers and each microchamber consisted of two inlet and two outlet ports, whereby one set of inlet and outlet port was connected to the top layer and one set of inlet and outlet ports to the bottom layer. To enable effective parallel perfusion of reagents to all eight microchambers on the same layer, a suitable peristaltic micropump with eight pumplines was necessary.

Each of the MainSTREAM micropump has eight pumplines [12,10,11] with integrated 240 μm wide circular channels spaced 2.25 mm center-to-center [7,8]. The pumplines also have integrated, reversibly sealing ball

joint interconnections with a self-aligning feature [10]. Thus, the peristaltic micropumps could easily be connected to the inlets or outlets of the microchip using four M2 screws. Having two sets of MainSTREAM micropumps and interconnection components enable the perfusion of reagents into and out from the respective 16 inlets and outlet ports on the microchip. Moreover, all components can be reversibly connected using standard screws [8]. This platform (with the MainSTREAM components) is robust, portable and reported to culture cells successfully for long periods [8]. Thus, the MainSTREAM peristaltic micropumps and components were suitable to be integrated onto the platform with the thiol-ene microchip.

Furthermore, by subjecting the entire system under pressure, the presence of air bubbles could be eliminated [13,14].

5.2 Materials and methods

5.2.1 Assembling of the microfluidic perfusion cell culture system

Base plate of cell culture system. The architecture of the fluidic platform consisted of an assembly of the system base plate, onto which various components were fixed by screws. Design of the assembly of the base plate was drawn using the CAD software, Autocad 2012 and micromilled (Figure 5.1). The assembly of the base plate consisted of two pieces of 5 mm thick polycarbonate (PC) blocks (Figure 5.1). Whereby the bottom piece was the microscope stage plate that had a recess matching the dimensions of the thiol-ene microchip. Attached on the microscope stage plate was the outer base plate that supported the reservoir racks and motors. Screws were used to fix the microscopic base plate and outer base plate in position.

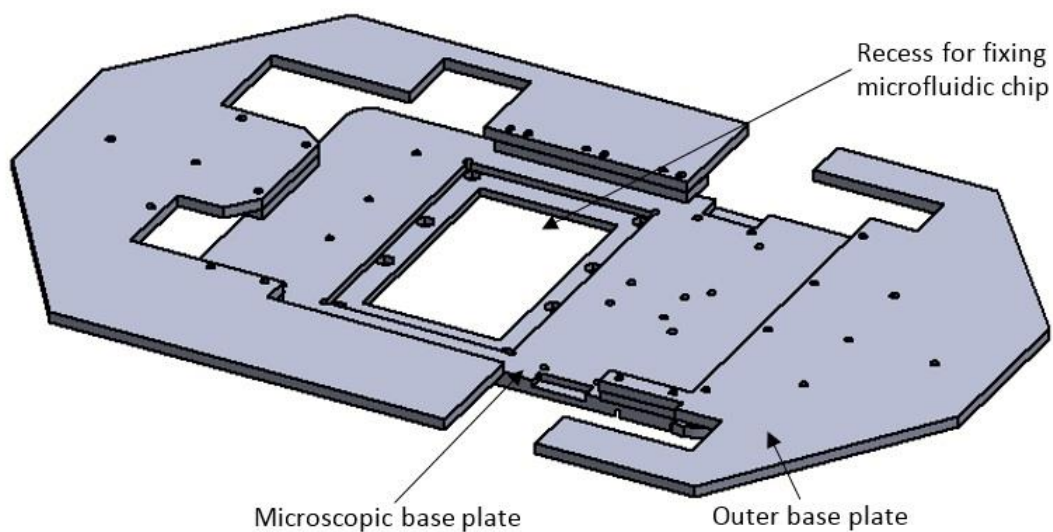


Figure 5.1 Schematic drawing of the assembly of base plate for the cell culture platform

Integrating microfluidic chip with the fluidic system. The thiol-ene microfluidic chip was assembled onto the platform and bolted down in place with eight M2 screws (Figure 5.2). The MAINSTREAM components adopted onto the platform for cell culturing with the thiol-ene microfluidic chip comprised of:

1. 2 x 8 pumplines in the peristaltic MAINSTREAM micropumps
2. 2 cell loading components
3. 2 intermediate connection components
4. Poly(tetrafluoroethylene) (PTFE) tubings (Bola, Germany). Inner diameter (ID) 0.8 mm for air pressure network and ID 0.2 mm for perfusing of reagents into and from microfluidic chip
5. Glass vials (Mikrolabs, Denmark)
6. 2 sets of LEGO MINDSTORM's motor and controller

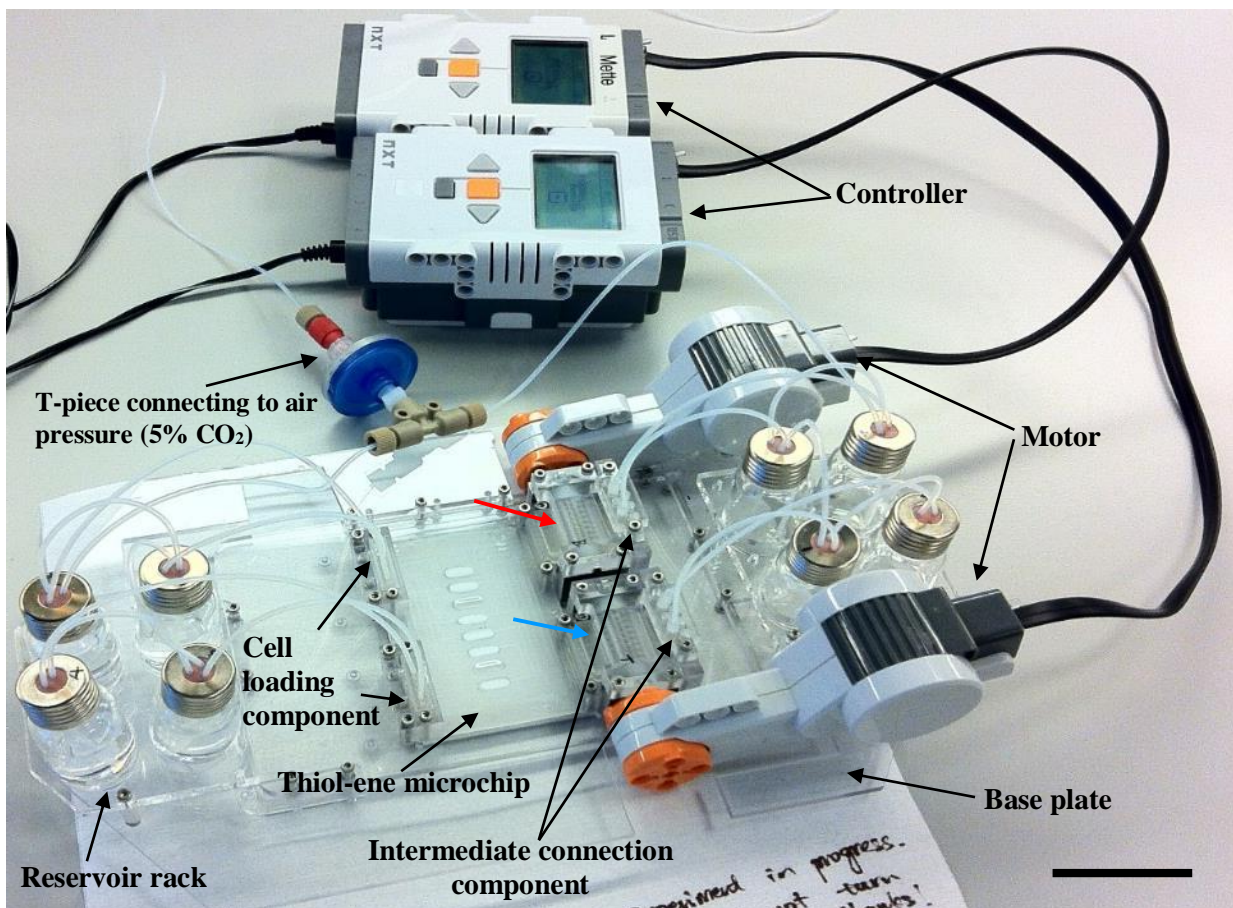


Figure 5.2 Assembled thiol-ene microfluidic chip (design 1) with the cell culture platform. Blue arrow indicating the micropump perfusing through the top layer. Red arrow indicating the peristaltic micropump perfusing through the bottom layer. (Scale bar = 5 cm)

Micropumps. The micropumps have integrated, reversibly sealing ball joint interconnections with a self-aligning feature [10]. Thus, the peristaltic micropumps could be easily connected to the outlets of the microchip using four M2 screws (Figure 5.2). The micropumps were programmed to pump the reagents through the microchip from the glass vials (positioned at the inlets of the microchip). The micropump indicated by blue arrow in Figure 5.2, was set to perfuse reagents through the top layer. While the other peristaltic micropump (indicated by the red arrow Figure 5.2) was set to perfuse reagents through the bottom layer.

Actuation and control of micropumps. Fluidic actuation was provided by LEGO® Mindstorms® MXT 2.0 robotics kit. The LEGO® Mindstorms® MXT 2.0 robotics kit provides servo motors (with 1° angle control), a small controller (Figure 5.2), and a software interface (powered by National Instruments LabView®) for programming of the motors. With the software, it was possible to pre-program the flow rates or breaks over time.

Sample to waste management. The glass vials were placed onto a rack, integrated onto the microfluidic cell culture platform. Glass vials were interfaced to the microchip and micropumps using tube connectors. The two cell loading components (Figure 5.2) were connected to the inlets of the microchip. The design and concept of the cell loading component have been reported previously [13,14]. Each of these cell loading components comprised of eight channels/wells, based on the connection of eight fluidic channels in one step. The cell loading chip was fabricated from polycarbonate (PC) with a middle piece casted in PDMS. The cell loading components were placed directly on top of the inlet holes of the microfluidic chip. The channels/wells of the cell loading component were connected to the glass vials with PTFE tubings (ID 0.2mm and OD 1.6mm). The middle piece made out of PDMS in the cell loading component, allowed the force-fitting of the PTFE tubes, thereby making a proper tight sealing.

An intermediate connection chip with an array of eight holes with inner diameter of 3 mm was interfaced with the micropump to allow fluids to be pumped from the micropump into the glass vials via PTFE tubings (Figure 5.2). Small pieces of silicone tube could be individually press fit into the holes as sealing gasket (Figure 5.2). This method has been found to be simple and leak-free [11].

Connection to pressurized air source. The glass vials were coupled with PTFE tubings and pressurized with an air and 5% CO₂ mixture (0.3 bar) through a sterile filter with a single Luer-Lok fitting (Figure 5.2). This principle of pressuring the entire system for cell culture was previously introduced [13,14].

5.2.2 Preparation of microfluidic system for cell culture

Prior to assembling the system, the glass vials and tubings were autoclaved. Once the entire system was assembled (described in section 5.2.1) the glass vials were filled with 70 % ethanol (Sigma, Denmark). Air

pressure was connected to the T-piece of the entire system at a pressure of 0.3 Bars. Next, the pumps were activated to pump at a flow rate of 5 $\mu\text{l}/\text{min}$. 70 % ethanol was perfused throughout the entire system for 2 hrs to sterilise the entire system. Following that, sterile water (Sigma; Denmark) was flushed into the entire system for an additional 2 hours. Perfusion of sterile water was required to remove all traces of ethanol.

An extra cellular matrix (ECM) mixture of 300 $\mu\text{g}/\text{ml}$ matrigel (Corning®, Sigma, Denmark), 50 $\mu\text{g}/\text{ml}$ collagen Type I (BD Bioscience, Denmark) in serum-free Dulbecco's Modified Eagle's medium (DMEM, Sigma, Denmark) was prepared. This mixture was flowed into the microchip for 2 hrs. During the coating procedure, the entire microfluidic system was incubated at 37°C with an air atmosphere of 5 % CO₂ in a standard cell culture incubator. After 2 hrs, normal cell culture medium was perfused through the entire system for more than 20 hrs at 37 °C with an air atmosphere of 5 % CO₂.

5.2.3 Cell seeding and cell culture in microfluidic system

Preparation of cell suspension for microfluidic system. Two different types of cell lines were used: HeLa cells (Passage 48) and Caco-2 cells (Passage 45). HeLa cells and Caco-2 cells were cultured separately in individual T-75 cell culture flasks. The cell culture medium used for culturing the cells was DMEM supplemented with 10% (v/v) heat-inactivated fetal bovine serum (FBS; Sigma, Denmark), 1% (v/v) nonessential amino acids (NEAA; Gibco, Denmark) and 1% (v/v) penicillin-streptomycin (P/S; Gibco, Denmark). The cells were harvested using a trypsin/EDTA solution (Sigma; Denmark). Subsequently, they were centrifuged at 125 xg for 5 min. After removing the supernatant, a culture medium containing 60 % FBS was added to the cell pellets to re-suspend the cells. The culture medium with a higher content of FBS was used to increase the density of the cell suspension. This would allow better distribution of the cells within the cell culture chamber during cell seeding procedure [14]. Cells were counted using the cell counter (Moxi-Z; Orflo, Denmark). The cell suspensions were prepared to concentrations of 0.5 x 10⁶ cells/ml and 10 x 10⁶ cells/ml for Caco-2 cells and 0.5 x 10⁶ cells/ml for HeLa cells.

Seeding of cells in microfluidic system. Prior to cell seeding, the Teflon tubings connecting to the cell loading components for the top fluidic layer were carefully removed. The re-suspended cell solutions were manually loaded into the cell loading channels/wells (Figure 5.2) with a 1 ml syringe attached with a 23G needle. To draw the cell suspensions into the microchambers, the micropumps (indicated with blue and red arrows in Figure 5.2) were activated to drag the cell suspensions at a rapid flow rate of $\approx 65 \mu\text{l}/\text{min}$.

Following that, the Teflon tubings were connected back to the cell loading channels/wells. Extra care was taken when connecting the tubes to prevent any introduction of air into the microchip. Next, the entire system was placed onto the microscope stage. The microchambers were observed microscopically to ensure the cells

were loaded into the chambers. Lastly, the entire system was placed in an incubator for 2 hr with no flow. This step was necessary to ensure the cells attached onto the ECM coated membrane prior to starting the flow. After 2 hrs, flow perfusing to the upper fluidic layer of the thiol-ene microchip was activated at a flow rate of 0.5 $\mu\text{l}/\text{min}$. 24 hrs later, flow perfusing to the bottom fluidic layer was also activated at a flow rate of 0.5 $\mu\text{l}/\text{min}$. The glass vials connected to the inlets were replenished with fresh cell culture media on alternate days.

5.2.4 Cell imaging and live/dead cell staining

The growth of the cells was microscopically monitored with an inverted microscope (Axio Observer Z1, Carl Zeiss, Germany). Phase contrast images of the cells were taken daily at four different positions of each chamber. During the microscopic imaging of cells, the flow of cell culture medium was discontinued.

Live/dead cell staining was performed on the cells on day 6 of cell culture for HeLa cells and day 11 for Caco-2 cells. Fluorescent dyes, calcein and ethidium homodimer-1 (Life Technologies; Denmark) were used for staining live and dead cells respectively. Sterile phosphate buffer saline (PBS; Sigma, Denmark) was first perfused into the chambers for 30 min at a flow rate of 5 $\mu\text{l}/\text{min}$ to remove all traces of DMEM. Next, the dyes diluted in PBS (1:1000 for calcein; 1:500 for ethidium homodimer-1) were flowed into the microchamber and incubated for 30 min at 37 °C. Following that, PBS was flowed into the system to remove all traces of the unbound stains in the channels prior to imaging the cells.

Fluorescent imaging of the cells were carried out with the inverted microscope. To image the live cells, excitation/emission wavelengths of 495/517 nm was chosen and for dead cells, excitation/emission wavelengths of 528/617 nm was chosen. The fluorescent images were processed by the software (AxioVision SE64Rel. 48).

5.2.5 Flow profile in microchamber

Fluid flow simulation. Simulation of the fluid flow was carried out based on the two different microchip designs discussed in Chapter 4 (Figure 4.1). 2-dimensional (2D) simulations were performed using the commercially available software, COMSOL 5.0 Multiphysics (COMSOL A/S, Denmark). The flow rate was set at 3 $\mu\text{l}/\text{min}$. The simulations were performed assuming the flow within the microchannels was laminar and the walls were stationary. The fluid velocities were solved with Navier-Stokes equations (eq 2.2):

$$\text{Eq. 2.2:} \quad \rho \left[\frac{\partial u}{\partial t} + (u \cdot \nabla)u \right] = -\nabla P + \eta \nabla^2 u$$

And the continuity equation is given by:

Eq. 2.3:
$$\nabla \cdot u = 0$$

where ρ is the density of fluid, u is fluid velocity, t is time, P is the pressure and η is fluid viscosity. No slip boundary at the walls of the microchannels was chosen for the simulation.

5.3 Results

5.3.1 System evaluation

All the results reported in this section were performed using thiol-ene microchip design 1 (described in chapter 4). Previously in chapter 3, two of the major set-backs in that entire system were the persistent appearance of bubbles and leaking in the microchip. To evaluate if this new fluidic platform was able to address those challenges, cell culture medium was perfused into the entire system at a flow rate of 5 $\mu\text{l}/\text{min}$. During perfusion of cell culture medium, the entire microfluidic paths (inlets to outlets) was pressurised at 0.3 bars. The microfluidics system was left to perfuse for at least 20 hrs in room temperature and incubator conditions.

In this preliminary study, cell culture medium was perfused through only two microchambers (microchamber 3 and 4). Once the pumps were activated, the system was carefully scrutinized for leaking at the interconnections between microchip and components and any bubble formation.

Leaking of fluids at the interconnections between the microchip and fluidic components was not observed when the system was functioning at room temperature or at 37 °C. Only the microchambers that supported cell culture medium perfusing through the microchannels, showed observable wetting of the porous membrane (black arrows in Figure 5.3). The microchambers appeared pink (Figure 5.3) and they were transparent to visible light. Furthermore, the microfluidic system was also able to operate successfully without any appearance of air bubbles in the microfluidic chip for at least 20 hrs at 37 °C.

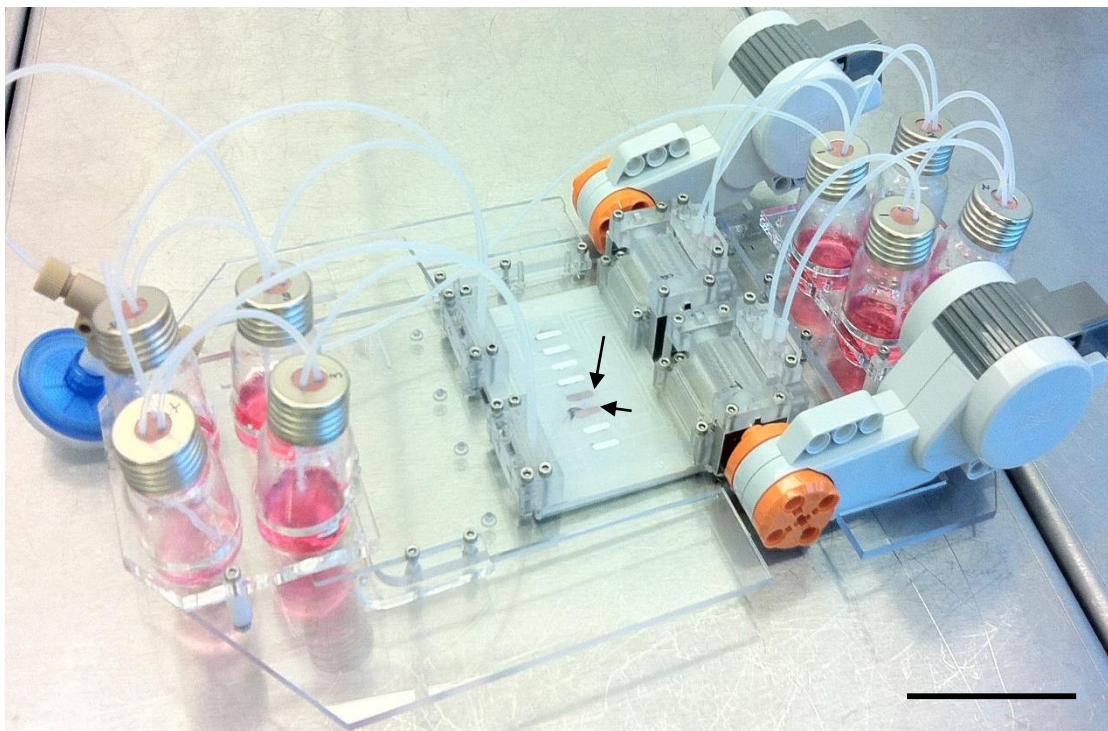


Figure 5.3 Assembled system with thiol-ene microchip. Cell culture medium was perfused into the system for chambers 3 and 4 (black arrows). Cell culture medium had perfused through the microchip for 20 hr in the incubator. (Scale bar = 5 cm)

Liquid reservoirs. The liquid reservoirs in the form of glass vials were connected to the micropumps and interconnection blocks via PTFE tubings (Figure 5.3). This form of liquid reservoirs are easily accessible and allowed easy changing of the liquids. Attempts to connect 16 glass vials to each inlet port and 16 glass vials to each of the outlet port failed to keep the entire system leak-free. Leaking was observed at the interconnections between the microfluidic chip and the components on the fluidic platform. The reason for leaking could be due to the added weight of the bottles on the base plate, which caused some form of bending moment of the base plate. Hence, when the microfluidic chip was integrated onto the fluidic platform, there was no tight sealing between the interconnection components and the microfluidic chip. To resolve the issue, the number of glass vials was reduced to eight bottles for the inlet ports and eight bottles to the outlet ports. Therefore, one glass vial was supplying to and collecting from two microchambers. However, the maximum volume of each of the glass vial was 10 ml (Figure 5.3). With a flow rate of $3 \mu\text{l}/\text{min}$, it would require the user to fill up the inlet bottles every day or risk emptying the bottles. To resolve this issue, glass vials with a larger volume (20 ml) would be used for future studies.

Another important thing to note was the breaking/chipping of the screw top of the glass vial. The screw top was susceptible to breaking/chipping when the cap of the glass vial was over tightened. If this happen, the

entire system would not be able to keep the pressure when pressurised. This would eventually risk the formation of air bubbles in the microchip. Therefore, during assembling of the entire platform, much care was required when tightening the screw caps of the glass vials.

5.3.2 Preliminary cell culture with HeLa cells and Caco-2 cells with thiol-ene microchip design 1 and fluidic system

HeLa and Caco-2 cells adhered onto the ECM coated Teflon membrane within 30 min after cell seeding. Caco-2 cells were observed to grow as clusters in certain regions of the cell culture chamber during the first 24 hrs of perfusion. The Caco-2 cells spread out and showed signs of proliferation during the subsequent days of culture (Figure 5.4b, e). By day 11, microchambers with low seeding density of Caco-2 cells displayed no full coverage (Figure 5.4b). In fact, numerous regions on the porous membrane were devoid of cells (yellow arrow in Figure 5.4b). By contrast, microchambers seeded with high Caco-2 cell density, the coverage was higher. By day 11, there was almost 80 % of Caco-2 cell coverage on the porous Teflon membrane (Figure 5.4e) using the higher cell seeding density.

Differentiation of the Caco-2 cells could be microscopically observed in the chamber with high Caco-2 seeding density (Figure 5.4e). Folds started to appear in the Caco-2 monolayers around day 8 (a suggestion of villous formation) (red arrows in Figure 5.4e) and it became more challenging to focus on all the cells simultaneously. This was consistent with an earlier study [2] which showed that Caco-2 cells cultured in microfluidic device, spontaneously displayed undulations and folds in the monolayer. This phenomenon could be due to the presence of continuous perfusion of cell culture medium across the Caco-2 cells. Furthermore, in certain regions of the microchamber, there were some observable regions of ‘dark patches’ on the cells (Blue arrows in Figure 5.4e). These ‘dark patches’ were highly suspected to be mucus. However, these two interesting morphologies were absent in the chamber with low seeding concentration of Caco-2 cells.

In the microchamber seeded with HeLa cells, the phase contrast images showed the HeLa cells proliferated well (Figure 5.4h). By day 6, the HeLa cells had reached close to 70 % confluency.

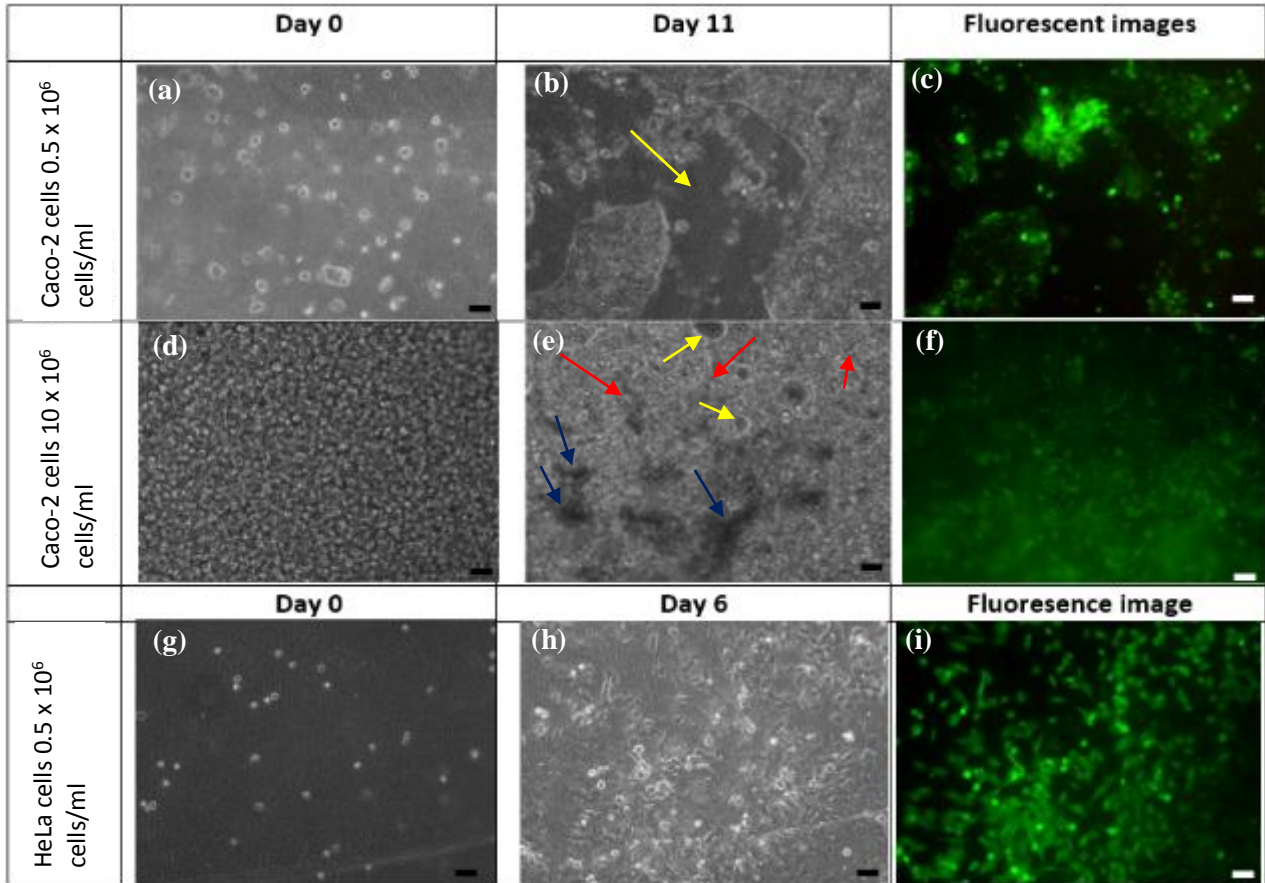


Figure 5.4 Images of Caco-2 cells and HeLa cells in the thiol-ene microchip after culturing for 11 days and 6 days respectively. (blue arrows indicate suspected mucus; red arrow indicate folds; yellow indicate region devoid of cells) Cells were fluorescently stained to investigate for live and dead cells (c, f and i). Live cells were stained green whereas dead cells were stained red. (Day 0 is the day that cells were seeded into the microchambers. Images were taken before flow was started. Images were taken with 10 x magnification). Scale bar = 50 μm .

Live/dead cell fluorescent images showed that there were > 90 % of the Caco-2 cells and HeLa cells alive on day 11 and day 6 respectively.

As mentioned earlier, there were observable patches devoid of cells (yellow arrow in Figure 5.4b) in the microchamber with low Caco-2 seeding density. This was also seen in the chamber with a high Caco-2 seeding density (yellow arrows in Figure 5.4e). These patches (devoid of cells) were more prominent in the regions on the membrane closer to the outlet (yellow arrows in Figure 5.5a). Furthermore, it was also observed that the cells closer to the inlet were differentiating more than the cells closer to the outlet. There were observable folds on the Caco-2 cells (red arrows in Figure 5.5b), an indication of differentiated Caco-2 cells. This observable gradient of cell proliferation and differentiation across the microchamber could be due to insufficient supply

of nutrients reaching the cells that were closer to the outlet. This will be discussed more in depth in the next section of this chapter.

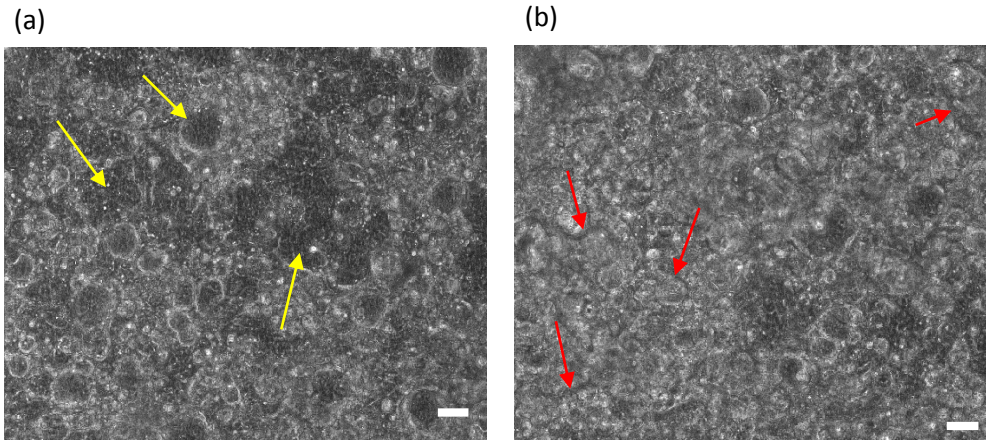


Figure 5.5 Phase contrast imaging of Caco-2 cells cultured in thiol-ene microchip (design 1) on day 10. Images were taken from two different positions of the same microchamber. (a) Position close to the outlet. Yellow arrows indicate regions devoid of cells on the Teflon membrane. (b) Position close to the inlet. Red arrows indicate folds on the Caco-2 cells. (Scale bar = 50 μm)

5.3.3 Effect of inlet dimensions on flow profile and cell growth in microchamber

Fluid flow is a crucial feature in microfluidic devices for cell culture and cell handling [6,9]. The rate of cell growth and differentiation is dependent on the amount of nutrients available in the culture media. In a microfluidic system, varying the flow rate of the culture medium or the microchamber geometries (often the channel height) are the straightforward means of optimising the mass transport of nutrients in the cell culture medium to the cells [6,9].

To understand the effect of inlet geometry on the flow profile within the microchamber, flow simulations on two different widths of the inlet and outlet channels were performed (Figure 5.6). The designs of the microchannels simulated were based on the designs presented earlier in Figure 4.1. Widths of the inlet microchannels used in the simulations were 0.6 mm and 1 mm respectively. In order to study the fluid distribution within the microchambers (boxed-up region in Figure 5.6a, c), the horizontal velocity field fluctuations in the middle of chamber were analysed. Considering the geometric symmetry of the rectangular microchamber (boxed up region in Figure 5.6a, c), only one velocity profile was analysed at the center of the horizontal plane. The velocity magnitude across the horizontal plane in the center of the microchamber displayed parabolic profiles in both microchip designs (Figure 5.6b, d). The parabolic velocity distribution was observed in both microchip designs because the flow was pressure-driven. Therefore resulting in higher velocities in the middle of the microchannel as compared to the velocities closer to the wall. It should be noted

that the fluidic velocities in both designs were similar throughout the middle section of the cell culture chamber $\approx 0.3\mu\text{m/s}$ (Figure 5.6 b,d). The only difference is the fluid velocities in the inlet and outlet channels leading to and from the microchambers. Fluid velocities in the smaller inlet and outlet channels design (Fig 5.6a) showed higher fluid velocities as compared to the larger inlet and outlet channel design (Fig5.6c).

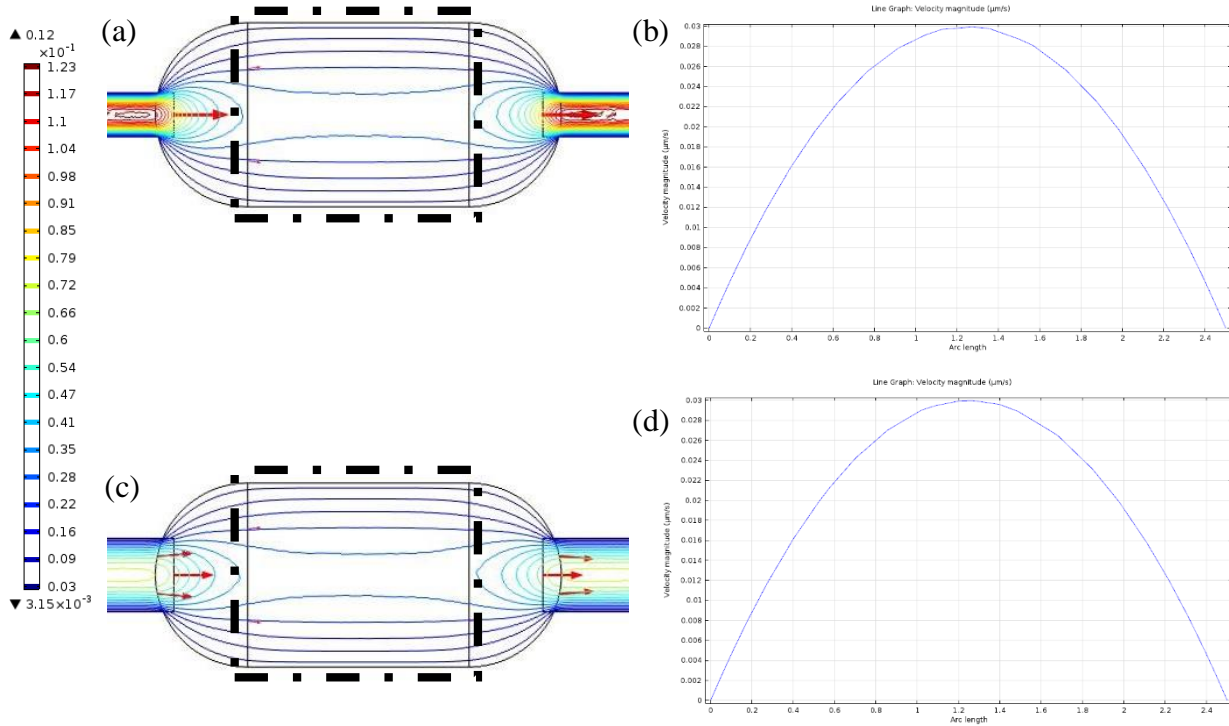


Figure 5.6 Simulated flow contours in the microchambers with respect to different inlet and outlet widths. (a) Flow contours for microchamber connected to inlet and outlet channel width = 1 mm. (velocity = $\mu\text{m/s}$) (b) Velocity magnitude across the middle of the microchamber for the 1 mm (width) inlet and outlet. (c) Flow contours for microchamber connected to inlet and outlet channel width = 0.6 mm. (velocity = $\mu\text{m/s}$) (d) Velocity magnitude across the middle of the microchamber for 0.6 mm (width) inlet and outlet.

Microscopic phase contrast images of the Caco-2 cells cultured in the microchip with the narrower inlet showed that the Caco-2 cells closer to the inlet were proliferating. There were numerous patches close to the outlet where they were devoid of cells (Figure 5.7d, f). The Caco-2 cells cultured in the microchamber with narrower inlet and outlet microchannels, also showed little villous-like folds in the Caco-2 monolayer. These villous-like folds were only present in regions close to the inlet. As seen from the simulation (Figure 5.7b), the surface velocities in the microchamber were very low. Therefore, the rate at which the cell culture medium was being replenished and removal of wastes would also be slow.

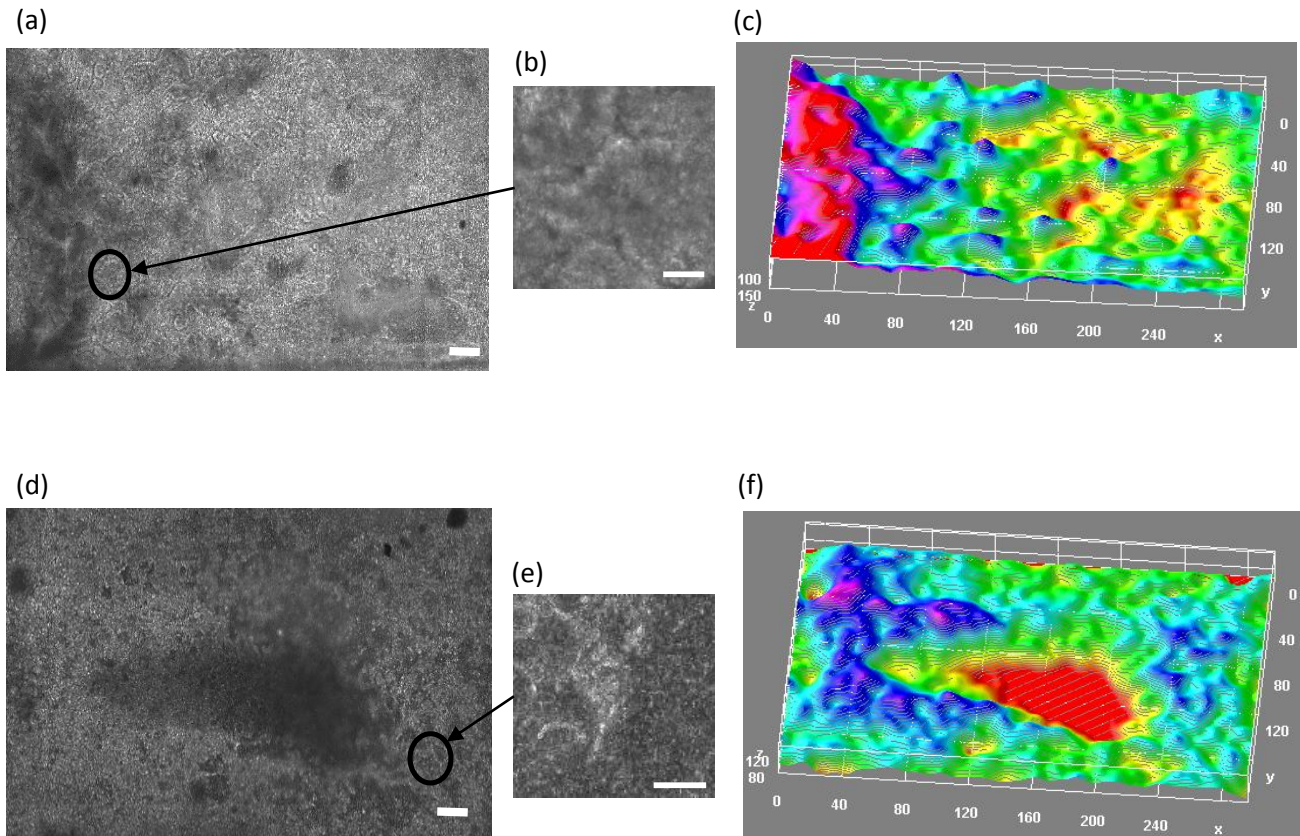


Figure 5.7 Effect of channel dimensions on cell growth. a) Phase contrast of Caco-2 cells cultured in microchambers with inlet and outlet width of 1mm. (b) Enlarged view of circled region in (a). (c) Intensity plot of the cell coverage on the porous membrane in microchamber with inlet and outlet width = 1 mm. (d) Phase contrast of Caco-2 cells cultured in microchambers with inlet and outlet width of 0.6mm. (e) Enlarged view of circled region in (d). (f) Intensity plot of cell coverage on the porous membrane in microchamber with inlet and outlet width = 0.6mm. Where z = height on the intensity surface plot. (Scale bar = 50 μm)

Phase contrast images of the Caco-2 cells cultured in the microchamber with the larger inlet and outlet (width 1 mm) microchannels showed uniform proliferation of cells throughout the microchamber. Villous-like folds were observed on the Caco-2 monolayer throughout the microchamber (Figure 5.7a-c). There was also 100 % confluency of Caco-2 cells on the Teflon membrane. This clearly showed that sufficient nutrients reached the cells throughout the microchamber. From this study, it was clearly displayed that the inlet and outlet channel dimensions microchannel dimensions were very important factors for good Caco-2 cell culture in the microfluidic device.

5.4 Discussion

The microfluidic perfusion platform comprising of MainSTREAM components and the thiol-ene microchip was established and investigated. The results showed that the Caco-2 cells could be cultured with satisfactory cell attachment, proliferation and morphologies. Furthermore, demonstrations on the dimensions of the inlet

of the microchannel showed potential effect on the growth and maintenance of the cells. These are further discussed in the sections below.

5.4.1 Fluidic system for cell culture

Micropumps. The MainSTREAM peristaltic micropump has many advantages over the conventional syringe pump. With its compact size, it allowed easy integration and assembly onto a system platform. Furthermore with eight pump lines, it enabled increased throughput. However, it was noticed that for the micropumps to perform optimally, the rotor bed [8] of the micropumps must be tightened sufficiently well (but not over-tightened) with the M2 screws. One of the serious problems observed was the malfunctioning of the micropumps when the screws of the rotor bed were over tightened. This would result in insufficient nutrients being perfused to the cells. The problem was resolved by loosening the screws a little but still sufficient to enable the micropump to function properly. It was also necessary to calibrate and calculate the flow rate of the micropumps before performing the cell culture studies.

Evaluation of system. The platform consisting of the MainSTREAM components effectively resolved the major challenges (bubble formation and leaking) that were persistent in the previous system discussed in Chapter 3. Previously in chapter 4, the PDMS molds were discovered to shrink by 0.7 % during thermal curing and this would be transferred to the cured thiol-ene fluidic layers. Therefore, to compensate the shrinkage, the designs of the PMMA master molds were enlarged by 0.7%. From the results reported in this chapter, there were no observable leaking at the interconnections between the microfluidic chip and the components on the fluidic platform. Therefore, all 32 ports on the thiol-ene microfluidic chip were well aligned with the pump lines and interconnection blocks. Thus, the overall enlargement of the PMMA master molds by 0.7 % was sufficient to compensate the shrinkage of the PDMS molds to ensure a well aligned and leak-free system.

5.4.2 Thiol-ene microchip for cell culture

Previously in chapter 4, it was mentioned that the porous membrane embedded between the fluidic layers of the microchip was changed to the Teflon membrane due to its transparency to visible light when wetted. The results presented in this chapter have further confirmed the transparency of the Teflon membrane when wetted. This enabled real-time microscopic monitoring of the cells.

Both HeLa and Caco-2 cells were observed to proliferate in the thiol-ene microfluidic chip. The results also showed that the seeding concentration of Caco-2 cells was crucial in producing good coverage of cells on the membrane. This would eventually affect the formation of a confluent layer of Caco-2 monolayer that is necessary for transport studies. From the results, a high seeding concentration of Caco-2 cells ($\approx 10 \times 10^6$

cells/ml) was necessary to provide sufficiently good coverage of Caco-2 cells in the microchamber (Figure 5.4e).

The Caco-2 cells cultured in the microfluidic device, even displayed differentiation with the formation of folds in the cells (Figure 5.4e). However, the appearance of folds in the Caco-2 cells were only observed when the Caco-2 cells were seeded at sufficiently high concentrations. To our knowledge, only one group reported on the observation of folds in the Caco-2 cells cultured in a microfluidic device [2,15]. The authors claimed the appearance of folds in the Caco-2 monolayers was the result of fluid flow and cyclic strain in the microfluidic device [2,15]. However, the Caco-2 cells cultured in the thiol-ene microfluidic device were subjected to only continuous peristaltic flow of fluid. Therefore, we hypothesized the appearance of the folds in the Caco-2 cells could be due to the presence of the flow of reagents on the cells.

Additionally, the growth and maintenance of the cells in the microfluidic chip were also dependent on the amount of nutrients present. In a microfluidic cell culture chip, the amount of nutrients present is dependent on the rate at which the nutrients are being perfused, dimensions of the microchamber, number of cells present and rates of nutrient uptake by the cells [9]. It is important to understand the relationship between culture media flow rate and the chamber dimensions, which collectively determine the average fluid velocity within the cell culture chamber as showed in Figure 5.6 and Figure 5.7. The results showed the microchamber connected to a narrower inlet had poor cell growth and differentiation compared to the microchamber connected to a larger inlet. Folds in the Caco-2 monolayer were observed throughout the microchamber connected to the larger inlet. We hypothesize that the poor cell growth in the microchamber connected to the narrower inlet could be the result of the low flow velocities. This may have resulted in regions where the combined convective and diffusive transport was insufficient to provide adequate nutrients to the cells as well as removal of wastes from the cells. Therefore resulting in patchy cell growth.

5.5 Conclusion

Integrating the microfluidic chip with the platform comprising of the MainSTREAM components and the constant supply of a pressure of 0.3 bar of atmospheric air and 5% CO₂, had resolved the formation of bubbles in the microchambers. There was also no observable leakage at the interconnections between the microchip and fluidic platform.

Preliminary cell culture studies using Caco-2 cells and HeLa cells clearly demonstrated that the fabricated thiol-ene microchip allowed real time microscopic observation of the cells and it was also able to support long term cell culture (more than 10 days). From the live/dead cell fluorescent images, it was clearly demonstrated

that > 90% of the Caco-2 cells and HeLa cells were viable. Folds were also observed on the Caco-2 cells, which was one of the morphologies of differentiated Caco-2 cells. The results thus far showed that the microenvironment of the microchambers on the thiol-ene microchip was suitable for cell culture.

To further understand the effect of inlet dimensions on the flow profiles and velocities in the microchambers, 2D simulations were performed. The results from the simulations clearly showed that the geometry of the inlet had a great impact on the flow distributions and velocities in the microchamber. To verify the simulated results, experimental cell culture studies were performed. The Caco-2 cells cultured in microchip design 2 (discussed in chapter 4 (Figure 4.1)) showed 100 % confluency in the microchamber and there was uniform differentiation of the Caco-2 monolayer. Therefore, this design will be used for further studies carried out in chapters 6, 7 and 8.

5.6 Outlook

As mentioned earlier in Chapter 2, one of the unique features of the Caco-2 monolayer is the tight barrier it exhibits. However, currently there is no real-time monitoring means of the integrity of the Caco-2 monolayer cultured in the thiol-ene microchip. One of the widely used methods for investigating the barrier integrity of the cells, is by measuring the trans-epithelial electrical resistance (TEER) across the cell monolayer [1,2,16–22]. This is a label-free and non destructive means to characterize the Caco-2 monolayers. To realise this goal, the next chapter will discuss and demonstrate embedding electrodes on the thiol-ene microchip.

In this chapter, from the cell culture on the thiol-ene microchip, ‘dark’ patches on the Caco-2 cells were observed. As mentioned earlier, these ‘dark’ patches were suspected to be mucus on the cells. More studies will be carried out to identify these ‘dark’ patches. This will be brought up in chapter 7 of the thesis.

References

- [1] L.M. Griep, F. Wolbers, B. de Wagenaar, P.M. ter Braak, B.B. Weksler, I.A. Romero, et al., BBB on chip: microfluidic platform to mechanically and biochemically modulate blood-brain barrier function, *Biomed. Microdevices*. 15 (2013) 145–50.
- [2] H.J. Kim, D. Huh, G. Hamilton, D.E. Ingber, Human gut-on-a-chip inhabited by microbial flora that experiences intestinal peristalsis-like motions and flow, *Lab Chip*. 12 (2012) 2165–74.
- [3] H. Kimura, T. Yamamoto, H. Sakai, Y. Sakai, T. Fujii, An integrated microfluidic system for long-term perfusion culture and on-line monitoring of intestinal tissue models, *Lab Chip*. 8 (2008) 741–6.

- [4] Y. Imura, Y. Asano, K. Sato, E. Yoshimura, A microfluidic system to evaluate intestinal absorption, *Anal. Sci. Int. J. Japan Soc. Anal. Chem.* 25 (2009) 1403–1407.
- [5] K.A. Southam, A.E. King, C.A. Blizzard, G.H. McCormack, T.C. Dickson, Microfluidic primary culture model of the lower motor neuron-neuromuscular junction circuit, *J. Neurosci. Methods.* 218 (2013) 164–9.
- [6] E.W.K. Young, D.J. Beebe, Fundamentals of microfluidic cell culture in controlled microenvironments, *Chem. Soc. Rev.* 39 (2010) 1036–1048.
- [7] P. Skaft-Pedersen, M. Hemmingsen, D. Sabourin, F.S. Blaga, H. Bruus, M. Dufva, A self-contained, programmable microfluidic cell culture system with real-time microscopy access, *Biomed. Microdevices.* 14 (2012) 385–99.
- [8] D. Sabourin, P. Skaft-Pedersen, M.J. S e, M. Hemmingsen, M. Alberti, V. Coman, et al., The MainSTREAM component platform: a holistic approach to microfluidic system design, *J. Lab. Autom.* 18 (2013) 212–28.
- [9] L. Kim, Y.-C. Toh, J. Voldman, H. Yu, A practical guide to microfluidic perfusion culture of adherent mammalian cells, *Lab Chip.* 7 (2007) 681–94.
- [10] D. Sabourin, D. Snakenborg, M. Dufva, Interconnection blocks with minimal dead volumes permitting planar interconnection to thin microfluidic devices, *Microfluid. Nanofluidics.* 9 (2009) 87–93.
- [11] P. Skaft-Pedersen, D. Sabourin, M. Dufva, D. Snakenborg, Multi-channel peristaltic pump for microfluidic applications featuring monolithic PDMS inlay, *Lab Chip.* 9 (2009) 3003–6.
- [12] D. Sabourin, D. Snakenborg, M. Dufva, Interconnection blocks: a method for providing reusable, rapid, multiple, aligned and planar microfluidic interconnections, *J. Micromechanics Microengineering.* 19 (2009) 035021.
- [13] P. Skaft-Pedersen, Microfluidic cell culture systems for real-time studies of cells, Technical University of Denmark, 2011.
- [14] M. Hemmingsen, Usability and Applicability of Microfluidic Cell Culture Systems, Technical University of Denmark, 2012.
- [15] H.J. Kim, D.E. Ingber, Gut-on-a-chip microenvironment induces human intestinal cells to undergo villus differentiation, *Integr. Biol.* 5 (2013) 1130–40.
- [16] N. Ferrell, R.R. Desai, A.J. Fleischman, S. Roy, H.D. Humes, W.H. Fissell, A microfluidic bioreactor with integrated transepithelial electrical resistance (TEER) measurement electrodes for evaluation of renal epithelial cells, *Biotechnol. Bioeng.* 107 (2010) 707–16.
- [17] M. Odijk, A.D. van der Meer, D. Levner, H.J. Kim, M.W. van der Helm, L.I. Segerink, et al., Measuring direct current trans-epithelial electrical resistance in organ-on-a-chip microsystems., *Lab Chip.* 15 (2015) 745–52.
- [18] M.J. Briske-Anderson, J.W. Finley, S.M. Newman, The influence of culture time and passage number on the morphological and physiological development of Caco-2 cells, *Proc. Soc. Exp. Biol. Med.* 21 (1997) 248–257.
- [19] R. Booth, H. Kim, Characterization of a microfluidic in vitro model of the blood-brain barrier (μ BBB)., *Lab Chip.* 12 (2012) 1784–92.

- [20] S.B. Petersen, G. Nolan, S. Maher, U.L. Rahbek, M. Guldbrandt, D.J. Brayden, Evaluation of alkylmaltosides as intestinal permeation enhancers: comparison between rat intestinal mucosal sheets and Caco-2 monolayers, *Eur. J. Pharm. Sci.* 47 (2012) 701–12.
- [21] C. Piana, I. Güll, S. Gerbes, R. Gerdes, C. Mills, J. Samitier, et al., Influence of surface modification on vitality and differentiation of Caco-2 cells, *Differentiation*. 75 (2007) 308–317.
- [22] P.D. Ward, T.K. Tippin, D.R. Thakker, Enhancing paracellular permeability by modulating epithelial tight junctions, *Pharm. Sci. Technolo. Today*. 3 (2000) 346–358.

CHAPTER 6: Embedding electrodes onto thiol-ene microfluidic chip for trans-epithelial electrical resistance (TEER) measurements

The thiol-ene microchip presented in chapter 5 was capable of supporting long term Caco-2 cell culture. However, the integrity of the Caco-2 monolayers cultured in the thiol-ene microchip could not be validated. One of the most common techniques for real-time monitoring of the integrity of Caco-2 monolayers is by measuring the trans-epithelial electrical resistance (TEER). TEER is a non-destructive and label free method for characterizing the barrier property of epithelial and endothelial cells. In this chapter, the design, the process of embedding the electrodes in the microfluidic device and the reliability of the electrodes in the microchip are presented. Biocompatibility of the electrodes was also verified. Likewise, some preliminary TEER measurements are presented.

The traditional static Transwell inserts for Caco-2 cell culture were used as reference studies. Comparisons of the TEER results between the two different systems are presented in the later sections of this chapter.

6.1 Trans-epithelial electrical resistance measurement across Caco-2 monolayer

As described in Chapter 2, there are two pathways for ion transport across the Caco-2 cell monolayer, namely the transcellular pathway and the paracellular pathway. The tight junctions between adjacent cells govern the transport of the solutes through the paracellular space of epithelial and endothelial cell layers. As mentioned earlier, integrity of the tight junctions can be monitored by measuring the TEER [1].

The epithelial layer can be simplified to a simple electrical circuit of resistances [1,2]. The electric model of the cell layer in Figure 6.1a is only applicable for transfer of direct current (DC) signals. In the equivalent circuit diagram (Figure 6.1a) the resistance of the transcellular pathway is the sum of the apical cell membrane resistance (R_a) and the basolateral cell membrane resistance (R_b). The resistance of the paracellular pathway is the sum of the tight junction resistance (R_{TJ}) and the intercellular resistance (R_{IC}). Especially at the start of epithelial and endothelial cell culture, the paracellular pathway is more dominant in the overall TEER measurements. The reason being the tight junctions between adjacent cells have not yet formed [2].

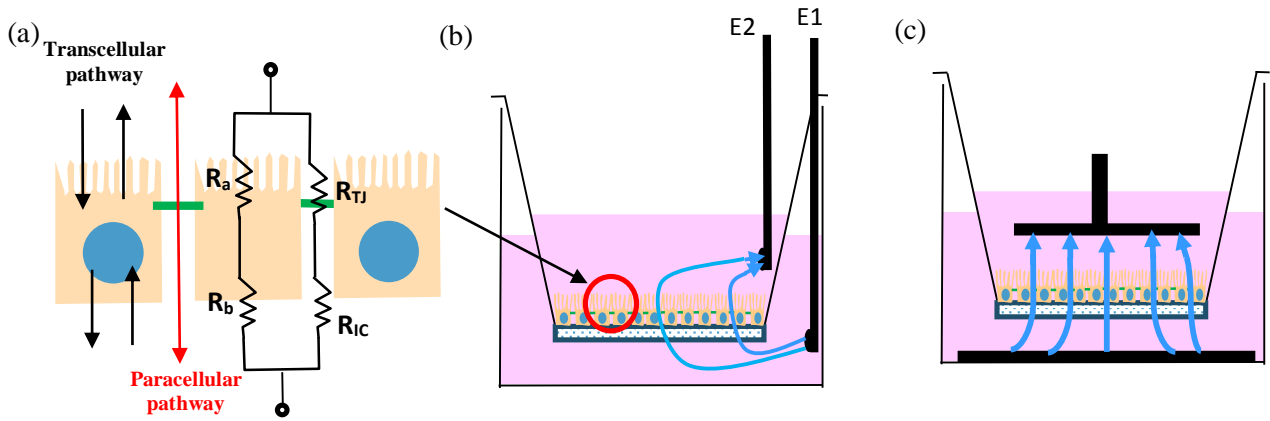


Figure 6.1 Schematic illustrations of the electrical circuit and flow of current across Caco-2 monolayers. (a) Schematic electrical equivalent circuit of Caco-2 monolayer for transfer of DC signals. (b) TEER measurements carried out in the Transwell set-up using the chopstick-like electrodes (E1 and E2). Blue arrows indicate the unidirectional flow of current for DC signals (c) TEER measurements carried out in the Transwell inserts using the 2-electrode system. Black bars indicate electrodes. Blue arrows indicate the unidirectional flow of current for DC signals

The mechanism behind TEER measurements is based on Ohm's Law:

$$\text{Eq 6.1:} \quad V = IR$$

Where R is resistance, V is voltage, I is current. In TEER measurements, a current or voltage is applied across the cell layer. By measuring the respective returning voltage or current, the resistance measurement is determined [3]. TEER values ($\Omega \cdot \text{cm}^2$) are determined by eq 6.2.

$$\text{Eq. 6.2:} \quad TEER = (R_1 - R_o)A$$

Where R_1 (Ω) is the apparent resistance, R_o (Ω) is the baseline resistance recorded without cells and A (cm^2) is the cell culture area of the porous membrane.

Most of the commercially available systems for measuring TEER across cells cultures in microporous filters or inserts use volt-ohm resistance meters such as the EVOM2 (World Precision Instruments) and Millicell ERS-2 (Millipore), equipped with either a 4-point measurement with silver/silver chloride (Ag/AgCl) chopstick electrodes (Figure 6.1b) or chamber electrodes (Figure 6.1c) [2,3]. These volt-ohm meters use a near DC (12.5 Hz) current of $10 \mu\text{A}$. In this project, TEER measurements in the microfluidic device were acquired using DC signals, as it is main measurement method used in most past reports on acquiring TEER values.

6.2 Design considerations

The format of measuring TEER using the ‘chopstick’ electrodes or chamber electrodes are limited to static or macroscopic cell environments and are difficult to be adapted to microchannels. Due to the small cell culture area, a simple and robust method for embedding electrodes in the microfluidic chip is required.

Incorporating electrical properties into microfluidic devices is not something that is foreign nor new. For decades, much had been reported on acquiring electrical measurements from microfluidic systems for electrochemical detection [4], electrophoresis [5,6], flow cytometry [5–8] etc. Recently, there are literature reporting on TEER measurements in microfluidic devices [3,9–17]. To fabricate the TEER measuring electrodes on the microchip there were some points that must be considered:

- 1) the fabrication technique should be simple and electrodes should be easily integrated on the thiol-ene chip
- 2) the electrode material must be biocompatible for Caco-2 cell culture
- 3) the electrode material must not deposit toxic compounds in the microchambers when electrical signals are activated
- 4) the positions of connecting wires of electrodes should still allow microscopic monitoring of Caco-2 monolayers in microchambers
- 5) Electrodes must be fixed in positions on the microchip to prevent variations of measurements in the same microchamber

6.2.1 Positioning of electrodes

Due to the compactness of the structures on the thiol-ene microchip (microchip design 2 shown in Figure 4.1b), a simplified and straight-forward method for fabricating the electrodes with the metal of interest was necessary. One simple method considered was to insert the electrodes directly to the top and bottom of the microchambers (Figure 6.2). This will allow the electrodes to be in close proximity with the Caco-2 cells in the microchamber. Placing the electrodes in close proximity with the cells will reduce the noise imposed on the readings by cell culture medium [10]. However, the contact points of the bottom electrodes must exit from the top of the microfluidic chip. This will still allow the use of an inverted microscope to conduct real-time microscopic monitoring of the Caco-2 cells.

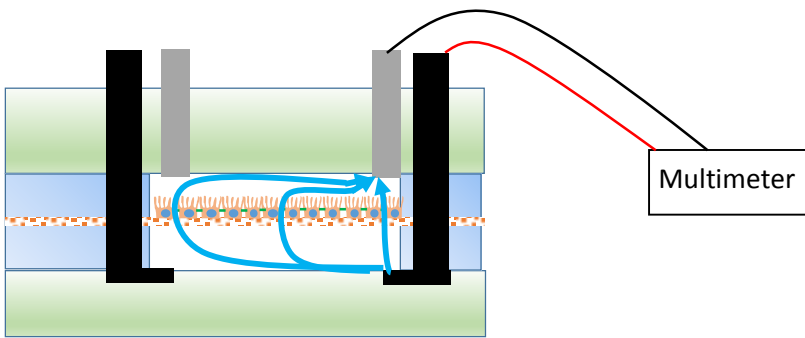


Figure 6.2 Schematic cross-sectional view of the microchamber in a microfluidic chip with electrodes connected to the multimeter. Electrodes are placed in close contact with the Caco-2 monolayer. Blue arrow indicate the direction of current flow. In DC signals, direction of current flow is uni-direction. DC signals are supplied to the electrodes to acquire TEER measurements.

6.2.2 Material selection of electrode and fabrication technique

The most commonly used materials for fabricating electrodes in microfluidic systems are Ag/AgCl [2,10–13] and platinum (Pt) [15]. However Sun et. al. [16] reported on fabricating gold-plated electrodes covered with a conducting polymer (polypyrrole doped with polystyrene sulfonate), for reducing the influence of the double layer capacitance. Other conductive metals such as aluminium (Al) and copper (Cu) have also been explored for TEER measurements in microfluidic systems [14]. Although all these metals are suitable electrode material, the accompanying methodologies (e.g., clean room technologies, attaching of electrodes to microchip with ferrules, inserting electrodes to the sides of the microchip or inlet tubes etc) of fabricating the electrodes are not feasible for the thiol-ene microchip. As mentioned in the earlier section, a simple and low cost fabrication method allowing more than one set of electrodes to be embedded on the same microchip was necessary. Keeping all these in mind, two metals were chosen to fabricate the electrodes in the thiol-ene microchip: indium alloy (InBiSn; In 51 % Bi 32.5 % Sn 16.5 % by weight; Indium Corp, USA) and platinum (Pt; Advent, UK).

Bottom electrodes. InBiSn is a eutectic metal with a melting temperature of 62 °C. InBiSn was chosen as the material for the bottom electrodes because it could be easily embedded in the completed microchip. At an elevated temperature (> 62 °C), it could be easily molded into the desired electrode shape in the electrode channel on the microfluidic chip. This particular metal is non-toxic [18], is mechanically stable in room temperature [19] and has a relatively high electrical conductivity of $\approx 2.4 \times 10^6$ S/m [18]. InBiSn metal had reportedly been used for fabrication of electrodes for picoinjection [20], electroporation of cells [18] etc. Therefore, InBiSn is an attractive and suitable material for fabricating the electrodes on the thiol-ene microchip.

It was decided the melted metal filling approach would be implemented to fabricate the bottom electrodes. In this method, InBiSn metal was first heated to above melting temperature, so the melted metal could be easily drawn into the electrode cavities by (Figure 6.2a) pressure and capillary forces.

Top electrodes. Another metal for fabricating the top electrodes was necessary as the method for fabricating the bottom electrodes (by heating the metal) could not be applied for fabricating the electrodes. By heating the microchip in order to soften the microchip layers for inserting the InBiSn metal would result in melted metal dripping into the microchamber. Alternatively, by force-fitting the metal into the electrode ports resulted in breakage of the metal. The reason being InBiSn is quite brittle (Brinell hardness = 11 HB [21]), therefore this poses some challenges to force-fit the metal into the electrode ports on the microchip for the top electrodes. Due to this challenge, another harder, inert, non toxic metal was chosen. Pt (Brinell hardness = 299 MPa [22]) with high conductivity was chosen as the metal for the top electrodes.

6.2.3 Electrode design on microfluidic chip

As mentioned in the earlier section, the thiol-ene microchip (design 2 in Figure 4.1b) consisted of numerous structures. Thus, the best positioning of the electrodes was directly to the top and bottom of the microchamber. Moreover, fabrication of the electrodes should be simple and not time consuming. Keeping these criteria in mind, two electrode channels were designed on the bottom of the fluidic layer and two holes for the top electrodes were designed for the upper fluidic layer (Figure 4.1b). The sections below will describe in detail of the electrodes for the respective fluidic layers.

Bottom electrodes. Two straight electrode channels with dimensions of 2 mm (length) x 0.5 mm (width) x 0.2 mm (height) were designed on the bottom fluidic layer (figure 6.3a). The lines are positioned with one end at the edge of the microchamber (Figure 6.3a). The size of the electrodes could be controlled by the amount of melted metal and geometry of the electrode cavity. The direction in which the melted metal flows is guided by the geometry of the electrode cavity. Copper wires will be inserted into the melted electrodes to serve as connection to the measuring equipment (e.g., Multimeter) (Figure 6.3a).

Top electrodes. The top electrodes were fabricated by inserting Pt wires into the electrode ports that were drilled into the top fluidic layer of the microchip (Figure 6.3b). The Pt wires used for the electrodes have a dimension of 0.5 mm for diameter and a length of 10 mm. Similar to the bottom electrodes, copper wires would be soldered to the Pt electrodes to allow a measuring equipment to be connected for TEER measurements.

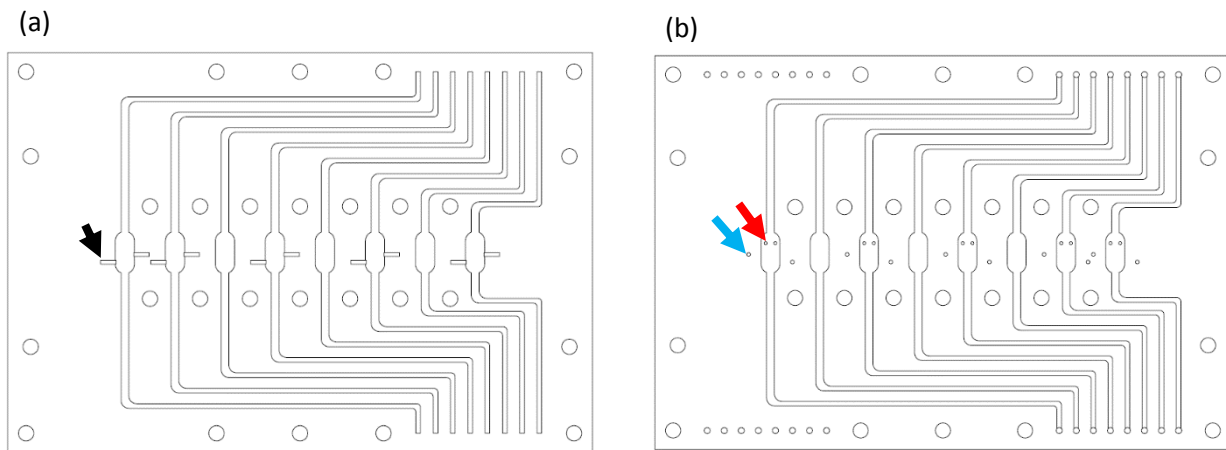


Figure 6.3 Schematic drawings of the fluidic layers. (a) Schematic drawing of the bottom fluidic layer of microchip. Two electrode grooves were drawn for placement of the bottom electrodes in each of the microchambers. (Black arrow indicating the electrode groove on the bottom fluidic layer) (b) Schematic drawing of the electrode ports drawn on the top layer of the microfluidic layer. (Blue arrow indicate electrode port for bottom electrode, red arrow indicate electrode port of top electrode)

6.2.4 System for obtaining TEER measurements

As mentioned earlier in section 6.1, DC signals would be supplied to the microfluidic device to acquire the TEER measurements. There are some concerns of the DC signals interfering with cellular processes due to membrane polarization or intracellular charge displacements when cells are exposed to DC signals [23]. Nonetheless, DC measurements can be adequately employed in studies whereby the cells are exposed to short durations of DC signals. Furthermore, using DC techniques – by means of the commercial systems mentioned in section 6.1 – to acquire the TEER measurements is the most widely used method reported in literature [24–30].

The Millicell ERS-2 meter uses a fixed current of 10 μA . However, due to the high resistances in the microchannels, this will result in potentials that exceed the maximum measurable membrane potential of 200 mV [31]. Therefore, a sensitive multi-meter (Keithley, USA) was chosen to obtain the TEER measurement read-outs from the microfluidic chips as this multi-meter is capable of reading resistance from 100 $\mu\Omega$ to 100 M Ω and has an input voltage ranging from 100 nV to 1 kV (Figure 6.4).

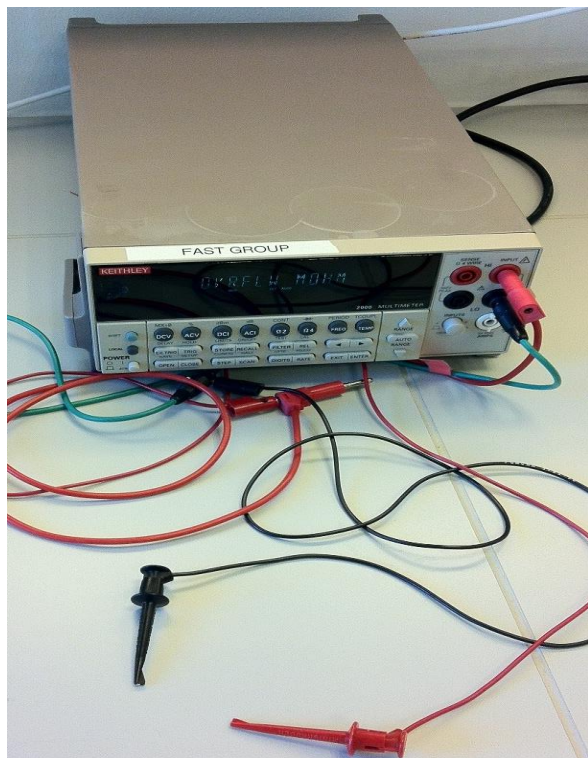


Figure 6.4 Multi-meter used for recording the TEER measurements from microfluidic chip.

6.3 Materials and methods

6.3.1 Fabrication of electrodes on microchip

The thiol-ene microchip fabrication process was described in detail in section 4.3.1 in the thesis. Referring to the fabrication process in section 4.3.1, at step 4 of the fluidic layer fabrication process (Figure 4.3A) electrode grooves in the bottom fluidic layer were micromilled onto the cured thiol-ene layer. Electrode ports were drilled through the top fluidic layer and the cured thiol-ene modified Teflon membrane at step 5 of membrane fabrication process (Figure 4.3B). Once these were completed, the layers were aligned against each other and bonded (microchip fabrication final procedure Figure 4.3) to form a sealed microchip.

Bottom electrodes. To fabricate the bottom electrodes, the sealed microchip was first placed onto a hotplate set at 80 °C. This was to allow the entire thiol-ene microchip to reach a temperature of more than 62 °C. 10 min later, pieces of the InBiSn metal, with length of 5 mm, were inserted into the electrode ports (connecting to the lower fluidic layer) on the thiol-ene microchip. InBiSn metal melted due to the heat from the hotplate. Slight pressure was applied manually to push the melted metal into the electrode groove. Once the electrode

was formed, electric wire of diameter 0.4 mm were inserted to the liquid metal. This would act as the connecting wire to the multimeter. Once the microchip was cooled down in room temperature, the InBiSn electrode hardened, retaining the shape (Figure 6.5b). The size of electrode for measuring TEER, was about 0.6 – 0.8 mm in diameter and thickness of 0.3 mm (Figure 6.5c).

Top electrodes. Next, two pieces of Pt wires (diameter of 0.5 mm, length of 5 mm) were forced fit into the electrode ports drilled through the top fluidic layer. Two connecting Cu wires were soldered to the Pt wires (Figure 6.5a). To fix the electrodes in position, UV-epoxy (NOA81; Norland, USA) was applied at the junctions between connecting wires and thiol-ene chip. The entire chip was exposed to UV light for 30 s. The entire procedure of embedding the electrodes on the microchip could be carried out in ambient environment, eliminating the use of expensive, sophisticated instruments in environment-controlled cleanroom.

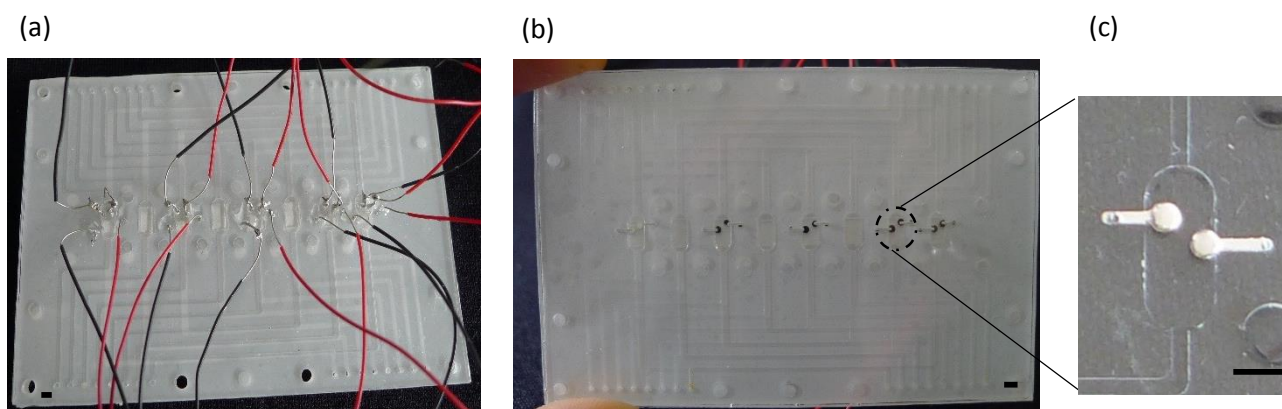


Figure 6.5 Electrodes on microfluidic chip for TEER measurements. (a) Top view of the completed microchip with embedded electrodes and connecting wires. (b) Underside of thiol-ene microfluidic chip with the InBiSn electrode embedded in the microchamber. (b) Expanded view of the InBiSn electrode. (Scale bar = 2mm)

6.3.2 Biocompatibility studies of InBiSn metal

Pieces of the InBiSn alloy (2 cm) were first sterilized with 70 % ethanol for 5 min before rinsing with sterile water for another 5 min. Once the pieces were cleaned, they were transferred to 6-well microplate wells. InBiSn metal was present in three microwells and three other control microwells did not have the InBiSn metal. Caco-2 cells harvested from T-75 flasks with trypsin/ETDA solution (Sigma, Denmark) were centrifuged at 125 \times g for 5 min. The supernatant was removed and fresh cell culture medium was added to re-suspend the cell pellets. Caco-2 cells were counted with the cell counter and prepared to a concentration of 2.5×10^5 cells/ml. 1.5 ml of the prepared Caco-2 cell was pipette into each of the microwell. Following that, the microplate was placed into an incubator (37°C, 5 % CO₂). The growth of the Caco-2 cells was monitored daily using a bright field microscope.

Live/dead cell staining. Vitality of the Caco-2 cells were investigated by performing live/dead staining on the cells. The live/dead cell staining procedure is described in Chapter 5. Briefly, cell culture medium was first removed, followed with rinsing the cells three times with phosphate buffer saline (PBS; Sigma, Denmark). 1 ml of the stains diluted in PBS (Live cell stain: calcein (1:1000); dead cell stain: ethidium homodimer-1 (1:500)) was added to the cells. Next, the cells were incubated with the stains for 30 min. After 30 min, the staining solution was removed and the cells were rinsed with PBS for three times. Fresh PBS was added to the cells and imaged immediately at excitation/emission wavelengths of 495/517 nm for live cells and excitation/emission wavelengths of 528/617 nm for dead cells with a confocal microscope (Axio Observer; Zeiss, Germany). An image software (Zen lite; Zeiss, Germany) was used to process the images.

6.3.3 Characterization studies of electrodes

Different standard solution of sodium chloride (NaCl; Sigma, Denmark) solutions (final concentrations of NaCl: 0.187 M, 0.287 M, 0.637 M and 1.137 M) were prepared for the characterization studies. NaCl solutions were prepared by mixing concentrated NaCl with PBS as the diluent.

Microfluidic system. PBS was first flowed into the upper and lower fluidic layers for 30 min at a flow rate of 5 $\mu\text{l}/\text{min}$. Following that, the flow was stopped and the resistance measurements were recorded. Different concentrations of the NaCl solutions were pumped into the microchannels. For each concentration, NaCl was introduced into the microfluidic device for 30 min before measuring the resistance. All the characterisation experiments were conducted in room temperature at static conditions. Each TEER measurement was acquired by connecting only one set of electrode (one top electrode and one bottom electrode) in a microchamber to the multimeter (Figure 6.2).

Transwell system. Electrical measurements were also recorded for the Transwell cultures. The electrical resistance measurements for the Transwell cultures were obtained using the handheld chopstick Ag/AgCl electrodes connected to the ERS-2 volt-ohm reader (Millicell, Denmark). Baseline readings were first obtained using PBS. PBS was added to both the apical side (500 μl) and basolateral side (1500 μl) of the porous Transwell inserts. Following that, the TEER was measured. Next, PBS was replaced with the different standard solutions and resistance measurements were recorded accordingly. Eq 6.2 was used to calculate the TEER values ($\Omega\cdot\text{cm}^2$).

6.3.4 TEER measurements of Caco-2 cells cultured in microchip

The microchip (Microchip design 2 (Figure 4.1b)) and fluidic system were prepared using the procedure discussed in chapter 5. Caco-2 cells in the concentration of 2.4×10^5 cells/ cm^2 were seeded onto the ECM treated porous Teflon membrane in the microchip. The Caco-2 cells were cultured over 10 days.

Before seeding cells into the microchambers, the apical and basolateral chambers were primed with cell culture medium and a blank membrane resistance was measured. This first set of TEER measurements was recorded as the baseline TEER readings for each of the microchamber with electrodes.

After the Caco-2 cells were cultured in the microfluidic chip, TEER measurements were recorded from day three of cell culture and subsequently daily. TEER was only recorded from day 3 onwards because it would be 24 hrs after the cells were exposed to fluid flow in both the apical and basolateral sides.

Before recording TEER measurements, the entire system was removed from the incubator and left to cool in room temperature for 15 min. This was to prevent any interference of temperature difference with TEER recordings [29]. To prevent any implications on fluid flow on the resistance measurements, all resistance measurements were recorded at static flow conditions. Resistance measurements were measured by using alligator clips to connect wires of the electrodes to the multimeter. Stabilization of each set of electrode took about 3 min for recording the apparent resistance measurements. TEER was calculated using eq 6.2. Area of the microchamber was 0.1 cm^2 .

6.3.5 Introducing membrane enhancer to Caco-2 monolayers in microchip

Studies on the effect of the membrane enhancer on the barrier integrity of the Caco-2 monolayers were investigated on day 10 of cell culture. Two different concentrations of the membrane enhancer, tetradecyl- β -D-Maltoside (TDM; Sigma, Denmark) were prepared in buffer⁺ as the diluent. Buffer⁺ was prepared by mixing the Hank's buffered saline solution (HBSS; Gibco, Denmark) and 10 mM HEPES (HEPES; Sigma, Denmark) at pH 7.4. TDM solutions were prepared in the concentrations of 100 μM and 400 μM TDM. To prepare the cells for the studies, HBSS was first pumped into the microfluidic chip for 1 hr at a flow rate of 3 $\mu\text{l}/\text{min}$. Following that, TEER measurements were recorded. Next, the TDM solutions were set to perfuse into the microchambers for 1.5 hr at a flow rate of 3 $\mu\text{l}/\text{min}$. After 1.5 hrs of continuous flow through, the TEER measurements of the Caco-2 monolayers were recorded. Following the experiments, the cells were rinsed with PBS (perfused into the microchip for at least 1 hr at a flow rate of 3 $\mu\text{l}/\text{min}$) and recovered with continuous perfusion of cell culture medium for 24 hr. Subsequently, TEER measurements were recorded 24 hrs later. During perfusion of reagents through the microchannels, the entire system was placed in the incubator (37°C; 5% CO_2). We also carried out control studies with the Caco-2 cells by perfusing the HBSS buffer without TDM.

Data analysis of TEER values in the presence of TDM. The ratio between the measured TEER in the presence of TDM and the measured baseline TEER is defined as the drop in TEER values.

Eq. 6.3:
$$\% \text{ drop in TEER} = \left(\frac{TEER_{sample}}{TEER_{baseline}} \right) \times 100 \%$$

A drop in TEER values indicates the barrier integrity of the Caco-2 monolayer is disrupted.

6.3.6 Static Transwell cultures of Caco-2 monolayers

Control studies of the effect of TDM on Caco-2 monolayers were demonstrated using static cultures of Caco-2 cells in 12 well Transwell plates (Corning Inc, Lowell, MA). Each insert contained a porous polycarbonate membrane (1.1 cm², 0.4 μm pores). Caco-2 cells cultured in T-75 flasks were first harvested with trypsin/EDTA solution. The harvested Caco-2 cells were centrifuged at 125 xg at room temperature for 5 min. Following that, the supernatant was removed and fresh cell culture medium was added to re-suspend the cell pellets. Caco-2 cells were counted with a cell counter (Moxi-Z, Denmark) and prepared to a concentration of 1.5 x 10⁵ cells/ml. 500 μl of the prepared Caco-2 cell suspension was seeded onto the top surface of the porous Transwell membrane. The Caco-2 cells were cultured for 21 days in cell culture medium, with cell culture medium change every second day.

TEER measurements. Measurements of the TEER values in Transwell experiments were recorded using a pair of chopstick Ag/AgCl electrodes coupled to the ERS-2 volt-ohm meter shown in Figure 6.6. The entire system was purchased from Millicell, Denmark. The shorter electrode (E2, Figure 6.6) was immersed in the Transwell insert and the longer electrode (E1; Figure 6.6) was immersed in the microwell.

The electrodes were sterilized in 70 % ethanol, followed by equilibrating in cell culture medium in a biosafety cabinet for 15 min before use. Caco-2 cell cultures in Transwell experiments were allowed to cool to room temperature for 20 min in a biosafety cabinet. Next, the electrodes were placed into the cell culture medium in the respective compartments as shown in Figure 6.6a. About 1 min was required for the resistance to stabilise before recording.

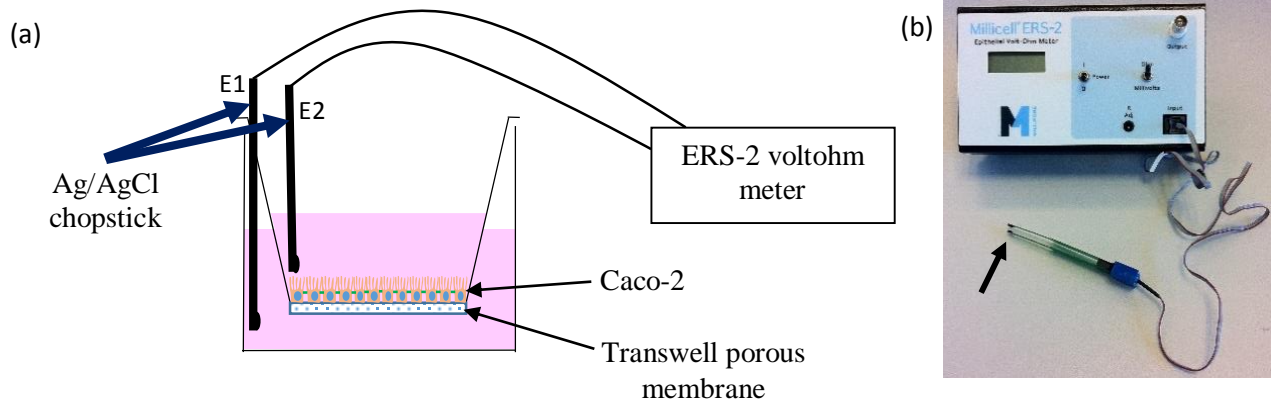


Figure 6.6 TEER measurement in Transwell system. (a) Schematic drawing of TEER measurements using the chopstick Ag/AgCl electrodes coupled to the ERS-2 voltohmmeter. (b) Commercial TEER system, millicell ERS-2 volt-ohm meter and the chopstick electrodes. Arrow indicate the Ag/AgCl electrodes.

Similar to the microfluidic device, resistance measured from Transwell inserts without Caco-2 cells cultured were used as baseline resistance. Finally, eq. 6.3 was used to calculate the TEER measurements of the Caco-2 cells cultured in the Transwell inserts. TEER measurements of the Caco-2 cells cultured in the Transwell inserts were recorded on alternate days.

Challenging Caco-2 monolayers with membrane enhancer in Transwell. On day 21 of cell culture, the Caco-2 monolayers in the Transwell inserts were rinsed three times (on both the apical and basolateral sides) with PBS. Next, HBSS was added to both the apical (500 μ l) and basolateral (1500 μ l) sides of the cells and incubated at 37 °C for 1 hr. At this point, TEER measurements of the Caco-2 monolayers were recorded. Next, the HBSS solution in the apical side of the Caco-2 monolayers was replaced with the prepared membrane enhancer (TDM) solutions. The cells were incubated with the TDM solutions for 1 hr prior to obtaining the last TEER measurements. After the experiments, the Caco-2 monolayers were rinsed 3 times with PBS followed by replenishing with cell culture medium for 24 hr. TEER measurements were also recorded post 24 hr recovery.

Data analysis of TEER values in the presence of TDM. Similar to the microfluidic device, equation 6.3 was used to calculate the percentage drop in TEER values.

6.4 Results

6.4.1 Biocompatibility tests on InBiSn metal

The growth of Caco-2 cells cultured in the microwells were monitored daily by microscopic means. Phase contrast microscopic images confirmed that the Caco-2 cells cultured in the microwells containing the InBiSn metal, multiplied (Figure 6.7). By day 3 of cell culture, the Caco-2 cells cultured in the microwells were mostly spread out (Figure 6.7(b), (g)), a sign of the cells adhering to the surface of the microwell. The shape and size of the Caco-2 cells in the microwells containing the metal piece were comparable to the Caco-2 cell cultured in the control wells. The Caco-2 cells were multiplying close to the pieces ($< 1\text{mm}$) and even growing beneath the metal (due to buoyancy, at times, the metal floated in the microwell).

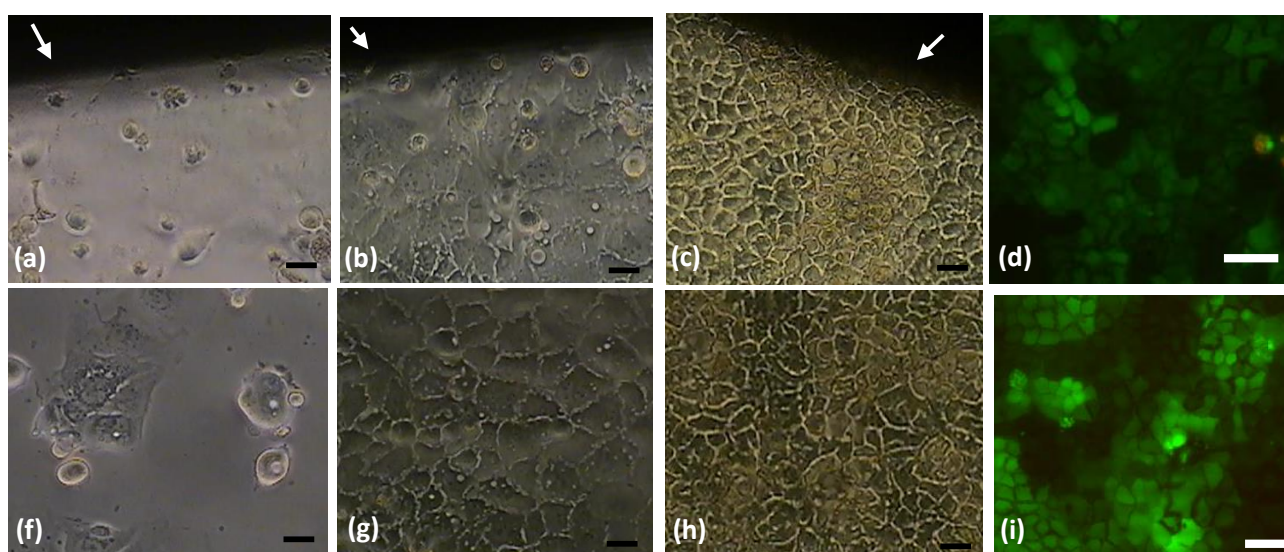


Figure 6.7 Biocompatibility tests of InBiSn alloy. Microscopic images of Caco-2 cells cultured in microwells in the presence of InBiSn metal (a) – (d) and without the metal (f) – (i). Microscopic images were taken on day 1 (a and f), day 3 (b and g) and day 6 (c and h) of Caco-2 cell culture. White arrows in (a) – (c) indicate the InBiSn metal. Live/dead fluorescent images were taken on day 6 of cell culture. Live cells were fluorescently stained with calcein, as shown in green, and dead cells are stained with ethidium homodimer-1 as shown in red. Magnification at 10 x. (Scale bar = 50 μm)

By day 6 of cell culture, there was 100 % coverage of Caco-2 cells on the bottom surface in all three microwells containing the metal (Figure 6.7c). These Caco-2 cells were more regular in sizes as compared to the Caco-2 cells on day 3 of cell culture. In all the microwells, the Caco-2 cells displayed distinct polygonal shape with clear, sharp boundaries (Figure 6.7c). Similar morphology of the Caco-2 cells were also observed in the control microwells. The studies showed that the Caco-2 cells in both the control microwells and microwells contacting the metals were forming monolayers in the microwells.

The viability of the Caco-2 cells was determined with the live/dead cell stains. The fluorescent images of the cells showed that the cell viability was $> 95\%$ in all the microwells containing the metal (Figure 6.7d). The results were comparable to the control microwells ($\approx 100\%$ cell viability) (Figure 6.7i). This is a clear indication that the InBiSn metal is biocompatible for Caco-2 cell culture.

6.4.2 Characterization of electrodes on microchip

The stability and reliability of the electrodes were investigated by conducting characterization studies using standard solutions with increasing concentrations of NaCl. Four NaCl solutions of increasing concentrations were prepared and introduced into the microfluidic device. Increasing the concentration of the NaCl solution will increase the resistivity of the electrolyte solution. This will in turn lead to a decrease in the resistance read-out.

The resistance values measured in the microfluidic device containing PBS had the highest resistance values ($\approx 78.2\text{ k}\Omega$) (Figure 6.8a). As expected, increasing the concentration of NaCl from 0.187 M to 1.137 M, resulted in a drop in the resistance values. The drop of resistance measured was $\approx 12.56\text{ k}\Omega$ (Figure 6.8a).

Similar studies were carried out in Transwell system and the same trend was also observed with the Transwell studies. The TEER values obtained from the Transwell inserts were much lower as compared with the TEER values obtained from the microfluidic device (Figure 6.8b). The huge difference between the two systems could be due to i) different electrodes used in the systems, ii) the size of electrodes and iii) the positioning of the electrodes in the different systems.

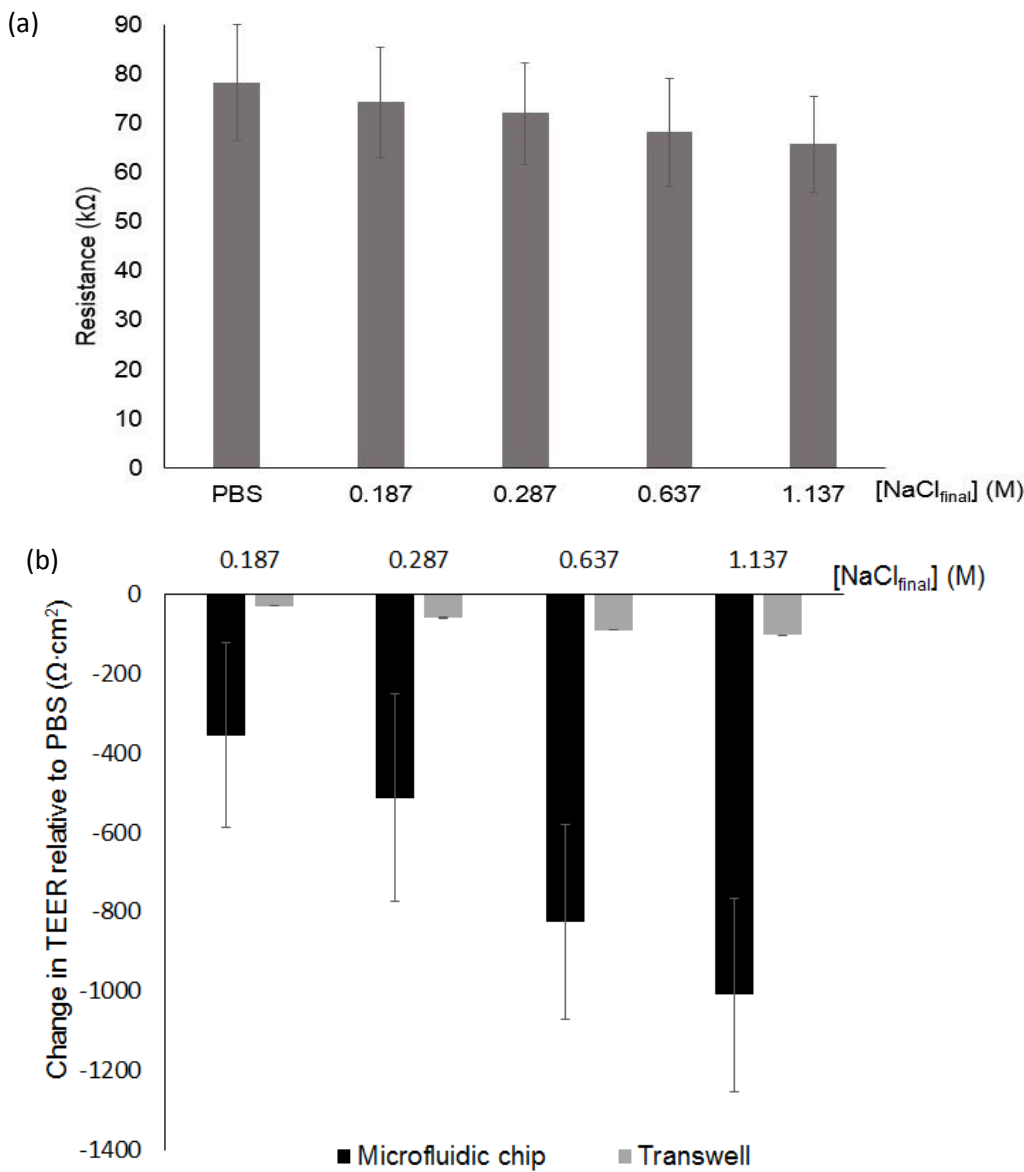


Figure 6.8 Characterisation of electrodes in microfluidic chip. (a) Raw resistance values measured for the varying NaCl concentrations. Impact of varying the concentrations of NaCl solution on the resistance measured on the system. (b) TEER values were calculated using PBS as the baseline for microfluidic device and Transwell inserts. (n = 3, Mean \pm SD)

The resistance obtained from the microfluidic devices could vary from microchamber to microchamber (Figure 6.9). This was most likely due to the variance in the positioning of the electrodes in each microchamber or the size of the electrodes. Lee et. al. [32] estimated that for every millimeter difference in the distance between the two recording electrodes resulted in the resistance changing by approximately 2.5 kΩ. Due to the variability of the resistance from microchamber to microchamber, it was therefore necessary to record the baseline resistance values for each microchamber prior to seeding the Caco-2 cells.

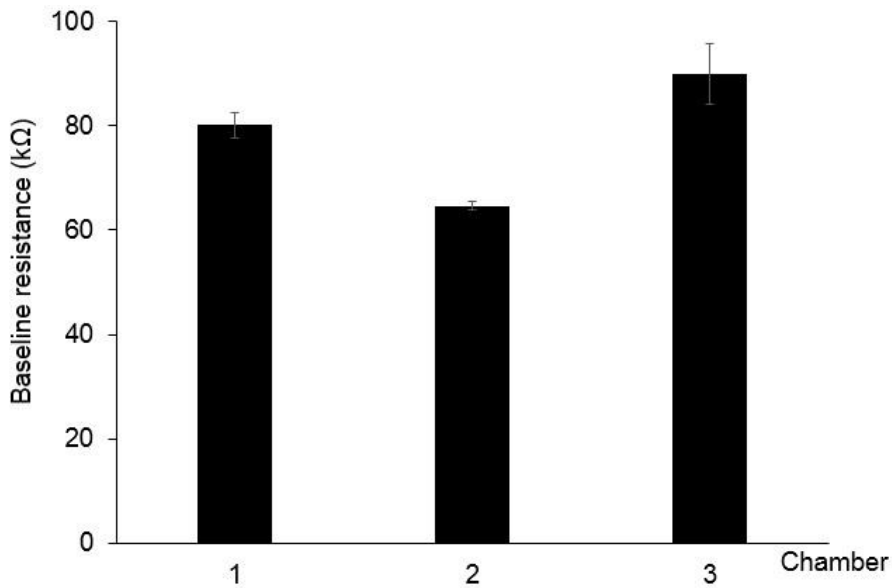


Figure 6.9 Baseline resistance of different chambers filled with PBS on the same microchip.

6.4.3 TEER measurements of Caco-2 cells cultured in microchip

TEER measurements from the microfluidic device were recorded under two different conditions. i) chambers seeded with Caco-2 cells; ii) chambers without Caco-2 cells. TEER measurements were recorded from day 3 of cell culture. The TEER measurements recorded from the microchambers without cells were used to determine the stability of electrodes under long-term exposure of serum containing medium. Figure 6.10 shows low readings fluctuating in the range of -100 to $+100 \Omega \cdot \text{cm}^2$ for the microchambers without Caco-2 cells cultured. The resistance measurements do not appear to trend either upward or downward as a function of time. We hypothesize that the fluctuations of the TEER values could result from the noise or error in the system as well as other variable that could not be perfectly controlled such as temperatures or resistivity of the cell culture medium. The results illustrated that the electrodes in the microfluidic system were stable for long term experimental measurements in serum-containing medium.

Importantly, the resistance measurements recorded from the microchambers seeded with Caco-2 cells displayed a steady increase in the TEER values from day 0, peaking at day 7 ($\approx 1400 \Omega \cdot \text{cm}^2$) and decreasing slightly (Figure 6.10).

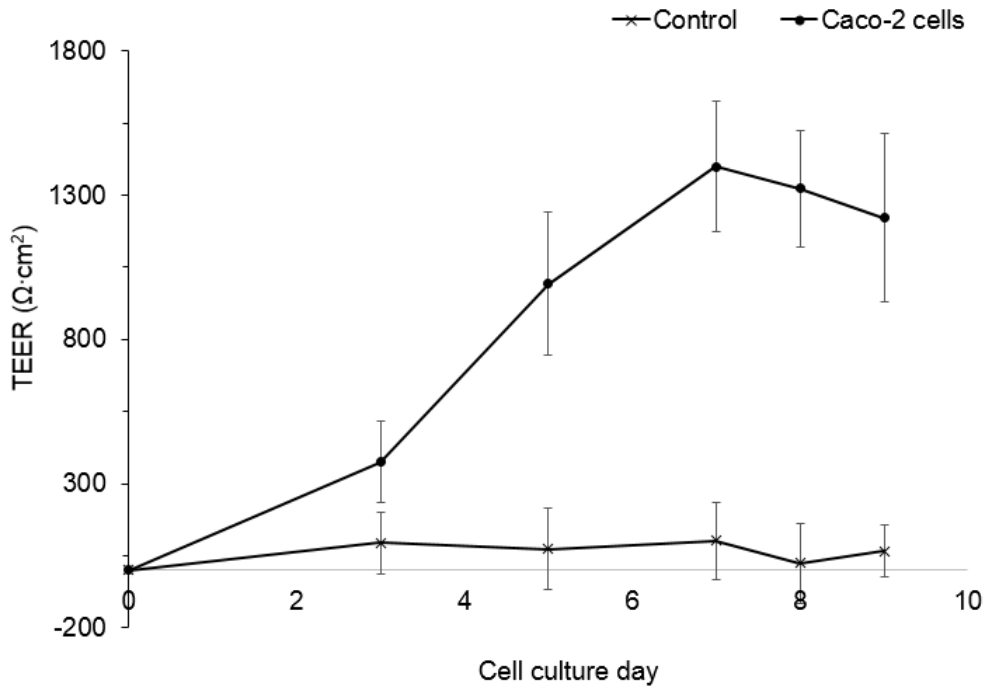


Figure 6.10 TEER measurements recorded with Caco-2 cells and no Caco-2 cells (Control) in microfluidic device. (n = 12)

Comparison of TEER measured on microchip and Transwell inserts. The TEER measurements recorded for Caco-2 monolayers cultured in the microfluidic device were compared with the TEER measurements recorded for the Transwell inserts. The TEER values recorded for the Transwell system increased steadily from day 0, peaking at $\approx 976.1 \Omega \cdot \text{cm}^2$ and plateauing from day 5. This similar trend was also observed in the microfluidic device. However TEER values in the microfluidic device drop slightly from day 7 to $\approx 1222.8 \Omega \cdot \text{cm}^2$ at day 9. The TEER values recorded in the microfluidic device were higher than the readings recorded from the Transwell cultures (Figure 6.11). This difference in TEER values between the two systems were also observed in the characterization studies (Figure 6.8b).

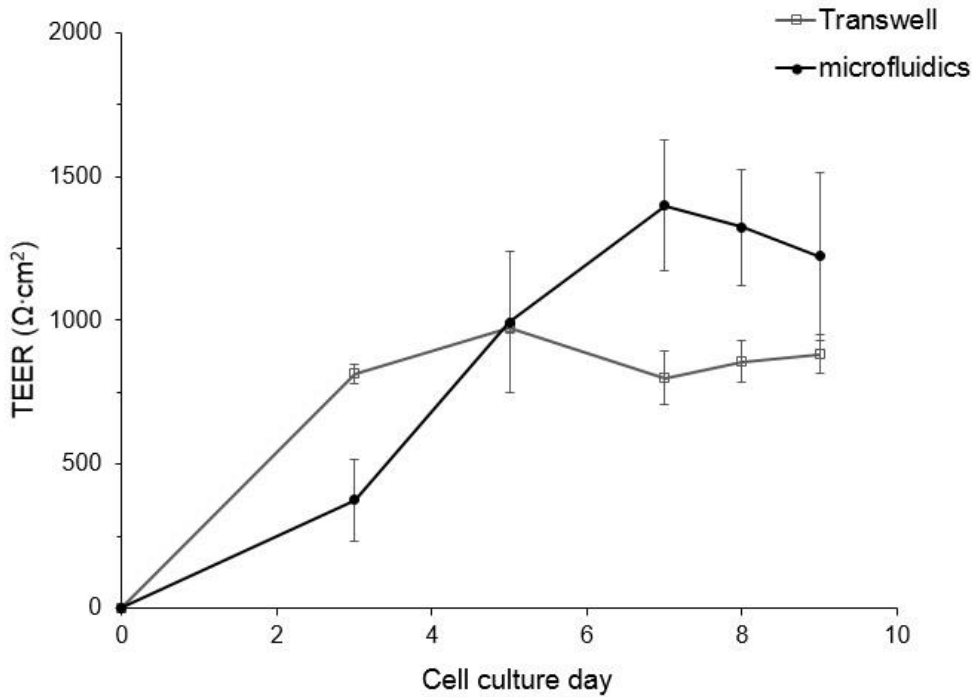


Figure 6.11 TEER measurements of Caco-2 cells cultured in thiol-ene microchip and Transwell inserts. For the same cell concentration of 2.55×10^5 cells/cm². (where $n = 12$ for microfluidic set-up; $n = 5$ for Transwell inserts)

6.4.4 Effect of membrane enhancers on TEER measurements

To further demonstrate that the electrodes in the microfluidic device can detect dynamic resistance changes in response to chemical factors, TDM was introduced to the Caco-2 monolayers cultured in the microfluidic and Transwell systems.

Challenging the Caco-2 cells cultured in the Transwell system with 100 μ M of TDM resulted in a decrease in TEER values of $\approx 67.7\%$ of initial values. Increasing the TDM concentration from 100 μ M to 400 μ M resulted in a 50% decrease in TEER values (Figure 6.12). Similar drop in TEER values was also observed in the microfluidic system (Figure 6.12). In the microfluidic device, challenging the cells with 100 μ M and 400 μ M of TDM resulted in percentage decrease in TEER values of 30% and 20.9%, respectively, of initial values (Figure 6.12). The percentage decrease in TEER values recorded for the microfluidic system were lower compared to the Transwell inserts. When the cells were exposed to 100 μ M of TDM, the percentage drop in TEER for the microfluidic device was almost two times lower than the data from Transwell cultures (Figure 6.11).

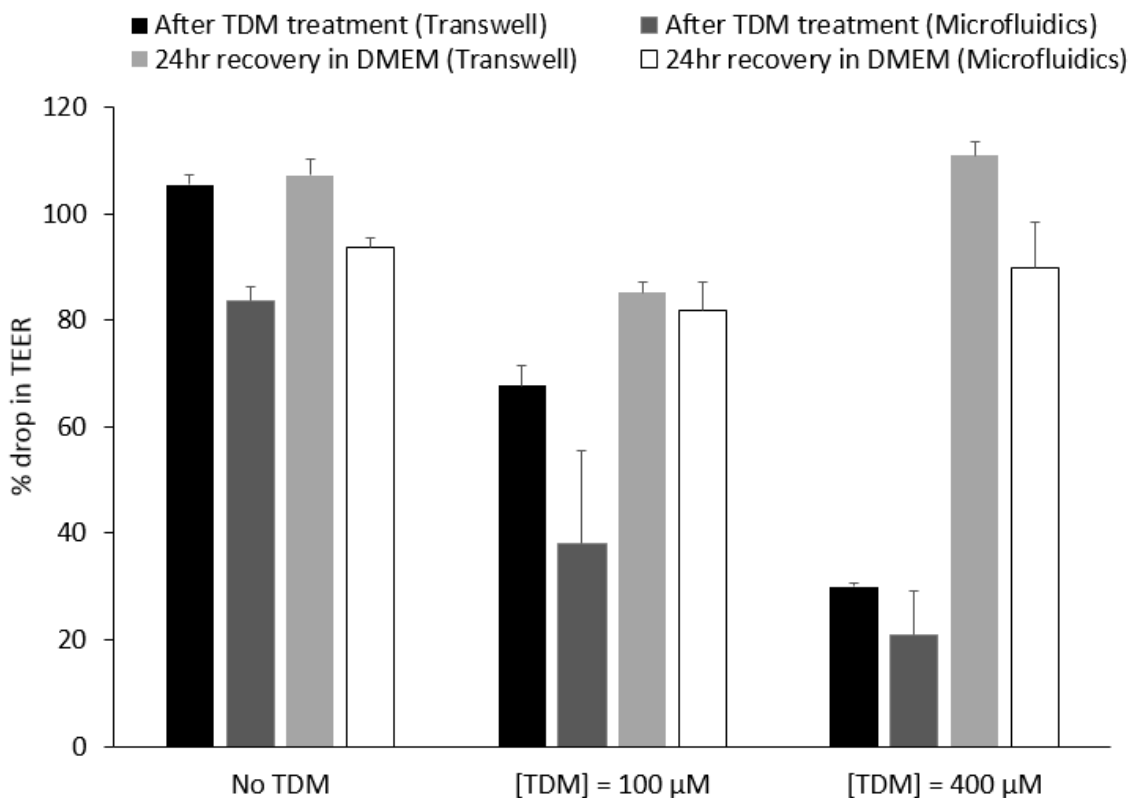


Figure 6.12 Impact of different concentrations of TDM on TEER measurements. (n = 3)

When the cells in the two systems were left to recover in normal cell culture medium, both systems showed signs of recovery. TEER values recorded from the Transwell system after 24 hr recovery for 100 μM and 400 μM was 85.2% and 110.9% respectively. Importantly, the TEER values recorded from the microfluidic device for the 100 μM and 400 μM after 24 hr of recovery was 81.9 % and 90 % respectively. The preliminary studies clearly demonstrated that the microelectrodes in the microfluidic system could sense changes in the Caco-2 monolayers.

6.5 Discussion

Biocompatibility studies of InBiSn metal with Caco-2 cells.

As the metal would be in direct contact with the cell culture media for long periods (> 10 days of cell culture), it was vital to investigate the biocompatibility of the electrode metal with Caco-2 cells. Biocompatibility studies with Caco-2 cells were only conducted with InBiSn metal, as it is common knowledge that Pt is biocompatible and is widely used in medical devices [33]. The biocompatibility studies of InBiSn metal with Caco-2 cells showed very promising results. Caco-2 cells were observed to multiply during the 6 days of cell

culture and mean vitality was > 95% near the metal. Having this knowledge is powerful because this will allow us to confirm the use of this metal as an electrode material in the microfluidic chip.

Microelectrode fabrication.

Previous reports [2,11,12] showed that inserting Ag/AgCl electrodes into the inlet tubes that were connected to the microfluidic device. However, this may risk introducing air bubbles into the system. Booth et. al. [9] reported sputtering Ag/AgCl electrodes in the microfluidic device. Such method is time consuming and may obstruct microscopic visualization of the cells. Ferrell et. al. [13] reported inserting the Ag/AgCl electrodes directly on the microchamber with the wiring of the bottom electrodes exiting from the bottom fluidic layer. Although such method was simple, the wiring of the bottom electrodes would prevent the use of an inverted microscope. Furthermore, the entire system must be on an elevated platform to prevent the Ag/AgCl wires from being crushed. Griep et. al. [15] and Douville et. al. [10] also reported on inserting the electrodes through the sides of the microchip. Due to the compactness of the designs on the thiol-ene microchip, the above mentioned positioning of the electrodes was not feasible. The reported positioning of the electrodes described in this chapter was the most appropriate for the thiol-ene microchip. Placement of the electrodes directly above and below the porous membrane enabled the electrodes to be in close proximity with the cells. As mentioned earlier, this would reduce the noise imposed on the resistance measurements by the cell culture medium [10].

The reported procedure of embedding the microelectrodes presented in this chapter was simple and did not require unique metal deposition. Furthermore, the metals used for fabricating the microelectrodes were inexpensive and were commercially available. This method also allowed more than one set of electrodes to be embedded on the same microfluidic chip. However, with more than one set of electrodes on the same microchip also meant more than one set of connecting wires from the electrodes. As shown in Figure 6.5a, there were numerous connecting wires on the microchip. Therefore, much care was required to ensure the right set of connecting wires were connected to the multimeter when recording the TEER values. Additionally, it was important to ensure the wires did not get into the way of the motors on the fluidic system. If the wires were caught in the motors on the fluidic system, the motor would stall or the leaking would start at the junction where the electrode was attached to the microchip. Furthermore, the wires may get in the way during microscopic imaging. Therefore, the wires needed to be arranged to allow proper microscopic imaging of the cells on the microchip.

Reliability of microelectrodes for TEER measurements.

To our understanding, there are no reports on using InBiSn or a combination of InBiSn and Pt metals for acquiring TEER measurements. The characterization studies showed that the microelectrodes were able to detect increasing NaCl concentrations (Figure 6.7). Further TEER measurements from microchambers not seeded with Caco-2 cells showed consistent TEER values throughout the 10 days in the incubator (37°C, 5% CO₂). This was an indication that there were no undesirable changes on the electrode surfaces despite being immersed in cell culture medium for long periods. Importantly, the TEER measurements (Figure 6.10, 6.11) illustrated that the electrodes were positioned appropriately to measure TEER in real time from cells cultured over a small surface area without disrupting the integrity of the cells. Additionally, when the Caco-2 cells were challenged to the membrane enhancer, TDM, the microelectrodes could detect dynamic changes in the integrity of the Caco-2 cells. The results showed that the electrodes were reliable and promising. The only drawback of the fabricated microelectrodes was the necessity of obtaining baseline readings for each set of the microelectrodes to ensure accurate measurements and comparisons of TEER values.

Comparisons of TEER values between the microfluidic device and Transwell cultures when challenged with membrane enhancer

In this study, the membrane enhancer, TDM, was used to disrupt the integrity of the Caco-2 monolayer. The concentrations used in our studies were previously reported [26] that will sufficiently disrupt the integrity of the Caco-2 monolayer. However, the concentration used will allow the Caco-2 monolayers to regain its barrier integrity after incubation for 24 hr in cell culture medium. Therefore, one will expect the TEER values to drop after challenging the Caco-2 monolayers to TDM and an increase of TEER values after 24 hrs recovery period in cell culture medium. Our results presented in Figure 6.12 showed this trend.

Moreover, when the Caco-2 monolayers were challenged to TDM, significant differences of the recorded TEER values between the microfluidic device and Transwell cultures were showed in Figure 6.12. This significant difference between the two systems maybe due to two reasons: i) the presence of a thick unstirred fluid layer in the static Transwell cultures [34]. This phenomenon may lead to lower numbers of tight-junctions interacting with TDM. Conversely, in the microfluidic device, the presence of fluid flow might have increased the interaction of TDM with the tight junctions in the Caco-2 monolayer and therefore resulting in a leakier Caco-2 monolayer in the microfluidic device. ii) The relatively small cell culture area in the microfluidic system as compared to the Transwell inserts. A minor defect in the Caco-2 layer can have a major impact on the recorded TEER values [2].

Comparison of TEER values measured on microfluidic device and Transwell cultures.

TEER values acquired from the Caco-2 monolayers may vary between labs [24]. TEER values may be influenced by various factors such as temperatures [29], physical support for cell culture [30], cell passage number [35] as well as the material, quality and surface state of the electrodes.

In previous reported literature, TEER values in microfluidic chips were often different from the TEER values measured from the Transwell set-up, despite using the same cell-types [2,9,11,12,15,17]. As mentioned earlier, the difference in readings between the two systems could be due to the different size of electrodes used, positions of the electrodes [9,10,15]. The results reported in Figures 6.8b, 6.11 and 6.12 further confirmed this. The difference in TEER measurements can result from specific measurement-related effects in microfluidic systems rather than due to biological effects [2]. Even TEER values measured in microfluidic devices can also vary greatly and this could be caused by small variations in cell confluency [2]. Therefore, comparisons of the apparent TEER values between the two different systems might not be reliable to determine which system is the better of the two. Rather it was more important to analyse the trend of the TEER plotted against the cell culture day (Figure 6.11) and the calculated percentage drop in TEER values when the Caco-2 cells were challenged to TDM (Figure 6.12).

6.6 Conclusion

In this chapter, a novel integration of inert metal electrodes with microfluidic device for cell culture was described. The manner of fabricating and embedding the microelectrodes in the thiol-ene microchips was simple, did not require any costly or specialized microelectrode fabrication techniques and could be conducted in ambient temperatures. Besides, this form of embedding the electrodes on the microchip allowed the electrodes to be in close proximity with the cells.

The feasibility of the electrodes was demonstrated by measuring the TEER measurements across the Caco-2 monolayers cultured in the microchip. The TEER values acquired from the microfluidic device agreed with the expected results (increased plateau) from the Transwell studies. The electrodes in the microchip were also capable of detecting dynamic resistance changes across the Caco-2 monolayers. This was demonstrated by introducing a membrane enhancer to the Caco-2 monolayers. The acquired TEER values from the microfluidic chip also agreed with the expected results (drop in TEER values) from the Transwell studies.

References

- [1] D.W. Powell, Barrier function of Epithelia, *Am. J. Physiol.* 4 (1981) 275–288.
- [2] M. Odijk, A.D. van der Meer, D. Levner, H.J. Kim, M.W. van der Helm, L.I. Segerink, et al., Measuring direct current trans-epithelial electrical resistance in organ-on-a-chip microsystems., *Lab Chip.* 15 (2015) 745–52.
- [3] J.A. Stolwijk, K. Matrougui, C.W. Renken, M. Trebak, Impedance analysis of GPCR-mediated changes in endothelial barrier function: overview and fundamental considerations for stable and reproducible measurements, *Pflugers Arch.* 467 (2014) 2193–218.
- [4] R.S. Pai, K.M. Walsh, M.M. Crain, T.J. Roussel, D.J. Jackson, R.P. Baldwin, et al., Fully integrated three-dimensional electrodes for electrochemical detection in microchips: fabrication, characterization, and applications, *Anal. Chem.* 81 (2009) 4762–9.
- [5] S.K. Sia, G.M. Whitesides, Microfluidic devices fabricated in poly(dimethylsiloxane) for biological studies, *Electrophoresis.* 24 (2003) 3563–76.
- [6] J. Wang, G. Chen, A. Muck Jr, Movable contactless-conductivity detector for microchip capillary electrophoresis, *Anal. Chem.* 75 (2008) 4475–4479.
- [7] J. Chen, C. Xue, Y. Zhao, D. Chen, M.-H. Wu, J. Wang, Microfluidic impedance flow cytometry enabling high-throughput single-cell electrical property characterization., *Int. J. Mol. Sci.* 16 (2015) 9804–30.
- [8] K. Cheung, S. Gawad, P. Renaud, Impedance spectroscopy flow cytometry: on-chip label-free cell differentiation., *Cytom. Part A.* 65A (2005) 124–32.
- [9] R. Booth, H. Kim, Characterization of a microfluidic in vitro model of the blood-brain barrier (μ BBB)., *Lab Chip.* 12 (2012) 1784–92.
- [10] N.J. Douville, Y.-C. Tung, R. Li, J.D. Wang, M.E.H. El-Sayed, S. Takayama, Fabrication of two-layered channel system with embedded electrodes to measure resistance across epithelial and endothelial barriers, *Anal. Chem.* 82 (2010) 2505–11.
- [11] D. Huh, B.D. Matthews, A. Mammoto, M. Montoya-Zavala, H.Y. Hsin, D.E. Ingber, Reconstituting organ-level lung functions on a chip, *Science* (80-.). 328 (2010) 1662–8.
- [12] H.J. Kim, D. Huh, G. Hamilton, D.E. Ingber, Human gut-on-a-chip inhabited by microbial flora that experiences intestinal peristalsis-like motions and flow, *Lab Chip.* 12 (2012) 2165–74.
- [13] N. Ferrell, R.R. Desai, A.J. Fleischman, S. Roy, H.D. Humes, W.H. Fissell, A microfluidic bioreactor with integrated transepithelial electrical resistance (TEER) measurement electrodes for evaluation of renal epithelial cells, *Biotechnol. Bioeng.* 107 (2010) 707–16.
- [14] P.A. Vogel, S.T. Halpin, R.S. Martin, D.M. Spence, Microfluidic transendothelial electrical resistance measurement device that enables blood flow and postgrowth experiments, *Anal. Chem.* 83 (2011) 4296–301.
- [15] L.M. Griep, F. Wolbers, B. de Wagenaar, P.M. ter Braak, B.B. Weksler, I.A. Romero, et al., BBB on chip: microfluidic platform to mechanically and biochemically modulate blood-brain barrier function, *Biomed. Microdevices.* 15 (2013) 145–50.
- [16] T. Sun, E.J. Swindle, J.E. Collins, J.A. Holloway, D.E. Davies, H. Morgan, On-chip epithelial barrier function assays using electrical impedance spectroscopy, *Lab Chip.* 10 (2010) 1611–7.

- [17] C. Huang, Q. Ramadan, J.B. Wacker, H.C. Tekin, C. Ruffert, G. Vergères, et al., Microfluidic chip for monitoring Ca²⁺ transport through a confluent layer of intestinal cells, *RSC Adv.* 4 (2014) 52887–52891.
- [18] A. Ainla, S. Xu, N. Sanchez, G.D.M. Jeffries, A. Jesorka, Single-cell electroporation using a multifunctional pipette., *Lab Chip.* 12 (2012) 4605–9.
- [19] J.-H. So, M.D. Dickey, Inherently aligned microfluidic electrodes composed of liquid metal, *Lab Chip.* 11 (2011) 905–11.
- [20] A.R. Abate, T. Hung, R.A. Sperling, P. Mary, A. Rotem, J.J. Agresti, et al., DNA sequence analysis with droplet-based microfluidics., *Lab Chip.* 13 (2013) 4864–9.
- [21] Solder Alloys, http://alasilir.com/reference/solder_alloys/.
- [22] W. Benenson, J.W. Harris, H. Stöcker, H. Lutz, *Handbook of physics*, 1st ed., Springer-Verlag New York, New York, 2002.
- [23] M.E. Mycielska, M.B.A. Djamgoz, Cellular mechanisms of direct-current electric field effects: galvanotaxis and metastatic disease, *J. Cell Sci.* 117 (2004) 1631–1639.
- [24] I. Hubatsch, E.G.E. Ragnarsson, P. Artursson, Determination of drug permeability and prediction of drug absorption in Caco-2 monolayers, *Nat. Protoc.* 2 (2007) 2111–9.
- [25] S.B. Petersen, L.G. Nielsen, U.L. Rahbek, M. Guldbrandt, D.J. Brayden, Colonic absorption of salmon calcitonin using tetradecyl maltoside (TDM) as a permeation enhancer, *Eur. J. Pharm. Sci.* 48 (2013) 726–34.
- [26] S.B. Petersen, G. Nolan, S. Maher, U.L. Rahbek, M. Guldbrandt, D.J. Brayden, Evaluation of alkylmaltosides as intestinal permeation enhancers: comparison between rat intestinal mucosal sheets and Caco-2 monolayers, *Eur. J. Pharm. Sci.* 47 (2012) 701–12.
- [27] V. Gupta, N. Doshi, S. Mitragotri, Permeation of insulin, calcitonin and exenatide across Caco-2 monolayers: measurement using a rapid, 3-day system, *PLoS One.* 8 (2013) e57136.
- [28] T. Yang, J.J. Arnold, F. Ahsan, Tetradecylmaltoside (TDM) enhances in vitro and in vivo intestinal absorption of enoxaparin, a low molecular weight heparin, *J. Drug Target.* 13 (2005) 29–38.
- [29] L.-F. Blume, M. Denker, F. Gieseler, T. Kunze, Temperature corrected transepithelial electrical resistance (TEER) measurement to quantify rapid changes in paracellular permeability, *Pharmazie.* 65 (2010) 19–24.
- [30] C.M. Lo, C.R. Keese, I. Giaever, Cell-substrate contact: another factor may influence transepithelial electrical resistance of cell layers cultured on permeable filters, *Exp. Cell Res.* 250 (1999) 576–80.
- [31] Millicell ERS-2 Voltohmmeter, <http://www.merckmillipore.com/>.
- [32] W.G. Lee, H. Bang, H. Yun, J.A. Kim, K. Cho, C. Chung, et al., Effect of geometry on impedance of cell suspended media in electrically mediated molecule uptake using a microstructure, *Curr. Appl. Phys.* 8 (2008) 696–699.
- [33] A. Cowley, B. Woodward, A healthy future: Platinum in medical applications, *Platin. Met. Rev.* 55 (2011) 98–107.
- [34] I.J. Hidalgo, K.M. Hillgren, G.M. Grass, R.T. Borchardt, Characterization of the unstirred water level in Caco-2 cell monolayers using a novel diffusion apparatus, *Pharm. Res.* 8 (1991) 222–227.

- [35] M.J. Briske-Anderson, J.W. Finley, S.M. Newman, The influence of culture time and passage number on the morphological and physiological development of Caco-2 cells, *Proc. Soc. Exp. Biol. Med.* 21 (1997) 248–257.

CHAPTER 7: Thiol-ene based microchip Caco-2 monolayer for passive transport studies

This chapter is a summary of the manuscript prepared for submission to a journal site.

In the preceding chapters (chapter 4 to 6), the presented thiol-ene based microfluidic chip showed promising results in supporting long-term cell culture. The incorporation of microelectrodes within in the microchip (Chapter 6) also increased the possibility of quantifying the integrity of the Caco-2 monolayers. However, further studies are required to understand the morphology and the barrier function of the Caco-2 cells cultured in the microchip.

In this chapter, microscopic techniques (phase contrast microscopy and fluorescent imaging) that were applied to study the morphology of Caco-2 cells cultured within the microchip are described. Model drug transport studies over the Caco-2 cell layer are described and discussed. The studies described in this chapter were conducted to better understand the behaviour of Caco-2 cells cultured under fluidic conditions.

7.1 Motivation

The Transwell intestinal culture system is the gold standard *in vitro* model for assessing and predicting permeability and absorption of oral drugs in the pharmaceutical industry. However, this platform does not mimic *in vivo* conditions as it does not support the application of any form of luminal flow conditions on the cells. Although the Transwell system is easy to implement, it requires a large amount of cells and at least 2-3 weeks are required to culture the Caco-2 cells before they can be used for drug permeability studies. Therefore, to address these limitations of Transwell inserts, the multi-layer multi-chamber thiol-ene microfluidic chip was engineered (presented in Chapter 4).

As previously mentioned in Chapter 2, Caco-2 cells form tight junctions and have the potential to exhibit structural and functional differentiation and polarization. The Caco-2 cells cultured in the microfluidic device required a shorter duration (7-8 days of cell culture) to form monolayers (from the reported TEER values in Chapter 6). Although the Caco-2 cells in the microfluidic device required a shorter duration to form monolayers, there was still a need to investigate if the Caco-2 cells had polarised and differentiated under continuous fluidic conditions. This is possible by measuring their expression of a specific brush border enzyme.

To further assess the barrier properties of the Caco-2 monolayers cultured in the microfluidic device, transport studies were carried out using three different test compounds. The compounds used in the studies were mannitol, fluorescein isothiocyanate (FITC)-labeled dextran (FD4) and insulin. Insulin was chosen as a proof-of-concept demonstration in using the Caco-2 monolayers cultured in the thiol-ene microchip for drug permeability studies. Insulin is usually administered by the subcutaneous route [1,2]. The lives of diabetic patients may be significantly improved if insulin could be routinely administered by oral delivery [1]. However, oral delivery of insulin has some limitations, due to insulin degradation by proteolytic enzymes in the gastrointestinal tract and poor permeability through the intestinal epithelium [2]. To overcome this, attempts have been made to facilitate the absorption of insulin by co-administering membrane enhancers [3–7] (Figure 1). In this chapter, permeability studies conducted to examine the response of the Caco-2 monolayers to a specific membrane enhancer are described.

7.2 Materials and methods

7.2.1 Caco-2 cell culture

Human Caco-2 intestinal epithelial cells used in the experiments were obtained from American Type Culture Collection ((ATCC), HTB-37, Germany). The passages of the Caco-2 cell line used in the microfluidics studies ranged from the 40th to 50th passages, and for the Transwell studies, passages in the range of 40th to 65th were used. The Caco-2 cells were cultured routinely in Dubelco's Modified Eagle Medium (DMEM; Sigma, Denmark). The culture medium is supplemented with 10 % (v/v) heat-inactivated fetal bovine serum (FBS; Sigma, Denmark), 1% (v/v) nonessential amino acids (NEAA; Gibco, Denmark) and 1% (v/v) penicillin-streptomycin (P/S; Gibco, Denmark).

7.2.2 Morphological studies

Preparation of cells for fluorescence imaging in microfluidic device. Phosphate buffer saline (PBS) was first pumped into both the upper and lower fluidic layers for 45 min at a flow rate of 3 μ l/min. Next, the cells were fixed, by pumping 4 % paraformaldehyde into the microchambers for 30 min at a flow rate of 5 μ l/min. This was followed by permeabilising the cells with 0.1 % (v/v) Triton-X-100. Next, a blocking buffer (1 % BSA, 0.1 % Tween 20 in PBS) was introduced into the cells for 1 hr. All chemicals mentioned above were purchased from Sigma, Denmark.

To visualize tight junctions, immunofluorescence staining was performed using mouse anti-ZO-1 (ZO-1; Life Technologies, Denmark) diluted in the blocking buffer (1:100), and introduced to the cells. The samples were protected from light and left static overnight in the fridge at 4°C. Immunofluorescence staining was also carried out to stain the mucoprotein, mucin-2. Primary mouse monoclonal antibody (ab11197; AbCam, Denmark) prepared in blocking buffer (1:100), was introduced to the cells. The samples were protected from light and left static overnight in the fridge at 4°C. After which, the cells were rinsed with blocking buffer followed by introducing the secondary antibody (AlexaFluor 488 goat anti-mouse; Life technologies, Denmark) prepared in blocking buffer (1:200) and left static in room temperature for 2 hrs. The immunofluorescence staining for tight junctions and mucin were carried out in different microchambers.

Staining of the nucleus were carried out by diluting 7-aminoactinomycin D (AAD) in PBS and incubated with the cells for 1 hr at room temperature. Between each of the procedure, the cells are rinsed by pumping PBS the microchambers. Lastly mounting media (Vectashield; VWR, Denmark) was added to the cells to protect the fluorescent dyes.

Preparation of cells for fluorescence imaging in Transwell inserts. The dyes and procedure for cell staining were the same for the Transwell inserts. After the cells were stained, a scalpel was used to cut out the Transwell porous membrane. These cut out membranes were mounted onto microscopic glass slides. Mounting media was added onto the cells before placing a cover slip on the stained cells and stored in fridge (4°C) overnight before imaging the stained cells.

Imaging of stained cells. The stained cells were scanned using an upright scanning confocal microscope (ZEISS Axioscope; Carl Zeiss, Germany) equipped with a photomultiplier tube coupled to a UV laser (405 nm) and diode lasers with working wavelengths of 488nm and 555nm. To visualise the tight junctions and mucus, excitation/emission wavelength of 488/570 nm was chosen. The stained nuclei were visualised at excitation/emission wavelengths of 546/647 nm. The fluorescent images of the cells were recorded with the image software (Zen lite; Zeiss, Germany).

7.2.3 Aminopeptidase studies

L-alanine-4-nitroanilide hydrochloride (L-A4N; Sigma, Denmark) was prepared by dissolving the L-A4N substrate in Dulbecco's Modified Eagle Medium without phenol red (DMEM^{PR}; Gibco, Denmark) to a concentration of 1.5 mM.

Transwell insert studies. Experiments were carried out on cell culture day 21. The Caco-2 cells were first rinsed with DMEM^{PR} on both the apical and basolateral sides for 3 times. Next, 500 µl of L-A4N substrate solution was added to the apical side of the cells and 1500 µl of DMEM^{PR} was added to the basal lateral side

of the cells. The Caco-2 cells were then incubated at 37 °C. Sample aliquots of 100 µl was removed from the apical side at 30 min intervals and transferred to a 96-well microplate. Studies were carried out for a 2 hr period. Analysis of the sample aliquots were carried out with microplate reader (Victor 3V; Perkin Elmer) and DMEM^{PR} was set as the reference. The test was calibrated with a series of dilutions of 4-nitroanilide in DMEM^{PR}. One unit is defined as the hydrolysis of 1.0 µmol of 4-nitroanilide per minute. All of the reagents were prepared under the protection of light.

Microfluidic device. Aminopeptidase studies were carried out on day 5 of cell culture. Before starting the studies, DMEM^{PR} was perfused to both the top and bottom fluidic channels for 45 min at a flow rate of 3 µl/min. 200µl of DMEM^{PR} was added to each waste reservoirs. Next, 1.5 mM of L-A4N solution was flowed into the upper microchannels and microchambers of the thiol-ene microchip at a flow rate of 3 µl/min for 2 hr. Sample aliquots of 120 µl were removed from the outlets of the upper microchannels at every 30 min and transferred to a 96-well microplate. Similar to the Transwell studies, the sample aliquots from the microfluidic device were analysed for the cleaved product, 4-nitroanalide using a microplate reader. The test was calibrated with a series of dilutions of 4-nitroanilide in DMEM^{PR}. Studies were conducted in triplicates.

7.2.4 Permeability studies

Permeability studies for the microfluidic device were carried out on day 9 or day 10 of cell culture. Previously in Chapter 6 we observed the TEER in the microfluidic device peaking at day 7 of cell culture. It was believed the Caco-2 monolayers had formed a tight barrier by day 9 or day 10 of cell culture in the microfluidic device. Therefore permeability studies were conducted on day 9 or 10 of cell culture. Permeability studies in the Transwell system were conducted on day 21 of cell culture as reported by previous procedure [8].

Preparation of test compounds for permeability studies. Radioactively labelled [³H]-mannitol (PerkinElmer; USA), fluorescein isothiocyanate (FITC)-labeled dextran (FD4; 40kDa; Sigma, Denmark), insulin (Novo Nordisk, Denmark) and tetradecyl-β-D-Maltoside (TDM; Sigma, Denmark) were all prepared using buffer⁺⁺ as the diluent. Buffer⁺⁺ was prepared by mixing Hank's Buffered Saline solution (HBSS; Gibco, Denmark), 0.1% (wt/v) OVA (ovalbumin; from chicken egg white, Sigma, Denmark) and 10 mM HEPES (HEPES; Sigma, Denmark) at pH 7.4. The different compounds were prepared in the various concentrations: 0.8 µCi/ml [³H]-mannitol, 100 µM insulin (peptide/drug) or 540 µM FD4, and 0 or 400 µM TDM.

Permeability studies in microfluidic device. Before the start of experiment, the cell culture medium was replaced with buffer⁺⁺. Buffer⁺⁺ was flowed into the system for 1 hr at a flow rate of 3 µl/min. Following that, the buffer⁺⁺ was changed to the test solutions in the top fluidic layer. 200µl of buffer⁺⁺ was added to each waste reservoirs. Flow rate was set at 3 µl/min (in both the upper and lower layers) and sample aliquots of 100 µl

were collected at the outlets of the lower fluidic layer at every 15 min intervals for 1 hr. After the experiments, the test solutions were replaced with buffer⁺⁺ in the top fluidic layer. Buffer⁺⁺ was flowed in both the upper and lower fluidic layers for 45 min at a flow rate of 3 $\mu\text{l}/\text{min}$. Lastly, buffer⁺⁺ was changed to normal cell culture medium flowing through both upper and lower fluidic layers at a flow rate of 3 $\mu\text{l}/\text{min}$ for 24 hr recovery. Six set of permeability studies were conducted with the microfluidic system.

Permeability studies in Transwell inserts. Similar to the microfluidic studies, before carrying out the transport experiments, cell culture medium was changed to buffer⁺⁺. 400 μl of buffer⁺⁺ was added to the apical side and 1 ml of buffer⁺⁺ to the basolateral side. Next, the Transwell plate was placed into the incubator for 60 min. Following that, buffer⁺⁺ was replaced apically by 400 μl test solution at time zero, and the Transwell plates were incubated at 37°C and 5% CO₂ with gentle shaking. The gentle shaking was to ensure there was little unstirred diffusion layers of fluid in the basolateral region. Basolateral samples were collected every 15 minutes for 1 hr. After the experiments, the cells were washed twice with buffer⁺⁺ and replenished with medium for 24 hour recovery. Four sets of Transwell well permeability studies were carried out.

Analysis of sample aliquots. Analysis of [³H]-mannitol content was carried out in a scintillation counter (Packard TopCount; PerkinElmer), after mixing 1:1 with scintillation fluid (Microscint-40; PerkinElmer). FD4 content was analysed in a fluorescence plate reader (MD Spectramax Gemini, USA) with excitation/emission wavelengths of 490/525 nm, based on standard curves prepared from test solutions. Insulin content was analysed using commercial insulin enzyme immunoassay kit (EIA, Phoenix Pharmaceuticals, Germany), as recommended by the manufacturer (Phoenix Pharmaceuticals, Germany).

Data analysis of permeability results. The Caco-2 translocation of peptide or [³H]mannitol over Caco-2 layers is expressed as the apparent permeability (P_{app}). The expression of P_{app} was mentioned previously in chapter 2:

$$\text{Eq. (2.1):} \quad P_{app} = \frac{dQ}{dt} \frac{1}{A \cdot C_0}$$

Where dQ/dt is the steady-state flux across the cell layer (pmol/s), A is the surface area (1.12 cm² for Transwell, 0.1 cm² for microfluidic), and C_0 is the initial sample concentration [8].

The amount of insulin from the aliquot samples was estimated base on the calibration curve of insulin concentration fitted to eq. 7.1 using Prism-6 (GraphPad).

$$\text{Eq. (7.1):} \quad \text{Abs}(450\text{nm}) = A + \frac{B-A}{1+10^{((\log EC_{50}-x) \cdot C)}}$$

where x is $\log(\text{concentration})$ of peptide in M, and A , B , C and EC_{50} are fitting parameters [9].

Statistical analysis was carried out using the softwares, Origin and Prism, where unpaired Students t-tests were used for comparison, and a significant difference was considered if $p < 0.05$. Results were presented as the mean \pm standard deviation of the mean (SD).

Trans-epithelial electrical resistance (TEER) measurements. The methods for measuring TEER for the Transwell and microfluidic device were described and discussed in Chapter 6.

7.3 Results and discussion

7.3.1 Phase contrast imaging of Caco-2 monolayers

The cells were observed to adhere on the ECM coated Teflon membrane 30 minutes after cell seeding in the microfluidic chip. During the phase of active growth, it was observed that once the flow of cell culture media had started (first 24 hrs of cell culture), the Caco-2 cells were observed to spread out (results not shown).

During the first 24 hrs of cell culture, under continuous perfusion of cell culture, the Caco-2 cells were observed in having the possibility of growing as clusters (Figure 7.1a). However, over the days of cell culture the Caco-2 cells were observed to multiply and differentiate. By day 2, distinct polygonal shape with clear, sharp boundaries between the Caco-2 cells were observed in all the microchambers (Figure 7.1b). The shape and morphology of the Caco-2 cells in the microfluidic device were similar to the Caco-2 cells cultured in microplate (reported in Chapter 6 Figure 6.7g, h).

Confluent monolayers of Caco-2 cells were observed in the microfluidic device typically around day 3-5 of cell culture. Folds (red arrows in Figure 7.1c) started appearing in the monolayers around day 5 (a suggestion of villous formation) and it became more challenging to observe single cells by optical microscopy. From day 7 onwards, the appearance of 'dark' patches (white arrow in Figure 7.1d) were observed on the cells. As the cell culture period progressed, these 'dark' patches increased in area, or more 'dark' patches started appearing on the Caco-2 monolayers. However, these 'dark' patches were not observed when the cells were cultured at a flow rate of 0.5 $\mu\text{l}/\text{min}$ (results not shown). These results were consistent with published studies showing Caco-2 cell monolayers cultured in microfluidic device displaying folds and undulations [10].

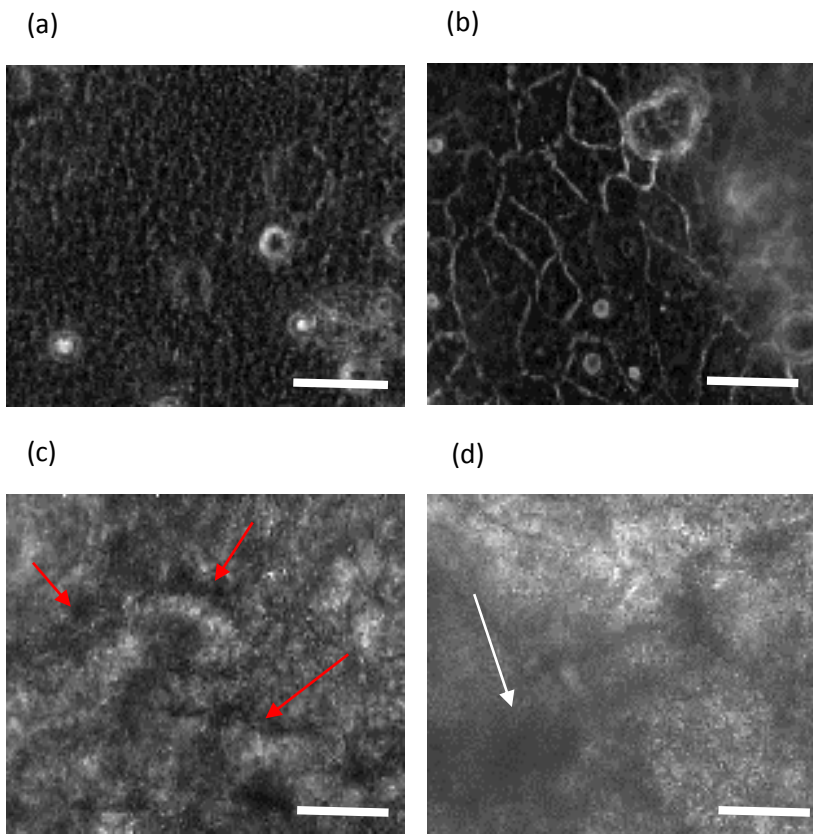


Figure 7.1. Phase contrast images of the Caco-2 cells cultured in the microchambers on the thiol-ene microchip over 10 days. (a) Day 1; (b) Day 2; (c) Day 5; (d) Day 8. Folds in the monolayer of Caco-2 cells start appearing from day 5 onwards (indicated by red arrows). Dark ‘patches’ on the Caco-2 monolayers from day 7 onwards. They become more prominent from day 8 of cell culture (indicated by white arrow). (Scale bar = 50 μm)

7.3.2 Fluorescent images of cells

The establishment of apical tight junctions determines the integrity of the human intestinal epithelial cell monolayer) [8]. Immunofluorescence microscopic studies using antibodies directed at the tight-junction protein, occludin, confirmed the formation of confluent Caco-2 monolayers, expressing tight junctions in the microfluidic device on day 3 (Figure 7.2a, b). Tight junctions were also observed in the Transwell samples on day 21 of cell culture (Figure 7.2d).

Further analysis of the vertical sections of the confocal images of the Caco-2 cells cultured in both systems (Figure 7.2b, e) revealed the tight-junction proteins were situated between neighbouring cells at the apical side of the Caco-2 cells (Figure 7.2c, e). Images of the cells cultured in the Transwell inserts at day 21 appeared cuboidal with heights of 14 – 20 μm (Figure 7.2e). However, the Caco-2 cells cultured in the thiol-ene microfluidic device (three days of cell culture) were observed to appear columnar in shape with heights of \approx 40 – 50 μm (Figure 7.2c). Our data is consistent with a previous report [10]. The Caco-2 cells cultured in the

microfluidic device were about the same columnar size and shape (30-40 μm) as reported in healthy human intestinal epithelial cells [11]. It was believed that the presence of continuous perfusion of cell culture medium in the microfluidic device may be responsible for stimulating the Caco-2 cells to polarise into columnar cells that were almost 2-fold taller than the cells from Transwell inserts.

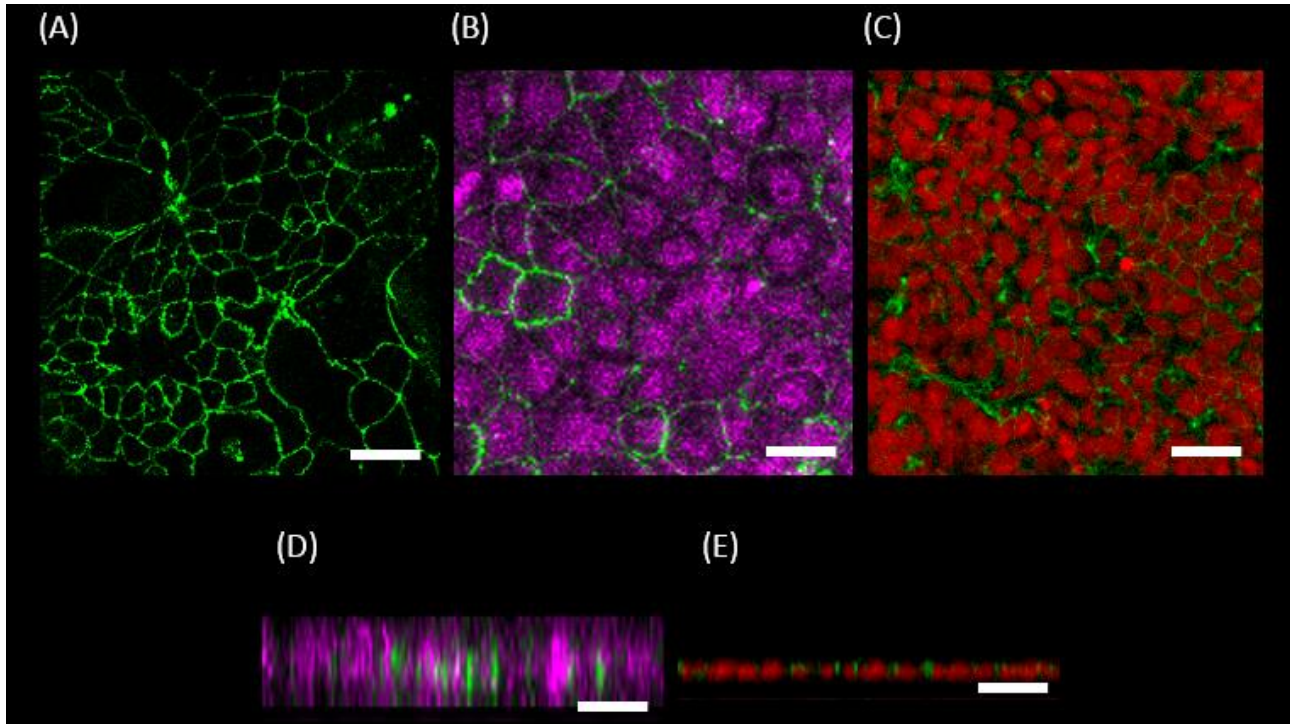


Figure 7.2 Immunostaining of tight junctions and nucleus of Caco-2 cells (a) – (c) cultured in microfluidic device. Cells were stained on day 3 of cell culture. Caco-2 cells cultured in Transwell inserts stained for nucleus and tight junctions (d) - (e). Cells were stained on day 21 of cell culture. a) The immunofluorescence image shows the distribution of the tight junction protein, occludin (green). b) Immunostaining of tight junctions (green) and nucleus (magenta). c) Vertical cross-section view of the Caco-2 monolayer (nucleus in magenta, tight junctions in green). The Caco-2 cells are $\approx 40 \mu\text{m} - 50 \mu\text{m}$ in height on day 3 of cell culture in the thiol-ene microfluidic chip. d) Top view of day 21 Caco-2 cells cultured in Transwell stained for nucleus (red) and tight junctions (green). e) Vertical confocal sectional view of Day 21 Caco-2 cells cultured in Transwell. Magnification of cells at 10 x. (Scale bar = 50 μm)

To identify and characterize the ‘dark’ patches (Figure 7.1d), the Caco-2 monolayers cultured in the microfluidic device were stained for the mucoprotein, Mucin-2 (MUC-2) on day 10 of cell culture. Mucin-2 is commonly found in human intestines. Our immunofluorescence staining directed towards Mucin-2, showed positive stains at the apical surfaces of the villous Caco-2 monolayers (Figure 7.3a). This was surprising as in an earlier study [10,12] claimed that the production of mucus on the Caco-2 cells cultured in a microfluidic device was due to fluid flow and cyclic peristaltic motions. However, the Caco-2 cells cultured in the thiol-ene microfluidic device were only exposed to low fluidic stresses ($\approx 0.008 \text{ dyn/cm}^2$). It was also reported the gastrointestinal tract has a tendency to protect itself from mechanical and other stresses by producing and

secreting a layer of lubricating mucus onto epithelial surfaces [13]. Therefore, we hypothesised the exposure to low fluidic shear stresses ($\approx 0.008 \text{ dyn/cm}^2$) might have resulted in the Caco-2 cells exhibiting some protective function by producing mucus on the apical side of the cells. To further confirm our observations, we also performed the same staining procedure on cells cultured in the Transwell inserts. Past studies reported that Caco-2 cells do not produce mucus when cultured in static culture conditions [14]. As expected the images of our Transwell cultures did not show the presence of mucin-2 on the Caco-2 monolayers (Figure 7.3b).

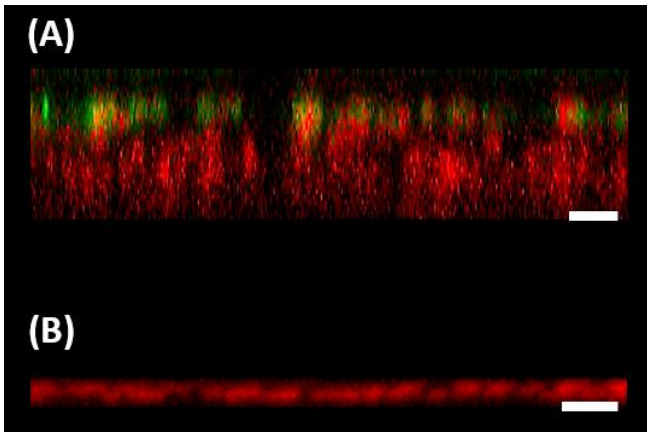


Figure 7.3 Immunofluorescence staining of nucleus and mucus on Caco-2 cells cultured in thiol-ene microchip on day 10 of cell culture (nucleus in red, Mucin-2 (MUC-2) in green). (a) Polarised Caco-2 cells cultured in microfluidic device, forming folds (villous-like structures) with heights of $\approx 100 \mu\text{m}$. (b) Cells cultured in Transwell were stained for nucleus and MUC-2 at day 21. Cells were taken at 10 x magnification. (Scale bar = $50 \mu\text{m}$)

The fluorescent images (Figure 7.3a) shows that the Caco-2 cells cultured in the microfluidic device formed folds and were capable of growing up to a height of $\approx 100 \mu\text{m}$ when they were cultured for long term (day 9 – 10). These results are consistent to an earlier study which showed that fluid flow can encourage the formation of villous structures in the Caco-2 monolayers [10,12].

7.3.3 Measurement of aminopeptidase activity

Once Caco-2 cells differentiate, they will form a monolayer of cells, coupled by tight junctions and express high level of brush border enzymes that are commonly found in small intestinal epithelial cells [15,16]. One of the brush border enzymes expressed is aminopeptidase.

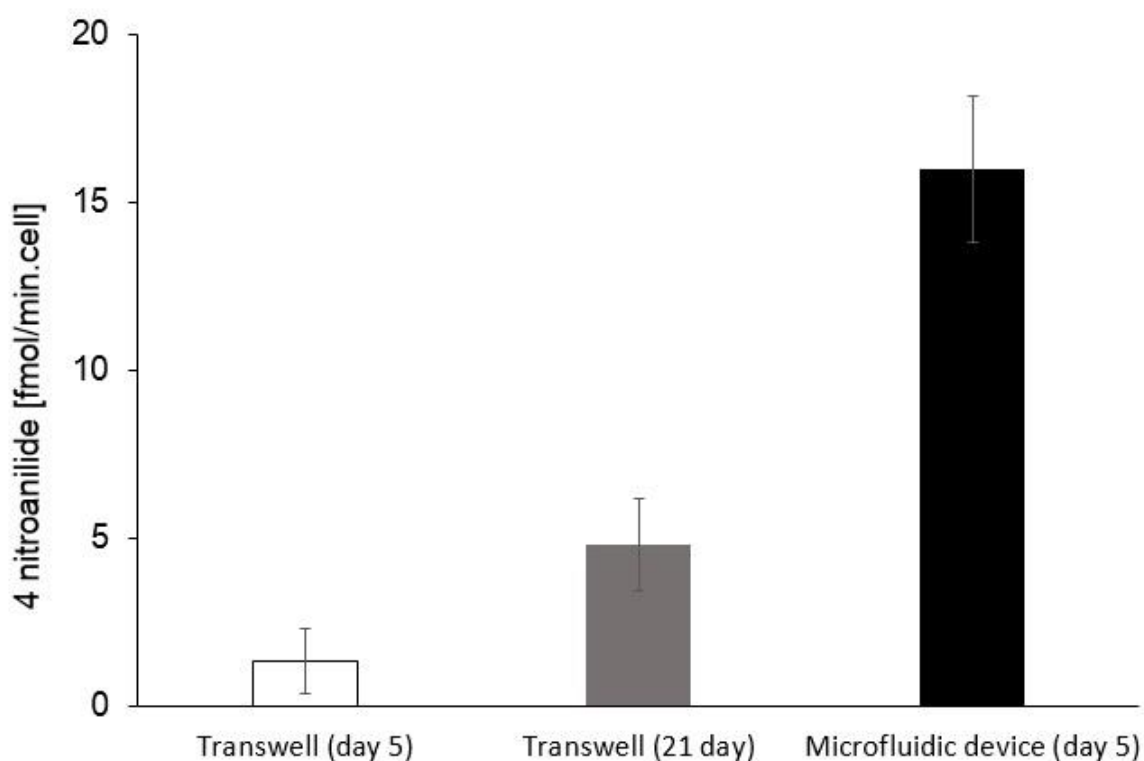


Figure 7.4 Differentiation of Caco-2 cells cultured in Transwell set-up and microfluidic device as indicated by the activity of the brush border enzyme aminopeptidase activity. (n = 3, mean \pm SD).

For the Transwell cultures, the measured amount of 4-nitroanilide for day 5 and 21 of cell culture was 1.34×10^{-15} mol/min-cell and 4.8×10^{-15} mol/min-cell respectively (Figure 7.4). Between days 5 and 21 of cell culture there was a 5-fold increase in aminopeptidase activity from the Transwell cultures. The increased in aminopeptidase activity between day 5 and day 21 of cell culture showed the Caco-2 cells in the Transwell cultures were still differentiating. Our data was also consistent with an earlier study [16]. Interestingly, an analysis of the samples collected from the thiol-ene microfluidic device at 5 days of cell culture, showed the aminopeptidase activity was 4 folds higher than the aminopeptidase activity in Transwell inserts at day 21 (Figure 7.4). These results clearly indicated that Caco-2 cells cultured under the presence of continuous flow (as in the microfluidic device) required a shorter time to polarise and differentiate.

7.3.4 Permeability studies of FITC–dextran (FD-4), mannitol and insulin in the presence or absence of membrane enhancer

Paracellular transport of compounds across the Caco-2 monolayers is governed by the presence of the tight junctions between adjacent cells. To assess if the Caco-2 monolayers cultured in the thiol-ene

microchip exhibit a rate-limiting barrier, the behaviour of three different test compounds (mannitol, fluorescein isothiocyanate (FITC)-dextran (FD 4) and insulin) was studied.

Permeability studies were carried out on day 9 or day 10 of cell culture for the microfluidic device. From the results recorded, the permeabilities (P_{app}) for mannitol, FD-4 and insulin were 3.94×10^{-6} cm/s, 2×10^{-7} cm/s and 9.43×10^{-7} cm/s, respectively, in the microfluidic chip. However, the P_{app} values of similar compounds in the static Transwell cultures were slightly lower as compared to the microfluidic device (Figure 7.5).

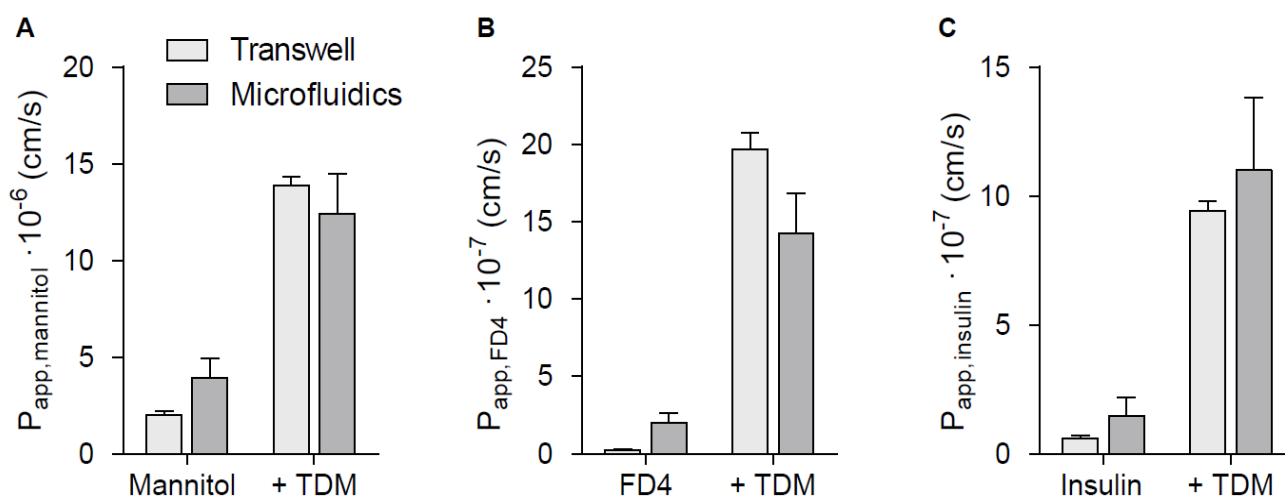


Figure 7.5 Permeability of A) mannitol, B) FD4 and C) insulin, alone or with TDM, across caco-2 monolayers grown in the Transwell or microfluidic setup. Data points represent mean of either 4 repeats (all Transwell values), 6 repeats for microfluidic experiments.

To further investigate whether the permeability of different test compounds was affected by the introduction of the membrane enhancer, TDM, we next challenged the Caco-2 monolayers in both the microfluidic device and the Transwell inserts to mixtures of test compounds with TDM. In both systems, the P_{app} values for all three compounds greatly increased (Figure 7.5) in the presence of TDM. In the microfluidic device, the P_{app} values for mannitol, FD-4 and insulin were 12.42×10^{-6} cm/s, 14.29×10^{-7} cm/s and 11.02×10^{-7} cm/s respectively (Figure 7.5). While the P_{app} values of the similar test compounds from the static Transwell cultures were 13.9×10^{-6} cm/s, 19.72×10^{-7} cm/s and 9.43×10^{-7} cm/s respectively. The permeability results clearly demonstrated that the addition of TDM effectively permeabilised the Caco-2 monolayers in both systems and allowed substantial transport of compounds across the Caco-2 monolayers. Additionally, the P_{app} values of the test compounds in the presence of TDM were comparable between the static Transwell cultures and the microfluidic system. The Caco-2 monolayers cultured in the microfluidic device could be a promising alternative *in vitro* model of the human intestines for drug transport studies.

7.3.5 TEER measurements across Caco-2 monolayers in the presence or absence of membrane enhancer

Similar to the membrane integrity study of the Caco-2 monolayers being challenged with TDM in Chapter 6, the Caco-2 monolayers in this study (in both the Transwell and microfluidic systems) clearly showed a decrease of the TEER values in the presence of TDM. The TEER values dropped to 29.5 % of initial values after challenging the Caco-2 cells with TDM in Transwell insert cultures. However, the TEER values increased to ≈ 107.2 % of initial values when the cells were left to recover in normal cell culture medium for 24 hr. TEER values measured in the microfluidic device dropped to ≈ 20.6 % of their initial values. When the Caco-2 monolayers were subjected to 24 hr continuous perfusion of cell culture medium, the TEER values recovered to ≈ 90 % of the initial values (Figure 7.6). This significant drop in TEER values in the presence of TDM and an increase in the TEER values during the 24 hr recovery in cell culture medium was consistent with the data acquired from the Transwell cultures (Figure 7.6).

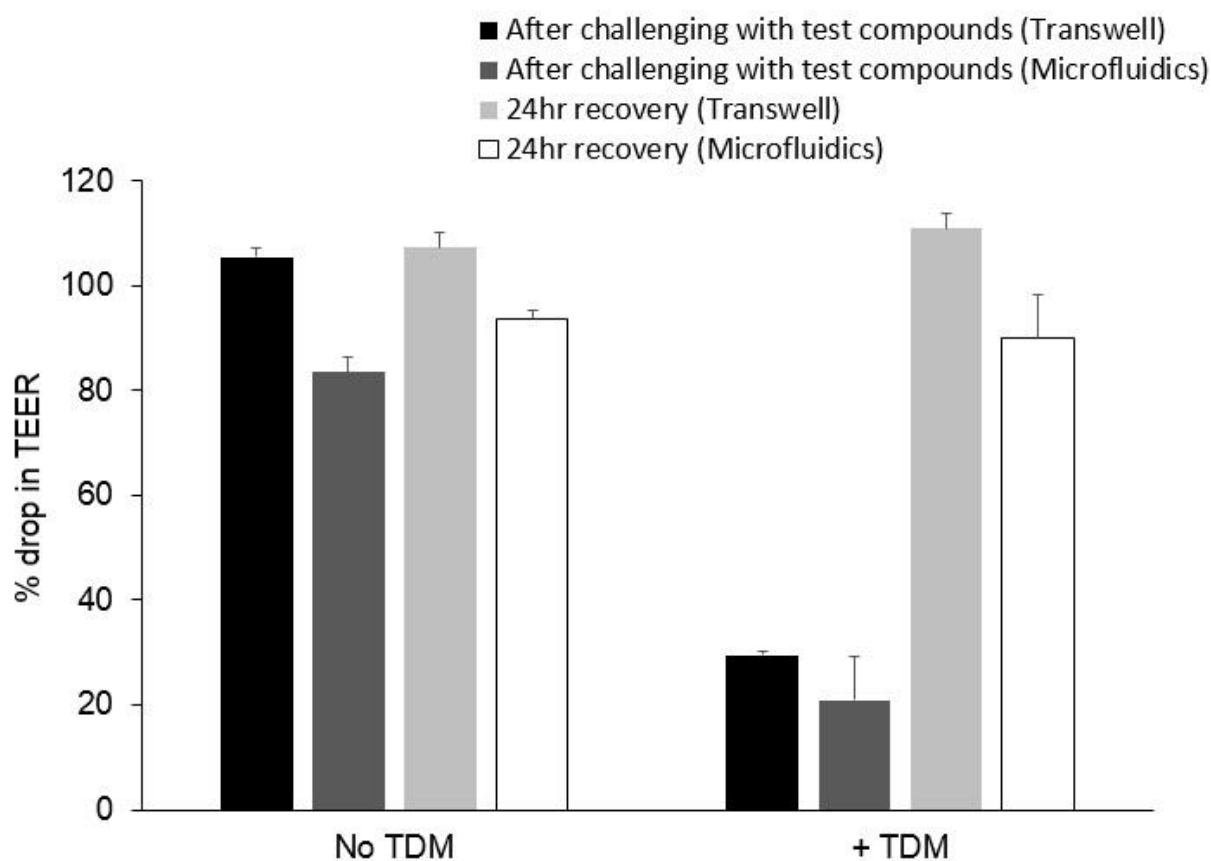


Figure 7.6 Effect of insulin/FD4 alone or with TDM on Caco-2 TEER in the Transwell or microfluidic setup, immediately after the experiment or 24 hr recovery in cell culture medium.

The TEER data acquired from the microfluidic device were comparable to the data acquired in static Transwell cultures (Figure 7.6). The TEER results recorded from the microfluidic device further indicated the electrodes

fabricated on the microfluidic device were sensitive to detect dynamic changes in the integrity of the Caco-2 monolayers.

7.4 Conclusion

In this chapter, a controlled platform supporting long-term Caco-2 monolayers for transport studies was demonstrated. Under continuous fluidic flow conditions, the growth of Caco-2 cells cultured in the microfluidic chip was accelerated. Furthermore, under continuous flow conditions, the Caco-2 cells cultured in the microchip developed villous morphogenesis and exhibited increased expression of brush border enzyme, aminopeptidase.

The permeability studies carried out with the Caco-2 monolayers cultured in the microfluidic device had also showed promising barrier function. The Caco-2 monolayers cultured in the microfluidic device revealed a tight barrier. Challenging the Caco-2 monolayers to the membrane enhancer, TDM, effectively permeabilised the monolayers. The apparent permeabilities of the test compounds increased. Furthermore, when the Caco-2 monolayers were subjected to 24 hr continuous perfusion of cell culture medium, the TEER values recovered to 90 % of the initial values. The TEER data acquired from the microfluidic device were comparable to the data acquired in static Transwell cultures.

In summary, this work had shown the Caco-2 cells cultured in the microengineered thiol-ene microfluidic chip may serve as an alternative *in vitro* human intestinal model for pharmaceutical, toxicological, cell-cell communication etc. studies. With 8 chambers fabricated on the same microchip, it allows for parallel studies to be carried out on the same microfluidic chip under basically identical conditions.

References

- [1] P. Fonte, F. Araújo, S. Reis, B. Sarmiento, Oral Insulin Delivery: How Far Are We?, *J. Diabetes Sci. Technol.* 7 (2013) 520–531.
- [2] G.P. Carino, E. Mathiowitz, Oral insulin delivery, *Adv. Drug Deliv. Rev.* 35 (1999) 249–257.
- [3] J.J. Arnold, F. Ahsan, E. Meezan, D.J. Pillion, Correlation of tetradecylmaltoside induced increases in nasal peptide drug delivery with morphological changes in nasal epithelial cells., *J. Pharm. Sci.* 93 (2004) 2205–13.

-
- [4] S.B. Petersen, L.G. Nielsen, U.L. Rahbek, M. Guldbrandt, D.J. Brayden, Colonic absorption of salmon calcitonin using tetradecyl maltoside (TDM) as a permeation enhancer, *Eur. J. Pharm. Sci.* 48 (2013) 726–34.
- [5] S.B. Petersen, G. Nolan, S. Maher, U.L. Rahbek, M. Guldbrandt, D.J. Brayden, Evaluation of alkylmaltosides as intestinal permeation enhancers: comparison between rat intestinal mucosal sheets and Caco-2 monolayers, *Eur. J. Pharm. Sci.* 47 (2012) 701–12.
- [6] T. Yang, J.J. Arnold, F. Ahsan, Tetradecylmaltoside (TDM) enhances in vitro and in vivo intestinal absorption of enoxaparin, a low molecular weight heparin, *J. Drug Target.* 13 (2005) 29–38.
- [7] T. Uchiyama, T. Sugiyama, Y.-S. Quan, A. Kotani, N. Okada, T. Fujita, et al., Enhanced permeability of insulin across the rat intestinal membrane by various absorption enhancers: their intestinal mucosal toxicity and absorption-enhancing mechanism of n-Lauryl- β -D-maltopyranoside, *J. Pharm. Pharmacol.* 51 (1999) 1241–1250.
- [8] I. Hubatsch, E.G.E. Ragnarsson, P. Artursson, Determination of drug permeability and prediction of drug absorption in Caco-2 monolayers, *Nat. Protoc.* 2 (2007) 2111–9.
- [9] G. Borchard, The absorption barrier, in: A. Bernkop-Schnürch (Ed.), *Oral Deliv. Macromol. Drugs*, Springer US, New York, 2009: pp. 49–64.
- [10] H.J. Kim, D. Huh, G. Hamilton, D.E. Ingber, Human gut-on-a-chip inhabited by microbial flora that experiences intestinal peristalsis-like motions and flow, *Lab Chip.* 12 (2012) 2165–74.
- [11] T.F. Bullen, S. Forrest, F. Campbell, A.R. Dodson, M.J. Hershman, M.D. Pritchard, et al., Characterization of epithelial cell shedding from human small intestine., *Lab. Invest.* 86 (2006) 1052–63.
- [12] H.J. Kim, D.E. Ingber, Gut-on-a-chip microenvironment induces human intestinal cells to undergo villus differentiation, *Integr. Biol.* 5 (2013) 1130–40.
- [13] G. Forstner, Signal transduction, packaging and secretion of mucins, *Annu. Rev. Physiol.* 57 (1995) 585–605.
- [14] P. Artursson, R.T. Borchardt, Intestinal drug absorption and metabolism in cell cultures: Caco-2 and beyond, *Pharm. Res.* 4 (1998) 1655–1658.
- [15] M. Pinto, S. Robine-Leon, M.-D. Appay, M. Kedinger, N. Triadou, E. Dussaulx, et al., Enterocyte-like differentiation and polarization, *Biol. Cell.* 47 (1983) 323–330.
- [16] S. Howell, A.J. Kenny, A.J. Turner, A survey of membrane peptidases in two human colonic cell lines Caco-2 and HT-29, *Biochem. J.* 284 (1992) 595–601.

CHAPTER 8: Co-culturing of Escherichia coli (*E. coli*) with Caco-2 cells

In this chapter, the focus was to explore the possibility of co-culturing the bacteria, Escherichia coli (*E. coli*), with the Caco-2 monolayers and to understand the interaction between them. Some preliminary investigations on culturing the bacteria, *E. coli*, on the Caco-2 monolayers were carried out in both the Transwell and microfluidic systems. This part of the project was carried out together with (visiting) Master's student, Jorien Brendensen from the University of Twente, Netherlands under the supervision of Hsih-Yin Tan.

8.1 Motivation of this project

The human intestines contain numerous microbial communities and these microbial communities form the gut flora [1]. The relationship between the host (in this case humans) and its resident microbiota can be mutually beneficial. The microbiota has substantial impact on human health, including dietary and nutritional processing, prevention of pathogen invasion and immune system maturation [2]. For many of these processes to take place properly, communication (in the form of chemical signals) between the human host and the microbiota is necessary [3]. Haller et. al. [4] reported on the non-pathogenic bacteria (*E. coli* and *Lactobacillus sakei*) eliciting cytokine/chemokine responses in leucocyte sensitised Caco-2 cells. Their results showed that maintenance of tissue homeostasis was possible due to the presence of bi-directional cross-talk between Caco-2 cells and the immunocompetent cells. Another study by Mathias et. al. [5] showed that by incubating the probiotics *Lactobacillus* and *Bifidobacterium* with Caco-2 monolayers resulted in modifications of several features of the Caco-2 cells (e.g., adhesion, permeability and signaling events that involved in nuclear translocation of NF- κ B and induction of immune mediators). The intestine therefore provides an extensive reservoir for intercellular signaling between the microbiota, the host and incoming pathogens [1–3,6,7].

One of the commonly found bacterium in the gut flora, is *E. coli* [8]. *E. coli* is commonly found in the lower portion of the intestines in warm-blooded organisms. *E. coli* has been largely considered as a commensal bacterium and starts colonizing the human gut at low abundance immediately after birth [9]. There are many strains of *E. coli*, and most of them are harmless. However, some strains are harmful and they may cause inflammatory bowel disease e.g. Crohn's disease, and other intestinal disorders [10]. Many *in vitro* studies using Caco-2 cells cultured in Transwell inserts have been conducted to understand intestinal disorders and the response of intestinal cells to the bacterium of interest [4,5,11–16]. However, the existing *in vitro* Caco-2

models in Transwell systems do not support luminal flow nor are they able to support more than 24 hr of co-culture. Therefore, in this project, we explored if the *in vitro* intestinal model in a microfluidic device could support the growth of microbial flora without compromising the viability of the intestinal epithelial cells. Co-cultures of the commensal bacteria, *E. coli*, with Caco-2 cells were carried out in both the Transwell and microfluidic systems.

8.2 Materials and methods

8.2.1 Culturing *E. coli*

E. coli (K12 ER2738 host strain) was obtained from New England Biolabs. The *E. coli* was grown in Luria broth (10 g of tryptone (Bacto-Tryptone; BD Biosciences, Denmark), 5 g of yeast extract (Bacto yeast extract; BD Biosciences, Denmark), 5 g sodium chloride (NaCl; Sigma, Denmark) in 1 liter of MilliQ water). This broth was sterilized by autoclaving before using for culturing *E. coli*.

8.2.2 Co-culturing *E. Coli* in Transwell inserts

Preparation of *E. Coli*. *E. Coli* cells were cultured overnight at 37 °C with shaking at 180 rpm. The cultured *E. Coli* was counted using a spectrometer (NanoDrop 2000C; Thermo Scientific). The bacteria was diluted in cell culture medium (Dulbecco's Modified Eagle's Medium (DMEM); Sigma, Denmark) to 1×10^6 bacteria/ml and 10×10^6 bacteria/ml respectively.

Caco-2 cell culture in Transwell inserts. The procedure for culturing and harvesting the Caco-2 cells for the *E. coli* studies was the same procedure described in Chapter 5. Caco-2 cells (Passage 35 (P35) and Passage (P47)) cultured in T-75 flasks were harvested with trypsin/ETDA solution. The harvested Caco-2 cells were centrifuged at 125 xg in room temperature for 5 min. Following that, the supernatant was removed and fresh cell culture medium was added to re-suspend the cell pellets. The cell culture medium used for Caco-2 cells was DMEM supplemented with 10 % (v/v) heat-inactivated fetal bovine serum (FBS; Sigma, Denmark), 1% (v/v) nonessential amino acids (NEAA; Gibco, Denmark) and 1% (v/v) penicillin-streptomycin (P/S; Gibco, Denmark). Caco-2 cells were counted using a cell counter (Moxi-Z; Orflo, Denmark) and prepared to a concentration of 1.5×10^5 cells/ml. 500 μ l of the prepared Caco-2 cell suspension (1.5×10^5 cells/ml) was seeded onto the top surface of the porous Transwell membrane. The Caco-2 cells were grown for 20 days in cell culture medium, with cell culture medium change every second day.

Co-culturing *E. Coli* on Caco-2 monolayers. On day 20 of cell culture, the cell culture medium in the Transwell inserts was changed to antibiotic-free medium (DMEM). Following that, the Transwell inserts were incubated in this new medium for at least 24 hr. After 24 hr incubation with DMEM, the DMEM on the apical side of the Caco-2 cells was removed and supplemented with prepared *E. coli* suspension.

500 μ l of the prepared *E. coli* suspension (1×10^6 bacteria/ml and 10×10^6 bacteria/ml) were seeded onto the apical side of the Caco-2 cells in respective Transwell inserts. Next, the Transwell inserts were placed in a humidified incubator (37 °C, 5% CO₂) for incubation periods of 5 hr, 15 hr and 24 hr. After the incubation periods, the Caco-2 monolayers were rinsed with phosphate buffer saline (PBS; Sigma, Denmark) on both the apical and basolateral sides for three times. Lastly, normal cell culture media supplemented with antibiotics was added to the apical (500 μ l) and basolateral (1500 μ l) sides of the Caco-2 monolayers and incubated 24 hrs for cell recovery in a humidified incubator.

8.2.2.1 Trans-epithelial electrical resistance (TEER) measurements

The integrity of the Caco-2 monolayers cultured in the Transwell inserts was monitored by measuring the TEER values. Similar to the Transwell experiments described in Chapter 6, TEER measurements were obtained using a handheld chopstick with Ag/AgCl electrodes coupled to a ERS-2 voltohm meter (Millicell, USA). The electrodes were first sterilized in 70 % ethanol, followed by equilibrating in cell culture medium in a biosafety cabinet for 15 min before use. Caco-2 cell cultures in Transwell experiment were allowed to cool to room temperature for 20 min in a biosafety cabinet before recording the TEER measurements.

During the co-culture studies, baseline TEER measurements were recorded before challenging Caco-2 cells with *E. coli*, after co-culturing *E. Coli* with Caco-2 cells and 24 hrs recovery in normal cell culture medium.

8.2.2.2 Cell staining

Live/dead cell staining. Live/dead cell staining was carried out using the live/dead cell staining procedure reported in Chapter 5 (section 5.2.5). After staining the cells, a scalpel was used to cut out the Transwell porous membrane on which the Caco-2 cells and *E. Coli* were co-cultured. These membranes were carefully mounted onto microscopic glass slides. A cover slip was placed over each microscopic slide before imaging. The cells were imaged at excitation/emission wavelength of 488/517 nm for live cells and 528/617 nm for dead cells with a confocal microscope (Axio Observer; Zeiss, Germany) using the image software (Zen lite; Zeiss, Germany).

Fluorescence staining. The staining procedure of the nucleus and tight junctions of the Caco-2 cells is found in Chapter 7 (Section 7.2.1). After completing the staining procedure, the membrane containing the fixed stained Caco-2 cells was removed using a scalpel. These cut out membranes were mounted onto microscopic glass slides. Mounting media was added onto the cells before placing a cover slip on the stained cells. Prior to imaging the cells with a confocal microscope, these microscopic slides with the stained cells were left in the fridge (4 °C) overnight. The tight junctions were imaged at excitation/emission wavelengths of 488/570 nm and the nuclei were imaged at excitation/emission wavelengths of 546/647 nm. The images were processed by an image software (Zen lite; Zeiss, Germany).

8.2.2.3 Permeability studies using phenol red

The permeability studies were carried out on the Caco-2 monolayers before seeding the *E. Coli* cells, after incubation with *E. Coli* and also 24 hrs recovery in normal cell culture medium. The tight junctional integrity was established by measuring the transport of phenol red (Sigma, Denmark). Phenol red solution was prepared by mixing phenol red powder with cell culture medium without phenol red (DMEM^{PR}, Gibco, Denmark) to a concentration of 50 µg/ml. In each of the permeability studies, Caco-2 monolayers were first rinsed with PBS for at least 3 times on the apical and basolateral sides. Next, 500 µl of the phenol red solution (DMEM^{PR}) was added to the apical side of the Caco-2 cells and 1500 µl of DMEM^{PR} was added to the basolateral side.

Every 15min, 100 µl of the sample aliquots were removed from the basolateral side while simultaneously replenishing with fresh DMEM^{PR}. Before analyzing the samples, 5 µl of 1M NaOH was added to each sample aliquot. NaOH was added to normalize the pH of the aliquot samples. The samples were analysed with a microplate reader set at a wavelength of 570 nm. The apparent permeability (P_{app}) of phenol red was calculated using equation 7.1 described previously in Chapter 7.

8.2.3 Co-culturing of *E. Coli* with Caco-2 cells in microfluidic system

The microchip (Design 2 described in Chapter 4) and fluidic system were prepared using the procedure discussed in chapter 5 (section 5.2.3). Fabrication procedure of the microelectrodes was described in detail in Chapter 6 of the thesis. Caco-2 cells (8.5×10^6 cells/ml) were seeded onto the ECM treated porous Teflon membrane in the microchip. The Caco-2 cells were cultured for 8 days. On day 8 of cell culture, the cell culture medium was switched to antibiotic-free cell culture medium. Antibiotic-free culture medium was perfused to both the upper and lower fluidic layers at a flow rate of 3 µl/min for at least 24 hr in an incubator (37 °C, 5% CO₂). Following this, the Teflon tubings connected to the cell loading component (red arrows in Figure 5.1) on the microfluidic platform were removed. Next, *E. Coli* prepared in antibiotic-free culture medium to a

concentration 10×10^7 bacteria/ml was introduced with a syringe into the cell loading reservoirs (red arrows in Figure 5.1). The motor connected to the upper microfluidic layer was activated to drag the *E. Coli* suspension very rapidly ($Q \approx 65 \mu\text{l}/\text{min}$) into the microchamber where the Caco-2 monolayers were. Extra care was taken to connect the Teflon tubings back to the cell loading component to prevent any introduction of air bubbles into the microchip. The entire system was then placed into an incubator (37°C , 5 % CO_2), for 2 hr with no flow. After 2 hr, antibiotic-free culture medium was perfused through both the upper and lower microchannels at a flow rate of $5 \mu\text{l}/\text{min}$. *E. coli* was co-cultured with Caco-2 cells in the microfluidic device for 24 hrs with continuous perfusion of cell culture medium with no antibiotics.

8.2.3.1 TEER measurements

The method for measuring TEER from the microfluidic device was similar to method described and discussed in detail in section 6.3.1 of Chapter 6 in the thesis. TEER measurements were acquired by connecting the embedded electrodes (one top electrode and one bottom electrode) in a microchamber to the multimeter (Keithley, USA). During the co-culture studies, TEER measurements were recorded before challenging Caco-2 cells with *E. Coli* and 24 hr after co-culturing *E. Coli* with Caco-2 cells. Equation 6.3 (in Chapter 6 of the thesis) was used to calculate the final TEER values.

8.2.3.2 Morphological studies

Live/dead cell staining. Viability of the Caco-2 cells co-cultured with *E. Coli* was investigated by staining the cells with live/dead cell stains. The stains used were similar to the ones used in the Transwell studies (Section 8.2.2.2) and previous studies (Chapter 5 and 6). After 24 hr of co-culturing with *E. Coli*, PBS was pumped into both the upper and lower layers of the microfluidic chip at a flow rate of $5 \mu\text{l}/\text{min}$ for 45 min. Following that, the prepared live/dead cell stains in PBS (live stain 1:1000; dead stain 1:500) were perfused to only the apical side of the Caco-2 monolayers at a flow rate of $5 \mu\text{l}/\text{min}$ for 30 min in an incubator (37°C , 5 % CO_2). Next, PBS was perfused to both the upper and lower microchannels at a flow rate of $5 \mu\text{l}/\text{min}$ for another 45 min to wash the cells. Lastly, the Caco-2 monolayers were imaged with a confocal microscope (Axio Observer; Zeiss, Germany) at excitation and emission wavelengths of 495/ 517 nm for live cells and excitation/emission wavelengths of 528/617 nm for dead cells using the image software (Zen lite; Zeiss, Germany).

Immunofluorescence staining. The Caco-2 monolayers were stained for tight junctions, nucleus and mucus. Phosphate buffer saline (PBS; Sigma, Denmark) was first pumped into both the upper and lower fluidic layers for 45 min at a flow rate of $3 \mu\text{l}/\text{min}$. Next, the cells were fixed, by pumping 4 % paraformaldehyde into the

microchambers for 30 min at flow rate of 5 $\mu\text{l}/\text{min}$. This would be followed by permeabilising the cells with 0.1 % (v/v) Triton-X-100 (Sigma, Denmark) for 30 min in room temperature. Next, a blocking buffer (1 % BSA, 0.1 % Tween 20 in PBS) was introduced into the cells for 1 hr. To visualize tight junctions, immunofluorescence staining was performed using mouse anti-ZO-1 antibody (ZO-1; Life Technologies, Denmark) diluted in the blocking buffer (1:100), and introduced into the cells. The samples were protected from light and left static overnight in the fridge at 4°C. Immunofluorescence staining was also carried out to stain the mucoprotein, mucin-2. Immunofluorescence staining of mucin-2 were carried in microchambers that were not stained for tight junctions. Primary mouse monoclonal antibody (ab11197; AbCam, Denmark) prepared in blocking buffer (1:100), was introduced to the cells. The samples were protected from light and left static overnight in the fridge at 4°C. After which, the cells were rinsed with blocking buffer followed by introducing the secondary antibody (AlexaFluor 488 goat anti-mouse; Life technologies, Denmark) prepared in blocking buffer (1:200) and left static at room temperature for 2 hrs.

Staining of the nucleus were carried out by diluting 7-aminoactinomycin D (AAD) in PBS and incubated with the cells for 1 hr at room temperature. Between each of the processing step, the cells were rinsed by pumping PBS the microchambers. Lastly mounting media (Vectashield; VWR, Denmark) was added to the cells.

Lastly, the Caco-2 monolayers were imaged with a confocal microscope (Axio Observer; Zeiss, Germany) at excitation and emission wavelengths of 495/517 nm for tight junctions and mucin-2 in separate microchambers. Excitation/emission wavelengths of 546/647 nm were chosen to image the nucleus of Caco-2 cells. The images were processed by an image software (Zen lite; Zeiss, Germany).

8.3 Results

8.3.1 Co-culturing of Caco-2 cells with *E. coli* in Transwell

Phenol red, a pH indicator was present in the cell culture medium. At 0 hr after co-culturing *E. coli* with the Caco-2 cells in the Transwell inserts, cell culture medium appeared red on the apical side (Figure 8.1a). However, 15 hrs later, distinct differences in the colours of the medium were observed in the Transwell inserts (Figure 8.1b). The medium in the apical side of the Caco-2 cells was yellow in colour. Conversely, the cell culture medium in the basolateral side of the Caco-2 cells still remained red. By visual observations, the lack of colour change of the medium in the basolateral side showed that the protons of the phenol red diffusing across the Caco-2 monolayer. This was an indication that the Caco-2 cultures in the Transwell inserts were exhibiting some form of barrier function.

From the change in colour (pink to yellow) in the apical side, it could be clearly discerned that the medium had turned acidic. However, in the control inserts, the cell culture medium was still red in both the apical and basolateral sides (results not shown). The observed change in media colour from the Transwell inserts in which the Caco-2 cells were challenged with *E. coli* could be due to the accelerated rate of metabolism and increased secretion of acidic by-products by the *E. coli* [17].

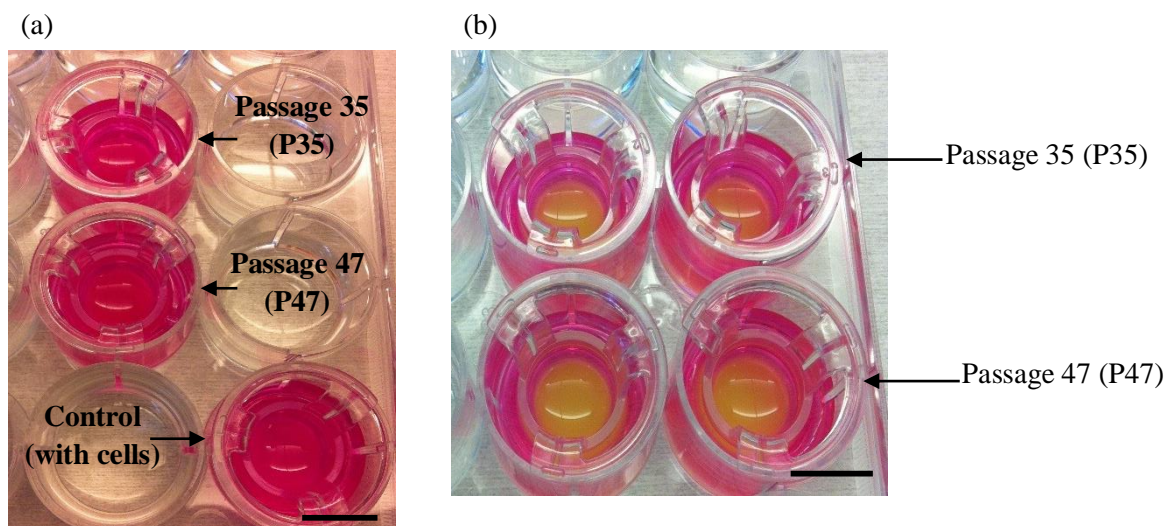


Figure 8.1 Transwell inserts with *E. coli* seeded on the apical side of Caco-2 monolayers. a) The Caco-2 monolayers were seeded with *E. coli* at 0 hr. b) Caco-2 monolayers incubated with *E. coli* for 15 hr. (scale bar = 1 cm)

8.3.1.1 Caco-2 cells viability

Live cells were fluorescently stained with Calcein and visualised. Dead cells were fluorescently stained with ethidium homodimer-1 and visualised in red. Two different passages of Caco-2 monolayers were investigated for their viability after 15 hr incubation with *E. coli*. One would expect the Caco-2 cells should be alive after being challenged with *E. coli*, since non-pathogenic *E. coli* can be found residing harmlessly in the intestinal lumen [8]. From the microscopic images, it was confirmed that the Caco-2 cells (P35) remained viable (> 90 %) after co-culturing with *E. coli* (Figure. 8.2a). Similarly for the higher passage number (P47), viability of the Caco-2 cells was > 90 % (Figure 8.2b).

From the fluorescence microscopic images, it was also clearly seen the passage number of Caco-2 cells did not have a great impact on the number of dead Caco-2 cells, after the Caco-2 monolayers had been subjected to *E. coli* incubation for 15 hr.

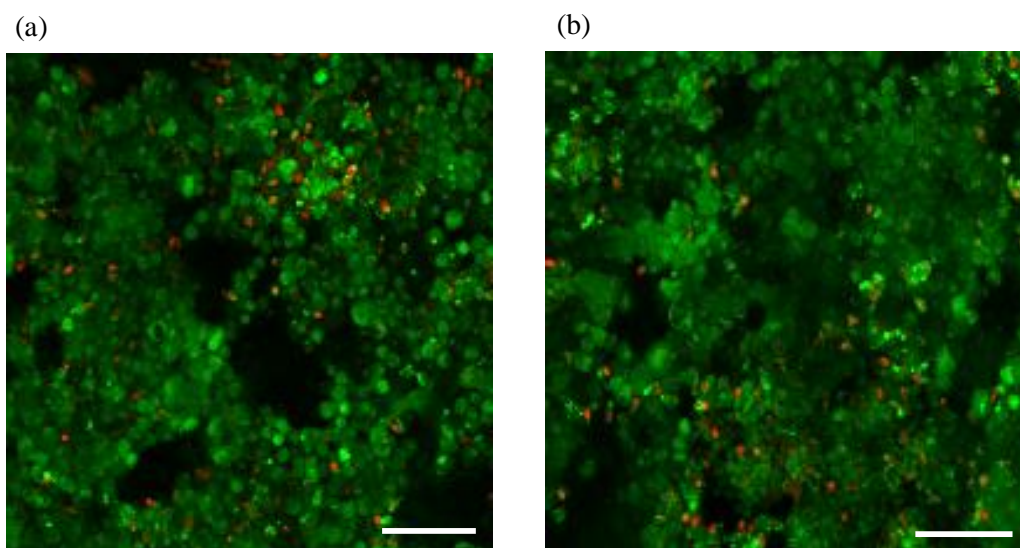


Figure 8.2. Live/dead cell staining on Caco-2 monolayers cultured in Transwell set-up. Caco-2 cells had undergone incubation with *E. coli* (concentration: 10×10^6 bacteria/ml) for 15 hr. Live cells were stained green and dead cells were stained red. (a) P 35 Caco-2 cells, (b) P 47 Caco-2 cells. (Scale bar = 50 μm)

8.3.1.2 Effect of co-culture duration on Caco-2 cells

Permeability studies carried out using phenol red as tracking molecule. As mentioned previously in chapter 7, permeability studies using a tracking molecule is a form of investigating the integrity of the barrier function of the Caco-2 monolayers. Permeability studies using phenol red as the tracking molecule was carried out on the Caco-2 monolayers incubated with the *E. coli* cells in Transwell inserts. Phenol red is a normal constituent found in most cell culture medium. Phenol red was chosen as the tracking molecule because it is non radioactive, easily collected without risking contamination of culture, and it is a simplified and reliable method for evaluating the integrity of Caco-2 monolayer [18].

The Caco-2 cells were challenged with two different *E. coli* concentrations. An increase in the transport of phenol red molecules across the Caco-2 monolayers was observed in all the Transwells chambers that were infected with *E. coli* (Figure 8.3). However, the P_{app} of phenol red was higher in cultures containing a higher concentration of *E. coli* (Figure 8.3). Caco-2 cells challenged with 10×10^6 bacteria/ml of *E. coli* showed $P_{\text{app}} = 3.53 \times 10^{-5}$ cm/s. The P_{app} of phenol red had increased by almost 26 folds as compared to the Caco-2 monolayers without *E. coli*. Furthermore, Caco-2 monolayers challenged with a lower *E. coli* concentration (1×10^6 bacteria/ml), the P_{app} of phenol red was 1.29×10^{-5} cm/s. This was almost 2.7 folds lower than the Caco-2 monolayers challenged with higher *E. coli* concentration.

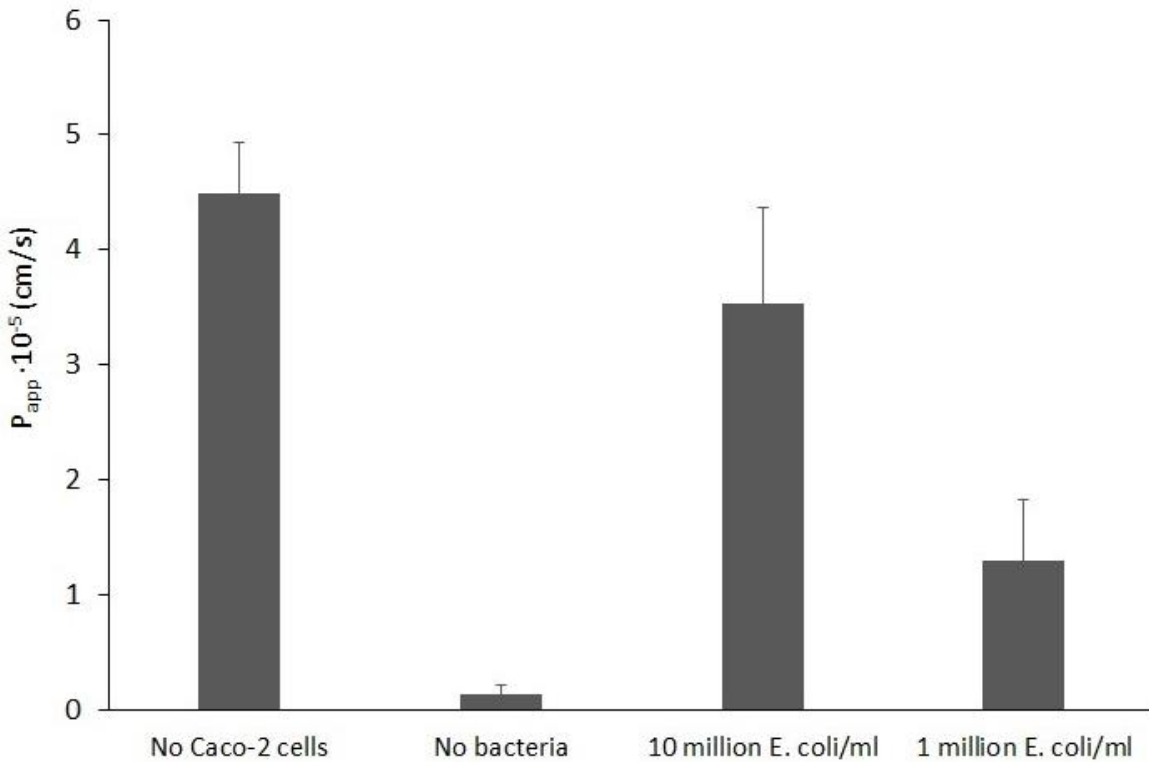


Figure 8.3 Apparent permeability (P_{app}) of phenol red across Caco-2 monolayers challenged with different concentrations of *E. coli* for 24 hr incubation period. Control are Transwells not containing any Caco-2 cells. ($n = 3$ for each Caco-2 passage)

Effect of co-culture duration on the integrity of Caco-2 monolayer. To investigate our hypothesis, we co-cultured *E. coli* with Caco-2 monolayers for different durations. We decided to use the concentration of 10×10^6 bacteria/ml. This concentration is within the range of *E. coli* that is present in human intestines [19]. After 5 hr of co-culture with *E. coli*, the apparent permeability of phenol red was low, $P_{app} = 2.21 \times 10^{-7}$ cm/s, but higher than the controls $\approx 5.2 \times 10^{-8}$ cm/s (Figure 8.4). This showed that the Caco-2 monolayers still exhibited tight barrier properties. The data is consistent with a past study that showed challenging the Caco-2 cells to *E. coli* for 6 hr did not compromise the integrity of Caco-2 monolayer [13]. However the P_{app} of phenol red increased slightly to $\approx 8.7 \times 10^{-7}$ cm/s after challenging the Caco-2 monolayers with *E. coli* for 15 hr.

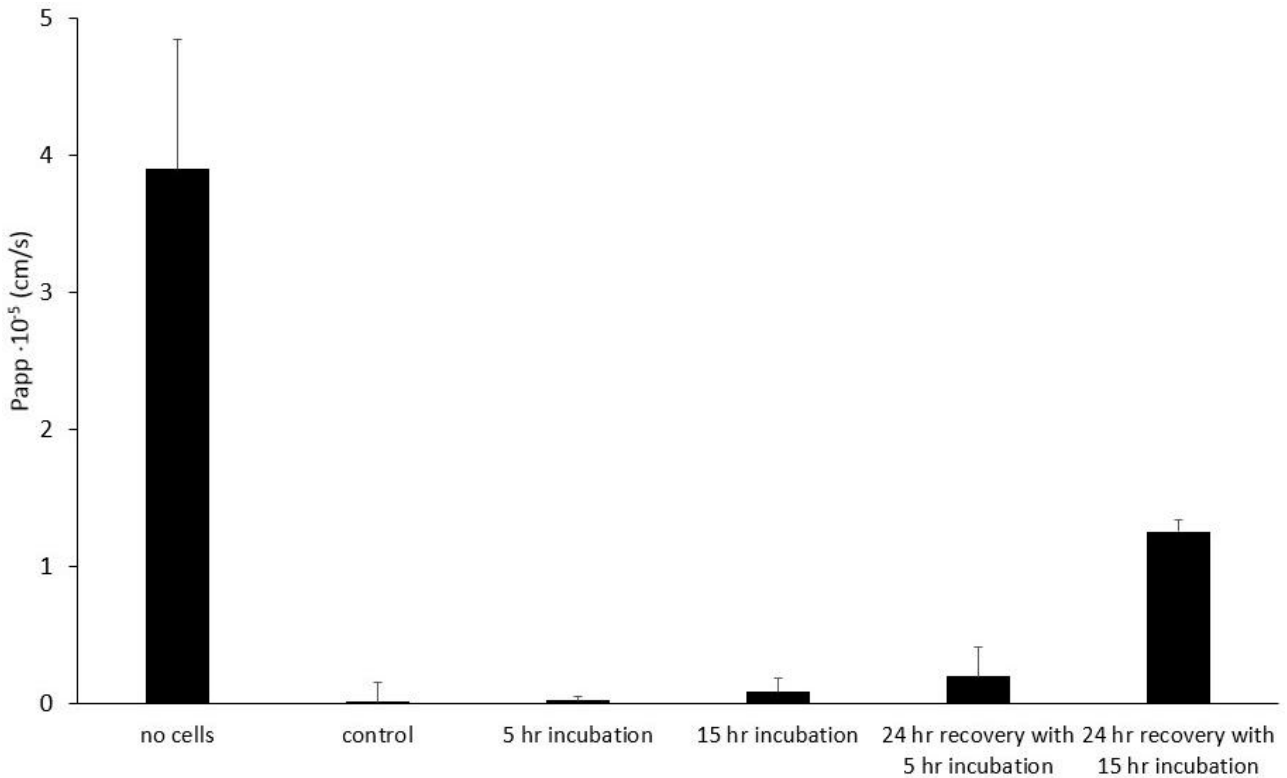


Figure 8.4 Phenol red permeability studies carried out on Caco-2 monolayers under different incubation duration with *E. coli* and 24 hr recovery with normal cell culture medium. (n = 6)

We also questioned if the permeability of phenol red was reversible after being challenged with *E. coli*. This may serve as interesting information for the correlation of reversible alteration of the tight junction proteins. When the Caco-2 monolayers were left to recover in normal cell culture medium with antibiotics for 24 hrs, the P_{app} of phenol red increased. The P_{app} of phenol red (24 hr recovery) was recorded as 2×10^{-6} cm/s and 1.3×10^{-5} cm/s for 5 hr and 15 hr incubation respectively (fig 8.4). Despite displaying apparent tight barrier properties immediately after incubation with *E. coli*, the barrier property of the Caco-2 monolayers weakened during 24 hr recovery period.

Upon comparing the data between the 15 hr incubation period with the 24 hr incubation period, the P_{app} was 3.53×10^{-5} cm/s and 1.3×10^{-5} cm/s respectively. The significant difference in phenol red permeability between the 15 hr incubation and 24 hr incubation period showed that the bacteria could have effected some major changes to the barrier property of the Caco-2 monolayers. However, more studies were necessary to further understand the happenings on the Caco-2 monolayers.

TEER measurements. The integrity of the Caco-2 monolayers was also measured by recording the TEER measurements. The TEER measurements of the Caco-2 monolayers were carried out concurrently with the permeability studies. The TEER measurements did not decrease in the values after incubating the Caco-2 monolayers with *E. coli* for 5 hr (Figure 8.5). This was a clear indication that the Caco-2 monolayer still exhibited barrier properties. The TEER measurements were also consistent with an earlier study [13], where the authors reported the TEER values were not affected after a 6 hr incubation period. However, the TEER measurements recorded for the 15 hr incubation showed a drop to $\approx 93\%$ of initial values (Figure 8.5). Our TEER measurements (Figure 8.5) were also consistent with the P_{app} data shown in Figure 8.4.

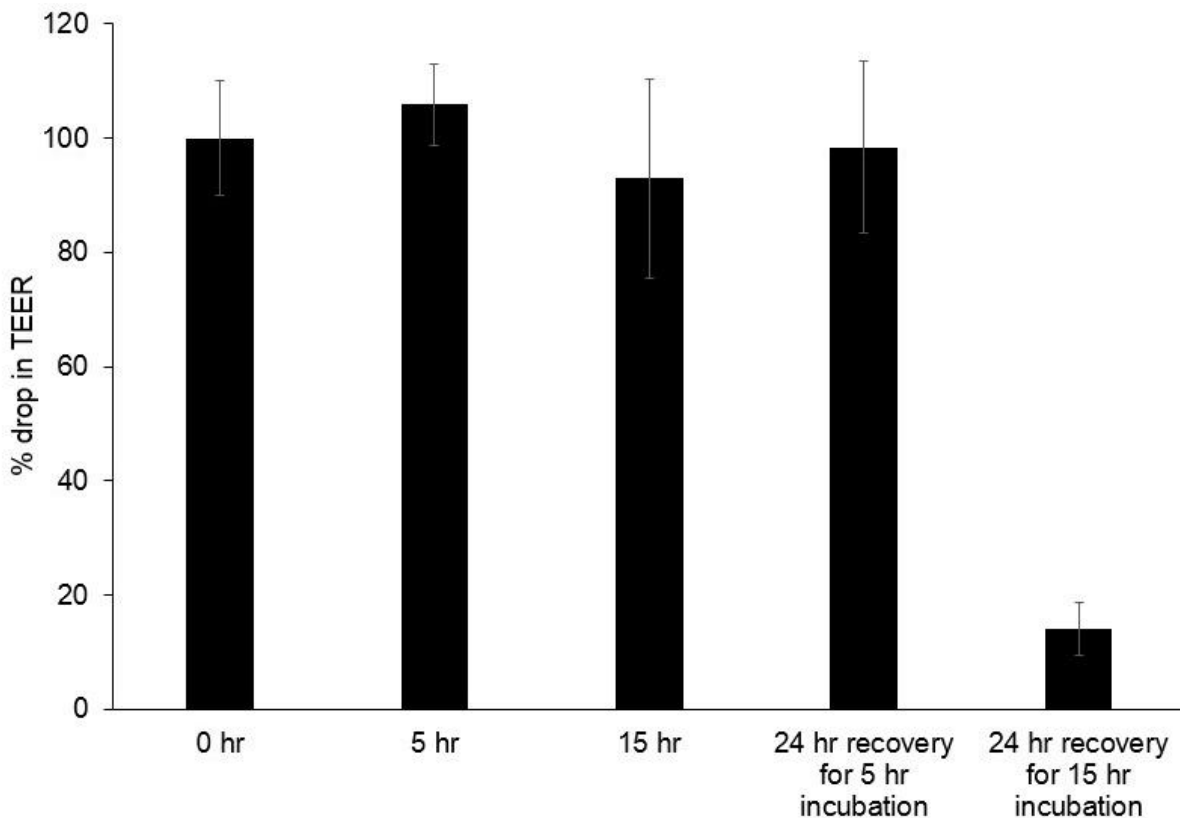


Figure 8.5 Percentage change in TEER measurements on Caco-2 monolayers co-cultured with *E. coli* for different duration and 24 hr recovery in cell culture medium with antibiotics.

From the presented data (Figure 8.5), it could be discerned that challenging the Caco-2 monolayers to different durations of *E. coli* might affect the integrity of the Caco-2 monolayers.

Measurements of the TEER values of the Caco-2 monolayers after 24 hrs recovery in normal cell culture medium with antibiotics were also recorded. The TEER values dropped slightly to $\approx 98.4\%$ of initial values for the 5 hr incubation period and a significant drop to $\approx 14\%$ of initial values for the 15 hr incubation period (Figure 8.5).

8.3.1.3 Morphological studies

Integrity of the barrier property of the Caco-2 monolayer is regulated by the presence of tight junctions between adjacent cells [20,21]. In the control sample (no *E. coli*), the Caco-2 monolayer was stained positive for tight junctions (Figure 8.6a). The web-like network of fluorescently stained tight junctions were observed. However, for the Caco-2 monolayer challenged with *E. coli* for 24 hr, there was absence of tight junctions (Figure 8.6b).

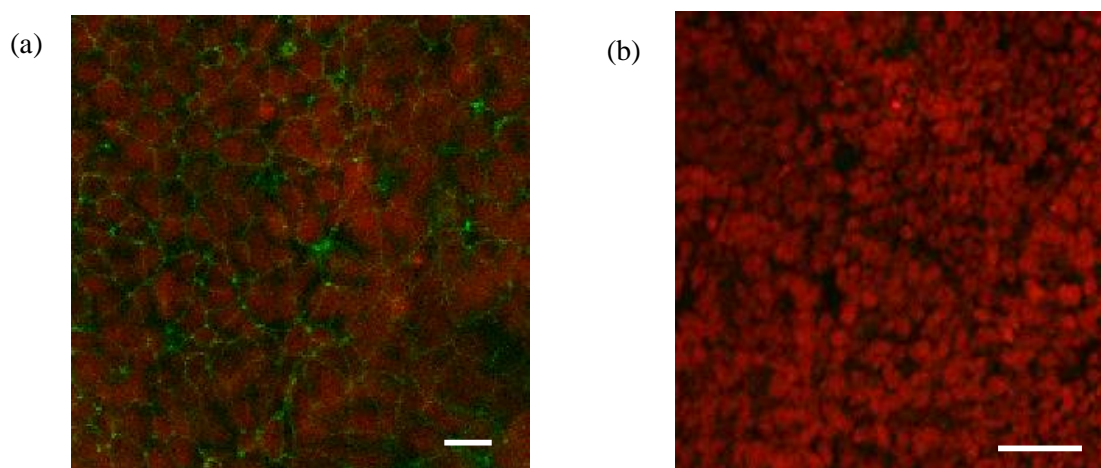


Figure 8.6 Top view of Caco-2 monolayers stained for nucleus (red) and tight junctions (green). (a) Control samples, no co-culturing of *E. coli* on Caco-2 monolayer. (b) Caco-2 monolayer had been challenged with *E. coli* for 24 hrs. (Magnification x 10) (scale bar = 50 μm)

8.3.2 Co-culturing *E. coli* in thiol-ene microfluidic system

Previously in Chapter 7, we showed that the Caco-2 cells cultured in the microfluidic device displayed tight barrier function, villous morphogenesis and presence of mucus. To further investigate if the Caco-2 cells cultured in the microfluidic device could support the growth of *E. coli* without compromising the viability of the cells, the Caco-2 cells were co-cultured with *E. coli* for 24 hr under constant perfusion of DMEM.

In our first studies, a flow rate of 3 $\mu\text{l}/\text{min}$ was set to perfuse through the upper and lower microchannels. However, within 24 hr, perfusing the medium through the upper microchannels was challenging. Antibiotic-free culture medium was observed to flow backwards into the glass vials connected to the inlets. Yellow coloured cell culture medium was observed in the glass vials connected to the inlets (Figure 8.7a). We suspected the backflow of cell culture medium could be due to the built up of pressure within the cell culture chamber from the accelerated growth of *E. coli* on the Caco-2 cells. The built-up of pressure could be the result of the gases released from the *E. coli*, which led to backflow of cell culture medium and contamination of the antibiotic-free culture medium in the inlet glass vials (Figure 8.7a). To overcome the increased pressure in the microchamber, the flow rate was increased to 5 $\mu\text{l}/\text{min}$ in the subsequent experiments. An increased flow rate would result in higher flow velocities within the microchambers. This would result in higher rate of waste

removal that may have resulted from the presence of *E. coli*. With this flow rate, no observable back flow and contamination of antibiotic-free culture medium in the inlet glass vials (Figure 8.7b).

When the flow rate was set at 5 $\mu\text{l}/\text{min}$, after 24 hr of continuous perfusion of cell culture medium, by visual observation of the microchambers, the microchambers containing *E. coli* appeared yellow (results are not shown). Contrastingly, the control chambers (devoid of *E. coli*) appeared pink after 24 hr of co-culture (results are not shown). This was a clear indication that the *E. coli* was successfully co-cultured with the Caco-2 cells in the microfluidic device. The colour in the microchambers also corresponded to the colour of the medium observed in the outlet glass vials as shown in Figure 8.7b.

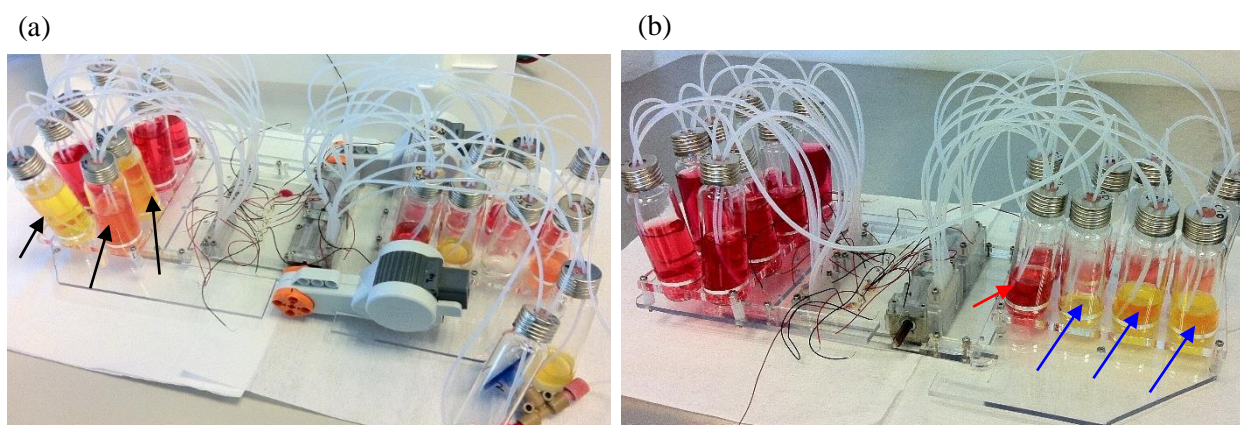


Figure 8.7. Microfluidic chip with *E. coli* co-cultured on the apical side of the Caco-2 monolayers. Image was taken 24 hr after continuous perfusion of antibiotic-free culture medium (a) Antibiotic-free culture medium was perfused at flow rate = 3 $\mu\text{l}/\text{min}$ in both upper and lower microchannels. (Black arrows indicating glass vials connected to inlet channels were contaminated due to back flow of antibiotic-free culture medium) (b) Antibiotic-free culture medium was perfused at flow rate = 5 $\mu\text{l}/\text{min}$. (Blue arrow indicating outlets of microchambers with *E. coli* and red arrow indicating the outlet for the control microchambers)

In our experimental system, two microchambers acting as the control chambers were not seeded with *E. coli*. The colour of the medium exiting from the control chambers appeared red in the outlet glass vials (red arrow in Figure 8.7b). Figure 8.7b illustrated that only the apical outlet glass vials connected to the microchambers with *E. coli* cells co-cultured with the Caco-2 monolayers) showed a change in the colour of the antibiotic-free culture medium.

8.3.2.1 TEER measurements in microfluidic device

As mentioned earlier in chapter 6 of the thesis, measurements of the TEER provide some insight into the integrity of the Caco-2 monolayers. In the co-culture studies, TEER measurements of the Caco-2 monolayers

with *E. coli* growing on the apical surface in the microfluidic device were also recorded. Surprisingly, we saw a slight increase in TEER values $\approx 1700 \Omega \cdot \text{cm}^2$ after co-culturing *E. coli* with Caco-2 monolayers for 24 hrs in the microfluidic chip (Figure 8.8a).

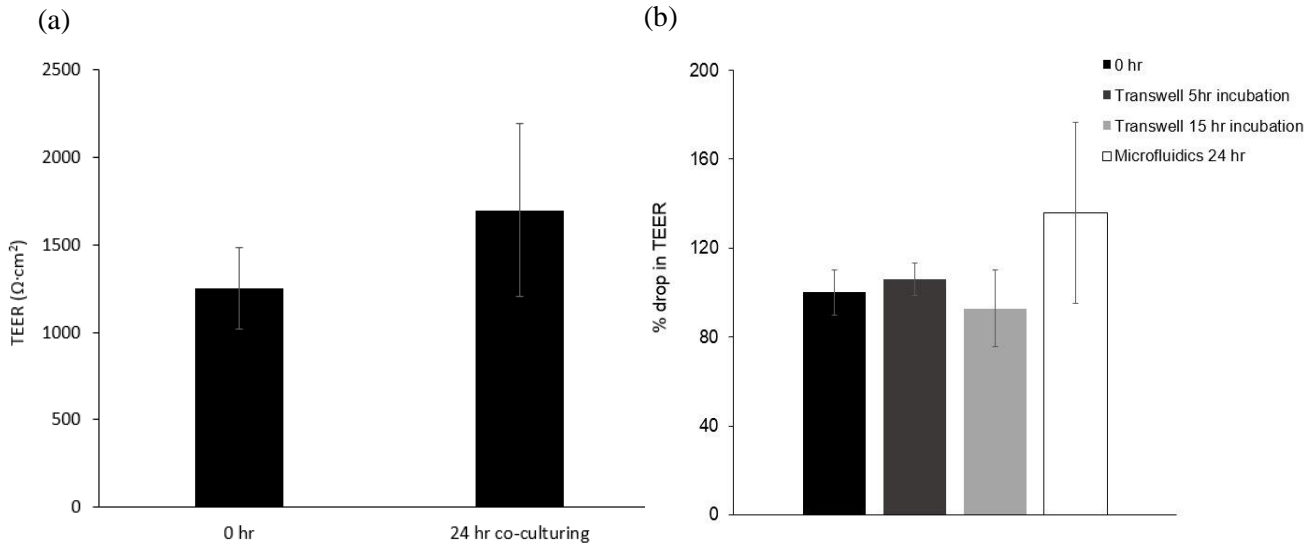


Figure 8.8 TEER measurements of co-culture studies in microfluidic device. (a) TEER values obtained for *E. coli* co-cultured with Caco-2 monolayers in thiol-ene microfluidic chip. (n = 6) (b) Comparisons of percentage drop in TEER values for different incubation periods in Transwell system and 24 hr incubation period in microfluidic device (n = 3 for each Transwell study and n = 6 for microfluidic device)

Comparing the data recorded from the microfluidic device with the data recorded for Transwell inserts, the TEER values from the microfluidic device were much higher than the 5 hr incubation from the Transwell set-up (Figure 8.8b). The results showed that the barrier property of the Caco-2 monolayers in the microfluidic device was not compromised with the presence of *E. coli*. To further confirm the barrier property of Caco-2 monolayers cultured in the microfluidic device was not compromised, we next performed immunofluorescence staining towards the tight junctional protein, occludin.

8.3.2.2 Morphological studies on Caco-2 cell incubated with *E. coli* in microfluidic system

Live/Dead cell staining. Similar to the Transwell studies, live/dead cell staining was performed on the Caco-2 monolayers to validate the viability of the Caco-2 cells in the microchambers after being challenged with *E. coli*. The viability of Caco-2 cells in the microfluidic device was higher compared to the viability of Caco-2 cells cultured in the Transwell. The fluorescent images of the live/dead cell staining of Caco-2 monolayers in the microchambers showed 100 % viability (Figure 8.10). This high percentage of cell viability in the

microfluidic device could also be due to the removal of dead cells by the continuous perfusion of cell culture medium through the microchambers.

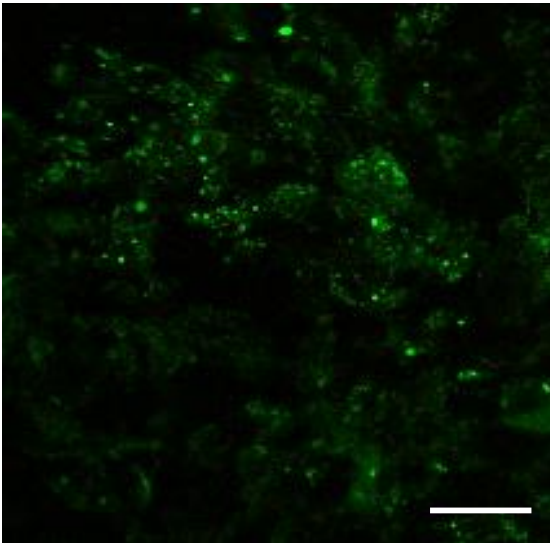


Fig 8.10 Live/dead cell staining on Caco-2 monolayers after challenged with *E. coli* for 24 hr in the microfluidic device. Antibiotic-free culture medium was perfused through both the upper and lower microfluidic layers for 24 hr at a flow rate of 5 μ /min. *E. coli* concentration seeded on the apical side of the Caco-2 monolayers was 10×10^6 cells/ml. Magnification $\times 10$. (Scale bar = 50 μ m)

Immunofluorescence imaging. Interestingly, the immunofluorescence microscopic studies using antibodies directed towards the tight junction protein, occludin, confirmed the presence of tight junctions in the Caco-2 monolayers after co-culturing with *E. coli* (blues arrows in Figure 8.11a). Distinct polygonal shapes of the Caco-2 cells could be observed on the Teflon membrane. The integrity of the Caco-2 monolayer was not compromised after co-culturing with *E. coli* for 24 hrs.

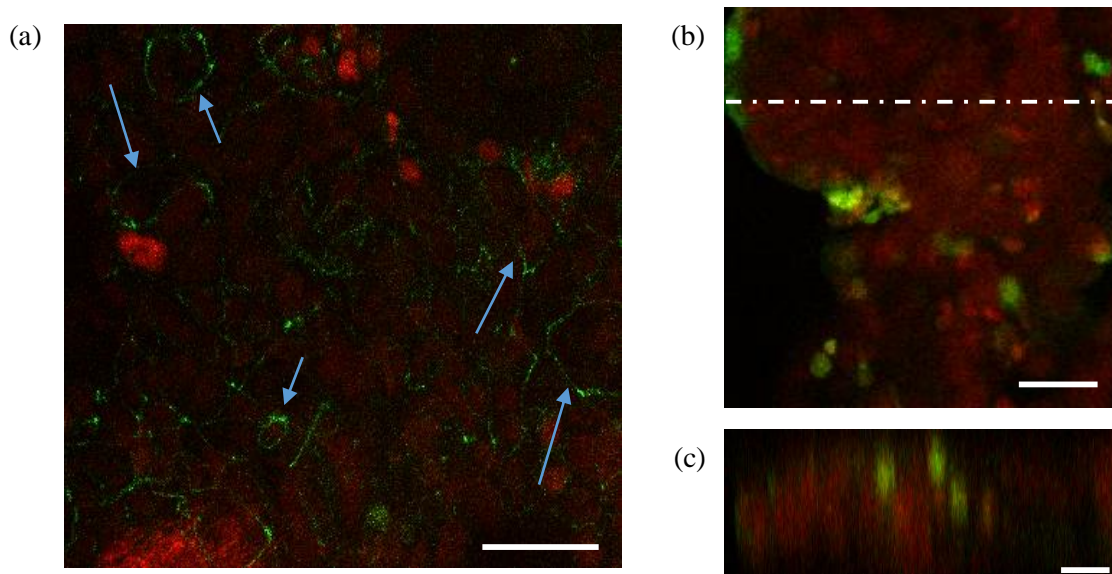


Fig 8.11 Immunofluorescent images of Caco-2 cells after 24 hr incubation with *E. coli*. a) Caco-2 cells were stained for tight junctions and nucleus. Tight junctions were stained green and nucleus were stained red. (Magnification x 15). (b) Top view of Caco-2 monolayers co-cultured with *E. coli* stained for nucleus (red) and mucus (green). (c) Confocal vertical view of the stained cells indicated by the dotted white line from (b). (Scale bar = 50 μm)

From the images of the Caco-2 cells stained for mucus and nucleus, mucus was positively stained on the Caco-2 monolayers (Figure 8.11b). However the mucus was no longer a layer on the apical surface of the Caco-2 cells, rather the mucus were observed in patches on the Caco-2 cells (Fig 8.11b, c). We also had some challenges in discerning the nucleus of the Caco-2 cells from the fluorescent stains. It later came to our knowledge that the nucleus stain also happens to stain the DNA of the *E. coli* cells [22].

8.4 Discussion

8.4.1 Challenging Caco-2 cells with *E. coli* in Transwell systems

Effect of incubation period of *E. coli* on Caco-2 barrier integrity. The *E. coli* k-12 used in the studies in this chapter is a commensal non-pathogenic bacterium. In our studies, an increase transport of phenol red molecules across the Caco-2 monolayers was observed after co-culturing with *E. coli* for 24 hr (Figure 8.3).

Our results presented in Figures 8.4 and 8.5 showed that incubating the *E. coli* with Caco-2 cells for 5 hrs did not disrupt the barrier integrity of the Caco-2 cells. These results were consistent with some earlier findings of incubating *E. coli* k-12 with *in vitro* intestinal models for less than 6 hrs, which did not compromise the barrier

integrity [13,23]. Conversely when the Caco-2 cells were challenged with *E. coli* for 15 hrs and 24 hr, the permeability of phenol red increased to 8.7×10^{-7} cm/s and 3.53×10^{-5} cm/s respectively. We believe that the changes and reactions caused by the *E. coli* on the Caco-2 would require sometime for the outcome of the changes to take effect.

Morphological studies of caco-2 cells after incubating with *E. coli*. The live/dead cell stains used are specific for mammalian cells, therefore there should not be any cross-staining for *E. Coli*. From the preliminary studies conducted with the Transwell inserts, the results showed that the viability of the cells was not affected by the presence of *E. coli* (Figure 8.2). However, from the immunofluorescence images, there was no signs of tight junctions in the Caco-2 cells after co-culturing with *E. coli* (Figure 8.6b). The absence of tight junctions in the Caco-2 layers was likely the cause for the drop in TEER measurements and increased transport of phenol red molecules across the Caco-2 monolayers.

In an earlier study, He et. al. reported that challenging the Caco-2 cells with *E. coli*, resulted in suppressing genes encoding for ion channels and membrane transporters [17]. The tight junctions are proteins that regulate the paracellular transport of compounds across the Caco-2 monolayer. The data presented in this chapter suggests that *E. coli* might have suppressed the genes encoding the proteins regulating the tight junctions. Due to the absence of tight junctions in the Caco-2 monolayers after co-culturing with *E. coli*, this might have resulted in the Caco-2 monolayers becoming leaky. The leakiness of the Caco-2 monolayers had been validated from our reported TEER values (Figure 8.5) and increased transport of the phenol red molecule across the Caco-2 monolayer (Figure 8.4).

Effect of *E. coli* on Caco-2 monolayers. He et. al. [17] reported on observing similar metabolic changes and inflammatory responses between the commensal *E. coli* k-12 and enterohemorrhagic *E. coli* O157:H7. The authors had suggested that in the static Transwell cultures, *E. coli* had direct contact with the Caco-2 cell cultures, therefore enabling the cells to have direct interaction with the host cells. Although the *E. coli* used in this present study was commensal and non-pathogenic, it might have exhibited some characteristics similar to the pathogenic *E. coli* strains [17] when in direct contact with the Caco-2 cells. One of the characteristics of pathogenic strains of *E. coli* was to alter tight junctional functions [23]. If so, this could explain the absence of tight junctions in the Caco-2 monolayers after co-culturing with *E. coli* for more than 15 hr.

Simonovic et. al. [23] reported the possibility of recovering the barrier property of infected intestinal cells after treatment with antibiotics and incubated overnight in cell culture medium. Conversely, our results (Figures 8.4, 8.5) showed the integrity the Caco-2 monolayers weakened during 24 hr recovery. The deterioration of barrier property may be due to several reasons: 1) *E. coli* adhered on the Caco-2 cells despite rinsing the monolayers and replacing the cell culture medium with antibiotics. 2) The amount of antibiotics present in the cell culture medium was not sufficient to eliminate the *E. coli* adhering onto the Caco-2 cells.

When *E. coli* is co-cultured with the Caco-2 cells, *E. coli* will compete with the Caco-2 cells for nutrients and energy [17]. Utilization of the nutrients and production of intermediate metabolites will reduce the energy available to the Caco-2 cells. In the static Transwell inserts, over time would result in depletion of nutrients available and accumulation of waste products from both the *E. coli* and Caco-2 cells. Consequently, this would result in poor maintenance of the cells.

8.4.2 Challenging Caco-2 cells with *E. coli* in microfluidic system

The human intestinal health and diseases are hugely determined by the human microbiome [2,6,24]. Therefore development of an *in vitro* platform that closely mimic *in vivo* conditions for such host-microbe studies would be of great interest to biologists, pharmaceutical scientists and physiologists.

Seeding *E. coli* to Caco-2 cell cultures in microfluidic device. One of the major advantages of a microfluidic device for cell culture is the ability to control the flow of reagents through the device. On the contrary, the presence of flow may also be a disadvantage. For example in our studies, the constant perfusion of cell culture medium could have remove any non-adhering *E. coli* from the microchamber. If this was so, then: 1) The concentration of *E. coli* adhering on the Caco-2 cells could be lesser than the initial seeding concentration of 10×10^6 bacteria/ml. 2) There might not be a uniform layer of *E. coli* adhering onto the Caco-2 after activating the micropumps.

Morphological studies of Caco-2 cells after incubating with *E. coli*. In human intestines, *E. coli* has a tendency to accumulate in the mucus layer that is on the apical side of the intestinal epithelium. Therefore, there is a lack of direct interaction between *E. coli* and the intestinal epithelial cells [17]. In the microfluidic device, our immunofluorescent staining showed that mucus is present on the Caco-2 cells (Figure 8.11b, c). This was showed previously in Chapter 7. Immunofluorescence staining of the tight junctions (Figure 8.11a) and the TEER measurements (Figure 8.8a) showed that the barrier integrity of the Caco-2 cells cultured in the microfluidic device was not weakened by the presence of *E. coli*. Unlike in the case of the Transwell system where the barrier integrity was disrupted after challenging the Caco-2 monolayers with *E. coli*. We attributed these contrasting results between the two systems to the presence and absence of mucus in the microfluidics and Transwell system respectively. The presence of the mucus on the Caco-2 cells allowed the *E. coli* to adhere onto the mucus, therefore preventing the bacteria from having direct interaction with the Caco-2 cells. Furthermore with the continuous perfusion of cell culture medium to the co-culture in the microchambers, a constant supply and nutrients and removal of wastes was provided, hence, allowing the microbe and host cells to co-exist for at least 24 hrs in the microfluidic device.

Our immunofluorescent images (Figure 8.11b, c) showed that the mucus was observed in patches rather than a complete layer on the Caco-2 cells when challenged with *E. coli*. We believe this non-uniformity layer of

the mucus could be due to several reasons. 1) The non-uniformity coverage of *E. coli* adhering onto the Caco-2 cells. In regions where the coverage of *E. coli* was poor, the mucus layer on the Caco-2 cells could be fluorescently stained. 2) The high flow rates ($\approx 65 \mu\text{l}/\text{min}$) supplied by the motors during seeding of the *E. coli* on the Caco-2 cells could have disrupted the uniformity of the mucus layer.

However, it should be stressed that the presented co-culture results for the microfluidic device thus far are preliminary investigations. The results presented in this chapter showed the barrier integrity of Caco-2 monolayers were not compromised after co-culturing with *E. coli* for 24 hrs. The implications of this are yet to be determined with longer co-culturing period of *E. coli* with Caco-2 cells in the microfluidic device.

8.5 Conclusion

The reported results showed that once the Caco-2 cells cultured in the microfluidic device had differentiated with the formation of villous structures and formation of a mucus layer, the Caco-2 monolayer was capable of supporting the growth of a commensal bacteria *E. coli*, commonly found in the human intestines. Tests of the co-culture system showed that Caco-2 barrier integrity was not compromised with the presence of *E. coli* after 24 hr of co-culture. Similar studies were conducted with Transwell cultures and the results were contrastingly different. The Transwell studies showed the barrier integrity of the Caco-2 cells were weakened after co-culturing with *E. coli*. The results presented in this chapter showed the microfluidic system was a better intestinal model as compared to the static Transwell cultures for such co-culture studies.

Furthermore, the continuous perfusion in the microfluidic device ensured there was a continuous supply of nutrients to the cells and removal of wastes, hence providing conditions for the microbe and Caco-2 cells to co-exist. Given that the microfluidic device has the possibility of mimicking *in vivo* conditions, it may be a possible alternative *in vitro* human intestinal model to facilitate host-microbiome studies as well as toxicological studies.

8.6 Outlook

Although, the preliminary studies carried out on the microfluidic device had shown some promising results. However, there are some areas that can be further improved.

For future studies, perhaps a longer duration of co-culturing the bacteria on Caco-2 monolayer in the microfluidic device could be carried out. This would enable better understanding of whether the *in vitro* intestinal model on the microchip could support long term microbe-host culture. Furthermore, some improvement could be made to the microchip design by increasing the microchannel height. This will enable an increased in the dilution rate of cell culture medium in the microchamber, hence providing the means to overcome the growth rate of *E. coli* with progressive culture days.

Lastly, in the studies presented in this chapter we could not show the amount of *E. coli* adhering onto the Caco-2 cells or if there were *E. coli* adhering onto the Caco-2 cells after the co-culture studies. For future studies, perhaps a fluorescently labelled *E. coli* strain (e.g., *E. coli*-green fluorescent protein) could be implemented in such co-culture studies. This will also enable real-time microscopic monitoring of the *E. coli* on the Caco-2 cells.

References

- [1] R.E. Ley, D.A. Peterson, J.I. Gordon, Ecological and evolutionary forces shaping microbial diversity in the human intestine, *Cell*. 124 (2006) 837–48.
- [2] C.L. Ohland, C. Jobin, Microbial activities and intestinal homeostasis: A delicate balance between health and disease, *Cell. Mol. Gastroenterol. Hepatol.* 1 (2015) 28–40.
- [3] S. Salminen, C. Bouley, M.C. Boutron-Ruault, J.H. Cummings, A. Franck, G.R. Gibson, et al., Functional food science and gastrointestinal physiology and function, *Br. J. Nutr.* 80 Suppl 1 (1998) S147–S171.
- [4] D. Haller, C. Bode, W.P. Hammes, A.M.A. Pfeifer, E.J. Schiffrin, S. Blum, Non-pathogenic bacteria elicit a differential cytokine response by intestinal epithelial cell/leucocyte co-cultures, *Gut*. 47 (2000) 79–87.
- [5] A. Mathias, M. Duc, L. Favre, J. Benyacoub, S. Blum, B. Corthésy, Potentiation of polarized intestinal caco-2 cell responsiveness to probiotics complexed with secretory IgA, *J. Biol. Chem.* 285 (2010) 33906–33913.
- [6] L. V. Hooper, Bacterial contributions to mammalian gut development, *Trends Microbiol.* 12 (2004) 129–34.
- [7] S. Macfarlane, J.F. Dillon, Microbial biofilms in the human gastrointestinal tract, *J. Appl. Microbiol.* 102 (2007) 1187–1196.
- [8] J.P. Nataro, J.B. Kaper, Diarrheagenic *Escherichia coli*, *Clin. Microbiol. Rev.* 11 (1998) 142–201.
- [9] R. Wall, R.P. Ross, C.A. Ryan, S. Hussey, B. Murphy, G.F. Fitzgerald, et al., Role of gut microbiota in early infant development, *Benef. Microbes.* 1 (2009) 45–54.

- [10] R.B. Sartor, S.K. Mazmanian, Intestinal microbes in inflammatory bowel diseases, *Am. J. Gastroenterol. Suppl.* 1 (2012) 15–21.
- [11] J. Cleary, L.-C. Lai, R.K. Shaw, A. Straatman-Iwanowska, M.S. Donnenberg, G. Frankel, et al., Enteropathogenic *Escherichia coli* (EPEC) adhesion to intestinal epithelial cells: role of bundle-forming pili (BFP), EspA filaments and intimin, *Microbiology*. 150 (2004) 527–538.
- [12] L.D. Kalischuk, F. Leggett, G.D. Inglis, *Campylobacter jejuni* induces transcytosis of commensal bacteria across the intestinal epithelium through M-like cells, *Gut Pathog.* 2 (2010) 14.
- [13] S.M. Man, N.O. Kaakoush, S.T. Leach, L. Nahidi, H.K. Lu, J. Norman, et al., Host attachment, invasion, and stimulation of proinflammatory cytokines by *Campylobacter concisus* and other non-*Campylobacter jejuni* *Campylobacter* species, *J. Infect. Dis.* 202 (2010) 1855–65.
- [14] D.J. Philpott, D.M. Mckay, W. Mak, M.H. Perdue, P.M. Sherman, Signal transduction pathways involved in enterohemorrhagic *Escherichia coli*-induced alterations in T84 epithelial permeability, *Infect. Immun.* 66 (1998) 1680–1687.
- [15] S. Resta-Lenert, K.E. Barrett, Live probiotics protect intestinal epithelial cells from the effects of infection with enteroinvasive *Escherichia coli* (EIEC), *Gut.* 52 (2003) 988–997.
- [16] A.M.D. Machado, M.O.A. Sommer, Human intestinal cells modulate conjugational transfer of multidrug resistance plasmids between clinical *Escherichia coli* isolates, *PLoS One.* 9 (2014) 1–5.
- [17] X. He, D.O. Mishchuk, J. Shah, B.C. Weimer, C.M. Slupsky, Cross-talk between *E. coli* strains and a human colorectal adenocarcinoma-derived cell line, *Sci. Rep.* 3 (2013) 3416.
- [18] M.J. Briske-Anderson, J.W. Finley, S.M. Newman, The influence of culture time and passage number on the morphological and physiological development of Caco-2 cells, *Proc. Soc. Exp. Biol. Med.* 21 (1997) 248–257.
- [19] W.-L. Hao, Y.-K. Lee, Microflora of the gastrointestinal tract: a review, in: J.F.T. Spencer, A.L.R. de Spencer (Eds.), *Public Heal. Microbiol. Methods Protoc.*, 1st ed., Humana Press, New York, 2004: pp. 491–502.
- [20] J.M. Anderson, C.M. van Itallie, Tight junctions of paracellular and the molecular permeability basis for regulation, *Am. J. Physiol. Liver Physiol.* 269 (1995) 467–475.
- [21] M. Cerejido, J. Valdes, L. Shoshani, R.G. Contreras, Role of tight junctions in establishing and maintaining cell polarity, *Annu. Rev. Physiol.* 60 (1998) 161–177.
- [22] W.M. Leevy, J.R. Johnson, C. Lakshmi, J. Morris, M. Marquez, B.D. Smith, Selective recognition of bacterial membranes by zinc(II)-coordination complexes, *Chem. Commun.* 1 (2006) 1595–7.
- [23] I. Simonovic, J. Rosenberg, A. Koutsouris, G. Hecht, Enteropathogenic *Escherichia coli* dephosphorylates and dissociates occludin from intestinal epithelial tight junctions, *Cell. Microbiol.* 2 (2000) 305–315.
- [24] P.J. Turnbaugh, R.E. Ley, M. Hamady, C.M. Fraser-Liggett, R. Knight, J.I. Gordon, The human microbiome project, *Nature.* 449 (2007) 804–10.

CHAPTER 9: Conclusion and outlook

9.1 Conclusion

The goal of the project presented in this thesis was to develop a microfluidic chip to support long-term Caco-2 cell culture for barrier and drug transport studies. Furthermore, the device should also allow real time microscopic imaging and monitoring of the integrity of the cultured epithelial cell layer.

The bulk of the thesis focuses on microchips fabricated using the thiol-ene ‘click’ chemistry. This method of fabricating the multi-layer microfluidic chip could be carried out in ambient temperatures and environments. The method also does not need costly or specialized cleanroom technologies. The presented microchip consists of three layers, where the middle layer was a thiol-ene-modified Teflon membrane. Modifying the Teflon membrane with thiol-ene allowed it to be easily bonded to another thiol-ene surface. Furthermore, during UV-exposure of the thiol-ene coated membrane, localised cell culture regions on the Teflon membrane could be protected with a plastic mask. Rinsing these localised regions of uncured thiol-ene with methanol allowed the recovery of the Teflon porous structures and, therefore, allowing cell culture to take place in these unmodified areas.

With the microfluidic device, we demonstrated that *in vivo* conditions could be more closely mimicked with the presence of continuous low flow on the Caco-2 cells. The Caco-2 cells cultured under such flow conditions in the microfluidic chip were observed to differentiate into columnar cells, spontaneously forming folds and producing mucus after 9-10 days of cell culture. Barrier integrity of the Caco-2 cells cultured in the microchip were demonstrated by measuring the paracellular transport of three different compounds. Introduction of low concentrations of membrane enhancer revealed that the barrier property of Caco-2 monolayers cultured in the microfluidic device could be changed reversibly. The data acquired from the microfluidic device were comparable to the data acquired from the traditional static Transwell cultures.

A simple and straightforward method for fabricating electrodes on the thiol-ene microfluidic chip was also demonstrated. The microelectrodes in the microchips were fabricated using an indium alloy (for the bottom electrodes) and platinum (for the top electrodes) for acquiring TEER measurements. The fabrication method enabled the placement of electrodes in fixed positions. These electrodes were in close proximity to the cells cultured on the porous Teflon membrane in the microchip. This method of embedding the electrodes in the microchip could be carried out in ambient environment, eliminating any forms of using multiple lithography technologies, hence reducing labour fabrication costs. The electrodes embedded in the microchip allowed acquiring real-time TEER measurements of the Caco-2 cells. Furthermore, these electrodes were also capable

in sensing the changes in the integrity of Caco-2 monolayers when challenged with low concentrations of membrane enhancer.

Some preliminary studies of co-culturing *E. coli* with Caco-2 cells were also demonstrated and discussed in the thesis. The preliminary studies showed that once the Caco-2 cells cultured in the microfluidic chip had differentiated, the Caco-2 monolayers could support the growth of the microbial flora. The barrier integrity of the Caco-2 monolayers was not damaged when incubated with *E. coli* for 24 hrs. Furthermore, the TEER measurements increased slightly. The barrier integrity of Caco-2 monolayer was further confirmed with immunofluorescence imaging of tight junctions. Thanks to the continuous perfusion of culture medium into the cell culture microchamber, nutrients are continuously supplied to the cells and wastes are also continuously removed, hence providing sufficient conditions for the microbes and Caco-2 cells to co-exist.

In summary, the presented work in this project has shown that Caco-2 cells cultured in a microengineered thiol-ene microfluidic chip may serve as an alternative *in vitro* platform for pharmaceutical, toxicological, and cell-cell communication studies, among others. With eight chambers fabricated on the same microchip, it allows parallel studies to be carried out on the same microfluidic chip under basically identical conditions.

9.2 Outlook

In this project, we have demonstrated that the multi-layer, multi-chamber thiol-ene microfluidic cell culture chip is a promising alternative *in vitro* human intestinal model for transport studies. The current system is still in its prototype phase. Although the preliminary transport studies reported in this thesis had showed promising results, investigations of transport studies could be further expanded by experimenting with more drugs or membrane enhancers.

Regarding the design of the microchip, the current small sizes of the cell culture microchambers in the reported microfluidic chip provides the opportunity to achieve high-throughput and high-resolution analysis. However, it can be a challenge in collecting samples for analysis, due to the small number of cells used and small amounts of products dispensed. Therefore, the microchannel dimensions and perfusion rates must be carefully considered in designing and operating the microfluidic device in order to meet the minimum requirements for detection and analysis of cellular products.

The current microfluidic system was shown to support co-culturing of *E. coli* with Caco-2 cells. However, a higher flow rate was required to perfuse the cell culture medium to the cells to overcome the increased fluidic resistances due to gases emitted from the *E. coli*. Increasing the flow rate will consequently increase the fluidic stresses acting on the cells. Improvements can be made to the design of the microfluidic chip by increasing the

height of the microchannels. Implementing this improvement would increase the rate of cell culture medium perfuse into the cell culture chamber. This will also increase the rate of waste removal from the cell culture chamber. This will therefore, allow cell maintenance in the microfluidic chip. Such improvements would also entail more in-depth analysis and kinetics of fluid dynamics (e.g., fluidic stresses) at the cellular level.

In general, this work has shown the possibilities of leveraging microfluidic technologies to create controlled microenvironments for cell culture that open avenues for drug transport studies. However, the need for improving the system's quality for any more routine use in the pharmaceutical sciences, toxicology etc. calls for further concerted efforts from different disciplines, such as molecular biology, microtechnology, bioengineering and pharmaceuticals.

APPENDIX

List of publications

A1. Manuscript for peer review paper

H. Y. Tan, S. Trier, M. Dufva, J. P. Kutter and T. L. Andresen, “A multi-chamber microchip platform for studying drug transport across tissue barriers”, in preparation for submission

B1. Poster presentation at conference

Presenting author is indicated with an asterisk.

H. Y. Tan*, M. Hemmingsen, J. P. Lafleur, J. P. Kutter, M. Dufva, T. L. Andresen, “Multi-chamber and multi-layer thiol-ene microchip for cell culture”, International Conference of Miniaturized Systems for Chemistry and Life Science (MicroTAS 2014), San Antonio, USA, October 26th – 30th 2014.

A1. Manuscript 1: Thiol-ene-based human intestinal microchip for passive transport studies

H. Y. Tan, S. Trier, M. Dufva, J. P. Kutter and T. L. Andresen, "Thiol-ene-based human intestinal microchip for passive transport studies", in preparation for submission to *PNAS*, 2015.

A multi-chamber microchip platform for studying drug transport across tissue barriers

Hsih-Yin Tan^{a,b}, Sofie Trier^{a,b,d}, Martin Dufva^a, Jörg P. Kutter^c, Thomas Lars Andresen^{a,b,1}

^a Technical University of Denmark, Department of Micro and Nanotechnology, Ørsteds Plads, 2800 Kgs. Lyngby, Denmark

^b Technical University of Denmark, Center for Nanomedicine and Theranostics, Ørsteds Plads, 2800 Kgs. Lyngby, Denmark

^c Department of Pharmacy, University of Copenhagen, Universitetsparken 2, 2100 Copenhagen, Denmark

^d Global Research, Novo Nordisk A/S, 2760 Maaloev, Denmark

Abstract

This paper presents the design and fabrication of a multi-layer and multi-chamber microchip system using thiol-ene ‘click chemistry’ aimed for drug transport studies across tissue barrier models. The tissue barrier model employed to test the device was based on Caco-2 intestinal model and mannitol, dextrane and insulin were used as drug molecules (in the presence or absence of membrane permeability enhancers) to investigate transport in the microfluidic barrier system in comparison to the conventional Transwell system. The developed fabrication process allows for rapid prototyping of multi-layer microfluidic chips using different thiol-ene polymer mixtures. We incorporated porous Teflon support membranes to accommodate cell growth by masked sandwiching thiol-ene-based fluid layers. Electrodes for TEER measurements were incorporated using low melting soldering wires melted into channels as in combination with platinum wires. We demonstrated that the thiol-ene-based microchip material including the electrodes does not induce adverse effects on the cells. The Caco-2 cells cultured on the thiol-ene microchip differentiated and showed signs of producing mucus and directional drug transport within 9 - 10 days of cell culture, indicating the formation of a robust barrier at a much faster rate than in conventional Transwell models. The presented microdevice for cell culture is useful for carrying out real-time studies of cellular barriers under optical monitoring, and enables transport studies of drugs, chemicals, and pathogens. The system may have additional uses in toxicological assessments.

Keywords: thiol-ene microchip, Caco-2 cell culture, membrane barrier studies, drug permeability

Significance statement

Transwell culture system is the gold standard *in vitro* model for assessing and predicting permeability and absorption of oral drugs in pharmaceutical industry. However, this platform cannot support any form of luminal flow conditions on the cells to more closely mimick *in vivo* conditions. Relevance of this study lies in engineering an eight chamber multi-layer microchip to support long-term studies of tissue barriers by using the Caco-2 cell intestinal model. We demonstrate the feasibility of using the *in vitro* intestinal model culture in the thiol-ene-based microchip for transport studies by using three different test compounds. Such a platform paves the way towards advanced *in vitro* intestinal model for high throughput screening of drugs, chemicals, pathogens as well as toxicological studies.

\body

Manuscript Text

Introduction

Covering the inner walls of the intestines is a single layer of epithelial cells that forms a rate limiting barrier to the absorption of drugs. Numerous experimental models have been developed for the prediction of intestinal permeability - including *in situ* isolated perfused intestinal systems (1–4). However, the use of animal models is time consuming, labour intensive and costly. Furthermore, animal models also raise ethical issues and are often not able to accurately predict the results in humans (5). Culturing and differentiation of epithelial cells derived from the intestine can provide relevant *in vitro* models for prediction of drug absorption in humans (6, 7). Caco-2 cells constitute a gold standard of intestinal model when cultured under specific conditions, i.e., grown on Transwell permeable filter supports, the cells will form a monolayer (8). They will further

spontaneously differentiate and proliferate, thus exhibiting many features of the small intestinal villus epithelium (9, 10). Some of the most prominent features of Caco-2 cells cultured in this way are the formation of brush border microvilli (10) on the upper side of the cells, development of intercellular tight junctions (11), and the presence of various metabolic enzymes present in the intestinal epithelium (10, 12). Due to the formation of a tight monolayer of Caco-2 cells, this provides a physical and biochemical barrier to the passage of ions and small molecules through the Caco-2 cell layer. Therefore, it is one of the most well-established human intestinal epithelial cell lines and has been extensively used as an *in vitro* intestinal model for pharmaceutical studies, e.g., ADME-Tox (adsorption, distribution, metabolism, excretion, and toxicology) studies. About three weeks are required for Caco-2 cells to fully differentiate and form confluent and tight monolayers in Transwell inserts (8). However, this *in vitro* model does not allow to recreate the presence of continuous fluid flow nor the presence of fluid shear stresses on the epithelial cells as can be found in their natural environment. It has been postulated that the fluid shear stress in the intestinal tract varies depending on the exact location and fluid shear stresses from 1 to 5 dyn/cm² have been reported (13).

By using micro total analysis system technology, various functional microfluidic systems can be developed to provide integrated microenvironments for cell maintenance, continuous perfusion and real-time monitoring of cells. Several groups have reported on the design and fabrication of polydimethylsiloxane (PDMS) based microdevices for Caco-2 cell culture (14–18). Kim et al. have reported that with the combination of peristaltic motion and fluid flow in the microfluidic device, the Caco-2 cells displayed intestinal villi with physiological growth up to several hundreds of microns in height, as well as increased expression of intestine-specific functions, including mucus production (17). However, the reported microfluidic devices are only capable of culturing one set of Caco-2 monolayers for analysis at any one time. In biological cell analysis studies or drug transport studies across Caco-2 monolayers, or other model tissue barriers, it is highly desirable to investigate different conditions in the same experimental system in a high throughput manner (19). Scaling up the number of cell culture microchambers on the microfluidic chip provides the possibility for analyzing more than one sample in parallel under controlled conditions, therefore allowing for controlled parameter comparisons. Although PDMS is an excellent material choice for fabricating microfluidic devices for cell culture, it may pose some challenges in studies that involve chemicals and drugs (20). Furthermore, PDMS has a tendency to absorb small hydrophobic molecules and this may compromise accurate measurements of drug efficacy and toxicity (21–23).

To pursue the goal of developing an alternative *in vitro* model of the human intestines for high throughput transport studies (Fig. 1), we have explored the use of thiol-ene chemistry and a novel membrane system for cell support within a microfluidic system to develop a multi-chamber microchip. To quantitatively evaluate the integrity of the Caco-2 monolayer, two pairs of electrodes were embedded in the microchambers on the microchip to acquire trans-epithelial electrical resistance (TEER).

Results and discussion

Development of thiol-ene-based microchip for Caco-2 cell culture. We designed and developed a thiol-ene based microchip that consists of eight cell culture micro-chambers where each cell culture chamber has two compartments (to become the apical and basal side of the cell layer, respectively) (Fig. 1). The developed microchip contains eight micro-chambers, thus allowing parallel culturing of Caco-2 cells or other tissue models. The design of eight channels allows for significant controls during drug transport studies and allowed us to employ the previously reported microfluidic flow system developed by some of the authors (24). Thiol-ene was chosen since thiol-ene polymers have been reported to show low affinity to absorb molecules, have low volume shrinkage (25, 26), and are biocompatible for use in cell culture (27). The thiol-ene-based microchip has an external dimension of 76 mm x 52 mm x 2.7 mm and consists of three layers. The top and bottom layers of the microchip were fabricated via the method reported by Lafleur et. al. (28) using a two-step UV exposure (29, 30) (*SI Text Fabrication of microfluidic device*). The middle layer was a porous Teflon membrane (BGCM 00010; Millipore, Denmark) (0.4 μm in pore size; 40 μm in thickness). This porous Teflon membrane was suitable for cell culturing and it became transparent to visible light when wetted (Fig. S2), thus allowing real-time and fluorescence microscopic monitoring of the Caco-2 cells cultured on it. The bonding of the thiol-ene top and bottom fluidic layers with the Teflon membrane required a dedicated modification of the membrane. The porous Teflon membrane was coated with a thiol-ene mixture and exposed to UV radiation with a plastic mask that protected the part of the membrane to be used for cell cultures. Methanol was used to

rinse the entire membrane to remove any traces of uncured thiol-ene. The end result was a thiol-ene modified membrane with regions, which were not coated with thiol-ene and thus allowed the porous Teflon membrane to be used for cell culturing. When examined with a scanning electron microscope (SEM), a smooth surface was observed in regions where the porous Teflon membrane was coated with thiol-ene and exposed to UV light. In regions that were masked and rinsed with methanol, the porous structure of the Teflon membrane was preserved (Fig 2D). This procedure clearly demonstrated that thiol-ene 'click' chemistry can be exploited to functionalize and pattern the membrane surface (29, 30). In the pressure burst studies of the microfluidic chip, the multi-layer microchip could withstand burst pressures of more than 6 bars (*SI Table ST1*). The presented method of fabricating the microfluidic chip can easily be carried out at room temperature and in standard laboratory environments, therefore eliminating the need for costly or specialized cleanroom facilities.

Caco-2 cell culture in microfluidic system. To investigate the feasibility of culturing Caco-2 cells in the microchambers of the thiol-ene microfluidic chip, Caco-2 cells were seeded into the microchamber at a density of 8.5×10^6 cells/ml. Cell culture medium was perfused through the upper and lower fluidic layers at a flow rate of 3 μ l/min for 9 – 10 days. Caco-2 cells were observed to adhere onto the extracellular matrix (ECM) coated Teflon membrane (*SI Text Cell culture in microfluidic system*) within 30 min after cell seeding. During the phase of active growth, it was observed that once the flow of cell culture media was started (first 24 hrs of cell culture), the Caco-2 cells spread out (31). Yet, in some regions the cells grew in clusters. By day 2 (Fig. 3B), distinct polygonal shapes with clear, sharp boundaries between the Caco-2 cells were observed in all the microchambers. The shape and morphology of the Caco-2 cells in the microfluidic device was similar to the cells cultured in a microplate (results not shown). Confluent monolayers of Caco-2 cells were observed in the microfluidic device typically around day 3-5 of cell culture. Folds started appearing in the monolayers around day 5 (a suggestion of villous formation) and it became more challenging to observe the cells through an optical microscope (Fig 3C). From day 7 and onwards, the appearance of 'dark' patches (Fig. 3D) were observed on the cells.

Caco-2 cell morphological studies. The establishment of apical tight junctions determines the integrity of the human intestinal epithelial cell monolayer (8). To visualise and validate the presence of apical tight junctions in the Caco-2 cells cultured in the microfluidic device, immunofluorescence staining using antibodies directed at the tight-junction protein, occludin, was carried out (*SI Text Morphological studies of Caco-2 cells in microfluidic and Transwell cultures*).

The immunofluorescence images confirmed the formation of confluent Caco-2 monolayers, expressing tight junctions (Fig 3E-F). Analysis of the vertical sections of the confocal images of the Caco-2 cells (Fig 3H) revealed that the tight-junction proteins were situated between neighbouring cells at the apical side of the Caco-2 cells (Fig 3F and 3H). Images of the cells cultured in the Transwell inserts at day 21 appeared cuboidal with heights of 14 – 20 μ m (Fig 3I). However, the Caco-2 cells cultured in the thiol-ene microfluidic device (three days of cell culture) were observed to appear columnar in shape with heights of \approx 40 – 50 μ m (Fig 3H). Our data is consistent with a previous report (17). The Caco-2 cells cultured in the microfluidic device is about the same columnar size and shape (40-50 μ m) as reported in healthy human intestinal epithelial cells (32). It is believed that the presence of continuous perfusion of cell culture medium in the microfluidic device may be responsible for stimulating the Caco-2 cells to polarise into columnar cells that were almost 2 fold taller than the cells from Transwell inserts (17). An earlier report showed that the flow rate of cell culture medium was a critical factor in controlling the Caco-2 cell shape and polarity (17).

In the reported microfluidic device, as the cell culture period progressed in the microfluidic device, from microscopic phase contrast images, there were observable regions of 'dark' patches (Fig 3D). These 'dark' patches started appearing from day 7 of cell culture, but became more prominent from day 8 onwards. We observed that these dark patches were absent when the cells were cultured at a low flow rate of 0.5 μ l/min (results not shown). To further investigate the nature or origin of these 'dark' patches, the Caco-2 monolayers were stained for the muco-protein, Mucin-2 (Mucin-2 is commonly found in human intestines) on day 10 of cell culture. Our immunofluorescence staining directed towards the protein Mucin-2 showed positive stains at the apical surfaces of the villous Caco-2 monolayers (Fig 3J). This is surprising as in an earlier study (17, 33) the authors claimed the production of mucus on the Caco-2 cells cultured in a microfluidic device was due to fluid flow and cyclic peristaltic motions. However, the Caco-2 cells cultured in the thiol-ene microfluidic

device were only exposed to low fluidic stresses ($\approx 0.008 \text{ dyn/cm}^2$) at $3 \mu\text{l/min}$. It was also reported the gastrointestinal tract has a tendency to protect itself from mechanical and other stresses by producing and secreting a layer of lubricating mucus onto epithelial surfaces (34). Therefore, we hypothesise the exposure to low fluidic shear stresses ($\approx 0.008 \text{ dyn/cm}^2$) may have resulted in the Caco-2 cells exhibiting some protective function by producing mucus on the apical side of the cells. To further confirm our observation, we also performed the same staining procedure on cells cultured in the Transwell inserts. Past studies have reported that Caco-2 cells do not produce mucus when cultured in static culture conditions (19). As expected the images of our Transwell cultures did not show the presence of Mucin-2 on the Caco-2 monolayers (Fig. 3K).

From the fluorescent images (Fig. 3J), it can also be observed that the Caco-2 cells cultured in the microfluidic device form folds and are capable of growing up to a height of $\approx 100 \mu\text{m}$ when they are cultured for a longer term (day 9 – 10). These results are consistent with an earlier study which showed fluid flow can encourage the formation of villous structures in the Caco-2 monolayers (17, 33).

Differentiation of Caco-2 cells. Another characteristic of differentiated Caco-2 cells is the high level expression of brush border enzymes that are commonly found in small intestinal epithelial cells (10, 12). To evaluate the differentiation of the Caco-2 cells that were cultured in our thiol-ene microchip, we measured the level of aminopeptidase activity by using the substrate L-alanine-4-nitroaniline hydrochloride (L-A4N). The aminopeptidase experiments were also carried out in the static Transwell inserts. The Transwell studies were carried out on day 5 and 21 of cell culture. In the microfluidic device, the aminopeptidase studies were carried out on day 5 of cell culture. Analysis of data from the Transwell cultures showed that the aminopeptidase activity increased by more than 5-fold between Caco-2 cells cultured for 5 days and 21 days, respectively. These data are consistent with earlier findings (12, 17). Interestingly, analysis of the samples collected from our microfluidic device, with only 5 days of cell culture, showed that the aminopeptidase activity was 4 times higher than the aminopeptidase activity in the Transwell inserts at day 21 (Fig 3L). Our results are comparable to earlier findings (14, 17). These results clearly confirmed that cells cultured in the presence of continuous flow (as in the microfluidic device) required a shorter time to polarize and differentiate.

Trans-epithelial electrical resistance (TEER) measurements. Trans-epithelial electrical resistance (TEER) is a widely used technique for quantifying the integrity of the tight junctions present between cells that govern the solute transport across the paracellular space of epithelial monolayers (10). To ensure as much as possible an equal potential drop over the entire membrane (35), the electrodes were embedded directly above and below the membrane in our microfluidic device. The electrodes embedded in the thiol-ene microfluidic chip were produced in-house using a low-melting indium alloy (InBiSn) (*SI Fabrication of microfluidic device*) for the bottom electrodes and platinum wires for the top electrodes. TEER measurements were obtained by coupling the electrodes to a multi-meter (Keithley, USA) that supplied DC signals (constant current = $10 \mu\text{A}$). TEER measurements of the Caco-2 monolayer cultured in the thiol-ene microchip were taken from day 3 onwards of cell culture and monitored over the remaining days of the experiments. Importantly, the TEER measurements of the Caco-2 cells cultured in the thiol-ene microchip showed a significant increase over the days of cell culture (Fig 4A). TEER values for the microfluidic system reached a maximum of about $1400 \Omega\cdot\text{cm}^2$ and the high values could be maintained from day 7-9. The standard deviation (SD) of the TEER values from the microfluidic device is much larger compared to the SD of the data from the Transwell inserts. This is attributed to the difference in electrode designs. Furthermore, the positions of the electrodes on the microfluidic device may vary slightly from microchamber to microchamber, and this may contribute to differences in measured resistances (36).

Effect of membrane permeability enhancer on TEER values. To validate the accuracy of the TEER values acquired from the electrodes on the microfluidic chip, a membrane enhancer, tetradecyl- β -D-maltoside (TDM), was introduced to the Caco-2 monolayers for two hours. The membrane enhancer, TDM, is a compound that interacts with lipid cell membrane to permeabilise it, therefore increasing the transcellular pathway (37–39). It also modifies the tight junctions between adjacent cells, hence causing a drop in the TEER values. This also causes an increase in the paracellular transport of compounds across the Caco-2 monolayer (37–39). The concentration of TDM used in this study is within the range that was reported previously (37–39). The concentration of TDM used in this study would disrupt the integrity of the Caco-2 monolayer while allowing

it to recover when subjected to 24 hours of recovery with cell culture medium (Fig. 4B). Therefore, one will expect the TEER values to drop after exposing the Caco-2 monolayers to TDM, and then an increase of TEER values after 24 hours recovery period in cell culture medium. Interestingly, with the introduction of TDM to the Caco-2 monolayers cultured in the microfluidic device, the TEER data acquired in the absence and presence of membrane permeability enhancers showed distinct differences. It could be clearly seen that in the presence of TDM, the TEER values measured in the microfluidic device dropped to 20.6 % of their initial values (Fig 4B). When the Caco-2 monolayers were subsequently subjected to 24 hours of continuous perfusion with cell culture medium, the TEER values recovered to 90 % of the initial values (Fig 5B). This significant drop in TEER values with the introduction of TDM and an increase in the TEER values during the 24 hour recovery in cell culture medium was consistent with the data acquired from the static Transwell cultures (Fig 5B). The TEER results recorded from the microfluidic device were also an indication that the electrodes fabricated on the microfluidic device were sensitive to detect dynamic changes in the integrity of the Caco-2 monolayers.

P-glycoprotein analysis. Another important characteristic present in differentiated Caco-2 cells is the presence of efflux transporter P-glycoproteins (P-gp). These P-gp transporters play an important role in determining the bioavailability of drugs, especially the orally administered drugs. We evaluated the presence of P-gp transporters in the Caco-2 monolayers cultured in the microfluidic system by carrying out permeability studies with a well characterized substrate, Rhodamine 123 (as a model drug for uptake and transport) (Rh 123). Rh 123 was flowed to either the apical or basal compartments and sample aliquots were collected accordingly from the basal or apical waste reservoirs. Our analysis yielded a value for the apparent permeability in the apical-to-basal direction of $P_{app(apical \rightarrow basal)} \approx 1.03 \times 10^{-6}$ cm/s. The results suggested that the absorptive transport of Rh 123 was not affected by the presence of P-gp. Rather, Rh 123 was transported across the Caco-2 monolayers via the paracellular route. In contrast, $P_{app(basal \rightarrow apical)} \approx 1.12 \times 10^{-5}$ cm/s, suggesting that Rh 123 was transported across the Caco-2 monolayer by the P-gp transporters. The resulting efflux ratio ≈ 10.82 was comparable to that obtained with static cultures that were previously reported (40–42). An efflux ratio of higher than 2 is a strong indicator that the P-gp transporters are secretory (43). To further confirm the presence of P-gp transporters in the Caco-2 monolayers, immunofluorescence staining towards the P-gp transporters was performed (Fig 4C).

Permeability studies of FITC–dextran (FD-4), mannitol and insulin in the presence or absence of membrane permeability enhancer. Paracellular transport of compounds across the Caco-2 monolayers is governed by the presence of the tight junctions between adjacent cells. To further assess the rate-limiting barrier of the Caco-2 monolayers cultured in the thiol-ene microchip, the behavior of three different test compounds (mannitol, fluorescein isothiocyanate (FITC)-labeled-dextran (FD 4) and insulin) was studied. Mannitol and dextrane were used as model drugs. Insulin was used due to the interest in oral delivery of this drug in the pharmaceutical industry to provide a proof of concept of the Caco-2 monolayers cultured in the thiol-ene microchip for drug permeability studies. Insulin is usually administered by the subcutaneous route (44, 45); however, orally delivered insulin is attracting considerable attention due to the improved compliance this would provide for diabetic patients (44). Oral delivery of insulin has major limitations, due to the degradation of insulin by proteolytic enzymes in the gastrointestinal tract and poor intestinal barrier permeability due to its molecular weight (45). To increase the oral bioavailability, various strategies have been made to investigate to facilitate the absorption and transportation of insulin. One of the more successful methods is to co-administer membrane permeability enhancers (37–39, 46, 47) (Fig. 1c) together with the drug. For this reason, we chose to investigate the use of permeability enhancer, TDM, for aiding insulin transport to further demonstrate the usability of microfluidic-based tissue barrier platforms for investigating drug transport.

Permeability studies were carried out on day 9 or day 10 of cell culture. We measured the permeabilities (P_{app}) for mannitol, FD-4 and insulin to be 3.94×10^{-6} cm/s, 2×10^{-7} cm/s and 9.43×10^{-7} cm/s, respectively, in the microfluidic chip. The P_{app} values of similar compounds in the static Transwell cultures were slightly lower as compared to the microfluidic device (Fig 5). To further investigate whether the permeability of different test compounds is affected by the introduction of TDM, we next exposed the Caco-2 monolayers in both the microfluidic device and the Transwell inserts to mixtures of test compounds with TDM. In both systems, the P_{app} values for all three compounds greatly increased (Fig. 5) in the presence of TDM. In the microfluidic device, the P_{app} values for mannitol, FD-4 and insulin were 12.42×10^{-6} cm/s, 14.29×10^{-7} cm/s

and 11.02×10^{-7} cm/s respectively (Fig 5). While the P_{app} values of the similar test compounds from the static Transwell cultures were 13.9×10^{-6} cm/s, 19.72×10^{-7} cm/s and 9.43×10^{-7} cm/s. The permeability results clearly demonstrated that the addition of TDM effectively permeabilised the Caco-2 monolayers in both systems and allowed substantial transport of compounds across the Caco-2 monolayers. Additionally, the P_{app} values of the test compounds in the presence of TDM were comparable between the static Transwell cultures and the microfluidic system. Therefore, the Caco-2 monolayers cultured in the microfluidic device could be an interesting alternative *in vitro* model of the human intestines for drug transport studies.

Conclusion

A thiol-ene based multi-chamber and multi-layer microfluidic chip was engineered to provide a controlled platform to sustain long-term Caco-2 cell cultures under fluidic flow for transport studies. Characterization of the microfluidic chip revealed that the functionality of the porous Teflon membrane (sandwiched between the top and bottom fluidic layers) could be changed by coating and curing it with a thiol-ene mixture, followed by ECM coating of the porous region of the Teflon. Thus, bonding the Teflon membrane between two cured thiol-ene layers within a fluidic system formed a microchip that could support long time cell culture. The experiments with the Caco-2 cells cultured in the thiol-ene microfluidic chip revealed, the growth and differentiation of the Caco-2 cell cultures accelerated under fluidic conditions. Furthermore, under continuous flow conditions, the Caco-2 cells cultured in the microchip developed villous morphogenesis, exhibited increased differentiation, formed a tight barrier and P-glycoprotein transporters, closely mimicking the human intestine. We showed that this intestinal model was adequate for transport studies.

In summary, this work has shown that the thiol-ene polymers used in fabricating the microfluidic chip were biocompatible, permitting long-term culturing of Caco-2 cells. Additionally, the Caco-2 cells cultured in a microengineered thiol-ene microfluidic chip may serve as a promising alternative *in vitro* platform for pharmaceutical, toxicological, and cell-cell communication studies, among others. With eight chambers fabricated on the same microchip, it allows for parallel studies to be carried out on the same microfluidic chip under basically identical conditions.

Materials and methods

Fabrication of thiol-ene microfluidic chip. Pentaerythritol tetrakis-(3-mercaptopropionate) (4 thiol moieties), tri-allyl-tri-azine (3 ene moieties) and trimethylpropane tris-(2-mercaptopropionate) (3 thiol moieties) used for fabricating the fluidic layers in the thiol-ene microfluidic chips were all purchased from Sigma Aldrich, Denmark. The commercially available Teflon membrane that was modified and sandwiched between the thiol-ene layers was purchased from Milipore, Germany. Methanol (Sigma, Denmark) was used for removal of uncured thiol-ene on the modified Teflon membrane. The microelectrodes embedded in the thiol-ene microchips were fabricated by inserting pieces of low-melting temperature indium alloy (InBiSn, In 51 % Bi 32.5 % Sn 16.5 % by weight) (Indium Corp., Utica, NY) for the bottom fluidic layer and platinum wire (Advent, UK). The detailed fabrication of the microfluidic device is reported in the *SI Text Fabrication of microfluidic device*.

Cell culture. Human Caco-2 intestinal epithelial cells used in the experiments were obtained from American Type Culture Collection ((ATCC), HTB-37, Germany). The passages of the Caco-2 cell line used in the microfluidics studies ranged from the 40th to 50th passages, and for the Transwell studies, passages in the range of 40th to 65th were used. The Caco-2 cells were cultured routinely in Dubelco's Modified Eagle Medium (DMEM; Sigma, Denmark). The culture medium is supplemented with 10 % (v/v) heat-inactivated fetal bovine serum (FBS; Sigma, Denmark), 1% (v/v) nonessential amino acids (NEAA; Gibco, Denmark) and 1% (v/v) penicillin-streptomycin (P/S; Gibco, Denmark).

Acknowledgements

This work is supported by The Danish Council for Independent Research (FTP) and the Lunbeck Foundation.

References

1. Stewart B, et al. (1995) Comparison of intestinal permeabilities determined in multiple *in vitro* and *in situ* models: Relationship to absorption in humans. *Pharm Res* 12(5):693–699.

2. Lozoya-Agullo I, González-Álvarez I, González-Álvarez M, Merino-Sanjuán M, Bermejo M (2015) In Situ perfusion model in rat colon for drug absorption studies: comparison with small intestine and Caco-2 cell model. *J Pharm Sci* 104(9):3136–45.
3. Svensson USH, Sandström R, Carlborg Ö, Lennernäs H, Ashton M (1999) High in situ rat intestinal permeability if artemisinin unaffected by multiple dosing and with no evidence of P-glycoprotein involvement. *Drug Metab Dispos* 27(2):227–232.
4. Zakeri-Milania P, et al. (2007) Human intestinal permeability using intestinal perfusion in rat. *J Pharm Pharm Sci* 10(3):368–379.
5. Holmes AM, Creton S, Chapman K (2010) Working in partnership to advance the 3Rs in toxicity testing. *Toxicology* 267(1-3):14–9.
6. Hilgers AR, Conradi RA, Burton PS (1990) Caco-2 cell monolayers as a model for drug transport across the intestinal mucosa. *Pharm Res* 7(9):902–910.
7. Stenberg P, Norinder U, Luthman K, Artursson P (2001) Experimental and computational screening models for the prediction of intestinal drug absorption. *J Med Chem* 44(12):1927–1937.
8. Hubatsch I, Ragnarsson EGE, Artursson P (2007) Determination of drug permeability and prediction of drug absorption in Caco-2 monolayers. *Nat Protoc* 2(9):2111–9.
9. Hidalgo IJ, Raub TJ, Borchardt RT (1989) Characterization of the human colon carcinoma cell line (Caco-2) as a model system for intestinal epithelial permeability. *Gastroenterology* 96(3):736–749.
10. Pinto M, et al. (1983) Enterocyte-like differentiation and polarization. *Biol cell* 47(323):323–330.
11. Anderson JM, et al. (1989) ZO-1 mRNA and protein expression during tight junction assembly in Caco-2 cells. *J Cell Biol* 109(3):1047–1056.
12. Howell S, Kenny AJ, Turner AJ (1992) A survey of membrane peptidases in two human colonic cell lines Caco-2 and HT-29. *Biochem J* 284(2):595–601.
13. Guo P, Weinstein AM, Weinbaum S (2000) A hydrodynamic mechanosensory hypothesis for brush border microvilli. *Am J Physiol Physiol* 10031(4):F698–F712.
14. Chi M, et al. (2015) A microfluidic cell culture device (μ FCCD) to culture epithelial cells with physiological and morphological properties that mimic those of the human intestine. *Biomed Microdevices* 17(3):9966.
15. Gao D, Liu H, Lin J-M, Wang Y, Jiang Y (2013) Characterization of drug permeability in Caco-2 monolayers by mass spectrometry on a membrane-based microfluidic device. *Lab Chip* 13(5):978–85.
16. Imura Y, Asano Y, Sato K, Yoshimura E (2009) A microfluidic system to evaluate intestinal absorption. *Anal Sci Int J Japan Soc Anal Chem* 25(12):1403–1407.
17. Kim HJ, Huh D, Hamilton G, Ingber DE (2012) Human gut-on-a-chip inhabited by microbial flora that experiences intestinal peristalsis-like motions and flow. *Lab Chip* 12(12):2165–74.
18. Kimura H, Yamamoto T, Sakai H, Sakai Y, Fujii T (2008) An integrated microfluidic system for long-term perfusion culture and on-line monitoring of intestinal tissue models. *Lab Chip* 8(5):741–6.
19. Artursson P, Borchardt RT (1998) Intestinal drug absorption and metabolism in cell cultures: Caco-2 and beyond. *Pharm Res* 4(12):1655–1658.
20. Huh D, et al. (2013) Microfabrication of human organs-on-chips. *Nat Protoc* 8(11):2135–57.
21. Lee JN, Park C, Whitesides GM (2003) Solvent compatibility of poly(dimethylsiloxane)-based microfluidic devices. *Anal Chem* 75(23):6544–54.
22. Toepke MW, Beebe DJ (2006) PDMS absorption of small molecules and consequences in microfluidic applications. *Lab Chip* 6(12):1484–6.
23. Wang JD, Douville NJ, Takayama S, ElSayed M (2012) Quantitative analysis of molecular absorption into PDMS microfluidic channels. *Ann Biomed Eng* 40(9):1862–73.
24. Sabourin D, et al. (2013) The MainSTREAM component platform: a holistic approach to microfluidic system design. *J Lab Autom* 18(3):212–28.
25. Carlborg CF, Haraldsson T, Öberg K, Malkoch M, van der Wijngaart W (2011) Beyond PDMS: off-stoichiometry thiol-ene (OSTE) based soft lithography for rapid prototyping of microfluidic devices. *Lab Chip* 11(18):3136–47.
26. Hoyle CE, Lee TY, Roper T (2004) Thiol-enes: Chemistry of the past with promise for the future. *J Polym Sci Part A Polym Chem* 42(21):5301–5338.

27. Hung L-H, Lin R, Lee AP (2008) Rapid microfabrication of solvent-resistant biocompatible microfluidic devices. *Lab Chip* 8(6):983–7.
28. Lafleur JP, Kwapiszewski R, Jensen TG, Kutter JP (2013) Rapid photochemical surface patterning of proteins in thiol-ene based microfluidic devices. *Analyst* 138(3):845–9.
29. Carlborg CF, et al. (2014) Functional off-stoichiometry thiol-ene-epoxy thermosets featuring temporally controlled curing stages via an UV/UV dual cure process. *J Polym Sci Part A Polym Chem* 52(18):2604–2615.
30. Natali M, Begolo S, Carofiglio T, Mistura G (2008) Rapid prototyping of multilayer thiolene microfluidic chips by photopolymerization and transfer lamination. *Lab Chip* 8(3):492–4.
31. Jokhadar SZ, Suštar V, Svetina S, Batista U (2009) Time lapse monitoring of Caco-2 cell shapes and shape dependence of the distribution of integrin $\beta 1$ and F-actin on their basal membrane. *Cell Commun Adhes* 16(1-3):1–13.
32. Bullen TF, et al. (2006) Characterization of epithelial cell shedding from human small intestine. *Lab Invest* 86(10):1052–63.
33. Kim HJ, Ingber DE (2013) Gut-on-a-chip microenvironment induces human intestinal cells to undergo villus differentiation. *Integr Biol* 5(9):1130–40.
34. Forstner G (1995) Signal transduction, packaging and secretion of mucins. *Annu Rev Physiol* 57(1):585–605.
35. Odijk M, et al. (2015) Measuring direct current trans-epithelial electrical resistance in organ-on-a-chip microsystems. *Lab Chip* 15(3):745–52.
36. Lee WG, et al. (2008) Effect of geometry on impedance of cell suspended media in electrically mediated molecule uptake using a microstructure. *Curr Appl Phys* 8(6):696–699.
37. Petersen SB, Nielsen LG, Rahbek UL, Guldbrandt M, Brayden DJ (2013) Colonic absorption of salmon calcitonin using tetradecyl maltoside (TDM) as a permeation enhancer. *Eur J Pharm Sci* 48(4-5):726–34.
38. Petersen SB, et al. (2012) Evaluation of alkylmaltosides as intestinal permeation enhancers: comparison between rat intestinal mucosal sheets and Caco-2 monolayers. *Eur J Pharm Sci* 47(4):701–12.
39. Yang T, Arnold JJ, Ahsan F (2005) Tetradecylmaltoside (TDM) enhances in vitro and in vivo intestinal absorption of enoxaparin, a low molecular weight heparin. *J Drug Target* 13(1):29–38.
40. Troutman MD, Thakker DR (2003) Rhodamine 123 requires carrier-mediated influx for its activity as a P-glycoprotein substrate in Caco-2 cells. *Pharm Res* 20(8):1192–1199.
41. Jia JX, Wasan KM (2008) Effects of monoglycerides on Rhodamine 123 accumulation, estradiol 17 β -D-glucuronide bidirectional transport and MRP2 protein expression within Caco-2 cells. *J Pharm Pharm Sci* 11(3):45–62.
42. Sachs-Barrable K, Thamboo A, Lee SD, Wasan KM (2007) Lipid excipients peceol and gelucire 44/14 decrease P-glycoprotein mediated efflux of Rhodamine 123 partially due to expression within Caco-2 cells. *J Pharm Pharm Sci* 10(3):319–331.
43. Giacomini KM, et al. (2010) Membrane transporters in drug development. *Nat Rev Drug Discov* 9(3):215–236.
44. Fonte P, Araújo F, Reis S, Sarmiento B (2013) Oral Insulin Delivery: How Far Are We? *J Diabetes Sci Technol* 7(2):520–531.
45. Carino GP, Mathiowitz E (1999) Oral insulin delivery. *Adv Drug Deliv Rev* 35(2-3):249–257.
46. Arnold JJ, Ahsan F, Meezan E, Pillion DJ (2004) Correlation of tetradecylmaltoside induced increases in nasal peptide drug delivery with morphological changes in nasal epithelial cells. *J Pharm Sci* 93(9):2205–13.
47. Uchiyama T, et al. (1999) Enhanced permeability of insulin across the rat intestinal membrane by various absorption enhancers: their intestinal mucosal toxicity and absorption-enhancing mechanism of n-Lauryl- β -D-maltopyranoside. *J Pharm Pharmacol* 51(11):1241–1250.

Figure Legends

Figure 1. Schematic illustration of the thiol-ene based microfluidic chip for intestinal transport studies. (A) Cross-sectional view of human intestinal microvilli. (B) Microarchitecture of one microchamber on the thiol-ene microfluidic chip consisting of upper and lower cell culture chambers separated by an ECM coated Teflon

membrane. (C) Presence of membrane enhancer causing compounds to be transported across Caco-2 monolayer

Figure 2. A) Schematic process of fabricating the thiol-ene coated membrane. B) Exploded view of the high throughput multi-layer thiol-ene microchip for cell culture (*Dimension of microchip: 76 mm x 52 mm x 2.7 mm*). Thickness of the modified membrane is 0.3 mm. The membrane is coated with a thiol-ene mixture on both sides to ensure good bonding between the chip layers. Fluids were pumped in the upper and lower layers. (C) SEM images of Teflon membrane (Top view). Surface morphology was changed significantly after coating a layer of thiol-ene. The surface of the membrane has become very smooth after coating and curing a layer of thiol-ene (as indicated by red arrow). D) Expanded view of Teflon membrane that was masked off and rinsed with methanol, thus maintaining its porous structure in these areas.

Figure 3. Caco-2 cells cultured in microfluidic system (A-G). Caco-2 cells cultured in Transwell system (H-I). Phase contrast images of the Caco-2 cells cultured in the microchambers on the thiol-ene microchip over 10 days. (A) Day 1; (B) Day 2; (C) Day 5; (D) Day 8. Cells multiply and differentiate over the days of culture. Folds in the monolayer of Caco-2 cells start appearing from day 4 of cell culture. The folds in the Caco-2 monolayers are more prominent from day 5 onwards (indicated by red arrows). Dark ‘patches’ also start appearing on the Caco-2 monolayers from day 7 onwards. They become more prominent from day 8 of cell culture (indicated by white arrow). (E) Immunofluorescence image showing the distribution of the tight junction protein, occludin (green) at day 3. (F) Immunostaining of tight junctions (green) and nuclei (magenta). (G) Caco-2 cells cultured in Transwell stained for nucleus and tight junctions (Nuclei in red and tight junctions in green) (Day 21). (H) Vertical cross-section view of the Caco-2 monolayer (nuclei in magenta, tight junctions in green). The Caco-2 cells are $\approx 40 \mu\text{m} - 50 \mu\text{m}$ in height on day 3 of cell culture in the thiol-ene microfluidic chip. (I) Vertical confocal image of Caco-2 cells in Transwell (Nuclei in red and tight junctions in green). Immunofluorescence staining of nucleus and mucus on Caco-2 cells cultured in: (J) Thiol-ene microchip on day 10 of cell culture (nucleus in red, mucoprotein 2 (MUC-2) in green). The fluorescent images of the cells demonstrate that the cells have polarised into columnar cells of about $100 \mu\text{m}$ in height and formed villous-like structures. (K) Cells in the Transwell inserts were stained for nucleus and mucoprotein 2 at day 21. Only the nuclei could be fluorescently imaged but not MUC-2. Height of cells were about $25 - 30 \mu\text{m}$ at day 21. Cells were photographed at 10 x magnification. (Scale bar = $50 \mu\text{m}$) (L) Differentiation of Caco-2 cells cultured in Transwell inserts and thiol-ene microchip as indicated by the activity of the brush border enzyme aminopeptidase. ($n = 3$, mean \pm SD)

Figure 4. TEER measurements of Caco-2 cells cultured in thiol-ene microchip and Transwell inserts for the same cell concentration of $2.55 \times 10^5 \text{ cells/cm}^2$. (Here, number of measurements per data point $n = 12$ for microfluidic device; and $n = 5$ for Transwell inserts). B) Effect of test compounds alone or with TDM on Caco-2 TEER in the Transwell or microfluidic system, immediately after the experiment or following 24 h recovery in medium. (C) Immunofluorescence staining of P-gp on Caco-2 cells cultured in microfluidic device (nucleus in magenta, P-gp in cyan). Magnification 20x. (D) Rh 123 accumulation profile in the basolateral and apical chambers across Caco-2 monolayers in microfluidic device Data points represent mean \pm SD ($n = 3$).

Figure 5. Permeability of A) mannitol, B) FD4 and C) insulin, alone or with TDM, across Caco-2 monolayers grown in the Transwell or microfluidic system. Data points represent mean \pm SD ($n = 4$ for all Transwell inserts), ($n = 4$ for each of the experiments carried out with the microfluidic device)

Figures

Figure 1.

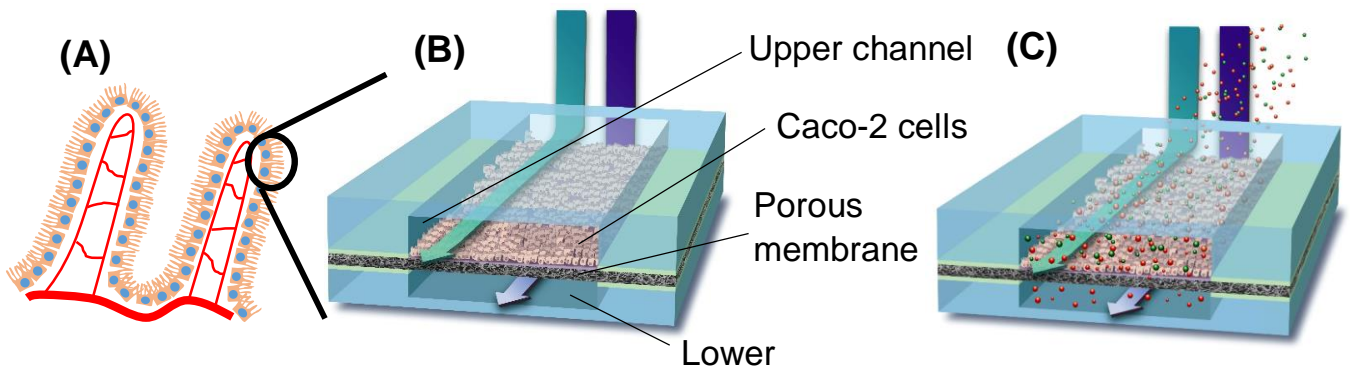


Figure 2.

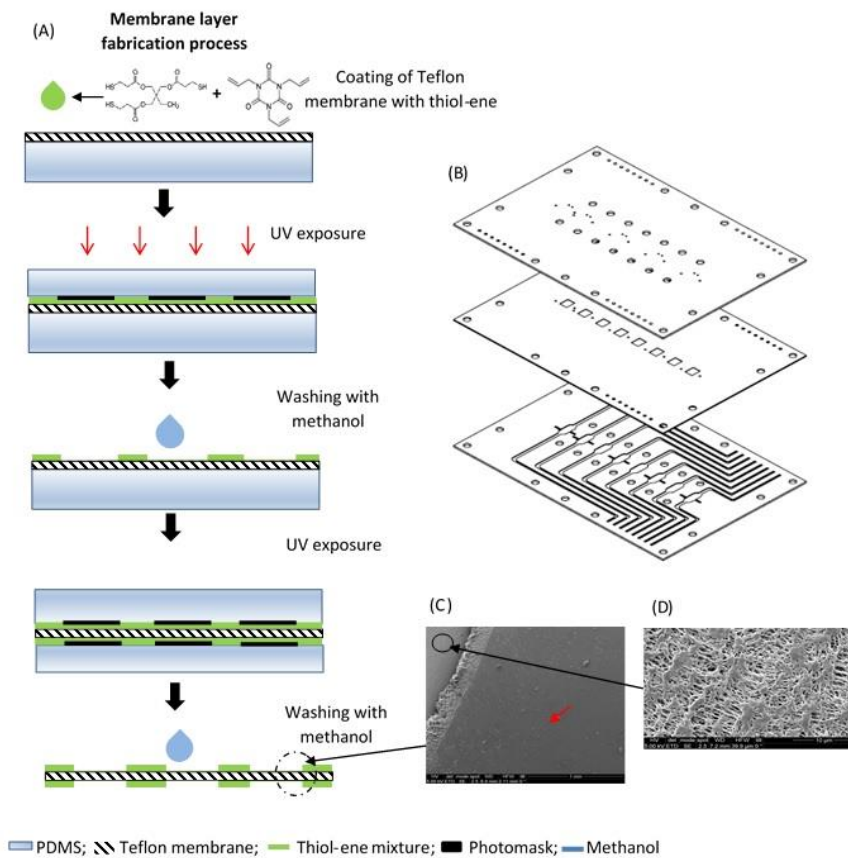


Figure 3.

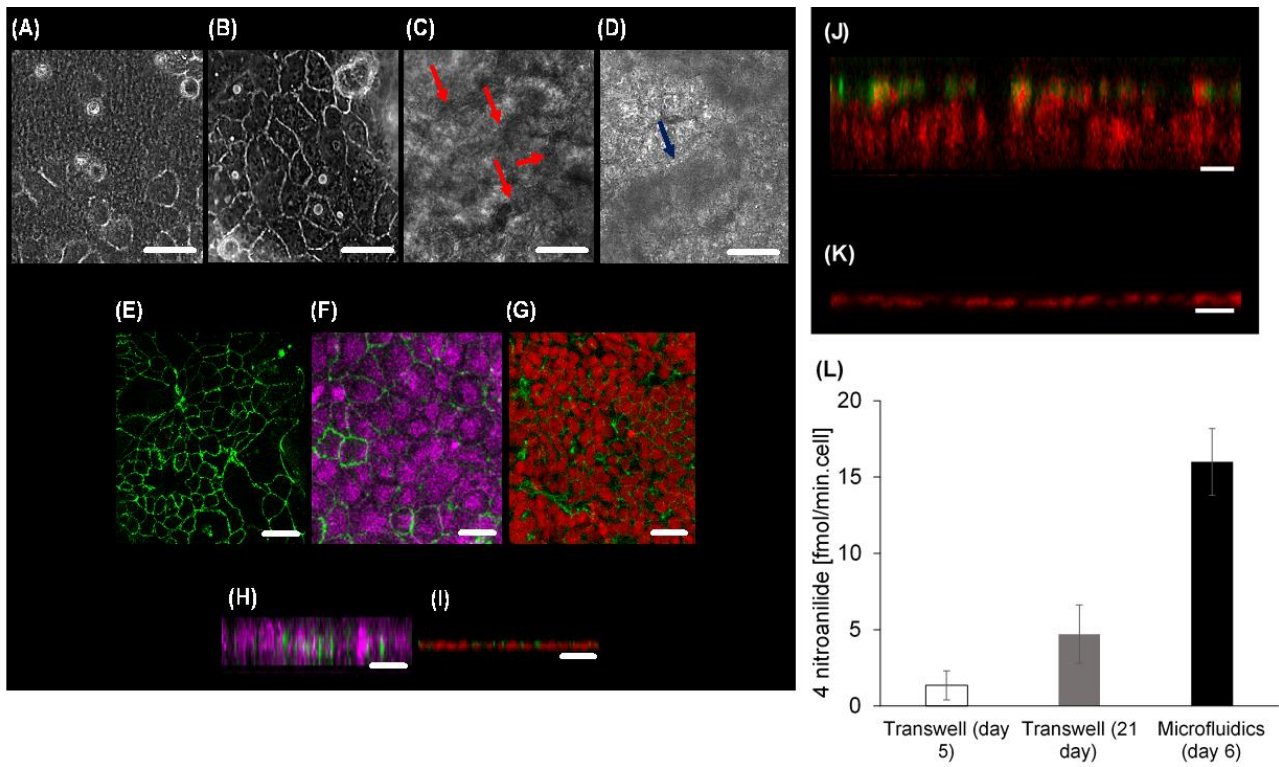


Figure 4

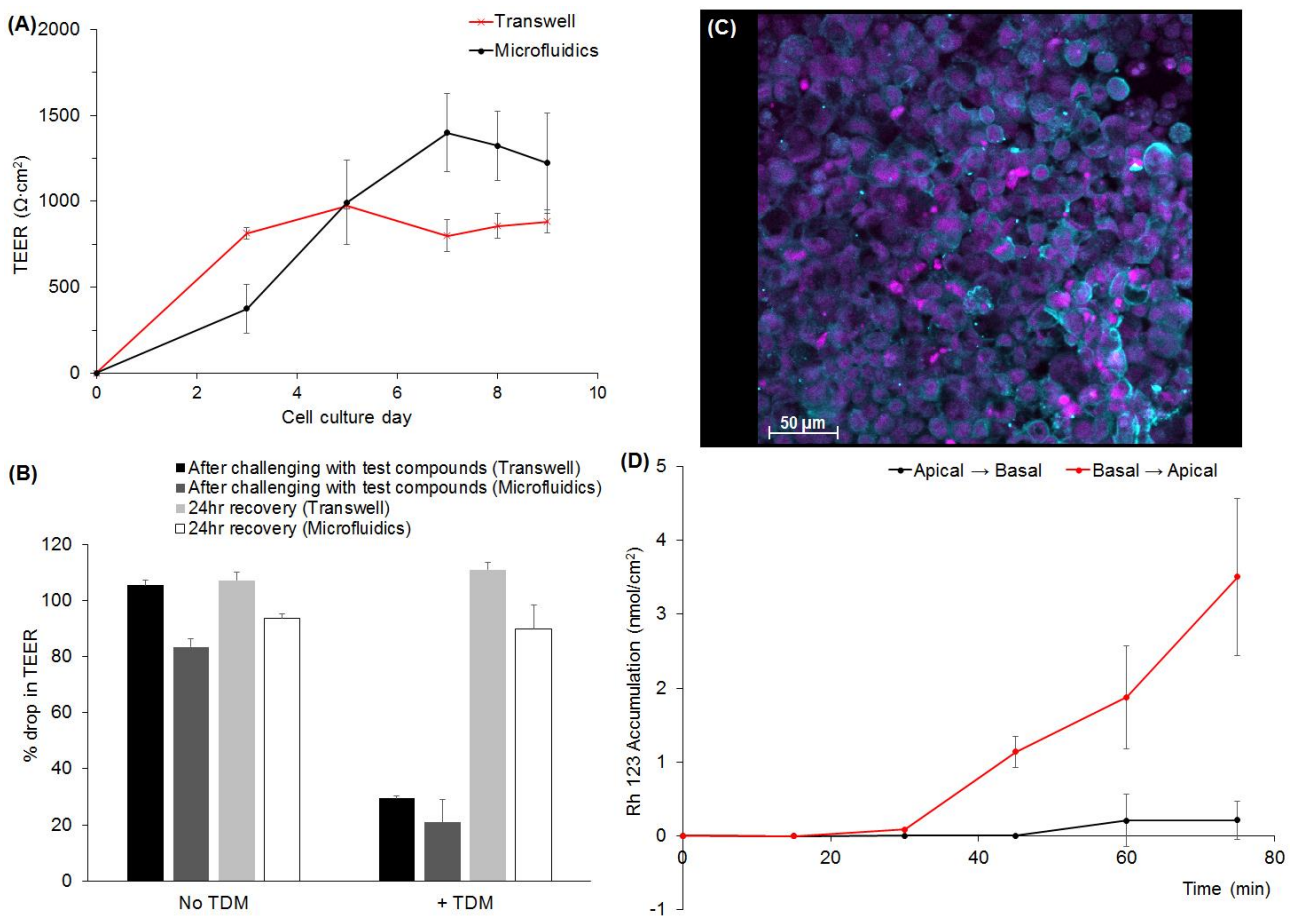
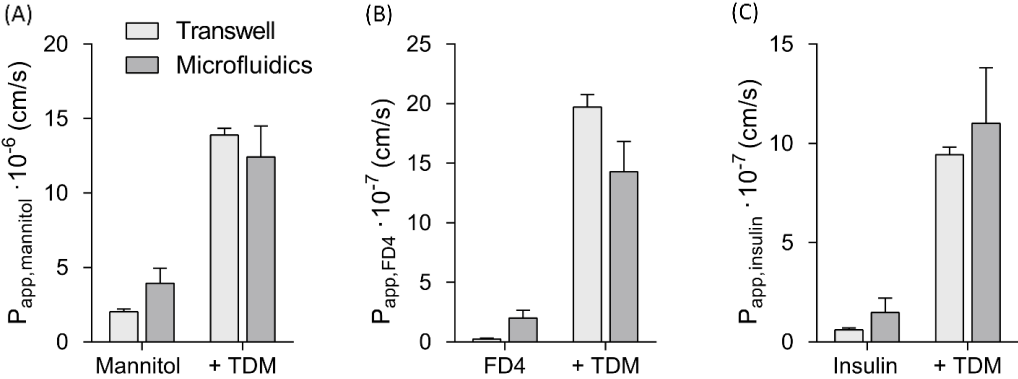


Figure 5.



Supporting Information

SI Text

Fabrication of microfluidic device. Two sets of molds were required to fabricate the fluidic layers of the thiol-ene microchip. The first mold was fabricated on polymethylmethacrylate (PMMA). The design of this mold was the exact replica of the thiol-ene microchip design. A second mold made from PDMS was the inverse design of the PMMA mold. The designs of the top and bottom layers of the microchip were first drawn with an engineering software, Autocad (Ver 18.1). To fabricate the first master molds, the drawings were converted to codes by EZ-CAM (ver 15.0, Germany) and micromilled (Mini-Mill/3, Minitech Machinery Corporation, GA, USA) onto 5 mm PMMA blocks. The second molds were fabricated by mixing poly dimethylsiloxane (PDMS; DowCorning, Germany) in the ratio of 1:10 (curing agent: pre-polymer), degassed under vacuum and poured onto the PMMA master mold. The liquid PDMS was cured in the oven at 70 °C for more than 20 hrs. Once the PDMS molds were cured, they were de-molded from PMMA molds, bearing the replicated design of the microchip layers.

Two different mixtures of thiol-ene were prepared for the microchip fabrication. The top and bottom layers, containing the fluidic microchannels and chambers were fabricated with a mixture of pentaerythritol tetrakis-(3-mercaptopropionate) (tetra-thiol moieties; Sigma, Denmark) (and 1,3,5 triallyl-1,3,5-triazine-2,4,6(1H,3H,5H)-trione (tri-allyl moieties; Sigma, Denmark) in stoichiometric ratios. The different components were mixed, poured onto the PDMS molds and exposed to UV (for 40 s on both sides (Dymax 5000-EC Series UV curing flood lamp, Dymax Corp., Torrington, CT, USA, ~40 mW cm⁻² at 365 nm) (Fig S1A).

To fabricate the thiol-ene coated Teflon membrane, a commercially available Teflon membrane (Millipore, Denmark) (0.4 μm in pore size; 40 μm in thickness) was modified to enable better bonding of the membrane to the thiol-ene parts containing the fluidic manifolds. A thiol-ene mixture consisting of trimethylpropane tris-(2-mercaptopropionate) (tri-thiol moieties; Sigma, Denmark) and the tri-allyl component as above, in stoichiometric ratios, was prepared and used to coat the membrane. The coated membrane was exposed to UV radiation for 25 s through a plastic mask (Infinite Graphics, Singapore) that protected the cell culture regions (Step 2 in Fig S1B). Thereafter, methanol (Sigma, Denmark) was used to rinse the entire membrane to remove any uncured thiol-ene (Step 3 in Fig. S1B). Before bonding the layers, holes for the inlets, outlets and electrode ports were drilled through the partial cured thiol-ene layers. Next, the layers (thiol-ene coated membrane and thiol-ene fluidic manifolds) were aligned onto each other. Slight pressure was applied with a roller over the layers to ensure good contact between the surfaces. To finalise the bonding, the combined layers were exposed to UV radiation for an additional minute on each side (Final step in Fig S1).

The completed microchip would have two sets of electrodes (top and bottom) embedded into selected chambers for measurement of the trans-epithelial electrical resistance (TEER). The bottom electrodes were fabricated using an Indium alloy (InBiSn (In 51 % Bi 32.5 % Sn 16.5 % by weight); Indium Corp, Utica, NY). Top electrodes were fabricated using Platinum wire (Pt, Advent, UK) (diameter 0.5 mm). To fabricate the bottom electrodes, the assembled microfluidic chip was first placed onto a hot plate set at 80 °C for 10 min. Pieces of the InBiSn metal, with length of 5 mm, were inserted into the electrode ports (connecting to the lower fluidic layer) on the thiol-ene microchip. Slight pressure was applied manually to push the melted metal into the electrode groove. Once the electrodes were formed, electric wires of diameter 0.4 mm were inserted to the liquid metal to act as connecting wires to the multimeter (Keithley, USA). To fabricate the top electrodes, pieces of Pt wires (diameter of 0.5 mm, length of 5 mm) were forced fit into the electrode ports drilled through the top fluidic layer. Two connecting Cu wires were soldered to the Pt wires. To fix the electrodes in position, UV-epoxy (NOA81; Norland, USA) was applied at the junctions between connecting wires and thiol-ene chip. The entire chip was exposed to UV light for 30 s. The entire procedure of embedding the electrodes on the microchip could be carried out in ambient environment, eliminating the use of expensive, sophisticated instruments in environment-controlled cleanroom.

Pressure burst studies of thiol-ene microchip layers. The burst pressure test of the different thiol-ene microfluidic chips were carried out at two different temperatures, namely room temperature (25°C) and incubator temperature (37 °C). The bond strength between the layers were investigated at 37 °C, which was the required temperature for cell culture of Caco2 cells. Therefore, this will also be the temperature that the

microfluidic chip would be subjected to for long periods. For the studies carried out at 37 °C, the microchip was first placed into an oven set at 37 °C, then transferred to a hotplate set at 37°C during the burst pressure tests. The system and method reported by Silkane et. al. (1) was used to carry out the burst pressure studies. The microchannels were first filled with diluted red food colour dye. Red dye was used to allow better visual observations during the pressure experiments. When testing the top layer, the inlets and outlets of the bottom layer and the outlet of the top layer were sealed with a layer of cured thiol-ene. These ports were sealed to prevent any leakage of pressure during the studies. The same procedure was carried out when testing the bottom fluidic layer. The instrument for the pressure test, as well as the chip filled with dye are shown in Fig. S2. Next, the microchip was connected to a mechanical clamp, where a pressure sensor was mounted onto a polycarbonate block. Via a tube, the system was connected to two 10 ml syringes. Pressure in the microchip was increased, by using the clamp to compress the air in the syringes. The entire system for the burst pressure test is shown schematically in Fig. S2a. The output of the pressure sensor was measured with an in-house written Labview program (National Instruments, Austin, TX, USA).

Cell culture in Transwell inserts and microfluidic chip

Transwell system. Control studies were carried out using static cultures of Caco-2 cells in 12 well Transwell plates (Corning, Sigma, Denmark). The inserts in the well plate each had a porous polycarbonate membrane (1.1 cm², 0.4 µm pores). In the Transwell studies, the Caco-2 cells harvested with trypsin/ETDA solution (0.05 %; Sigma, Denmark) were seeded on the top surface of the porous Transwell membrane at a density of 1 x 10⁵ cells/well. The Caco-2 cells were grown for 14–16 days in Dulbecco's Modified Essential Medium (DMEM; Sigma, Denmark) supplemented with 10 % (v/v) heat-inactivated fetal bovine serum (FBS; Sigma, Denmark), 1% (v/v) nonessential amino acids (NEAA; Gibco, Denmark) and 1% (v/v) penicillin-streptomycin (P/S; Gibco, Denmark). The medium was changed every second day of cell culture.

Microfluidic system. After the microchip was fabricated, it was assembled onto the platform with MAINSTREAM components (2). The Teflon tubings (inner diameter = 0.2 mm; Bola, Denmark) microcomponents and microchip were sterilised by perfusing 70 % ethanol throughout the entire system at a flow rate of 5µl/min for 2 hours. Following that, sterile water was flushed into the entire system for an additional 2 hours at a flow rate of 5µl/min. It was crucial to ensure good microenvironment in the cell culture chamber and good cell attachment during cell seeding in the microchip. To achieve this, extra cellular matrix mixtures (ECM) known to have the ability in improving the cellular microenvironment (3–5), was used to coat the Teflon membrane. An ECM mixture: 300 µg/ml matrigel (Corning, United Kingdom) and 50 µg/ml collagen (BD Bioscience, Denmark) and serum-free DMEM was flowed into the microchip to coat the porous membrane. The ECM mixture was flowed into the microchip for 2 hours at a flow rate of 5µl/min in an incubator. After the incubation, the microchip device was perfused with cell culture medium overnight in an incubator (37°C, 5 % CO₂). Following that, the harvested Caco-2 cells from the trypsin/EDTA solution was seeded into the microfluidic chip.

For cell seeding in the microfluidic microchip, the harvested Caco-2 cells was diluted with DMEM containing 60 % (v/v) FBS solution. The re-suspended cell mixture was syringed into the 'cell loading' reservoirs that were assembled onto the microfluidic platform. The peristaltic micropump on the microfluidic platform was activated at a very high flow rate (flow rate ≈ 65 µl/min) to draw the cell suspension into the cell culture chambers. The microchambers were seeded with Caco-2 cells at a concentration of 2.5 x 10⁵ cells/cm². A normal optical microscope was utilized to observe the distribution of the cells in the chambers. Caco-2 cells attached onto the ECM-coated Teflon membrane within 30 minutes. Next, the entire system with the microchip was placed in the incubator (37°C, 5% CO₂). After 2 hours, the peristaltic micropump was activated to perfuse culture medium through the upper microchannels and microchambers at a constant flow rate of 0.5 µl/min. Cell culture medium was flowed only in the upper layer on day 1 of cell culture. This was to ensure the Caco-2 cells establish an intact monolayer. From the second day of cell culture onwards, the micropump that was perfusing through the lower microchannels and microchambers was also activated. Flow rate was set at 3 µl/min for both top and bottom channels. Over the 9 - 10 days of cell culture, phase contrast images of the cells in four different positions of each of the microchambers were taken and compared.

Trans epithelial barrier measurements (TEER)

Transwell set-up. To acquire the TEER measurements (Ω) from the Transwell inserts, a Millicell ERS-2 (Millipore, USA) coupled to a pair of chopstick Silver/SilverChloride (Ag/AgCl) electrodes was used. TEER values ($\Omega \cdot \text{cm}^2$) were determined by subtracting the baseline measurements recorded in absence of cells, then multiply the cell culture area (cm^2) (eq. 1).

Microfluidic device. TEER measurements (Ω) of the Caco-2 cells cultured in the microfluidic device were obtained by coupling the connecting wires of the electrodes to a multimeter (Keithley, USA) using alligator clips. Similar to the Transwell studies, the final TEER values were determined by subtracting the baseline measurements recorded in the absence of cells, then multiply the cell culture area of the porous Teflon membrane (area 0.1 cm^2).

TEER measurements. The final TEER values ($\Omega \cdot \text{cm}^2$) from the microfluidic device were determined by subtracting the baseline measurement in the absence of cells (R_{baseline}) from the read out (R_1) and multiplying with the area of cell culture (A_o) as shown in equation 1.

Eq (1):
$$(R_1 - R_{\text{baseline}}) \times A_o = \text{TEER}$$

Morphological studies of Caco-2 cells cultured in microfluidic system and Transwell cultures. Phase contrast images of the Caco-2 monolayers were obtained using an inverted microscope (Carl Zeiss, Germany). Images were analysed with the imaging software (AxioVision 4.8.2, Carl Zeiss, Germany). Fluorescent confocal images of the monolayer morphology were obtained using a confocal microscope (Carl Zeiss, Germany). The procedure for cell staining and the dyes used were the same for both Transwell cultures and microfluidic device. PBS was used to rinse the cells between each processing step. The Caco-2 cells were fixed with 4% (vol/vol) paraformaldehyde for 30 min, following by permeabilisation with 0.1 % Triton X-100 for 30 min. After which, a blocking buffer (1% bovine serum albumin (BSA; Sigma, Denmark), 0.1% Tween-20 (Sigma, Denmark) in phosphate buffer saline (PBS; Sigma, Denmark)) was introduced to the cells for 1 hr. To visualize tight junctions, immunofluorescence staining was performed using mouse anti-ZO-1 (ZO-1; Life Technologies, Denmark) diluted in the blocking buffer 1:100, and introduced into the cells and left static overnight in the fridge at 4°C . Immunofluorescence staining was also carried out to stain the mucoprotein, mucin-2. Primary mouse monoclonal antibody (ab11197; AbCam, Denmark) prepared in blocking buffer (1:100), was introduced to the cells. The samples were protected from light and left static overnight in the fridge at 4°C . After which, the cells was rinsed with PBS followed by introducing the secondary antibody (AlexaFluor 488 goat anti-mouse; Life technologies, Denmark) prepared in blocking buffer (1:200) and left static in room temperature for 2 hrs. Similar immunofluorescence staining procedure was carried out to stain the P-glycoprotein transporters. Primary rabbit polyclonal antibody (ab129450; Abcam, Denmark) prepared in blocking buffer (1:200) was introduced to the cells and left static overnight in the fridge at 4°C . Following that, the cells were rinsed with PBS and stained with secondary antibody (AlexaFluor 488 goat anti-rabbit IgG H & L; Abcam, Denmark) prepared in blocking buffer (1:200). The cells were left in static condition in room temperature for 2 hrs. Staining of the nucleus and actin were carried out by diluting 7-aminoactinomycin D (7-AAD; Invitrogen, Denmark) ($32 \mu\text{M}$) and rhodamin phalloidin (RP; Life Technologies, Denmark)) to 1:100 in PBS and incubated with the cells for 1 hr. Lastly, mounting media (Vectashield; VWR, Denmark) was added to the cells to protect the fluorescent dyes. For the Transwell cultures, the membranes were removed from the inserts and mounted onto glass slides before microscopic imaging. Staining of cells in the microfluidic device, were performed *in situ* within the microchannels by flowing the different reagents into the microchannels and microchambers via MAINSTREAM platform. Visualisation of the tight junctions, mucus and P-gp transporters were carried out at excitation/emission wavelength of 488/570 nm was chosen. The stained nuclei were visualised at excitation/emission wavelengths of 546/647 nm. Fluorescent imaging of the stained Caco-2 cells on the thiol-ene microchip was performed through the thiol-ene layer on an upright microscope (ZEISS Axioscope; Carl Zeiss, Germany). The recorded images of the cells were analysed with an imaging process software AxioVision SE64 Rel4.8.

Aminopeptidase studies to determine differentiated Caco-2 cells. L-alanine-4-nitroaniline hydrochloride (L-4AN; Sigma, Denmark) was prepared by dissolving the L-A4N substrate in DMEM without phenol red (DMEM^{PR}, Gibco, Denmark) to a concentration of 1.5 mM. In the Transwell studies, the Caco-2 cells were first rinsed with DMEM^{PR} in both the apical and basolateral sides for 3 times. 500 µl of L-A4N substrate solution was added to the apical side of the cells and 1500 µl of DMEM^{PR} was added to the basal lateral side of the cells and incubated at 37 °C. Sample aliquots of 100 µl was removed from the apical side at 30 min intervals and transferred to a 96-well microplate. Studies were carried out for a 2 hr period. Analysis of the sample aliquots were carried out with a microplate reader (Victor 3V; Perkin Elmer). DMEM^{PR} was set as the reference. The test was calibrated with a series of dilutions of 4-nitroanilide in DMEM^{PR}. One unit is defined as the hydrolysis of 1.0 µmol of 4-nitroanilide per minute. All of the reagents preparation and experimental studies were conducted under the protection of light. The aminopeptidase experiments in the Transwell cultures were carried out on cell culture day 5 and 21.

In the microfluidic device, the aminopeptidase studies were carried out on day 5 of cell culture. DMEM^{PR} was first perfused to both the top and bottom fluidic channels for 45 min at a flow rate of 3 µl/min. Next, 1.5 mM of L-A4N solution was flowed into the upper microchannels and microchambers of the thiol-ene microchip at a flow rate of 3 µl/min. Sample aliquots of 120 µl were removed from the outlets of the upper microchannels at every 30 min and transferred to a 96-well microplate. Similar to the Transwell studies, the sample aliquots from the microfluidic system were analysed for the cleaved product, 4-nitroanalide with the microplate reader.

Permeability studies of fluorescein isothiocyanate–dextran (FD-4), mannitol and insulin in the presence or absence of membrane enhancer and Rhodamine 123 (Rh 123). The compounds used in the permeability studies, [3H]-mannitol (PerkinElmer; USA), fluorescein isothiocyanate (FITCH)-labeled dextran (FD4; 4kDa; Sigma, Denmark), insulin (Novo Nordisk, Denmark) and tetradecyl-β-D-Maltoside (TDM; Sigma, Denmark) were all prepared using buffer⁺ as the diluent. Buffer⁺ was prepared by mixing Hank's Buffered Saline solution (HBSS; Gibco, Denmark), 0.1% (wt/v) OVA (ovalbumin; from chicken egg white, Sigma, Denmark) and 10 mM HEPES (HEPES; Sigma, Denmark) at pH 7.4. The different compounds were prepared in various concentrations: 0.8 µCi/ml [3H]-mannitol, 100 µM insulin (peptide/drug) or 540 µM FD4, and 0 or 400 µM TDM.

In the Transwell studies, before carrying out the transport experiments, DMEM was changed to buffer⁺. 400 µl of buffer⁺ was added to the apical side and 1 ml to the basolateral prior to equilibrate the Transwell plate for 60 minutes. Buffer⁺ was replaced apically by 400 µl test solution at time zero, and the Transwell plates were incubated at 37°C and 5% CO₂ with gentle shaking. The gentle shaking is to ensure there was little unstirred diffusion layers of fluid in the basolateral region. Basolateral samples were collected every 15 minutes for 1 hour and analyzed along with apical test solutions, for [3H]-mannitol content in a scintillation counter (Packard TopCount; PerkinElmer), after mixing with scintillation fluid (Microscint-40; PerkinElmer), along with a peptide and FD4 content. We chose to use the peptide, insulin, as a proof-of-concept demonstration in using the Caco-2 monolayers cultured in the thiol-ene microchip for drug permeability studies. After experiments, cells were washed twice with buffer⁺ and replenished with medium for 24 hour recovery. In the microfluidic system, similar to the Transwell studies, before the start of experiment, the DMEM was replaced with buffer⁺. Buffer⁺ was flowed into the system for 1 hr. Subsequently, the buffer was changed to the test solutions in the top fluidic layer. Flow rate was set at 3 µl/min (in both the upper and lower layers). In the waste collection reservoirs, 200 µl of buffer was added to each of the waste reservoirs. This would enable sample aliquots of 100 µl collected at every 15 min intervals. During calculation of the permeability of the compounds across the cell monolayers, dilution of the sample aliquots were factored. Preparation of the test solutions can be found in *Materials and methods* segment.

For the Rhodamine 123 (Rh 123) efflux studies, Rh 123 (Sigma-Aldrich, Denmark) was prepared in buffer⁺ to a concentration of 10 µM. Before carrying out the Rh 123 studies, buffer⁺ was flowed to both the upper and lower channels for 1 hr. Following that Rh 123 (Sigma-Aldrich, Denmark) prepared in buffer⁺ to a concentration of 10 µM was flowed to the donor side – for absorptive the donor is the apical chamber and secretory transport the donor is the basolateral chamber. 200µl of buffer⁺ was added to each waste reservoirs. At each 15min interval, 150 µl was removed from the respective waste reservoirs with replacement of 150µl of buffer⁺. Studies were carried out in triplicates.

Data analysis of permeability results. The Caco-2 translocation of peptide, [³H]mannitol or Rh 123 over Caco-2 layers is expressed as the apparent permeability (P_{app}), given by:

$$\text{Eq. (E1):} \quad P_{app} = \frac{dQ}{dt} \frac{1}{A \cdot C_0}$$

Where dQ/dt is the steady-state flux across the cell layer (pmol/s), A is the surface area (1.12 cm² for Transwell, 0.1 cm² for microfluidic), and C_0 is the initial sample concentration (6) .

The basolateral samples were analyzed for insulin content using commercial insulin enzyme immunoassay kit (EIA, Phoneix Pharmaceuticals, Germany). Standards were prepared from test solutions, and were fitted to eq. 2 using Prism-6 (GraphPad).

$$\text{Eq. (E2):} \quad Abs(450nm) = A + \frac{B-A}{1+10^{((\log EC_{50}-x) \cdot C)}}$$

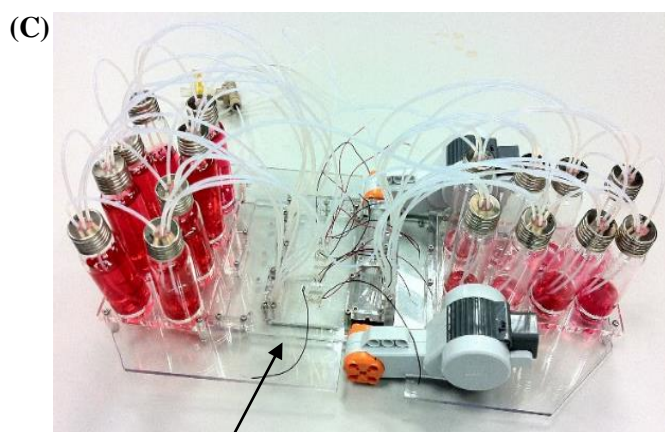
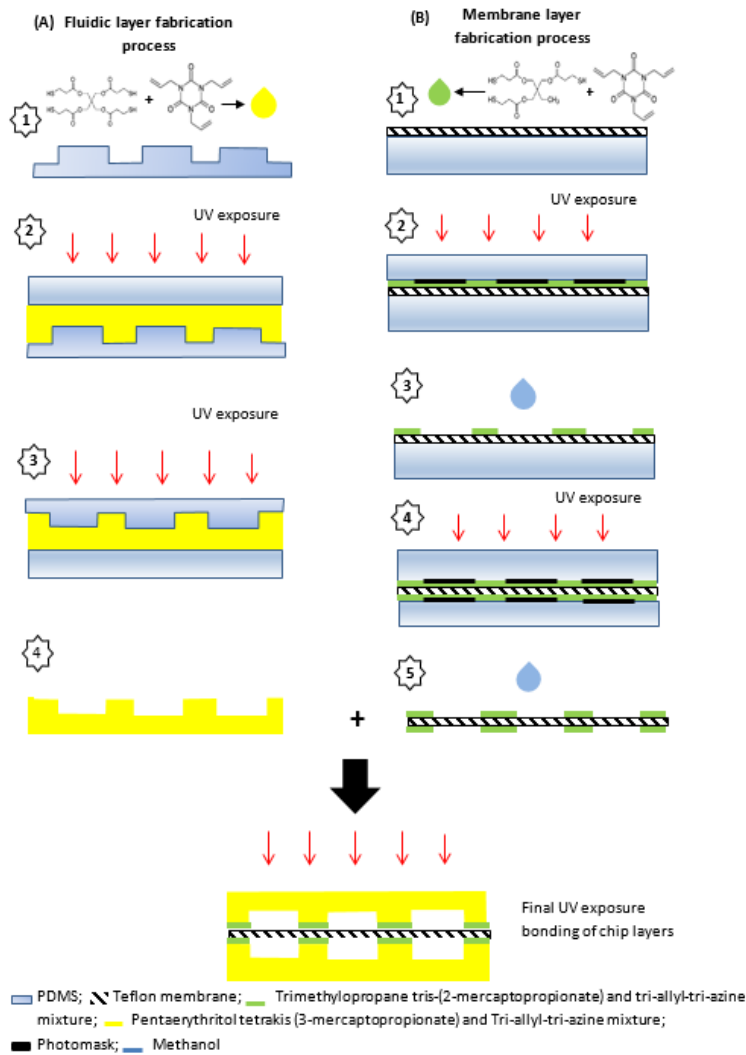
where x is $\log(\text{concentration})$ of peptide in M, and A , B , C and EC_{50} are fitting parameters (7).

Basolateral samples were analyzed for FD4 content in a fluorescence plate reader (MD Spectramax Gemini, USA) with excitation/emission of 490/525 nm, based on standard curves prepared from test solutions. Statistical analysis was carried out using the softwares, Origin (OriginPro, Ver 9.1) and Prism (GraphyPad, Ver 6), where unpaired Students t-tests were used for comparison, and a significant difference was considered if $p < 0.05$. Results are presented as the mean \pm standard deviation of the mean (SD).

For the P-gp studies, the collected samples were analysed for Rh 123 content using a fluorescence plate reader with excitation/emission of 485/546nm, based on standard curves prepared from test solutions. The efflux ratio of P-gp was determined by:

$$\text{Eq. (E3):} \quad \text{efflux ratio} = \frac{P_{app} (\text{Basal} \rightarrow \text{Apical})}{P_{app} (\text{Apical} \rightarrow \text{Basal})}$$

SI figures



Thiol-ene microfluidic chip

Figure S1. Schematic process of fabricating the thiol-ene microchip. (A) The upper and lower fluidic layer; (B) The thiol-ene coated Teflon membrane. (C) Final assembled system with microfluidic chip for cell culture. Microchambers on the microchip are embedded with the electrodes for acquiring TEER measurements.

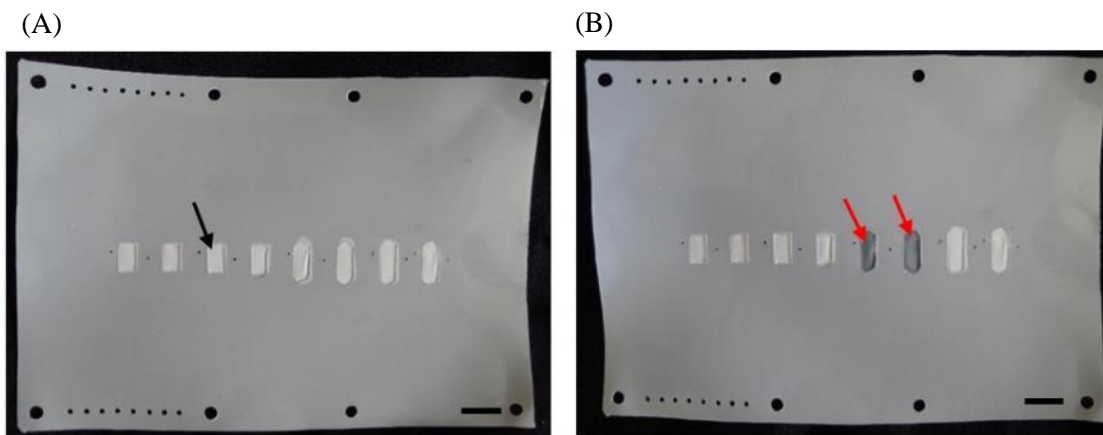


Figure S2. Porous Teflon membrane modified with a layer of cured thiol-ene mixture. Black arrow indicating the region on porous membrane that was protected by a plastic mask during UV-exposure. When dry, the region appeared white and opaque. (b) Two chambers were wetted with DI water, as indicated by red arrows. Teflon membrane becomes transparent in visible light. (Scale bar = 5 mm)

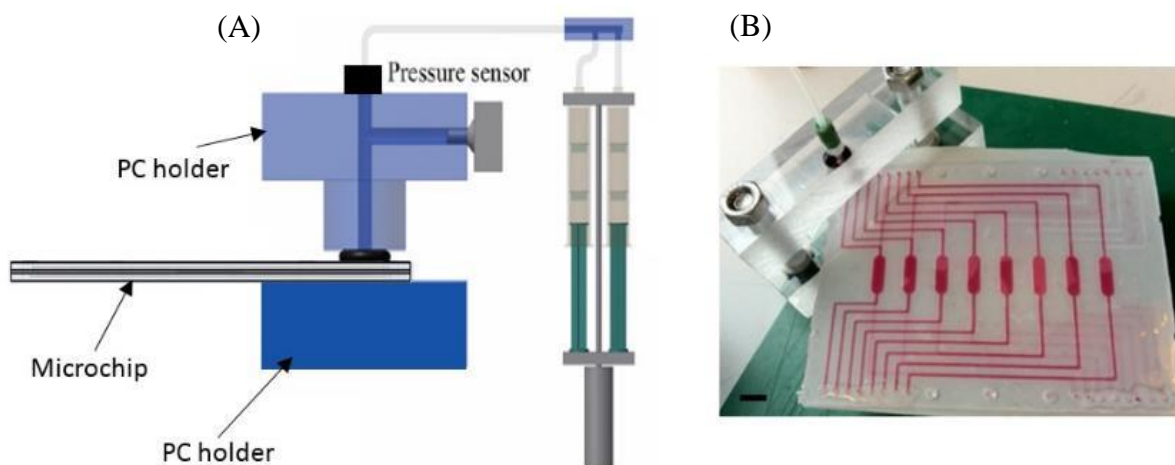


Figure S3. Burst pressure study for thiol-ene microchip. (a) Schematic view of the pressure system (1). The thiol-ene microchip was clamped between the PC holders. The pressure sensor on the top of the PC holder will measure the pressure of the set-up. The syringes are compressed to provide the pressure into the microchip. (b) Microfluidic chip filled with red dye. The inlet and outlet ports for the bottom fluidic layer and outlet for the top layer were sealed with cured thiol-ene. The inlet port of the top fluidic layer is clamped between the mechanical device.

Sample	Maximum pressure (Bars)	Temperature
3T3E + 3T3E	2.0 ± 0.66	

4T3E + 4T3E	Layers could not be bonded	25 °C
4T3E + 3T3E	> 6.0	
3T3E + 3T3E	< 0.3	37 °C
4T3E + 4T3E	Layers could not be bonded	
4T3E + 3T3E	> 6.0	

Table ST1. Tabulated data of the maximum pressure the different thiol-ene mixtures used for fabricating the microchips could withstand in different temperature conditions. All thiol-ene mixtures were prepared in stoichiometric ratios. Where 4T = tetra-thiol, 3T = tri-thiol and 3E = tri-allyl. (n = 6)

References

1. Sikanen TM, et al. (2013) Fabrication and bonding of thiol-ene-based microfluidic devices. *J Micromechanics Microengineering* 23(3):037002.
2. Sabourin D, et al. (2013) The MainSTREAM component platform: a holistic approach to microfluidic system design. *J Lab Autom* 18(3):212–28. Available at:
3. Kuschel C, et al. (2006) Cell adhesion profiling using extracellular matrix protein microarrays. *Biotechniques* 40(4):523–531.
4. Basson MD, Turowski G, Emenaker NJ (1996) Regulation of Human (Caco-2) Intestinal Epithelial Cell Differentiation by Extracellular Matrix Proteins 1. *Exp Cell Res* 305(225):301–305.
5. Zemljic Jokhadar S, Znidarcic T, Svetina S, Batista U (2007) The effect of substrate and adsorbed proteins on adhesion, growth and shape of Caco-2 cells. *Cell Biol Int* 31(10):1097–108.
6. Hubatsch I, Ragnarsson EGE, Artursson P (2007) Determination of drug permeability and prediction of drug absorption in Caco-2 monolayers. *Nat Protoc* 2(9):2111–9.
7. Borchard G (2009) The absorption barrier. *Oral Delivery of Macromolecular Drugs*, ed Bernkop-Schnürch A (Springer US, New York), pp 49–64.

B1. Peer review conference proceeding 1: Multi-chamber and multi-layer thiol-ene microchip for cell culture

H. Y. Tan*, M. Hemmingsen, J. P. Lafleur, J. P. Kutter, M. Dufva, T. L. Andresen, “Multi-chamber and multi-layer thiol-ene microchip for cell culture”, In Proceedings of the Eighteenth International Conference on Miniaturized Systems for Chemistry and Life Science (MicroTAS 2014), pp. 1749-1751.

MULTI-CHAMBER AND MULTI-LAYER THIOL-ENE MICROCHIP FOR CELL CULTURE

H. Y. Tan¹, M. Hemmingsen¹, J. P. Lafleur², R. V. Søndergaard¹, J. P. Kutter², M. Dufva¹ and T. L. Andresen¹

¹Technical University of Denmark, Denmark and

²University of Copenhagen, Denmark

ABSTRACT

We present a multi-layer and multi-chamber microfluidic chip fabricated using two different thiol-ene mixtures. Sandwiched between the thiol-ene chip layers is a commercially available membrane whose morphology has been altered with coatings of thiol-ene mixtures. Experiments have been conducted with the microchip and shown that the fabricated microchip is suitable for long term cell culture.

KEYWORDS: Thiol-ene, multi-chamber, multi-layer, cell culture

INTRODUCTION

Several groups have reported the use of thiol-ene as a material in microchip fabrication [1-4]. To our knowledge, this material has so far not been used for the fabrication and application of microchips for long term cell cultures. This paper reports on using thiol-ene as the main material in fabricating microchips for long term cell culturing. The presented microchip is comprised of three layers, where the middle layer is a thiol-ene-modified Teflon membrane. The fabricated microchip holds a total of eight individual chambers, thus allowing different cell concentrations and different types of cells to be cultured on the same device.

MICROCHIP FABRICATION

Two different mixtures of thiol-ene were prepared for the microchip fabrication. The top and bottom layers were fabricated with a mixture of pentaerythritol tetrakis(3-mercaptopropionate) (4 thiol moieties) and tri-allyl-tri-azine (3 ene moieties) in stoichiometric ratios. A commercially available Teflon membrane, which is known to be ideal for cell culture, was modified to enable bonding of the membrane to the thiol-ene parts containing the fluidic manifolds. A thiol-ene mixture consisting of trimethylpropane tris-(2-mercaptopropionate) (3 thiol moieties) and the same "ene" component as before in stoichiometric ratios was mixed and applied to both sides of the membrane. Following this, the coated membrane was exposed to UV radiation for about 25 s through a mask, which protected the cell culture chamber regions. After the thiol-ene was cured, the entire membrane was washed with methanol to remove any uncured thiol-ene. Next, the underside of the membrane was coated with another layer of thiol-ene and exposed to UV radiation. This was done to ensure good bonding with the chip layers in the next step. Figure 1 shows a schematic drawing of the exploded view of the microchip.

Microscopic inspection shows that the Teflon membrane's surface structure was modified after applying the thiol-ene. Figure 2 shows SEM images detailing the surface morphology of the Teflon membrane before and after curing of a coating of thiol-ene. To further investigate wetting behavior of the modified membrane, contact angle measurements were carried out with different materials to compare to the surface energy of the modified membrane. Figure 3 shows the contact angle measurements of different polymers in comparison with thiol-ene. The thiol-ene coated membrane was found to be hydrophobic.

After the different layers were fabricated, they were placed on top of each other and slight pressure was applied to ensure good contact between the surfaces. The combined layers were then exposed to UV radiation for another 1 min on each side of the entire chip.

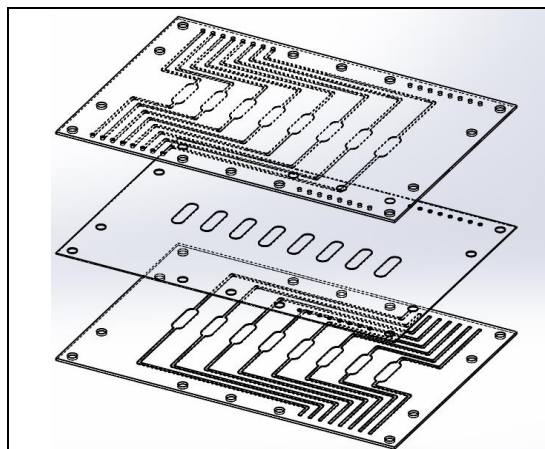


Figure 1: Schematic drawing of the 3 layer microchip. Dimension of microchip: 76mm x 52mm x 2.7mm. Thickness of modified membrane is 0.3mm. Membrane is coated with thiol-ene mixture on both sides to ensure good bonding between the chip layers. Fluids are pumped in the upper and lower layers.

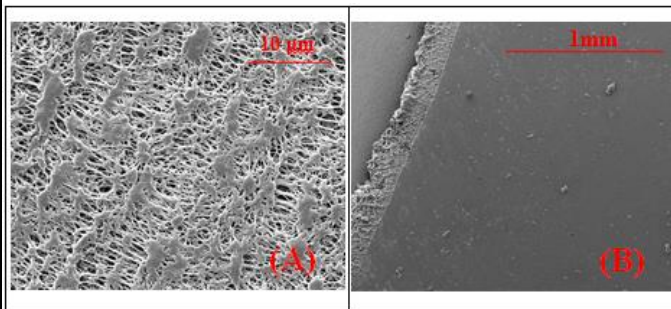


Figure 2: SEM images of a Teflon membrane. Surface morphology was changed significantly before and after curing a layer of thiol-ene. (A) Before coating and curing a layer of thiol-ene: observable pores on the membrane; (B) Teflon membrane after curing a layer of thiol-ene: no observable pores, the surface is very smooth. Top left side of membrane was uncoated.

Thiol-ene	Thiol-ene coated membrane	Polymethyl-Methacrylate (PMMA)	Polycarbonate (PC)	Poly-dimethyl-siloxane (PDMS)
Left angle = 95.87° Right angle = 95.03°	Left angle = 96.4° Right angle = 96.57°	Left angle = 76.73° Right angle = 77.13°	Left angle = 74.2° Right angle = 76.37°	Left angle = 113.13° Right angle = 113.93°

Figure 3. Contact angle measurement of materials typically used in microchip fabrication for cell culture. The contact angle measured on thiol-ene was compared to the other materials. Volume of droplet used for contact angle measurement was 4μl. The thiol-ene coated membrane was found to be hydrophobic.

RESULTS AND DISCUSSION

Different cells, specifically Caco-2 cells and Hela cells of different concentrations, were cultured in the reported microchip. The microchip was assembled to a pressurized system that utilised LEGO Mindstorm motors and controllers and a Lab View-based programming interface [5]. The cells seeded in the respective chambers were cultured in the chip for 7-11 days. Following this, live and dead cells staining was carried out to evaluate cell viability. Figure 4 shows the phase contrast and fluorescence images of stained Caco-2 cells cultured in the thiol-ene microchip.

	0.5 x 10 ⁶ cells/ml (seeding concentration)	10 x 10 ⁶ cells/ml (seeding concentration)
Phase contrast		

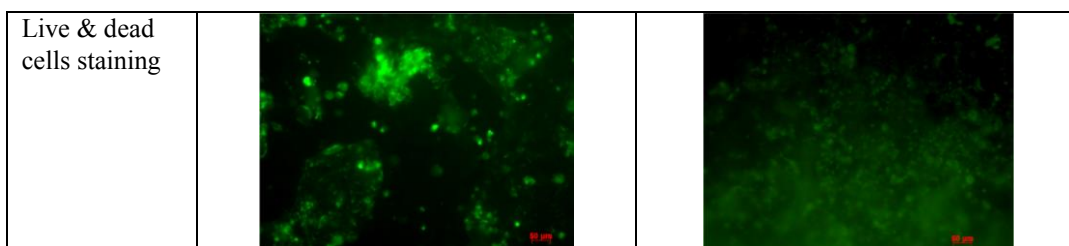


Figure 4. Images of Caco-2 cells in the thiol-ene microchip after culturing for 11 days. Green fluorescence indicates live cells whereas red fluorescence indicates dead cells. (Images were taken with 10x magnification)

CONCLUSION

We have successfully designed and fabricated a multi-layer microchip with thiol-ene as main substrate material for long-term cell culturing. Sandwiched between the thiol-ene layers is a commercially available Teflon membrane whose surface morphology had been altered with thiol-ene. Altering the morphology enabled the membrane to be bonded to the thiol-ene chip layers. The reported microchip is biocompatible and we have demonstrated that it is suitable for long-term cell culturing. Such a system provides an avenue for drug transport studies in cell lines.

ACKNOWLEDGEMENTS

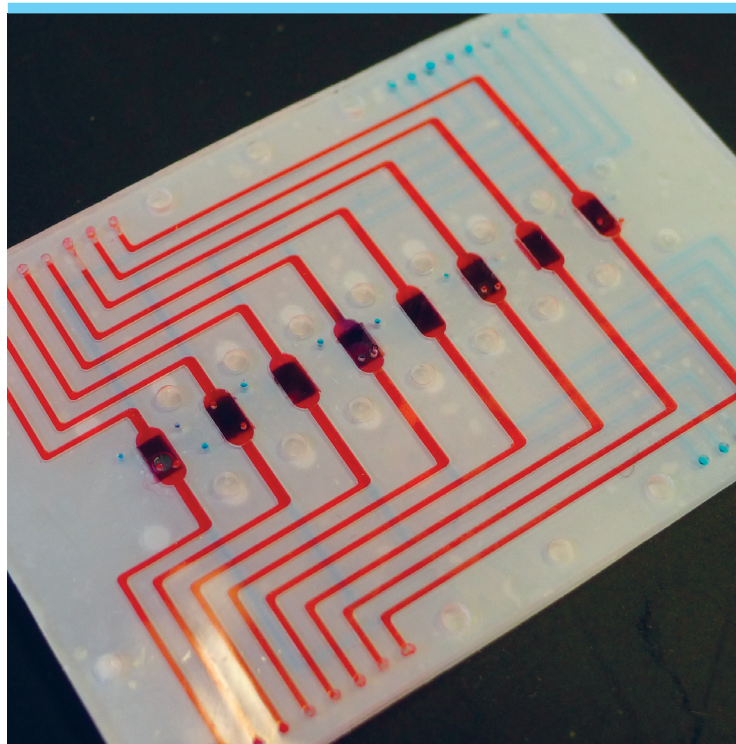
We would like to thank The Danish Council for Independent Research (FTP) for funding the research under the CAMNOT grant (12-126894).

REFERENCES

1. "Rapid prototyping of multi-layer thiolene microfluidic chips by photopolymerization and transfer lamination", M. Natali, S. Begolo, C. Carofiglio, G. Mistura, *Lab Chip*, 8, 492-494, (2008).
2. "Beyond PDMS: off-stoichiometry thiol-ene (OSTE) based soft lithography for rapid prototyping of microfluidic devices", C. F. Carlborg, T. Haraldsson, K. Oberg, M. Malkoch, W. van der Wijngaart, *Lab Chip*, 11, 3136, (2011)
3. "Biocompatibility of OSTE polymers studied by cell growth experiments", C. Errando-Herranz, A. Vastesson, M. Zelenina, G. Pardon, G. Bergström, W. van der Wijngaart, T. Haraldson, H. Brismar, K. B. Gylfason, *In Proc. microTAS*, (2013)
4. "Rapid photochemical surface patterning of proteins in thiol-ene based microfluidic devices", J. P. Lafleur, R. Kwapiszewski, T. G. Jensen, J. P. Kutter, *Analyst*, 138, (2013)
5. "The MainSTREAM component platform: a holistic approach to microfluidic system design", D. Sabourin, P. Skafte-Pedersen, M. J. Søb, M. Hemmingsen, M. A., V. Coman, J. Petersen, J. Emnéus, J. P. Kutter, D. Snakenborg, F. Jørgensen, C. Clausen, K. Holmstrøm, M. Dufva, *J. Lab. Automation*, 18, 3, (2012)

CONTACT

* H. Y. Tan; phone: +45 4525 5700; hsta@nanotech.dtu.dk



Copyright: Hsih-Yin Tan
All rights reserved

Published by:
DTU Nanotech
Department of Micro- and Nanotechnology
Technical University of Denmark
Ørsted's Plads, building 345C
DK-2800 Kgs. Lyngby